Westinghouse Electric Corporation Energy Systems

Box 355
Pittsburgh Pennsylvania 15230-0355

AW-96-1026

October 28, 1996

Document Control Desk
U.S. Nuclear Regulatory Commission
Washington, D.C. 20555

ATTENTION: T. R. QUAY

APPLICATION FOR WITHHOLDING PROPRIETARY INFORMATION FROM PUBLIC DISCLOSURE

SUBJECT: AP600 NOTRUMP VERIFICATION AND VALIDATION REPORT, DRAFT SECTIONS 5 AND 6

Dear Mr. Quay:

The application for withholding is submitted by Westinghouse Electric Corporation ("Westinghouse") pursuant to the provisions of paragraph (b)(1) of Section 2.790 of the Commission's regulations. It contains commercial strategic information proprietary to Westinghouse and customarily held in confidence.

The proprietary material for which withholding is being requested is identified in the proprietary version of the subject report. In conformance with 10CFR Section 2.790, Affidavit AW-96-1026 accompanies this application for withholding setting forth the basis on which the identified proprietary information may be withheld from public disclosure.

Accordingly, it is respectfully requested that the subject information which proprietary to Westinghouse be withheld from public disclosure in accordance with 10CFR Section 2.790 of the Commission's regulations.

Correspondence with respect to this application for withholding or the accompanying affidavit should reference AW-96-1026 and should be addressed to the undersigned.

Very truly yours,

Brian A. McIntyre, Manager
Advanced Plant Safety and Licensing

/nja

cc: Kevin Bohrer NRC 12H5

COPYRIGHT NOTICE

PROPRIETARY INFORMATION NOTICE

Transmitted herewith are proprietary and/or non-proprietary versions of documents furnished to the NRC in connection with requests for generic and/or plant specific review and approval.

In order to conform to the requirements of 10 CFR 2.790 of the Commission's regulations concerning the protection of proprietary information so submitted to the NRC, the information which is proprietary in the proprietary versions is contained within brackets, and where the proprietary information has been deleted in the non-proprietary versions, only the brackets remain (the information that was contained within the brackets in the proprietary versions having been deleted). The justification for claiming the information so designated as proprietary is indicated in both versions by means of lower case letters (a) through (f) contained within parentheses located as a superscript immediately following the brackets enclosing each item of information being identified as proprietary or in the margin opposite such information. These lower case letters refer to the types of information Westinghouse customarily holds in confidence identified in Section (4)(ii)(a) through (4)(ii)(f) of the affidavit accompanying this transmittal pursuant to 10 CFR2.790(b)(1).

AW-96-1026

AFFIDAVIT

COMMONWEALTH OF PENNSYLVANIA:

ss

COUNTY OF ALLEGHENY:

Before me, the undersigned authority, personally appeared Brian A. McIntyre, who, being by me duly sworn according to law, deposes and says that he is authorized to execute this Affidavit on behalf of Westinghouse Electric Corporation ("Westinghouse") and that the averments of fact set forth in this Affidavit are true and correct to the best of his knowledge, information, and belief:

Brian A. McIntyre, Manager
Advanced Plant Safety and Licensing

Sworn to and subscribed
before me this 28th day
of October, 1996

Janet A. Schwab
Notary Public

Notarial Seal
Janet A. Schwab, Notary Public
Monroeville Boro, Allegheny County
My Commission Expires May 22, 2000
Member, Pennsylvania Association of Notaries

2977A

(1) I am Manager, Advanced Plant Safety And Licensing, in the Advanced Technology Business Area, of the Westinghouse Electric Corporation and as such, I have been specifically delegated the function of reviewing the proprietary information sought to be withheld from public disclosure in connection with nuclear power plant licensing and rulemaking proceedings, and am authorized to apply for its withholding on behalf of the Westinghouse Energy Systems Business Unit.

(2) I am making this Affidavit in conformance with the provisions of 10CFR Section 2.790 of the Commission's regulations and in conjunction with the Westinghouse application for withholding accompanying this Affidavit.

(3) I have personal knowledge of the criteria and procedures utilized by the Westinghouse Energy Systems Business Unit in designating information as a trade secret, privileged or as confidential commercial or financial information.

(4) Pursuant to the provisions of paragraph (b)(4) of Section 2.790 of the Commission's regulations, the following is furnished for consideration by the Commission in determining whether the information sought to be withheld from public disclosure should be withheld.

(i) The information sought to be withheld from public disclosure is owned and has been held in confidence by Westinghouse.

(ii) The information is of a type customarily held in confidence by Westinghouse and not customarily disclosed to the public. Westinghouse has a rational basis for determining the types of information customarily held in confidence by it and, in that connection, utilizes a system to determine when and whether to hold certain types of information in confidence. The application of that system and the substance of that system constitutes Westinghouse policy and provides the rational basis required.

Under that system, information is held in confidence if it falls in one or more of several types, the release of which might result in the loss of an existing or potential competitive advantage, as follows:

(a) The information reveals the distinguishing aspects of a process (or component, structure, tool, method, etc.) where prevention of its use by any of Westinghouse's competitors without license from Westinghouse constitutes a competitive economic advantage over other companies.

(b) It consists of supporting data, including test data, relative to a process (or component, structure, tool, method, etc.), the application of which data secures a competitive economic advantage, e.g., by optimization or improved marketability.

(c) Its use by a competitor would reduce his expenditure of resources or improve his competitive position in the design, manufacture, shipment, installation, assurance of quality, or licensing a similar product.

(d) It reveals cost or price information, production capacities, budget levels, or commercial strategies of Westinghouse, its customers or suppliers.

(e) It reveals aspects of past, present, or future Westinghouse or customer funded development plans and programs of potential commercial value to Westinghouse.

(f) It contains patentable ideas, for which patent protection may be desirable.

There are sound policy reasons behind the Westinghouse system which include the following:

(a) The use of such information by Westinghouse gives Westinghouse a competitive advantage over its competitors. It is, therefore, withheld from disclosure to protect the Westinghouse competitive position.

(b) It is information which is marketable in many ways. The extent to which such information is available to competitors diminishes the Westinghouse ability to sell products and services involving the use of the information.

(c) Use by our competitor would put Westinghouse at a competitive disadvantage by reducing his expenditure of resources at our expense.

(d) Each component of proprietary information pertinent to a particular competitive advantage is potentially as valuable as the total competitive advantage. If competitors acquire components of proprietary information, any one component may be the key to the entire puzzle, thereby depriving Westinghouse of a competitive advantage.

(e) Unrestricted disclosure would jeopardize the position of prominence of Westinghouse in the world market, and thereby give a market advantage to the competition of those countries.

(f) The Westinghouse capacity to invest corporate assets in research and development depends upon the success in obtaining and maintaining a competitive advantage.

(iii) The information is being transmitted to the Commission in confidence and, under the provisions of 10CFR Section 2.790, it is to be received in confidence by the Commission.

(iv) The information sought to be protected is not available in public sources or available information has not been previously employed in the same original manner or method to the best of our knowledge and belief.

(v) Enclosed is Letter NSD-NRC-96-4863, October 28, 1996 being transmitted by Westinghouse Electric Corporation (W) letter and Application for Withholding Proprietary Information from Public Disclosure, Brian A. McIntyre (W), to Mr. T. R. Quay, Office of NRR. The proprietary information as submitted for use by Westinghouse Electric Corporation is in response to questions concerning the AP600 plant and the associated design certification application and is expected to be applicable in other licensee submittals in response to certain NRC requirements for justification of licensing advanced nuclear power plant designs.

This information is part of that which will enable Westinghouse to:

(a) Demonstrate the design and safety of the AP600 Passive Safety Systems.

(b) Establish applicable verification testing methods.

(c) Design Advanced Nuclear Power Plants that meet NRC requirements.

(d) Establish technical and licensing approaches for the AP600 that will ultimately result in a certified design.

(e) Assist customers in obtaining NRC approval for future plants.

Further this information has substantial commercial value as follows:

(a) Westinghouse plans to sell the use of similar information to its customers for purposes of meeting NRC requirements for advanced plant licenses.

(b) Westinghouse can sell support and defense of the technology to its customers in the licensing process.

Public disclosure of this proprietary information is likely to cause substantial harm to the competitive position of Westinghouse because it would enhance the ability of competitors to provide similar advanced nuclear power designs and licensing defense services for commercial power reactors without commensurate expenses. Also, public disclosure of the information would enable others to use the information to meet NRC requirements for licensing documentation without purchasing the right to use the information.

The development of the technology described in part by the information is the result of applying the results of many years of experience in an intensive Westinghouse effort and the expenditure of a considerable sum of money.

In order for competitors of Westinghouse to duplicate this information, similar technical programs would have to be performed and a significant manpower effort, having the requisite talent and experience, would have to be expended for developing analytical methods and receiving NRC approval for those methods.

Further the deponent sayeth not.

TABLE OF CONTENTS

LIST OF TABLES

LIST OF FIGURES

LIST OF FIGURES (cont.)

LIST OF FIGURES (cont.)

5 NOTRUMP ANALYSIS OF THE AUTOMATIC DEPRESSURIZATION SYSTEM TESTS

5.1 Introduction

This section contains the comparisons of the NOTRUMP predictions to the automatic depressurization system (ADS) stages 1 to 3 (1-3) full-scale tests from the VAPORE facility. The objectives of the analysis are to confirm that the flow models in NOTRUMP are appropriate for modeling the AP600 ADS.

The phenomena identification and ranking table (PIRT) ranking for the ADS 1-3 phenomena is shown in Table 1.1-1. The ADS 1-3 are key components that should be accurately simulated in the AP600 small-break transient. The phenomena of interest include the choking or critical flow behavior of the valves and the sparger, the two-phase pressure drop through the ADS piping, the valve loss coefficient, and the subcritical flow behavior of the ADS once IRWST injection begins.

The ADS 1-3 is ranked high during the blowdown, natural circulation phase of the transient to address the inadvertent opening of an ADS valve. In this case, the valve becomes the break and the critical flow through the valve determines the blowdown of the system. For the majority of the other small-break LOCA transients, the ADS 1-3 is ranked high during the ADS blowdown phase, where the break in another location has depressurized and drained the RCS down to the ADS setpoint in the CMT. At this time, the ADS valves open and control the system depressurization. Once the ADS blowdown phase is complete, ADS 1-3 is less important, because the ADS stage 4 valves will have opened and the primary vent path out of the RCS is through the fourth-stage valves. ADS 1-3 still provides a secondary vent path, which is available for the long-term cooling of the reactor.

5.2 NOTRUMP Automatic Depressurization System Validation Approach

5.2.1 NOTRUMP Model of the Automatic Depressurization System Phase B Test Facility

The NOTRUMP ADS 1-3 model uses the facility dimensions given by the drawings in the ADS Phase B Test Facility Description Report (Reference 5-1). Figure 5.2-1 is the schematic of the test facility with the major instruments indicated.

The noding scheme used to represent the ADS Phase B test facility is shown in Figure 5.2-2. All main components are simulated with the code. The quench tank is not directly simulated, but its effect is modeled using the pressure boundary condition in boundary node 1.

The whole ADS valve package is modeled with a single flowlink. The effective loss coefficient of the ADS package is not needed unless it appears that the flow is not choked for the tests that are analyzed. The VLI-1 valve is simulated with a flowlink with the flow area ramped to open in 30 seconds. The loss coefficient for the fully open area is used, which is converted from the manufacturer-supplied C_v value.

In the tests, VLI-2 valve is partially open at a different area for each test to provide the pressure drop needed to increase the flow quality. The loss coefficient for the valve is obtained from water tests and is used when flow is not choked at the valve.

The four arms of the sparger are modeled as one node. The loss coefficient between the sparger arms and the surrounding water in the quench tank is taken from the measurement in the ADS Phase A test.

5.2.2 Method Used to Simulate the Automatic Depressurization System Phase B Tests

The measured supply tank water level, pressure, and temperature are input as the initial conditions for a given transient. Since VLI-1 valve is initially closed, the pipes upstream of VLI-1 valve are filled with saturation water under the same pressure as that in the supply tank. The pressure in the boundary node that simulates the quench tank is assumed to be the atmospheric pressure plus the water head above the sparger arms. All pipes and the ADS valve downstream of VLI-2 valve are initially filled with saturation steam at the same pressure as the steam pressure in the boundary node at the sparger. In the actual test, the lines downstream of valve VLI-2 are initially filled with air. However, NOTRUMP cannot model the air field, so the pipes and valves are assumed to be filled with saturated steam. Since the air is immediately blown out of the piping once the test begins, it has no impact on the flows and pressure drops predicted by NOTRUMP.

The VLI-2 valve is set at a specific flow area for each test. To simulate a test, the VLI-1 valve area is modeled as a ramp to simulate the opening of the valve. The high-pressure, high-temperature water discharges from the supply tank, through the VLI-1 valve, and flows through restrictive flow areas, such as the VLI-2 valve, the ADS valve, and the sparger, and discharges to the boundary node. The

boundary node is at a much lower pressure, and flashing and choked flow is calculated at various locations along the piping. The resulting calculated mixture flow rate due to choking and flow resistance and the calculated quality due to flashing are then used to assess the NOTRUMP code's capability to model the ADS phenomena.

The ADS 1-3 configurations have different combinations of valves and orifices that hydraulically model the additional ADS valves since the ADS has two valves in series. Both the valves and the orifices have abrupt entrance geometries, which result in a vena contra that reduces the effective flow area through the component. The reduced flow area, divided by the nominal flow area, is an effective discharge coefficient for the valve or orifice. The flow and pressure drop data from the single-phase steam and water tests were examined for the ADS 1-3 components to determine a discharge coefficient. In addition, data from valve manufacturers were also checked to confirm the effective discharge coefficient, which is calculated from the single-phase ADS tests. The analysis of the steam data from the ADS test series indicates that there should be a discharge coefficient of approximately 0.62 applied to the true flow area to compensate for the vena contra that occurs when the flow is choked in the valves or orifices. Similar results were found from the valve manufacturer's data for a discharge coefficient.

The value of approximately 0.62 agrees with the classical discharge coefficient normally used in single-phase orifice calculations and is the value recommended by Zaloudek (Reference 5-2) for subcooled flow through short orifices; this value is also approximately the value recommended by Henry (Reference 5-3) for critical flow through short orifices and pipes.

Therefore, when modeling the ADS valves and orifices in the ADS piping in NOTRUMP, a discharge coefficient of 0.62 is used to multiply the true flow area to obtain the effective flow area through the component. This is applied to all ADS components as well as the upstream control valve when that valve chokes and controls the flow through the ADS valve package.

Applying a discharge coefficient multiplier to the valve as orifice area is a difference between the preliminary validation report (Reference 5-4) where this multiplier is, in effect, unity, and the current analysis, which uses a multiplier. The preliminary validation report shows that NOTRUMP consistently overpredicts the test-measured flow through the ADS test facility. Use of the discharge coefficient for the valves and orifices results in more consistent predictions of the tests.

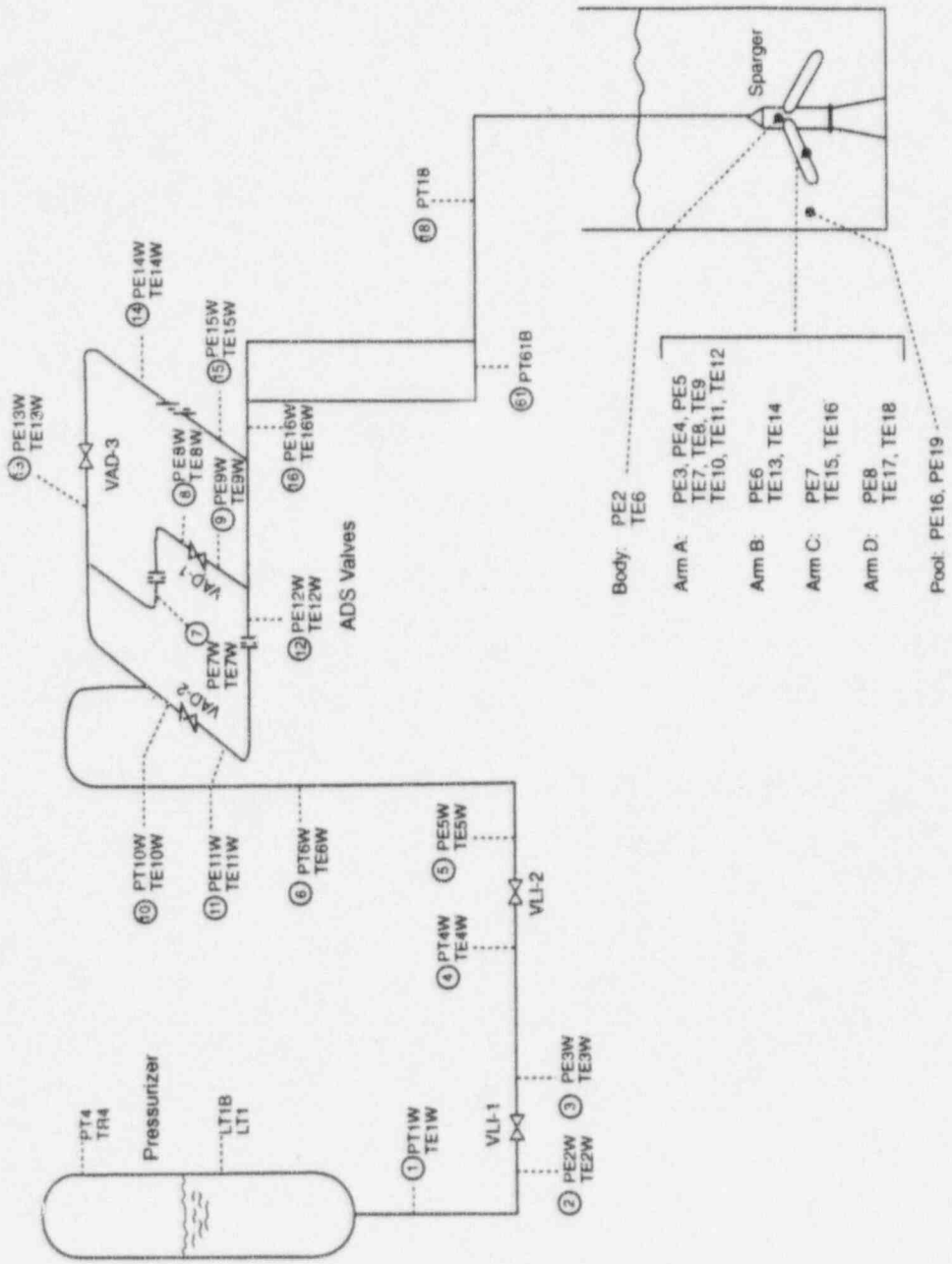

Figure 5.2-1 Schematic of the Automatic Depressurization System Phase B Test Facility

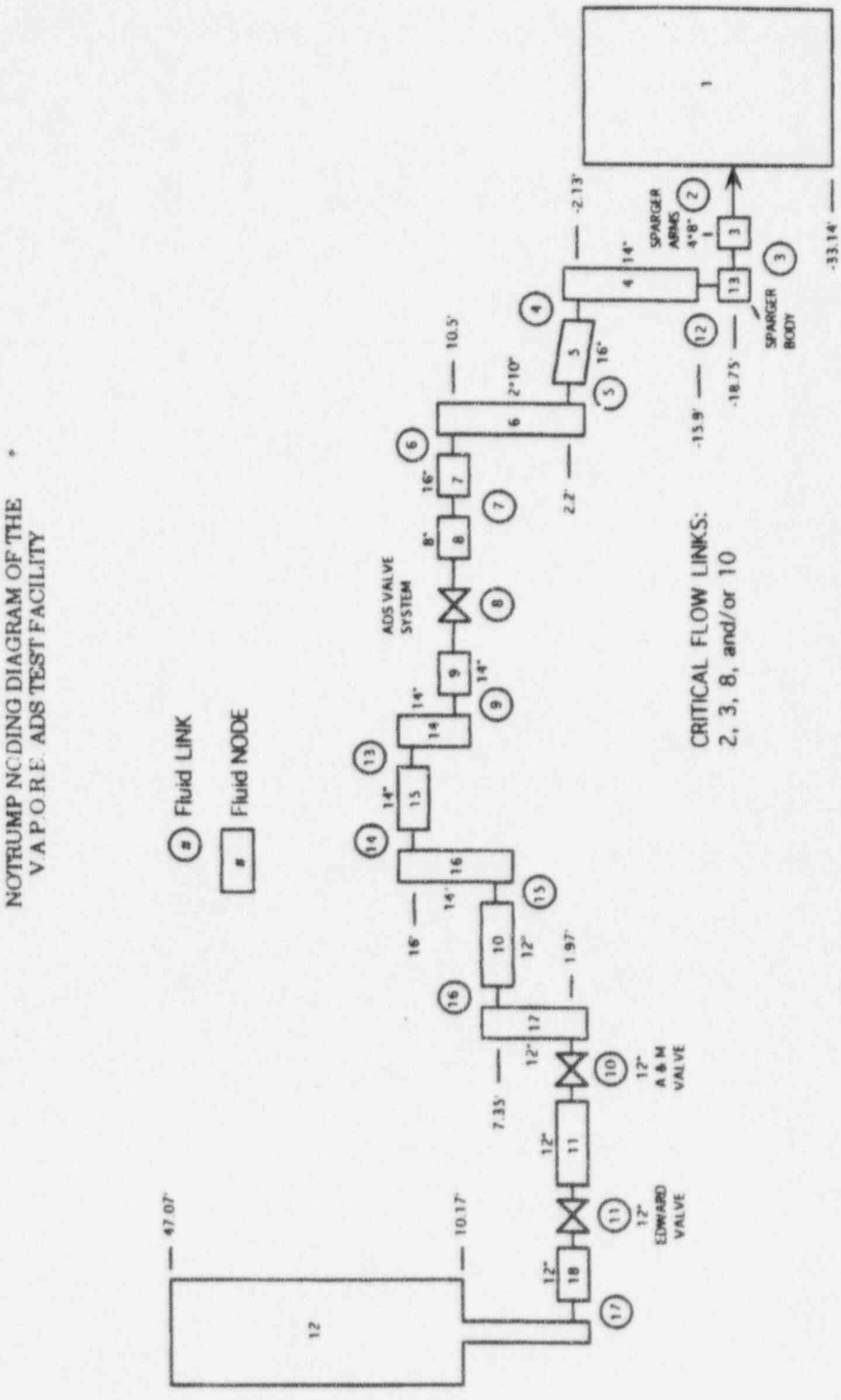

Figure 5.2-2 Automatic Depressurization System Phase B Test Facility Noding Diagram

5.3 NOTRUMP Analysis of the Automatic Depressurization System Test Data

5.3.1 Test Description

The ADS test matrix is shown in Table 5.3-1. There are three different test series. In the 100-series tests, the steam/water mixture is discharged from the top of the supply tank and flows through a moisture separator, where the water is separated. The steam then passes through the ADS valves and the sparger and quenches in the quench tank to give single-phase flow and pressure drop data for the ADS valve package. Data from the 100-series are used to initially benchmark the NOTRUMP code for the piping and valve resistances. For the 200- and 300-series tests, the flow is discharged from the bottom of the supply tank as a hot pressurized liquid.

The valve VLI-1 (see Figure 5.2-1) on the pipe connecting to the bottom of the supply tank is closed before the test is started. The supply tank is filled with water to about 60-percent capacity and is heated to the saturated conditions for the specified pressure. The valve VLI-2 is set to a specified opening area and stays open at that position once the test begins. The test is started by opening the valve VLI-1. The high-pressure saturated water in the supply tank flows from the bottom of the supply tank through valve VLI-1, valve VLI-2, the ADS valves, the sparger, and into the quench tank. The water flashes into the steam/water mixture as the pressure decreases and flows to the quench tank. The NOTRUMP calculations of pressure and flow have been compared to the test data. Special attention is given to the pressure drop across the valves and sparger. If the pressure drop is large, the critical flow (choke flow) is examined.

The tests that are analyzed are given in Table 5.3-2. The selected tests bound the conditions for the ADS to indicate the performance of the NOTRUMP code in predicting the phenomena associated with the ADS 1-3. The tests with the ADS stage 1 and 3 valves open are not included because they are similar to the tests with the ADS stage 1 and 2 valves open.

5.3.2 Possible Locations for Critical Flow

For the NOTRUMP critical flow model of the ADS valves, the Henry-Fauske correlation (Reference 5-3) for short tubes, nozzles, and orifices is used for low quality; and the homogenous equilibrium (Reference 5-5) model is used for high quality, with the transition between the two correlations beginning at a static quality of 10 percent. The transition behavior of the correlations is discussed in Section 2.2.

Figure 5.3-1 from test 212 is a typical pressure plot of the tests. It is a test with ADS stage 1 open, which indicates that critical flow occurs at the ADS stage 1 valve location because of large pressure drop. The locations of critical flow are determined by different methods in the ADS Test and Analysis Report (Reference 5-6). The pressure drop ratios across the valves and orifices were examined to observe if they are smaller than 0.53, which is a typical critical flow pressure drop ratio.

Also, the flow conditions, calculated from the data are used in the Henry-Fauske/homogeneous equilibrium critical flow calculations to compare the flow rate from the data to the value from the correlations. The potential choked flow for each test is given in the ADS Test and Analysis Report.

TABLE 5.3-1
AUTOMATIC DEPRESSURIZATION SYSTEM PHASE B1 TEST MATRIX

Facility Configuration	Matrix Test No.	ADS Simulation	Supply Tank Pressure	A&M Valve Flow Area
Saturated water blowdowns from bottom of supply tank, no orifices in spool pieces, cold quench tank water	310	Stages 1, 2, & 3 open	2235 psig	7 $in.^2$
"	311	Stages 1, 2, & 3 open	1200 psig	3.5 $in.^2$
"	312	Stages 1, 2, & 3 open	500 psig	14 $in.^2$
"	330	Stages 1 & 2 open	1800 psig	7 $in.^2$
"	331	Stages 1 & 2 open	1200 psig	21 $in.^2$
"	340	Stage 2 open (inadvertent opening)	2235 psig	35 $in.^2$
Saturated water blowdowns from bottom of supply tank, orifices installed in spool pieces	250	Stage 2 open (inadvertent opening)	1200 psig	7 $in.^2$
"	210	Stage 1 open	2235 psig	1.4 $in.^2$
"	211	Stage 1 open	2235 psig	2.1 $in.^2$
"	212	Stage 1 open	2235 psig	3.5 $in.^2$
"	220	Stages 1 & 2 open	1200 psig	3.5 $in.^2$
"	221	Stages 1 & 2 open	2235 psig	3.5 $in.^2$
"	230	Stages 1 & 3 open	1200 psig	3.5 $in.^2$
"	231	Stages 1 & 3 open	2235 psig	3.5 $in.^2$
"	240	Stages 1, 2, & 3 open	1200 psig	3.5 $in.^2$

TABLE 5.3-1 (Cont.)
AUTOMATIC DEPRESSURIZATION SYSTEM PHASE B1 TEST MATRIX

Facility Configuration	Matrix Test No.	ADS Simulation	Supply Tank Pressure	A&M Valve Flow Area
Saturated water blowdowns from bottom of supply tank, orifices installed in spool pieces	241	Stages 1, 2, & 3 open	500 psig	3.5 $in.^2$
"	242	Stages 1, 2, & 3 open	500 psig	7 $in.^2$
Saturated steam blowdowns from top of supply tank, orifices installed in spool pieces	110	Stage 1 open	2500 psig	N/A
"	120	Stages 1 & 2 open	1600 psig	N/A
"	130	Stages 1 & 3 open	1200 psig	N/A
"	140	Stages 1, 2, & 3 open	1600 psig	N/A
Saturated water blowdowns from bottom of supply tank, no orifices in spool pieces, quench tank water at 212°F (100°C)	320	Stages 1, 2, & 3 open	2235 psig	7 $in.^2$
"	321	Stages 1, 2, & 3 open	1200 psig	8.4 $in.^2$
"	322	Stages 1, 2, & 3 open	500 psig	14 $in.^2$
"	350	Stages 1 & 2 open	1800 psig	14 $in.^2$
"	351	Stages 1 & 2 open	1200 psig	21 $in.^2$

TABLE 5.3-2
AUTOMATIC DEPRESSURIZATION SYSTEM 1-3 TESTS ANALYZED WITH NOTRUMP, CONFIGURATIONS

Facility Configuration	Matrix Test No.	ADS Simulation	Supply Tank Pressure	A&M Valve Flow Area
Saturated water blowdowns from bottom of supply tank, orifices installed in spool pieces	210	Stage 1 open	2235 psig	1.4 $in.^2$
"	212	Stage 1 open	2235 psig	3.5 $in.^2$
"	220	Stages 1 & 2 open	1200 psig	3.5 $in.^2$
"	240	Stages 1, 2, & 3 open	1200 psig	3.5 $in.^2$
"	242	Stages 1, 2, & 3 open	500 psig	3.5 $in.^2$
"	250	Stage 2 open (inadvertent opening)	1200 psig	7 $in.^2$
Saturated water blowdowns from bottom of supply tank, no orifices in spool pieces, quench tank water at 212°F	320	Stages 1, 2, & 3 open	2235 psig	7 $in.^2$
Same as above but cold tank temperature	340	Stage 2 open (inadvertent opening)	2235 psig	35 $in.^2$

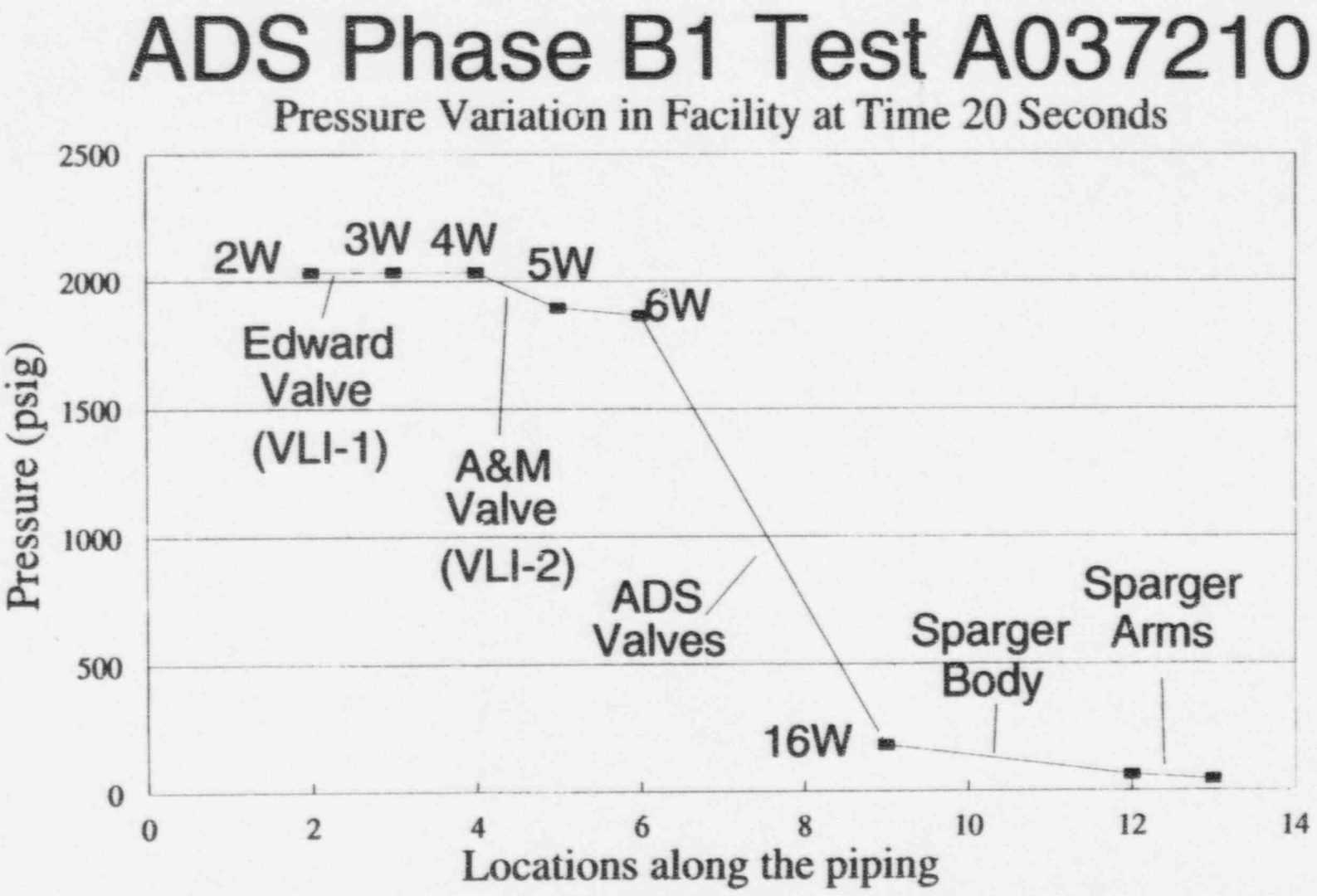

Figure 5.3-1 Test A037210 Pressure Variation in Facility at Time 20 Seconds

5.4 Comparison of NOTRUMP to the 200-Series Automatic Depressurization System Tests

In the NOTRUMP simulation of these tests, the sum of the area of the valves and orifices of the open stages is used as a single area for the ADS valve package, accounting for the discharge coefficient of 0.62. In the subsequent figures, NOTRUMP is compared to the ADS flow and pressure drop test data. The comparisons are made after the initial surge of flow through the system, once the flow and pressure drops have stabilized. This is usually 10 to 15 seconds into the test after the flow has been initiated.

5.4.1 Test 210

Figures 5.4-1 to 5.4-5 compare NOTRUMP predictions to the test data for test 210, which has a single stage 1 valve opened. Figure 5.4-1 shows that NOTRUMP correctly predicts the ADS flow rate, except for the hump early in the test, which is due to the filling of the loop downstream of the control valve. The ADS flow is calculated from the level measurement in the supply tank, whereas the NOTRUMP flow valves in the figure are given at the ADS valves. There are delay times both in the valve VL1-1 opening time, as seen in the supply tank pressure transient in Figure 5.4-2, as well as the transient time of the flow from the tank to the ADS valves. The level traces from the supply tank, given in Appendix C of the ADS data report (Reference 5-7), indicate a rapid decrease in the level for approximately 5 sec. as the flow is established in the facility piping between valve VL1-1 and the ADS valves. The time required to fill the piping compounds to the volumes between valve VL1-1 and the ADS valves divided by the initial volumetric flow from the supply tank. Once the flow reaches the ADS valves, it becomes checked and the flow is then limited through the valves.

The calculated NOTRUMP flow lies within the uncertainty of the flow data once the flow rate from the supply tank stabilizes. The comparison is excellent and indicates that NOTRUMP is predicting the correct flow for the given upstream condition. Figure 5.4-2 shows that NOTRUMP predicts a slower rate of pressure drop in the supply tank, which lies just outside the data uncertainty. Figure 5.4-3 shows that NOTRUMP overpredicts the VLI-2 valve pressure drop by 57 percent. The pressure drop across VLI-2 is much less than the pressure drop across the ADS valve, and critical flow does not occur at this point. Figure 5.4-4 shows that NOTRUMP overpredicts the ADS valve differential pressure by approximately 4.5 percent. The NOTRUMP-calculated pressure is within the data uncertainty for the conditions upstream of the ADS package and below the data uncertainty downstream of the valve package. The calculations do follow the data trend. The high differential pressure across the ADS valves indicates critical flow at this location. Figure 5.4-5 shows that NOTRUMP predicts a larger pressure drop across the sparger arms. NOTRUMP predicts the overall system pressure drop within a few psi, as shown by the plot of sparger arm pressure in Figure 5.4-5.

5.4.2 Test 212

Figures 5.4-6 to 5.4-10 compare NOTRUMP predictions to the test data for test 212, which has a stage 1 valve opened but a larger area for valve VLI-2. Figure 5.4-6 shows that NOTRUMP correctly

predicts the ADS flow rate within the uncertainty of the data. Figure 5.4-7 shows that NOTRUMP predicts a slightly higher pressurizer pressure, but the rate of decrease is identical. Figure 5.4-8 shows that NOTRUMP overpredicts the VLI-2 valve pressure drop by 36 percent and lies within the data uncertainty for the downstream pressure, but exceeds data uncertainty for the pressure for the upstream. The pressure drop across VLI-2 is much less than the pressure drop across the ADS valve, and critical flow does not occur at this point. Figure 5.4-9 shows that NOTRUMP underpredicts the ADS valve differential pressure by approximately 2 percent. The high differential pressure across the ADS valves indicates critical flow at this location. The calculation of the pressures is slightly outside the uncertainty bands on the data but follows the data trend. Figure 5.4-10 shows that NOTRUMP predicts a larger pressure drop across the sparger arms. NOTRUMP predicts the overall system pressure drop within a few psi, as shown by the plot of sparger arm pressure in Figure 5.4-10.

5.4.3 Test 220

Figures 5.4-11 to 5.4-15 compare NOTRUMP predictions to the test data for test 220. Figure 5.4-11 shows that NOTRUMP slightly underpredicts the ADS flow rate and lies outside the data uncertainty. Figure 5.4-12 shows that NOTRUMP predicts a slightly higher pressurizer pressure, but the rate of decrease is identical and is within the data uncertainty. Figure 5.4-13 shows that NOTRUMP underpredicts the VLI-2 valve pressure drop by 18 percent with the individual pressure values outside the data uncertainty but following the data trends. The pressure drop across VLI-2 is about the same as the pressure drop across the ADS valve so that critical flow should be occurring at these points. Figure 5.4-14 shows that NOTRUMP overpredicts the ADS valve differential pressure by approximately 69 percent and is outside the range of data uncertainty but is following the data trends. Figure 5.4-15 shows that NOTRUMP closely predicts the pressure drop across the sparger arms. NOTRUMP predicts the overall system pressure drop within a few psi, as shown by the plot of sparger arm pressure in Figure 5.4-15.

5.4.4 Test 240

Figures 5.4-16 to 5.4-20 compare NOTRUMP predictions to the test data for test 240. Figures 5.4-16 shows that NOTRUMP correctly predicts the ADS flow rate and is within the data uncertainty. Figure 5.4-17 shows that NOTRUMP predicts a slightly higher pressurizer pressure, but the rate of decrease is identical and is within the data uncertainty. Figure 5.4-18 shows that NOTRUMP predicts the VLI-2 valve pressure drop within 5 percent. The pressure drop across VLI-2 is larger than the pressure drop across the ADS valve, and critical flow occurs at VLI-2. Figure 5.4-19 shows that NOTRUMP overpredicts the ADS valve differential pressure by approximately 120 percent and lies outside the data uncertainty. The pressure drop across the ADS valves is low, and critical flow does not occur at this point. Figure 5.4-20 shows that NOTRUMP closely predicts the pressure drop across the sparger arms. NOTRUMP predicts the overall system pressure drop within a few psi, as shown by the plot of sparger arm pressure in Figure 5.4-20.

5.4.5 Test 242

Figures 5.4-21 to 5.4-25 compare NOTRUMP predictions to the test data for test 242. Figure 5.4-21 shows that NOTRUMP slightly overpredicts the ADS flow rate but is within the data uncertainty. Figure 5.4-22 shows that NOTRUMP predicts a slightly higher pressurizer pressure, but the rate of decrease is identical and is within the data uncertainty. Figure 5.4-23 shows that NOTRUMP predicts the VLI-2 valve pressure drop within 10 percent. The test data indicate that pressure drop across VLI-2 is larger than the pressure drop across the ADS valve, and critical flow occurs at VLI-2. Figure 5.4-24 shows that NOTRUMP overpredicts the ADS valve differential pressure by approximately 150 percent and is outside the data uncertainty. The pressure drop across the ADS valves is low, and critical flow does not occur at this point. Figure 5.4-25 shows that NOTRUMP closely predicts the pressure drop across the sparger arms. NOTRUMP overpredicts the overall system pressure drop, as shown by the plot of sparger arm pressure in Figure 5.4-25.

5.4.6 Test 250

Figures 5.4-26 to 5.4-30 compare NOTRUMP predictions to the test data for test 250. Figure 5.4-26 shows that NOTRUMP correctly predicts the ADS flow rate and is within the data uncertainty. Figure 5.4-27 shows that NOTRUMP accurately predicts the pressurizer pressure with the data uncertainty. Figure 5.4-28 shows that NOTRUMP underpredicts the VLI-2 valve pressure drop by 32 percent and the calculation lies outside the data uncertainty. The pressure drop across VLI-2 is smaller than the pressure drop across the ADS valve, and critical flow does not occur at VLI-2. Figure 5.4-29 shows that NOTRUMP overpredicts the ADS valve differential pressure by approximately 38 percent and the calculation lies outside the data uncertainty. The pressure drop across the ADS valves is high, and critical flow occurs at this point. Figure 5.4-30 shows that NOTRUMP closely predicts the pressure drop across the sparger arms. NOTRUMP predicts the overall system pressure drop within a few psi, as shown by the plot of sparger arm pressure in Figure 5.4-30.

5.4.7 Test 320

Figures 5.4-31 to 5.4-35 compare NOTRUMP predictions to the test data for test 320. Figure 5.4-31 shows that NOTRUMP correctly predicts the ADS flow rate within the data uncertainty. Figure 5.4-32 shows that NOTRUMP accurately predicts the pressurizer pressure within the data uncertainty. Figure 5.4-33 shows that NOTRUMP predicts the VLI-2 valve pressure drop within 12 percent but the predictions are outside the data uncertainty. The pressure drop across VLI-2 is much larger than the pressure drop across the ADS valve, and critical flow occurs at VLI-2. Figure 5.4-34 shows that NOTRUMP overpredicts the ADS valve differential pressure by approximately 63 percent. Figure 5.4-35 shows that NOTRUMP closely predicts the pressure drop across the sparger arms. NOTRUMP predicts the overall system pressure drop within a few psi, as shown by the plot of sparger arm pressure in Figure 5.4-35.

5.4.8 Test 340

Figures 5.4-36 to 5.4-40 compare NOTRUMP predictions to the test data for test 340. Figure 5.4-36 shows that NOTRUMP correctly predicts the ADS flow rate usually within the data uncertainty. Figure 5.4-37 shows that NOTRUMP accurately predicts the pressurizer pressure within the data uncertainty. Figure 5.4-38 shows that NOTRUMP overpredicts the VLI-2 valve pressure drop by 34 percent. The pressure drop across VLI-2 is smaller than the pressure drop across the ADS valve, and critical flow does not occur at VLI-2. Figure 5.4-39 shows that NOTRUMP overpredicts the ADS valve differential pressure by approximately 57 percent and is outside the data uncertainty. The pressure drop across the ADS valves is high, and critical flow occurs at this point. Figure 5.4-40 shows that NOTRUMP closely predicts the pressure drop across the sparger arms. NOTRUMP underpredicts the overall system pressure drop by about 30 psi, as shown by the plot of sparger arm pressure in Figure 5.4-40.

a,b

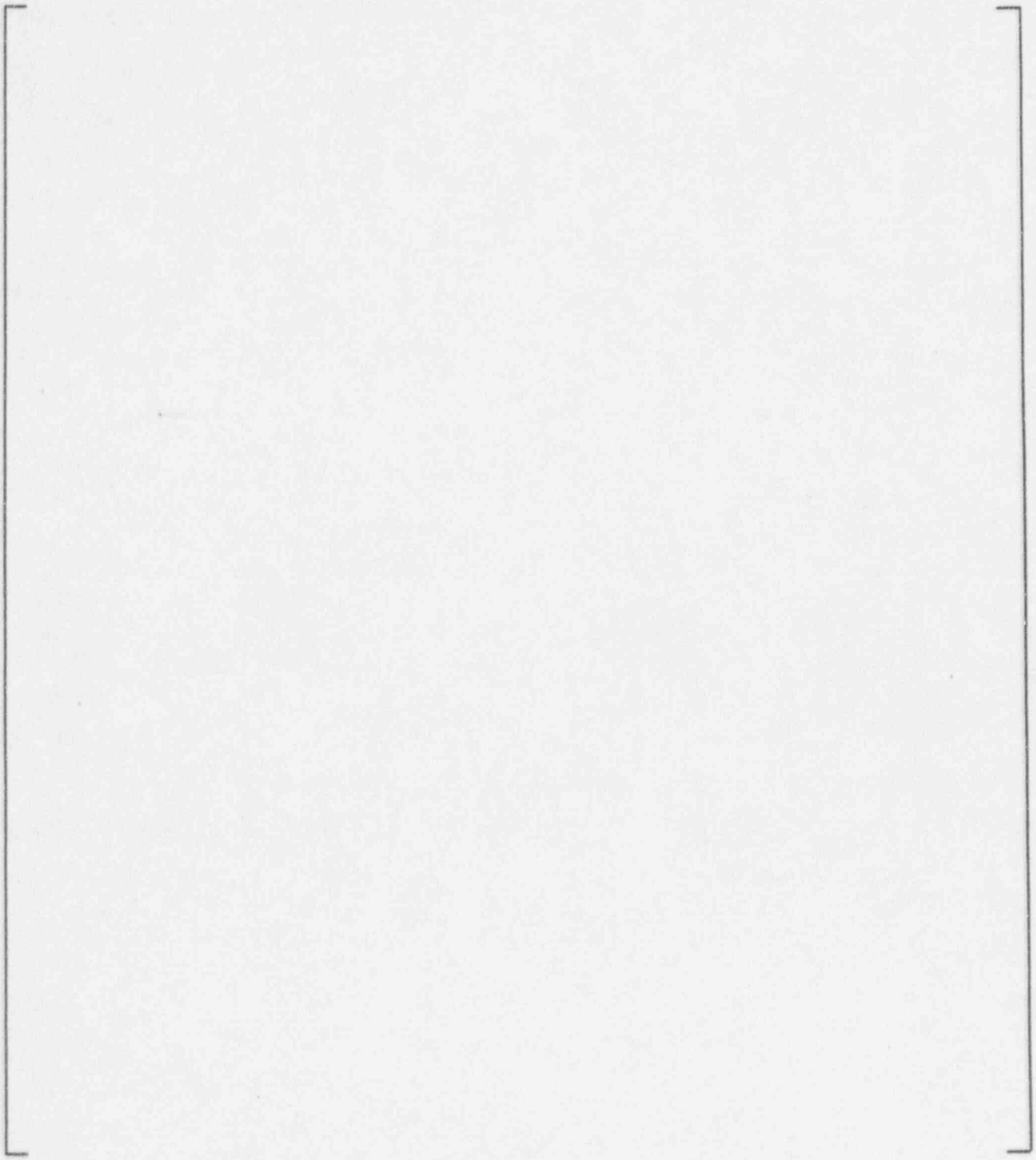

Figure 5.4-1 NOTRUMP Comparison to the Automatic Depressurization System Flow Rate for Test 210

a,b

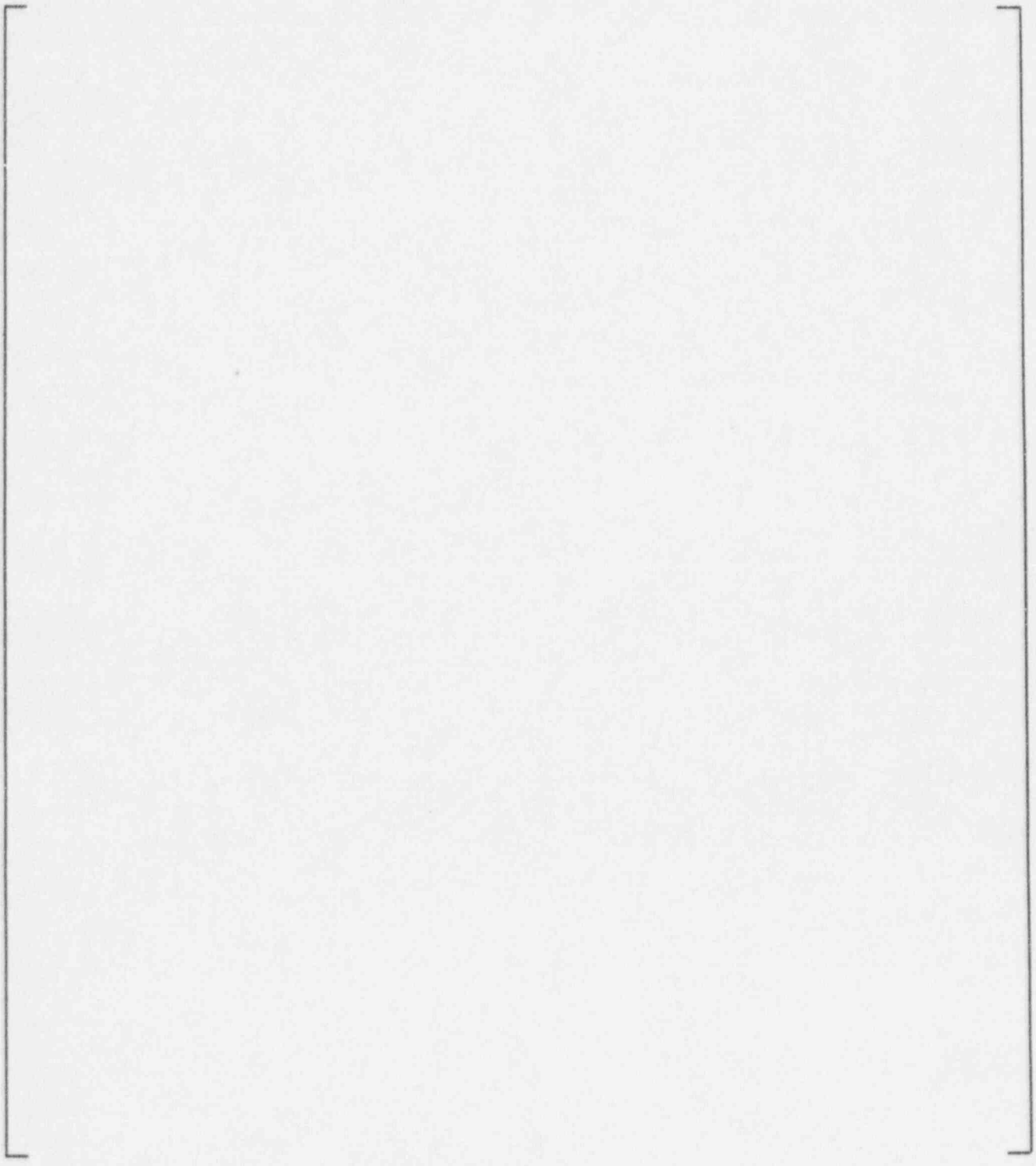

Figure 5.4-2 NOTRUMP Comparison to the Automatic Depressurization System Supply Tank (Pressurizer) Pressure for Test 210

a,b

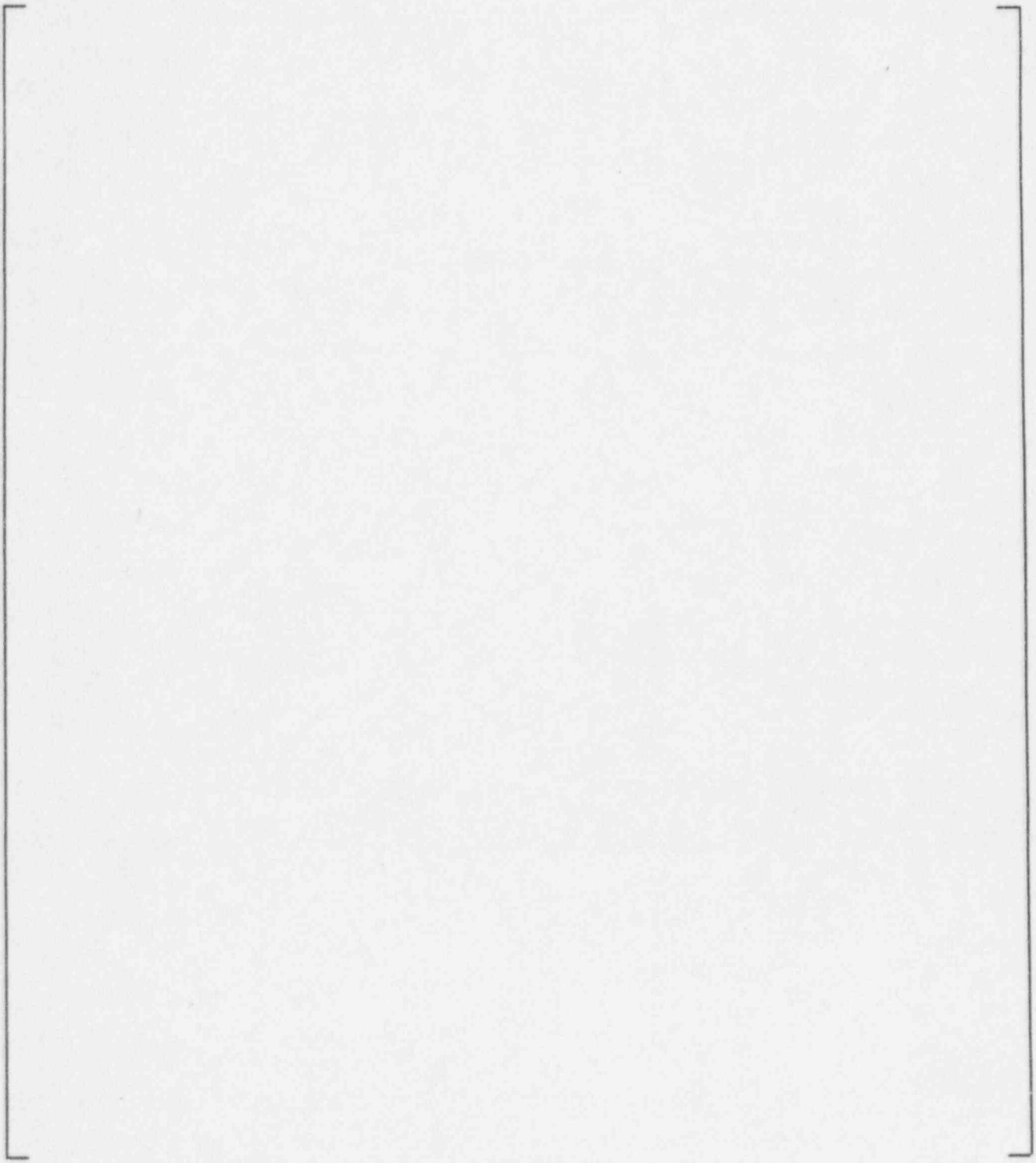

Figure 5.4-3 NOTRUMP Comparison to the Upstream and Downstream Pressures across Valve VLI-2 (A&M) for Test 210

a,b

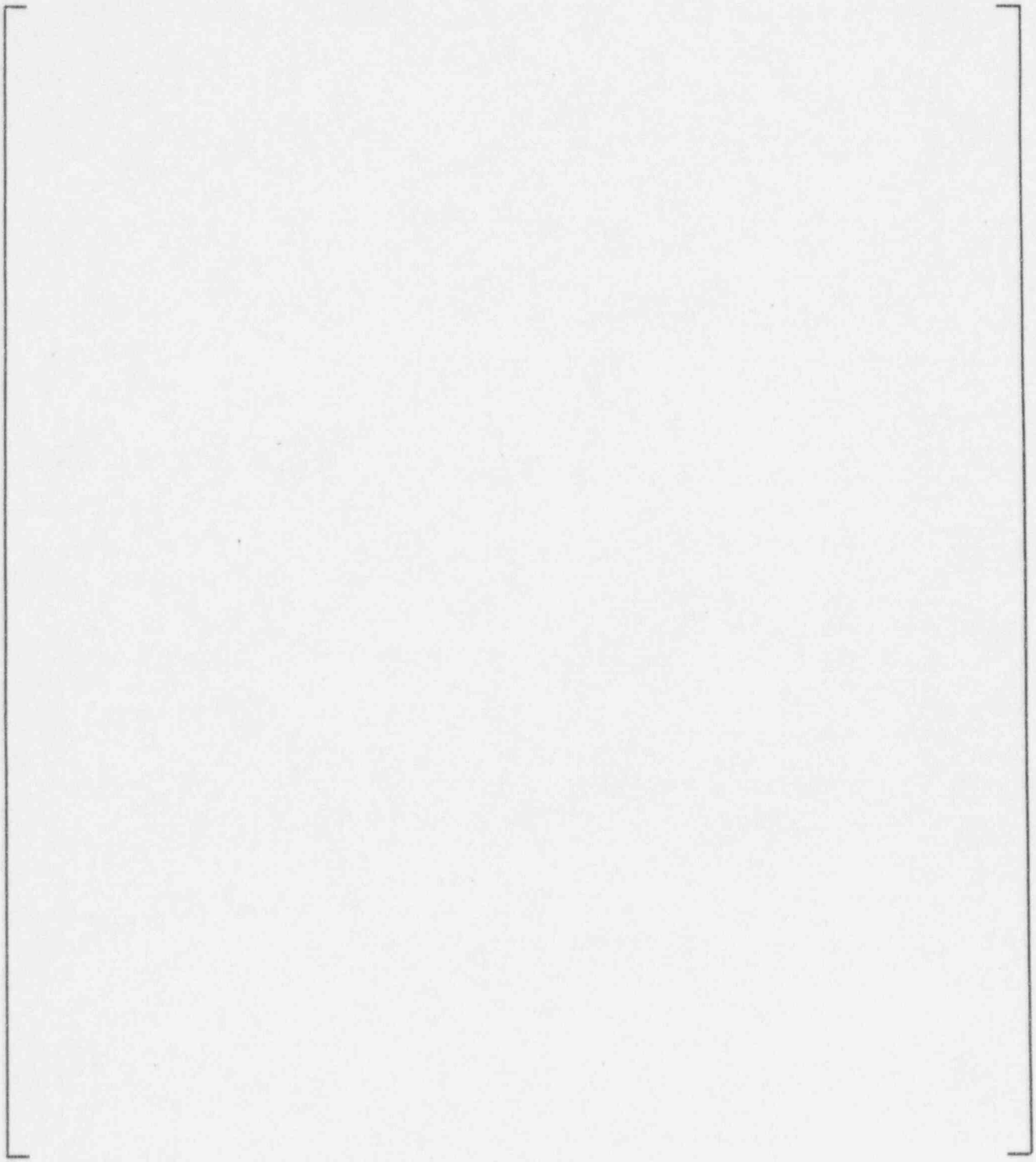

Figure 5.4-4 NOTRUMP Comparison to the Upstream and Downstream Pressures across the Automatic Depressurization System Valve Package for Test 210

a,b

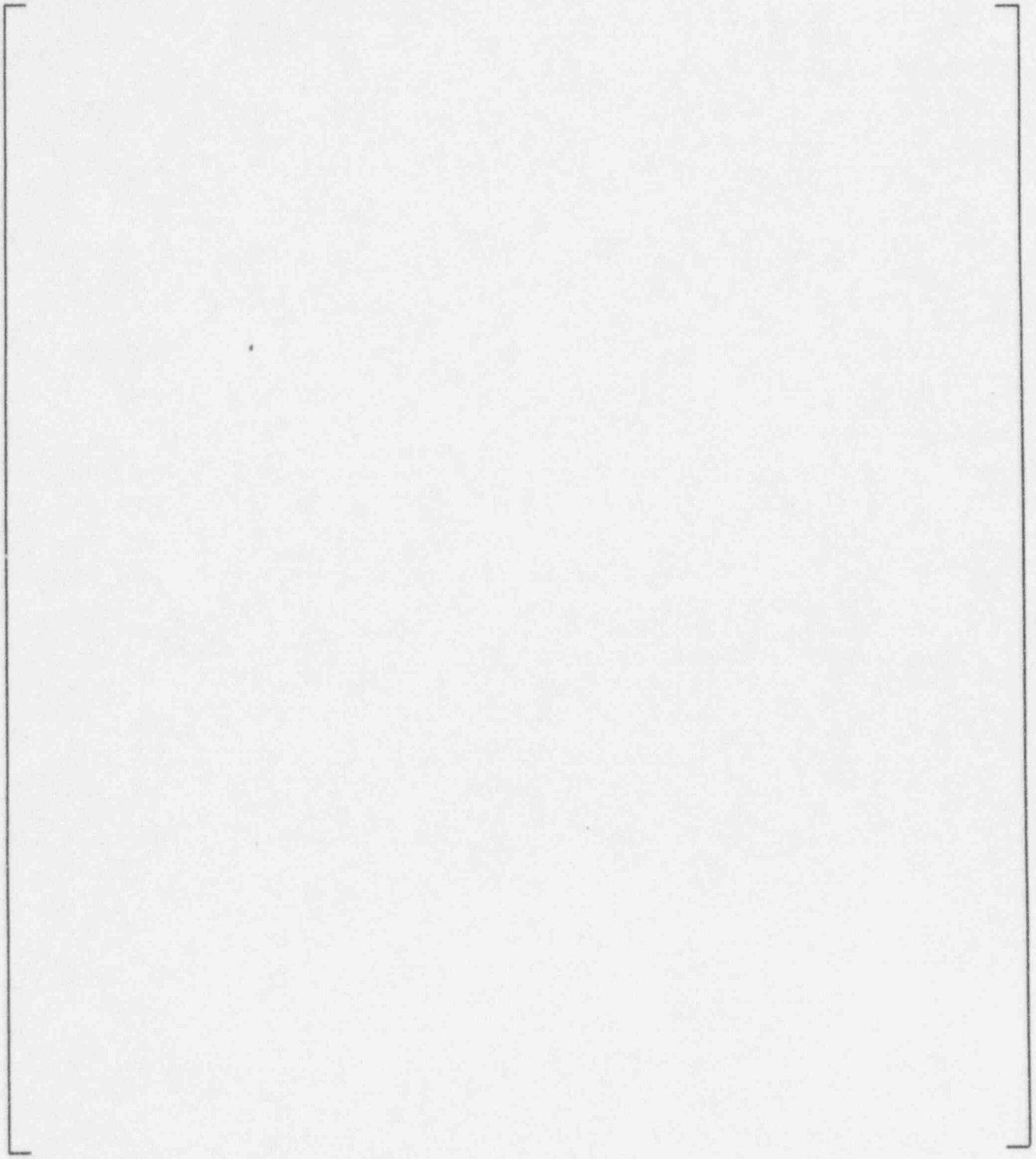

Figure 5.4-5 NOTRUMP Comparison to the Sparger Body and Sparger Arms Pressures for Test 210

a,b

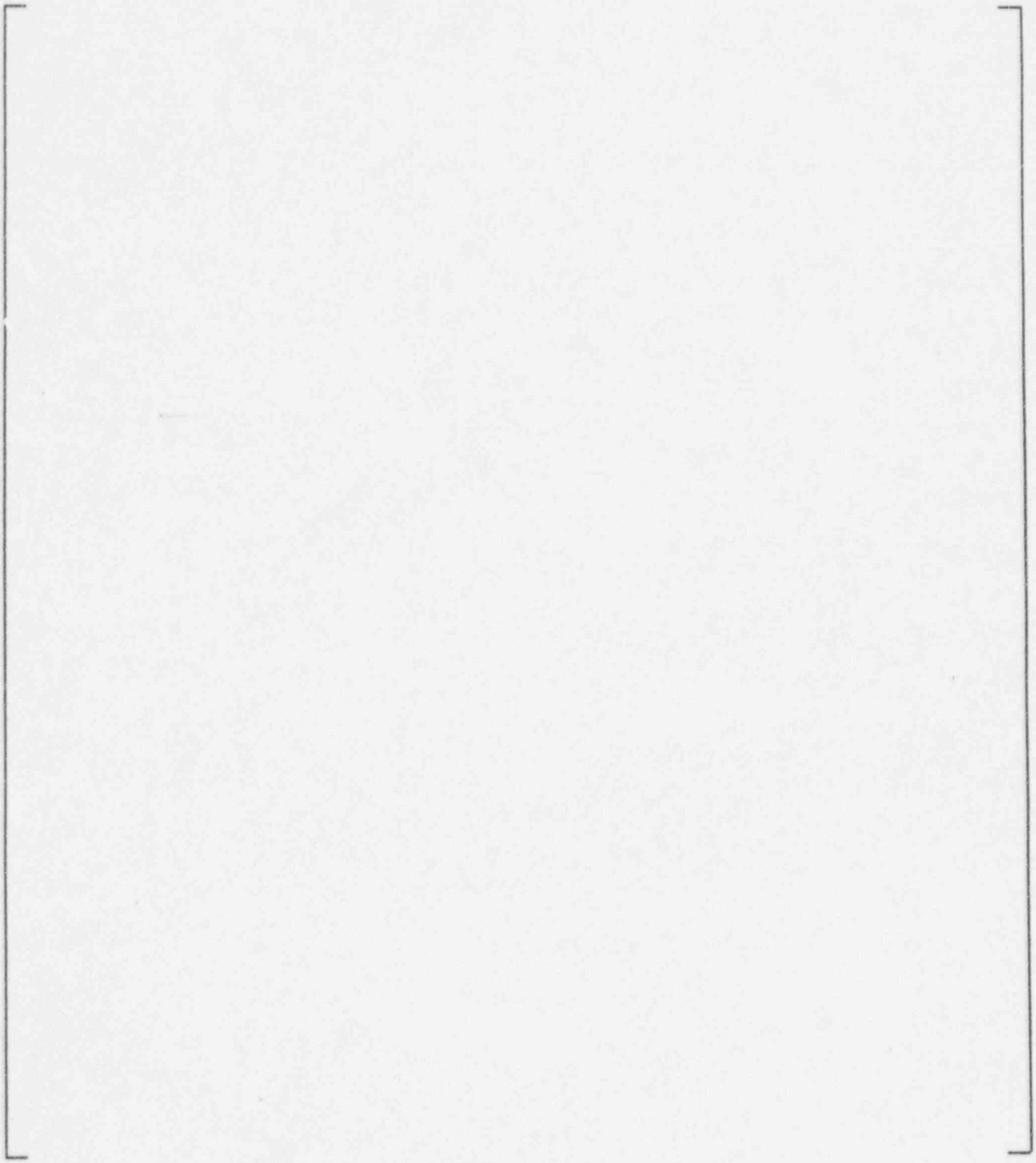

Figure 5.4-6 NOTRUMP Comparison to the Automatic Depressurization System Flow Rate for Test 212

a,b

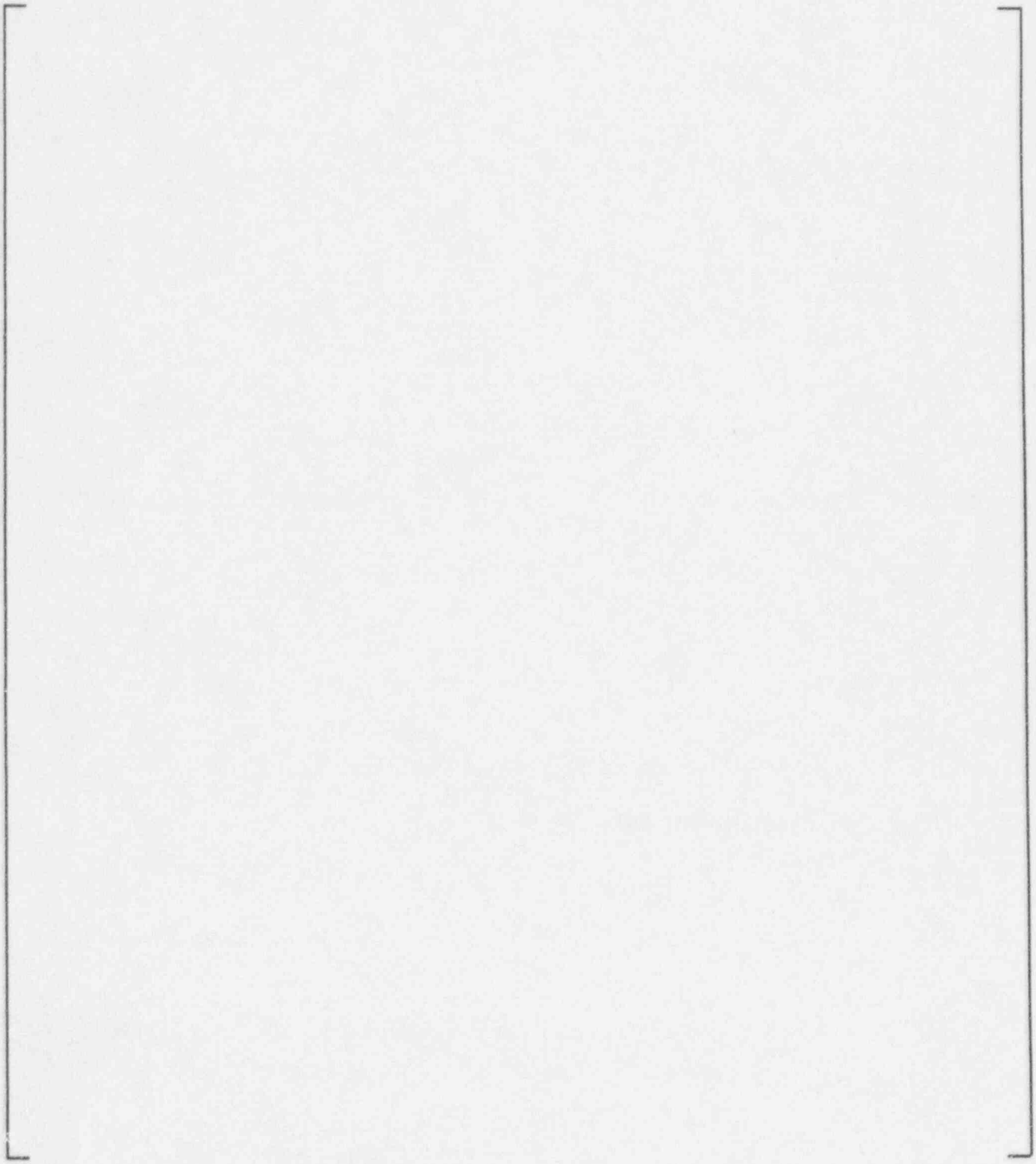

Figure 5.4-7 NOTRUMP Comparison to the Automatic Depressurization System Supply Tank (Pressurizer) Pressure for Test 212

a,b

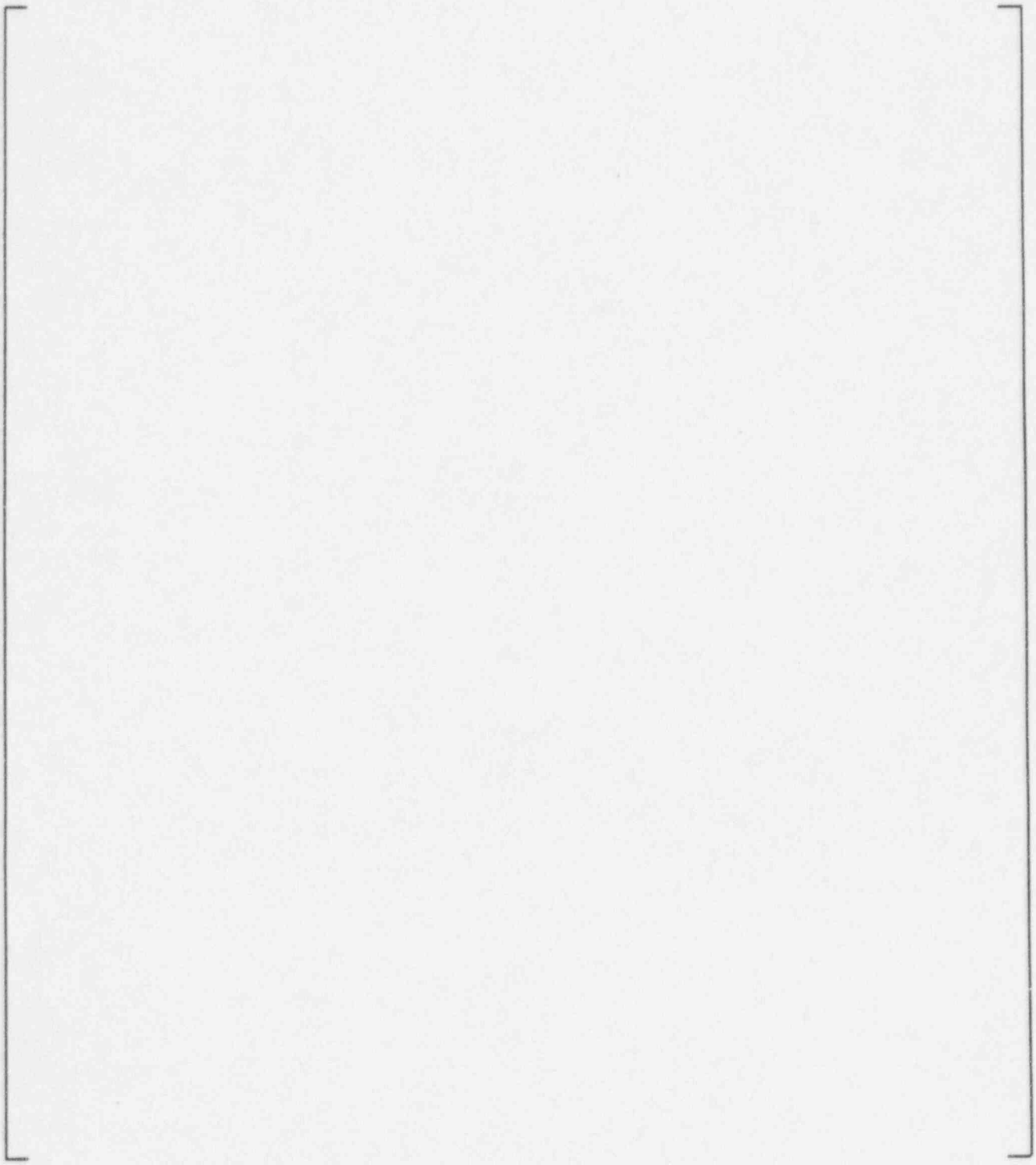

Figure 5.4-8 NOTRUMP Comparison to the Upstream and Downstream Pressures across Valve VLI-2 (A&M) for Test 212

a,b

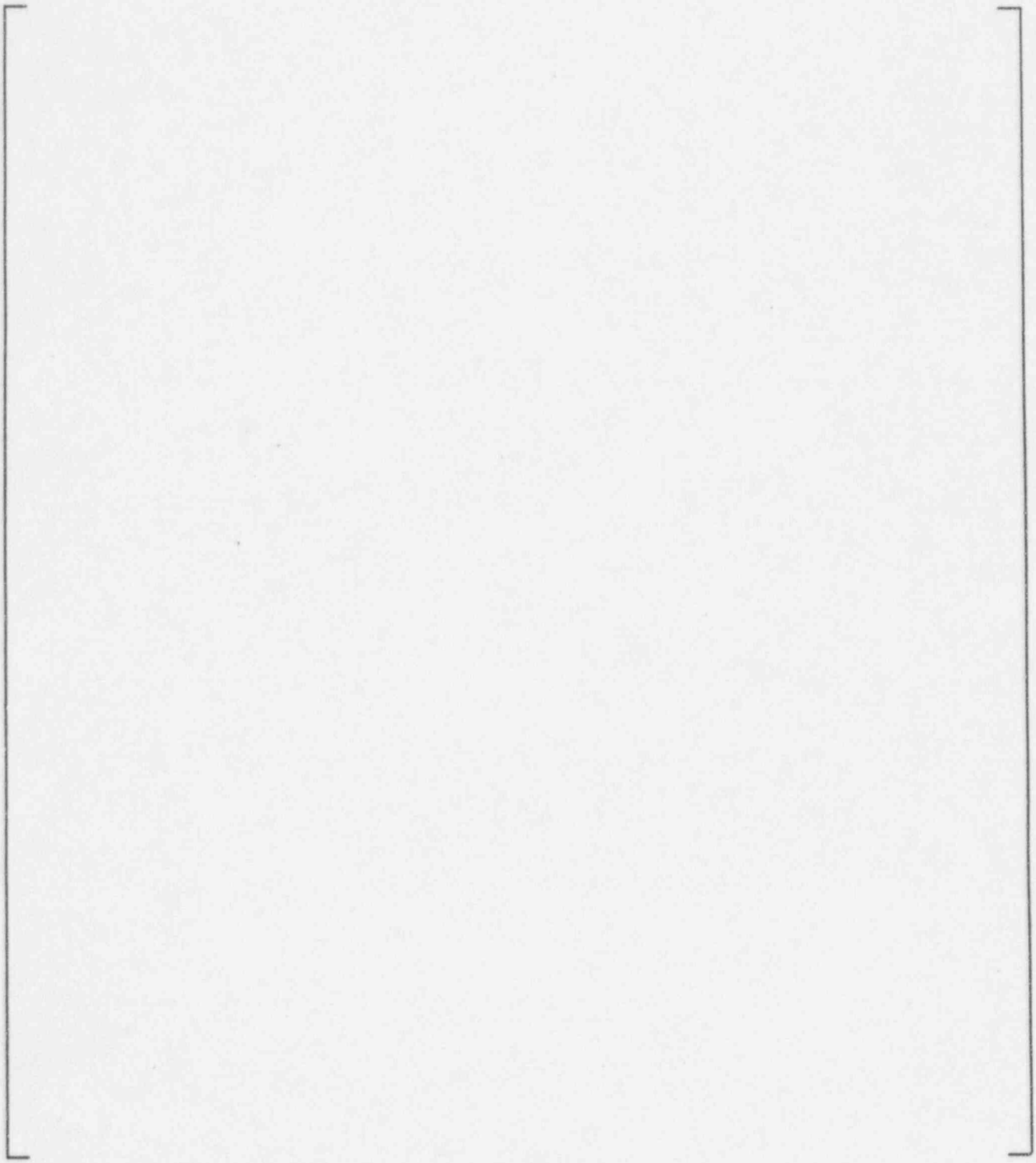

Figure 5.4-9 NOTRUMP Comparison to the Upstream and Downstream Pressures across the Automatic Depressurization System Valve Package for Test 212

a,b

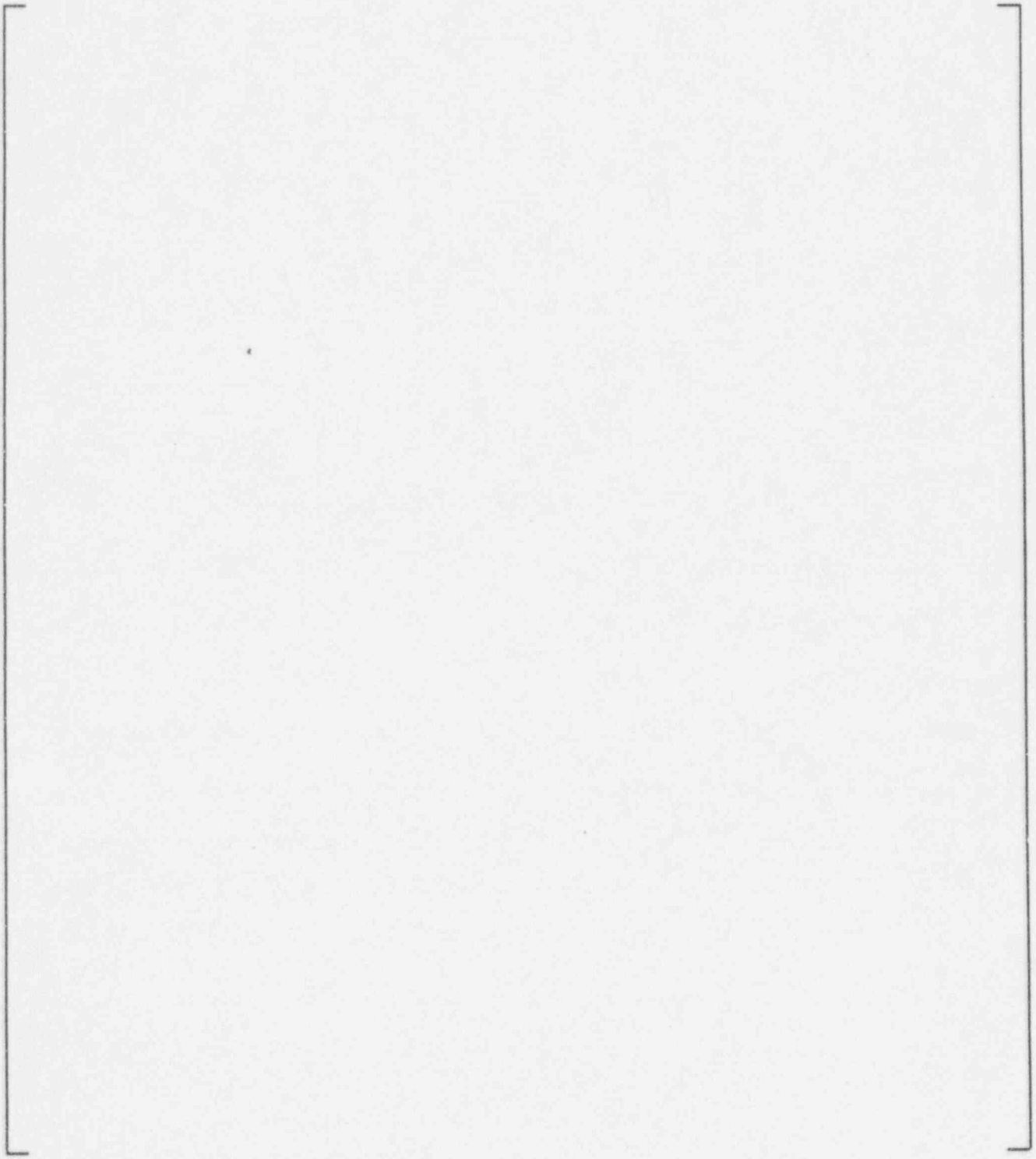

Figure 5.4-10 NOTRUMP Comparison to the Sparger Body and Sparger Arms Pressures for Test 212

a,b

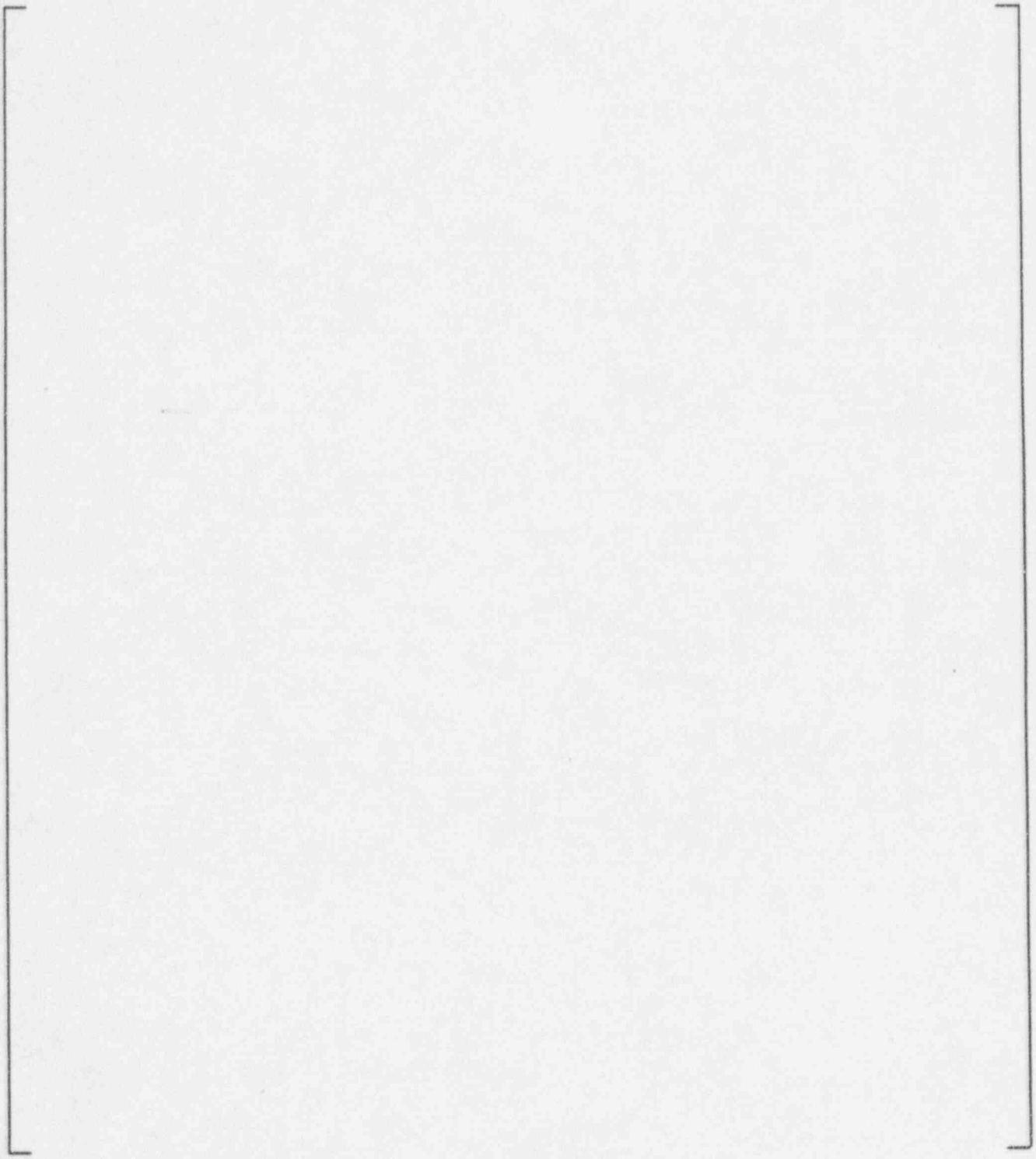

Figure 5.4-11 NOTRUMP Comparison to the Automatic Depressurization System Flow Rate for Test 220

a,b

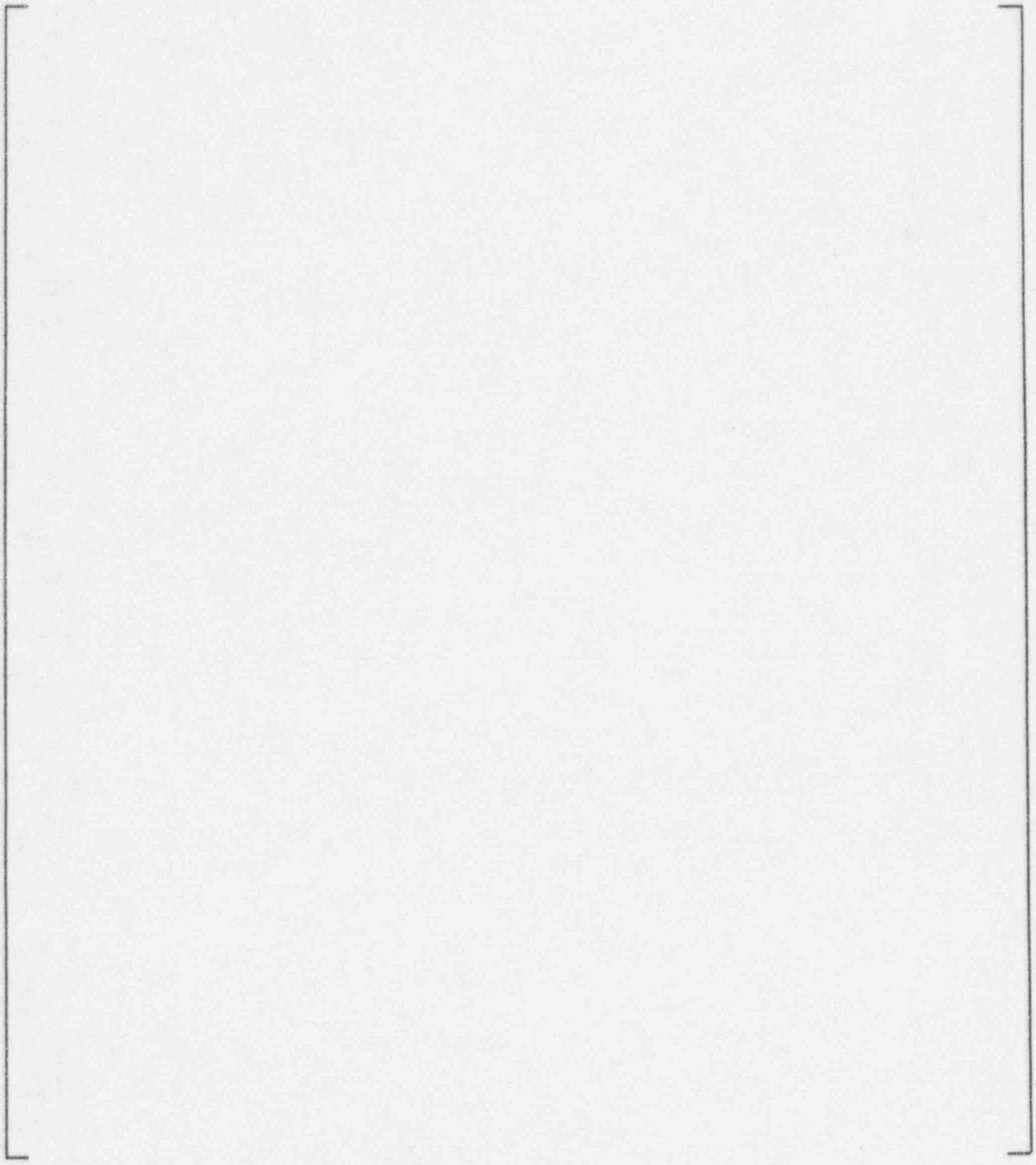

Figure 5.4-12 NOTRUMP Comparison to the Automatic Depressurization System Supply Tank (Pressurizer) Pressure for Test 220

a,b

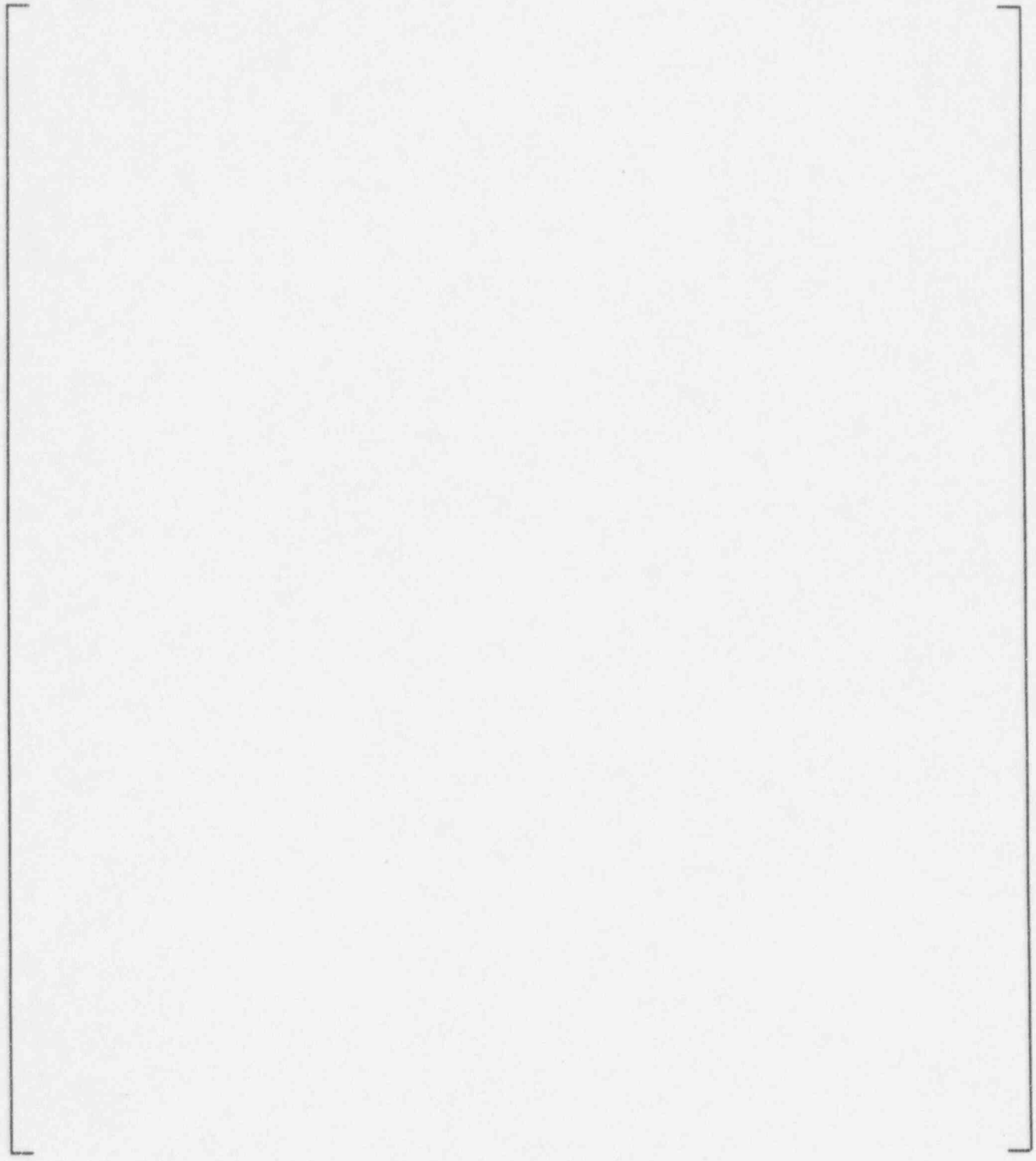

Figure 5.4-13 NOTRUMP Comparison to the Upstream and Downstream Pressures across Valve VLI-2 (A&M) for Test 220

a,b

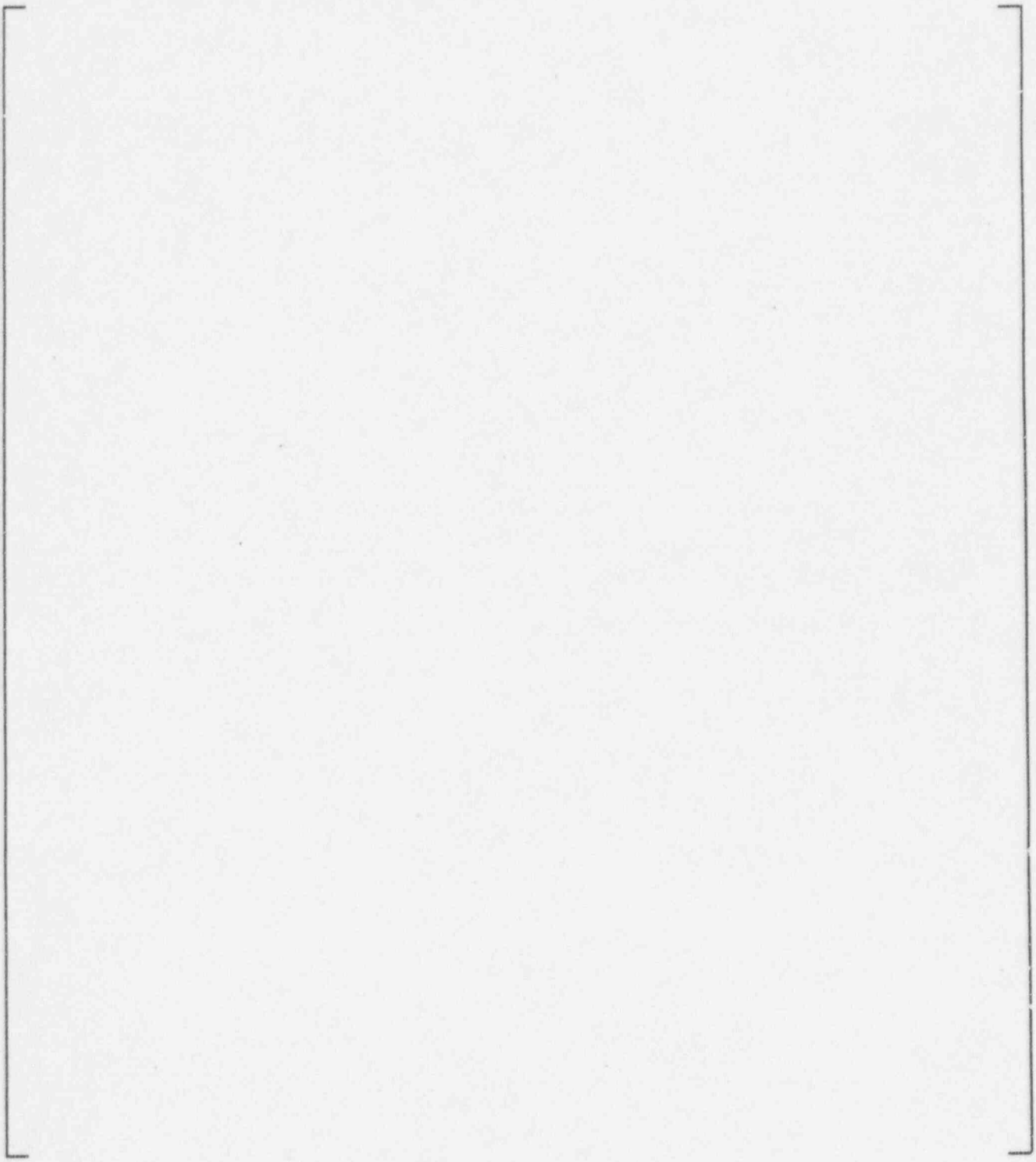

Figure 5.4-14 NOTRUMP Comparison to the Upstream and Downstream Pressures across the Automatic Depressurization System Valve Package for Test 220

a,b

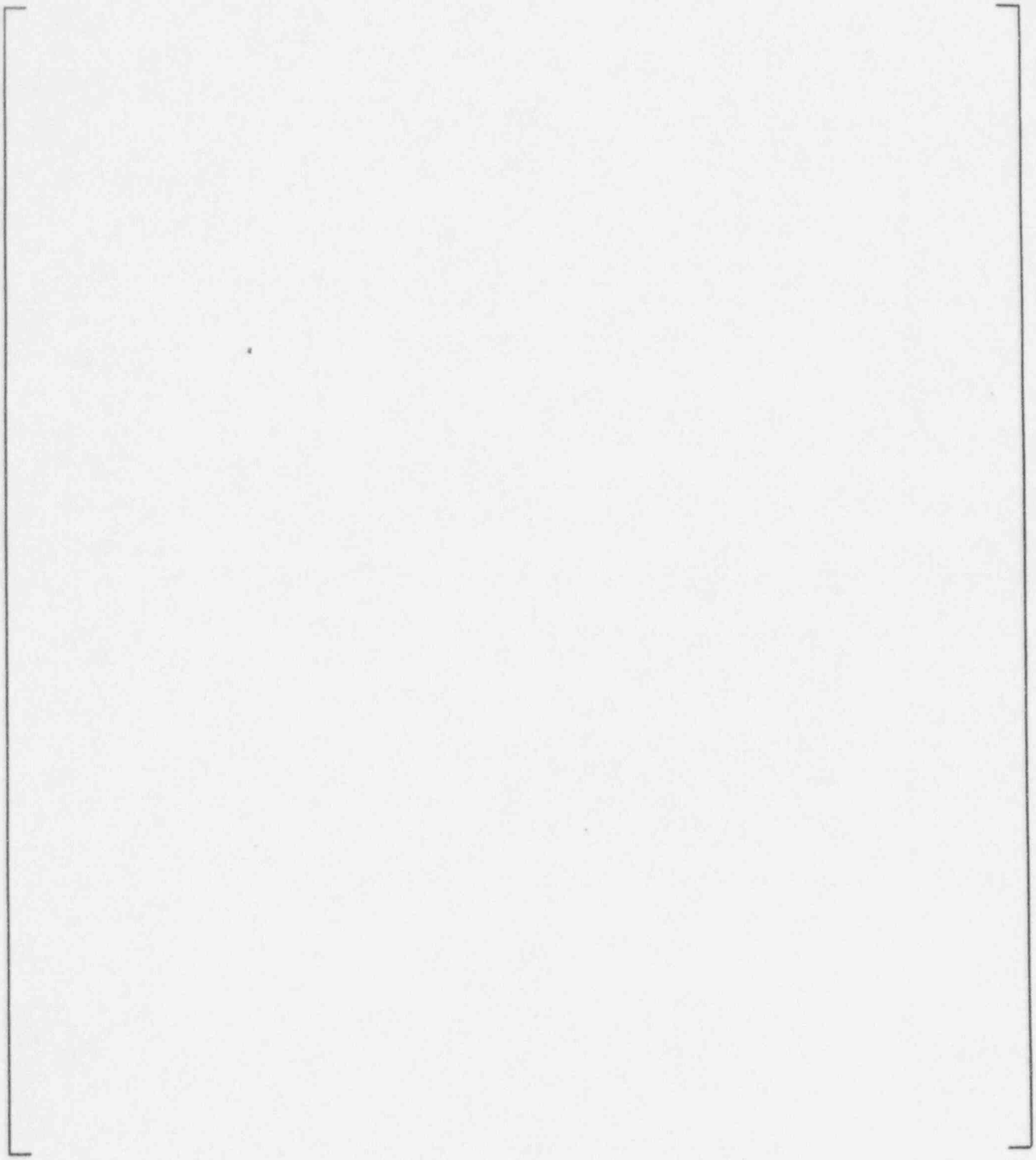

Figure 5.4-15 NOTRUMP Comparison to the Sparger Body and Sparger Arms Pressures for Test 220

a,b

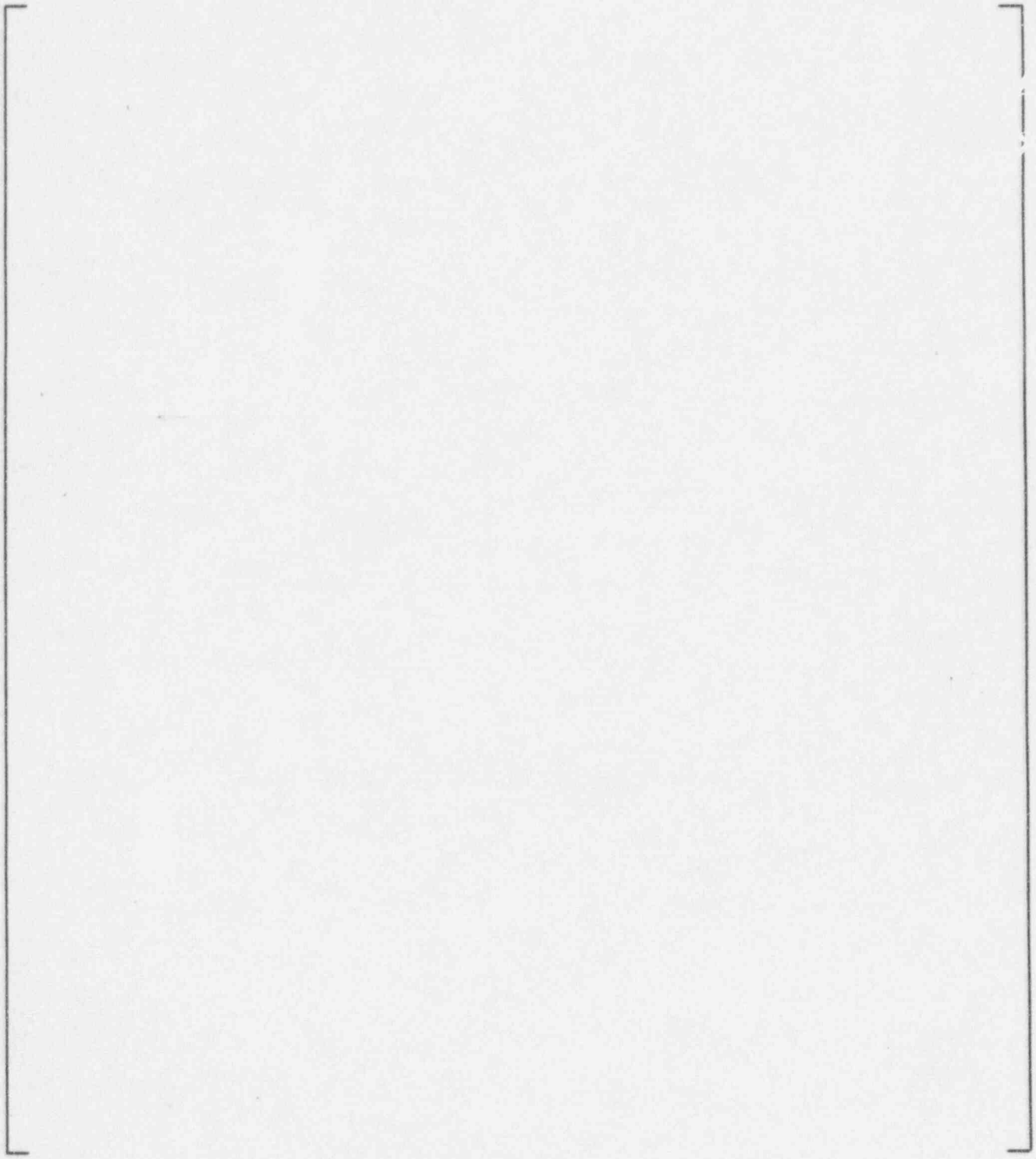

Figure 5.4-16 NOTRUMP Comparison to the Automatic Depressurization System Flow Rate for Test 240

a,b

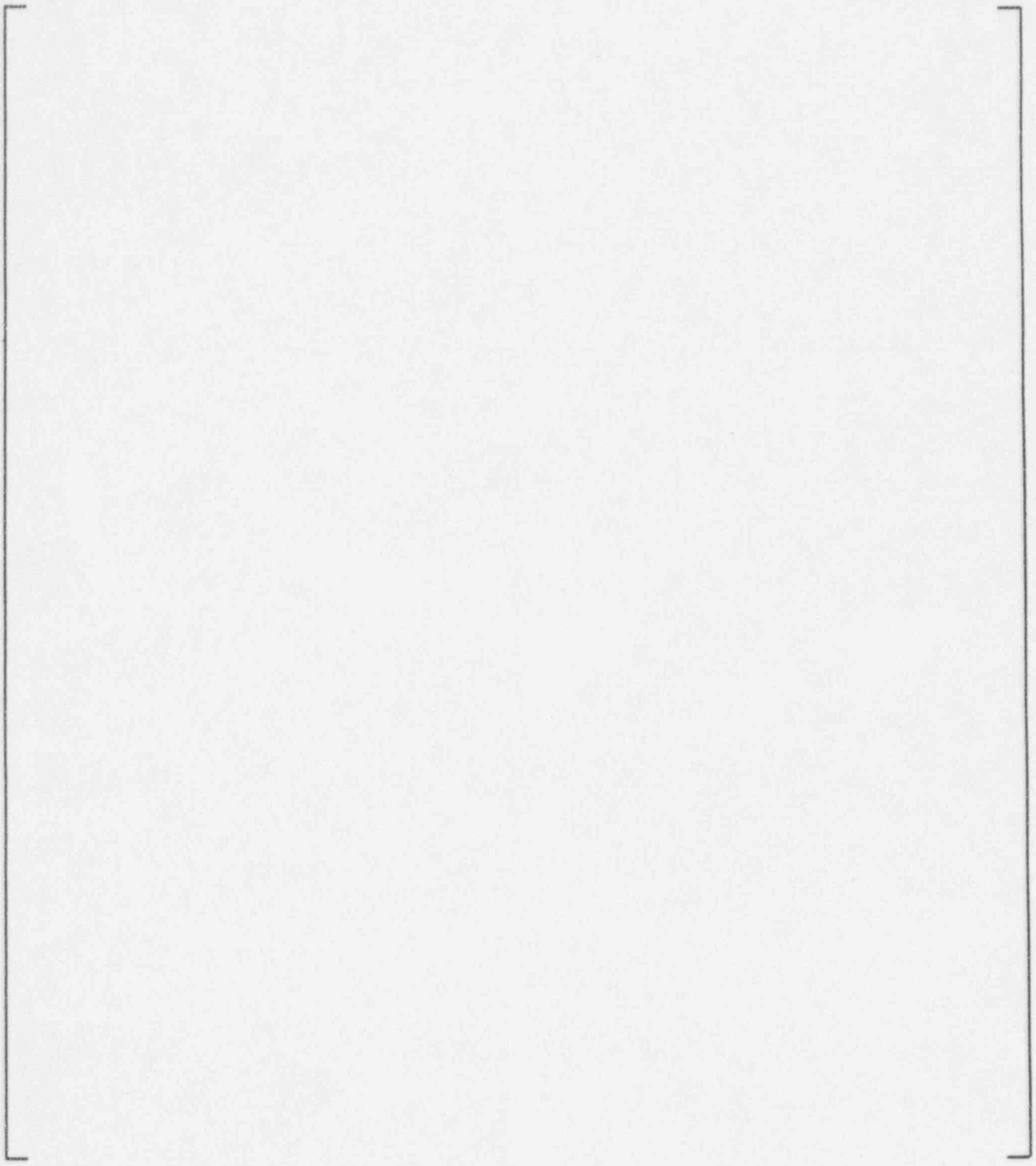

Figure 5.4-17 NOTRUMP Comparison to the Automatic Depressurization System Supply Tank Pressure for Test 240 (Pressurizer)

a,b

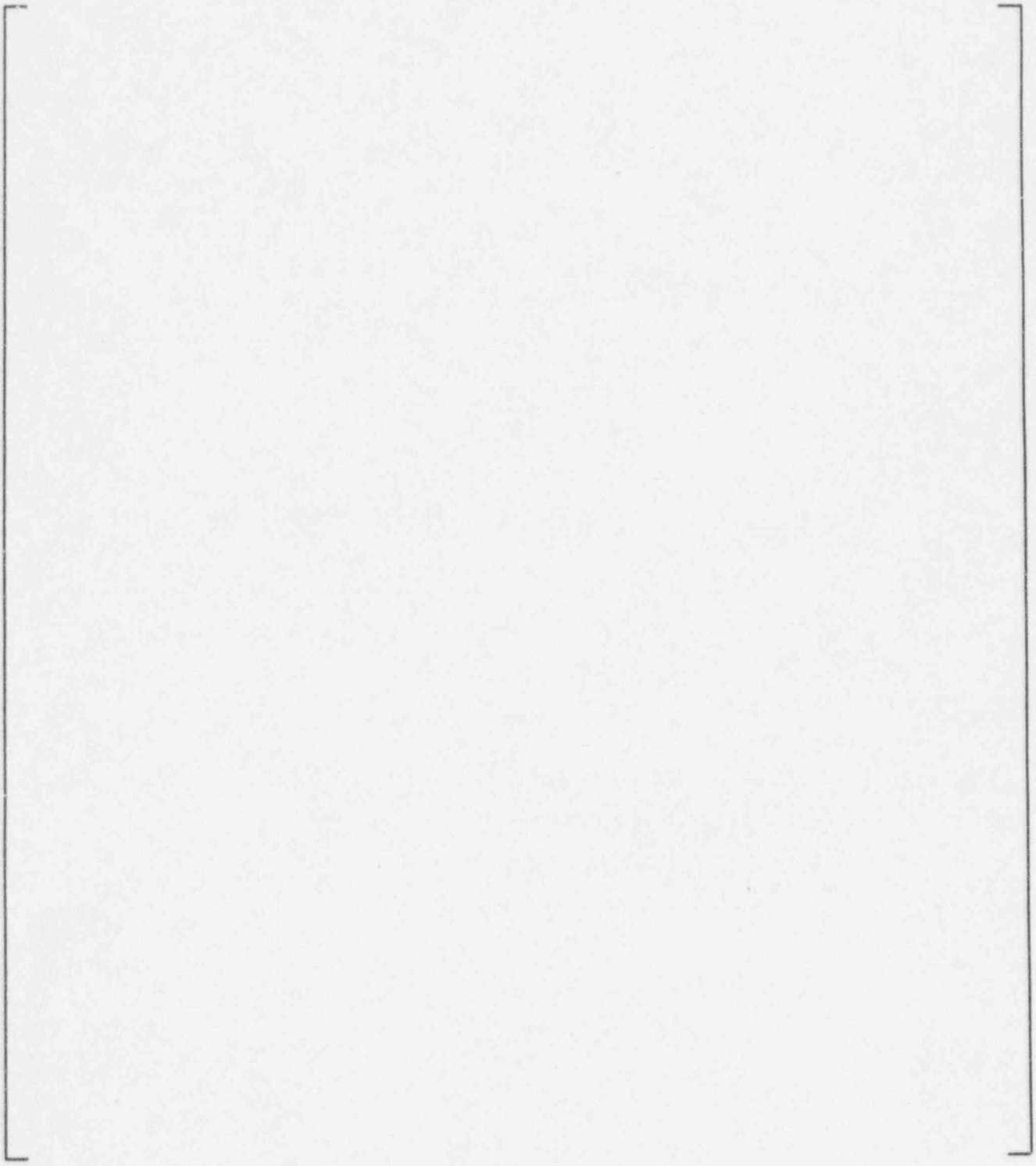

Figure 5.4-18 NOTRUMP Comparison to the Upstream and Downstream Pressures across Valve VLI-2 (A&M) for Test 240

a,b

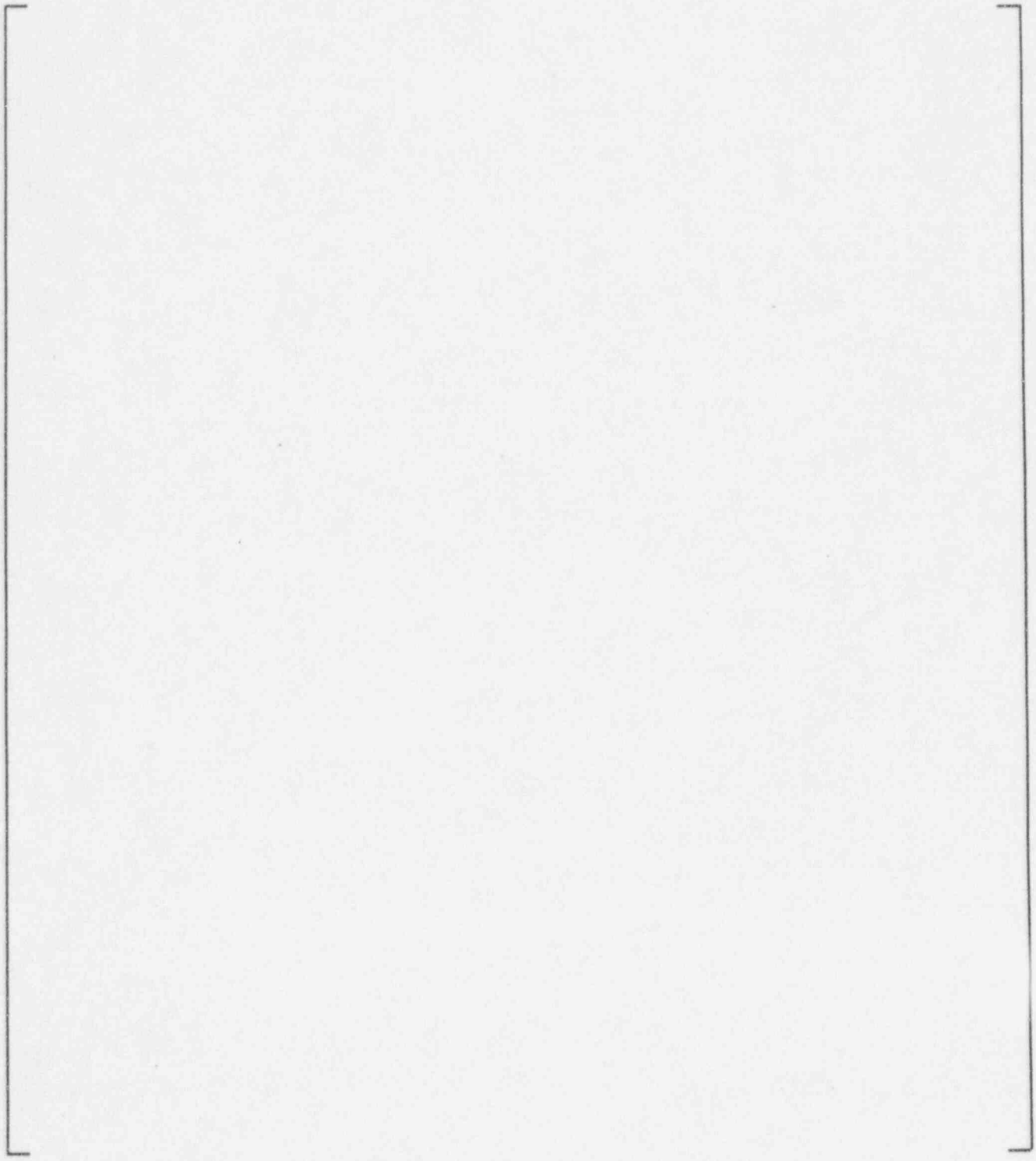

Figure 5.4-19 NOTRUMP Comparison to the Upstream and Downstream Pressures across the Automatic Depressurization System Valve Package for Test 240

a,b

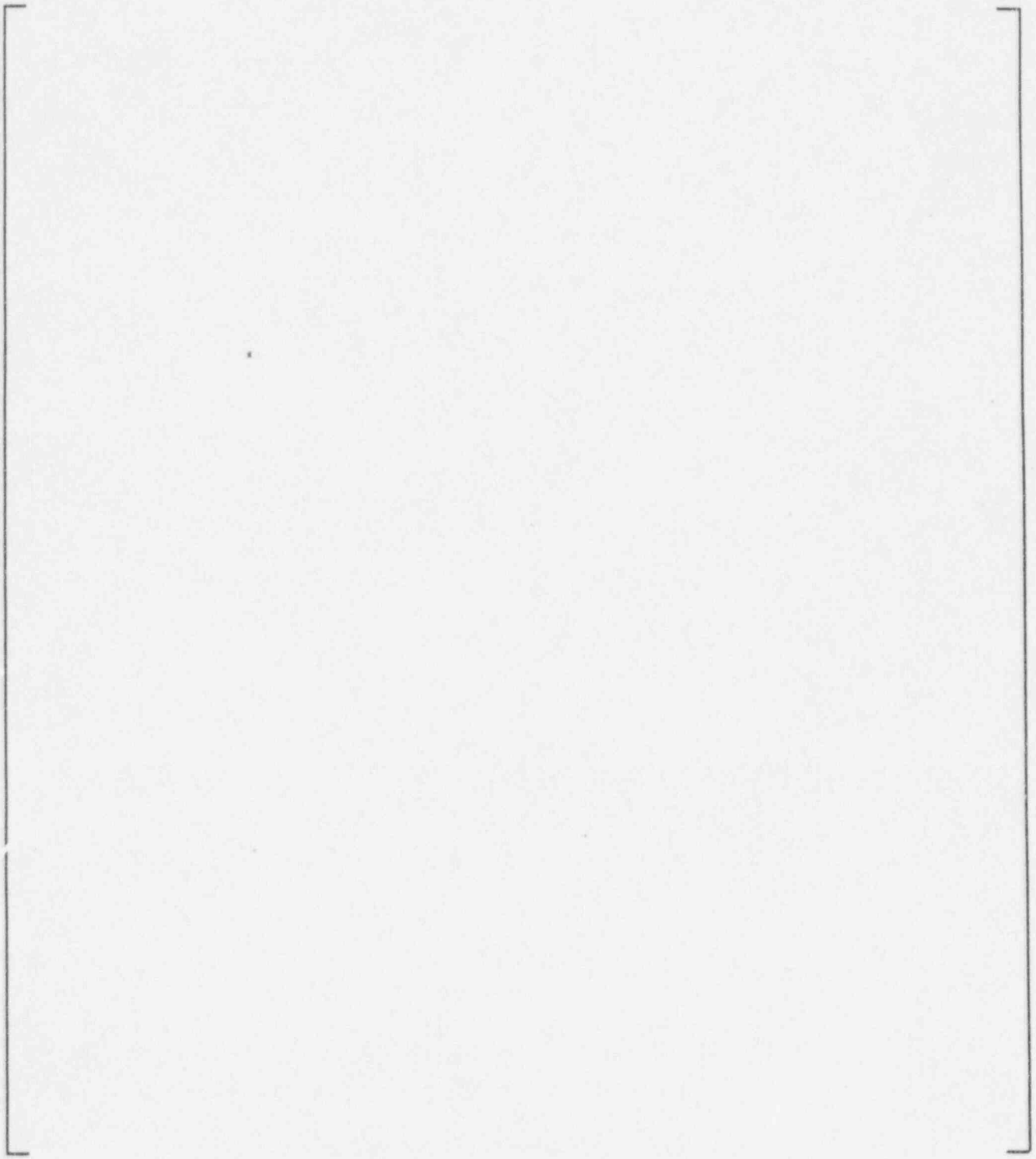

Figure 5.4-20 NOTRUMP Comparison to the Sparger Body and Sparger Arms Pressures for Test 240

a,b

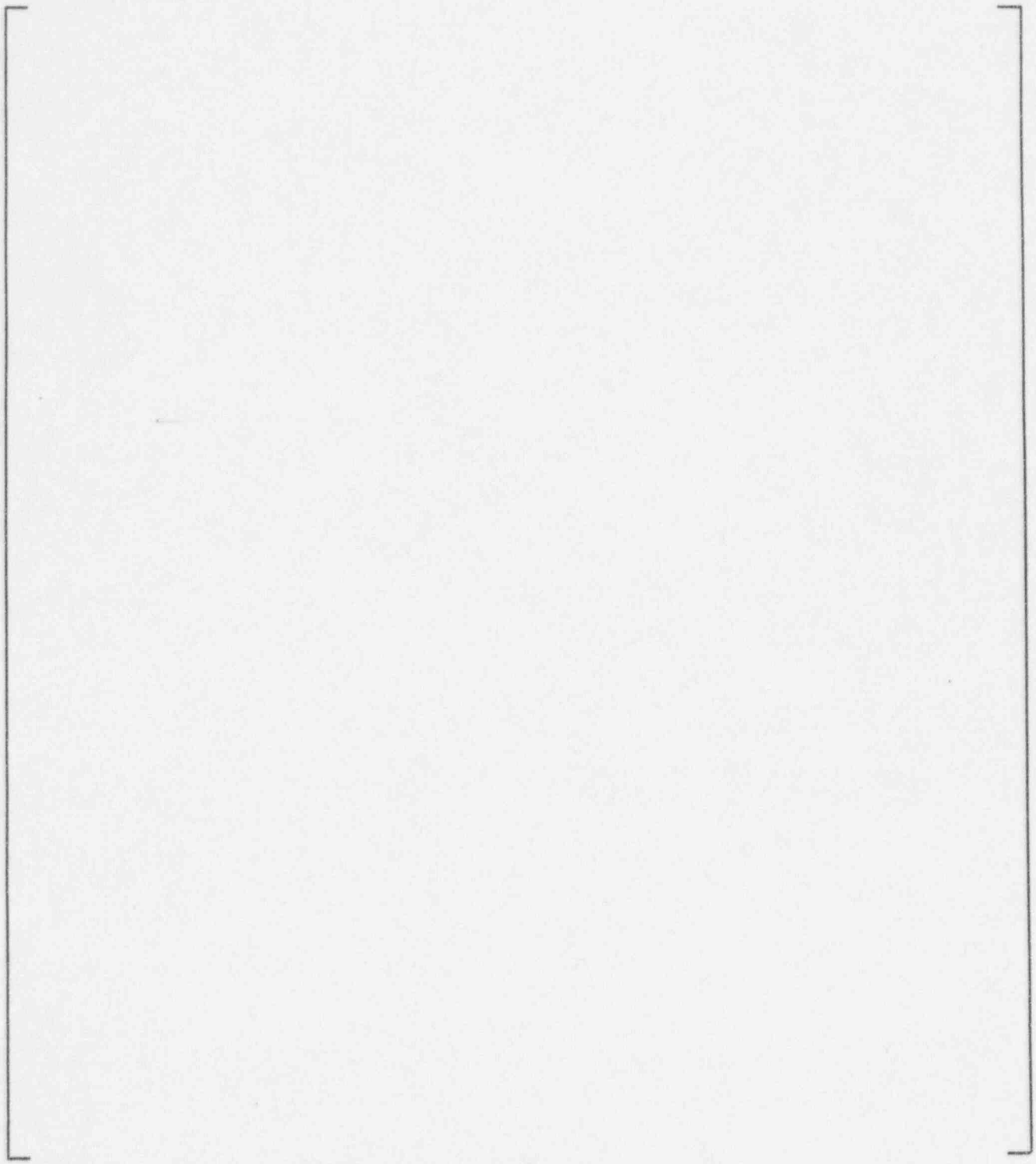

Figure 5.4-21 NOTRUMP Comparison to the Automatic Depressurization System Flow Rate for Test 242

a,b

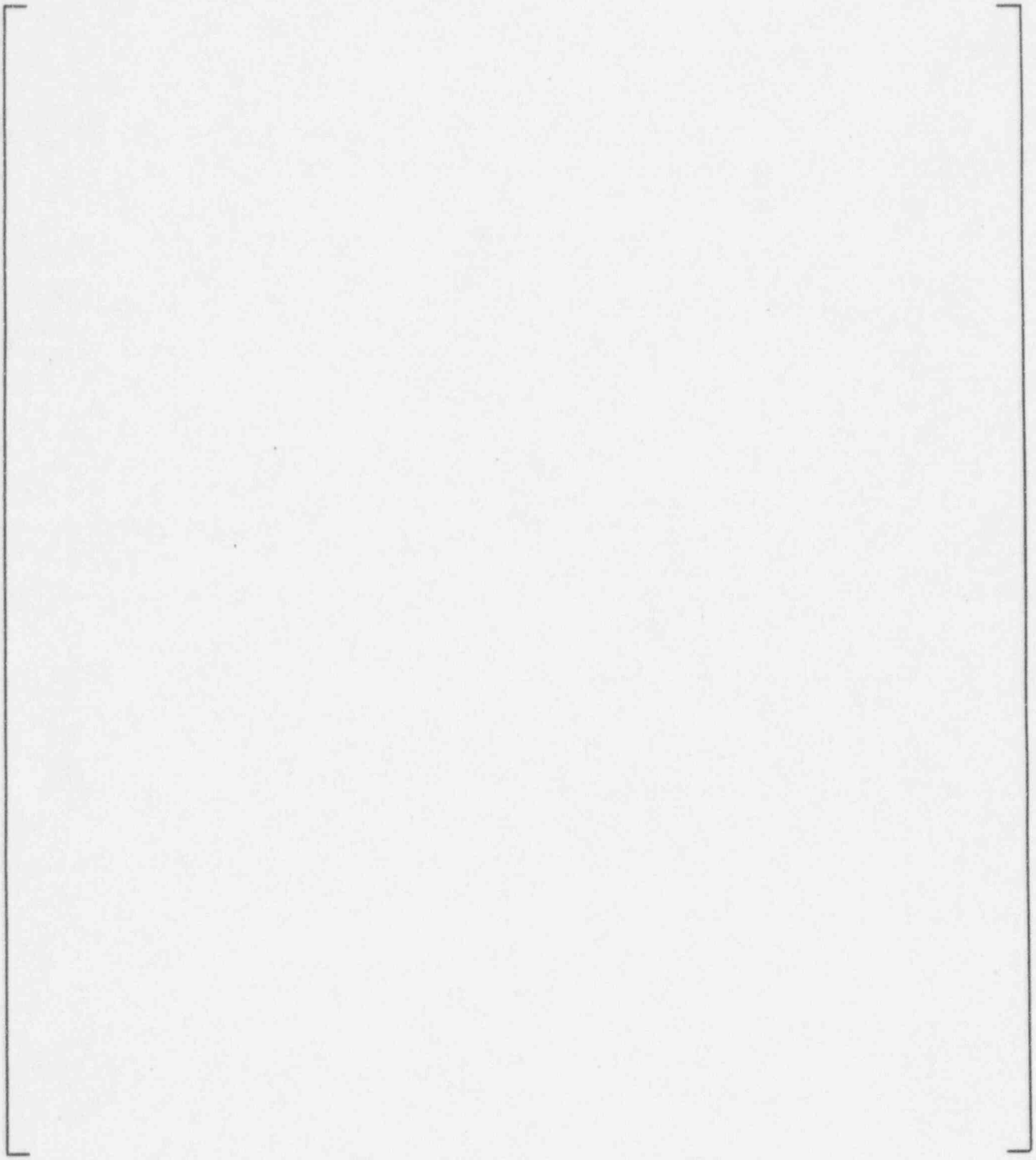

Figure 5.4-22 NOTRUMP Comparison to the Automatic Depressurization System Supply Tank (Pressurizer) Pressure for Test 242

a,b

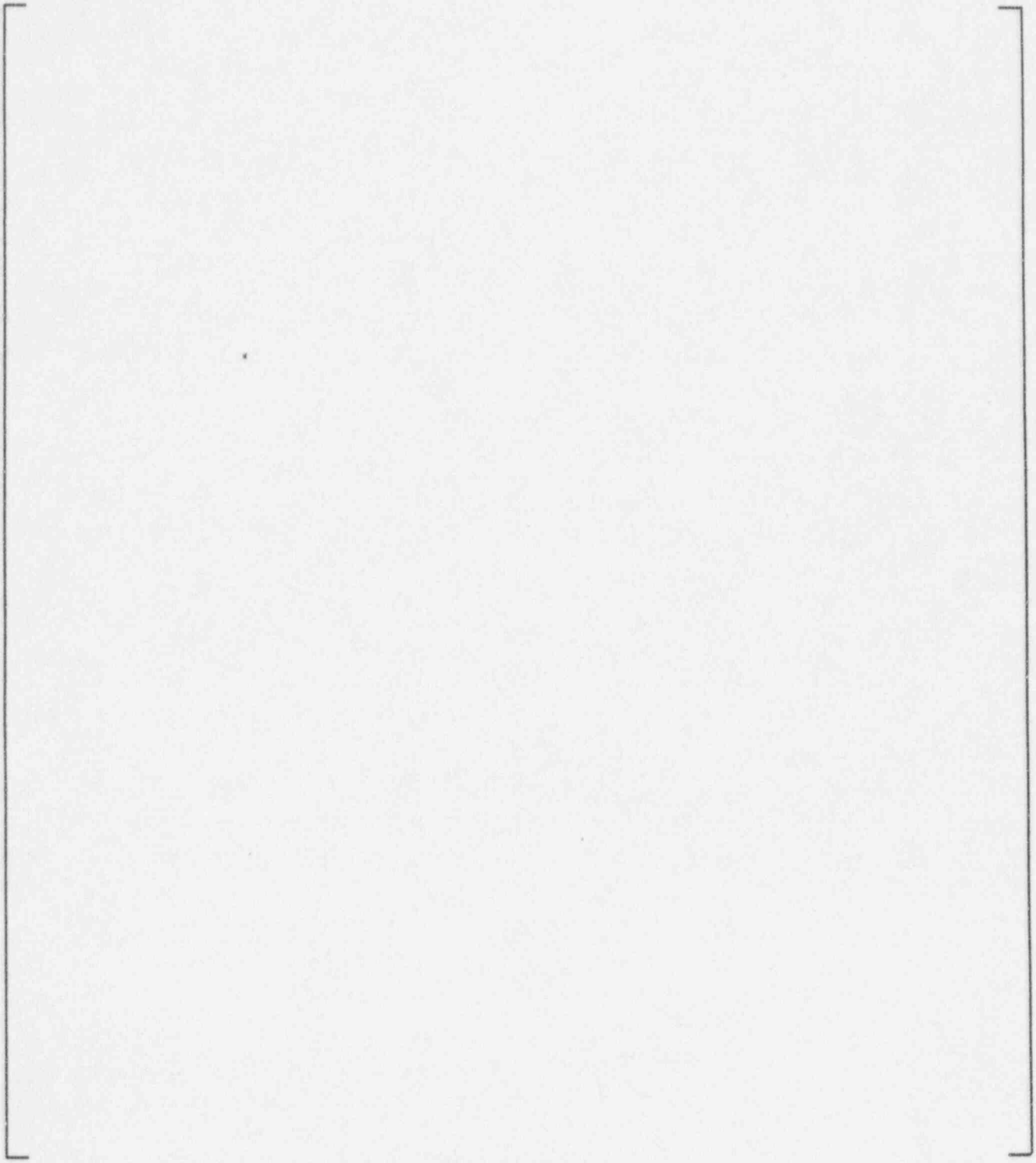

Figure 5.4-23 NOTRUMP Comparison to the Upstream and Downstream Pressures across Valve VLI-2 (A&M) for Test 242

a,b

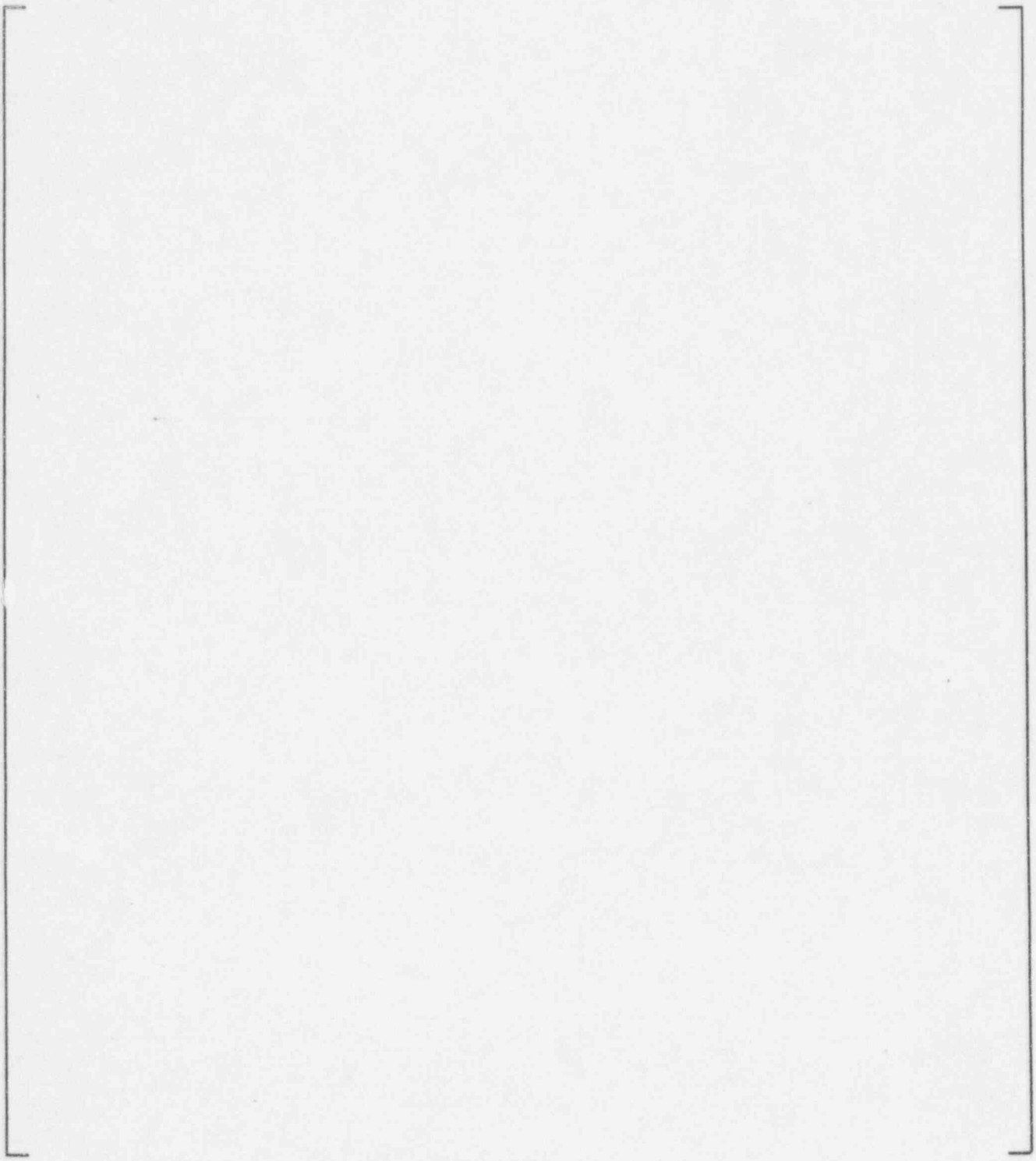

Figure 5.4-24 NOTRUMP Comparison to the Upstream and Downstream Pressures across the Automatic Depressurization System Valve Package for Test 242

a,b

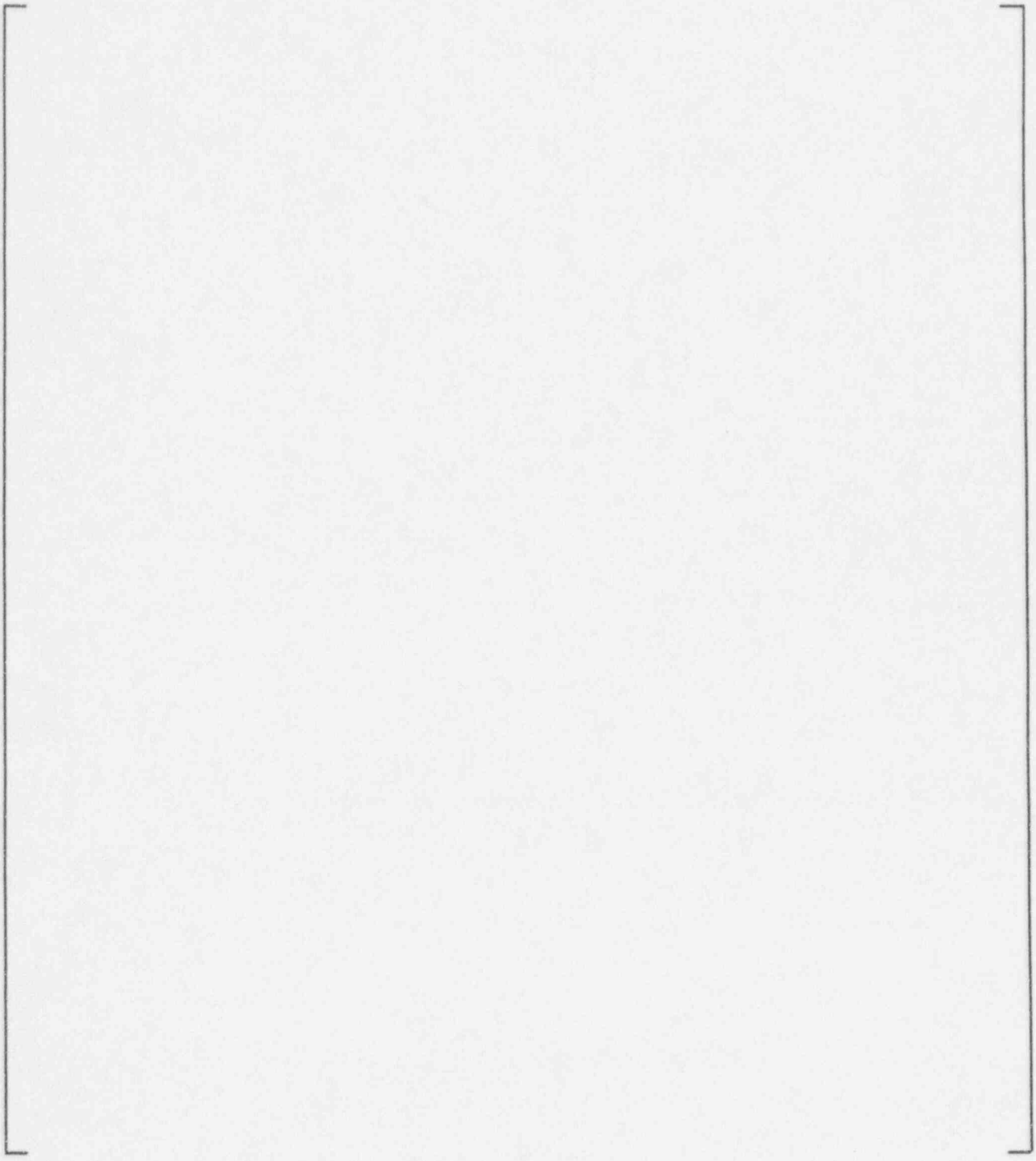

Figure 5.4-25 NOTRUMP Comparison to the Sparger Body and Sparger Arms Pressures for Test 242

a,b

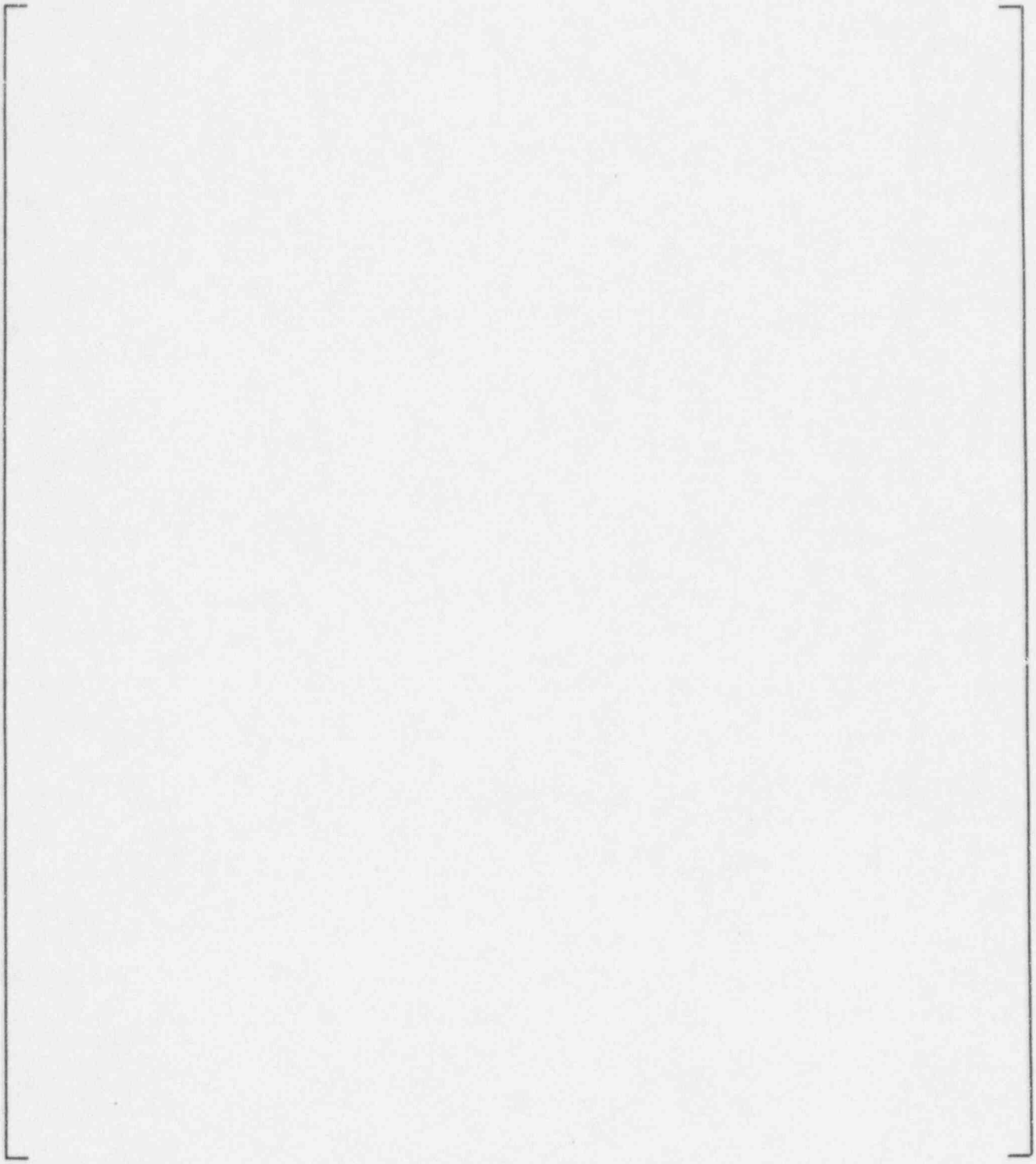

Figure 5.4-26 NOTRUMP Comparison to the Automatic Depressurization System Flow Rate for Test 250

a,b

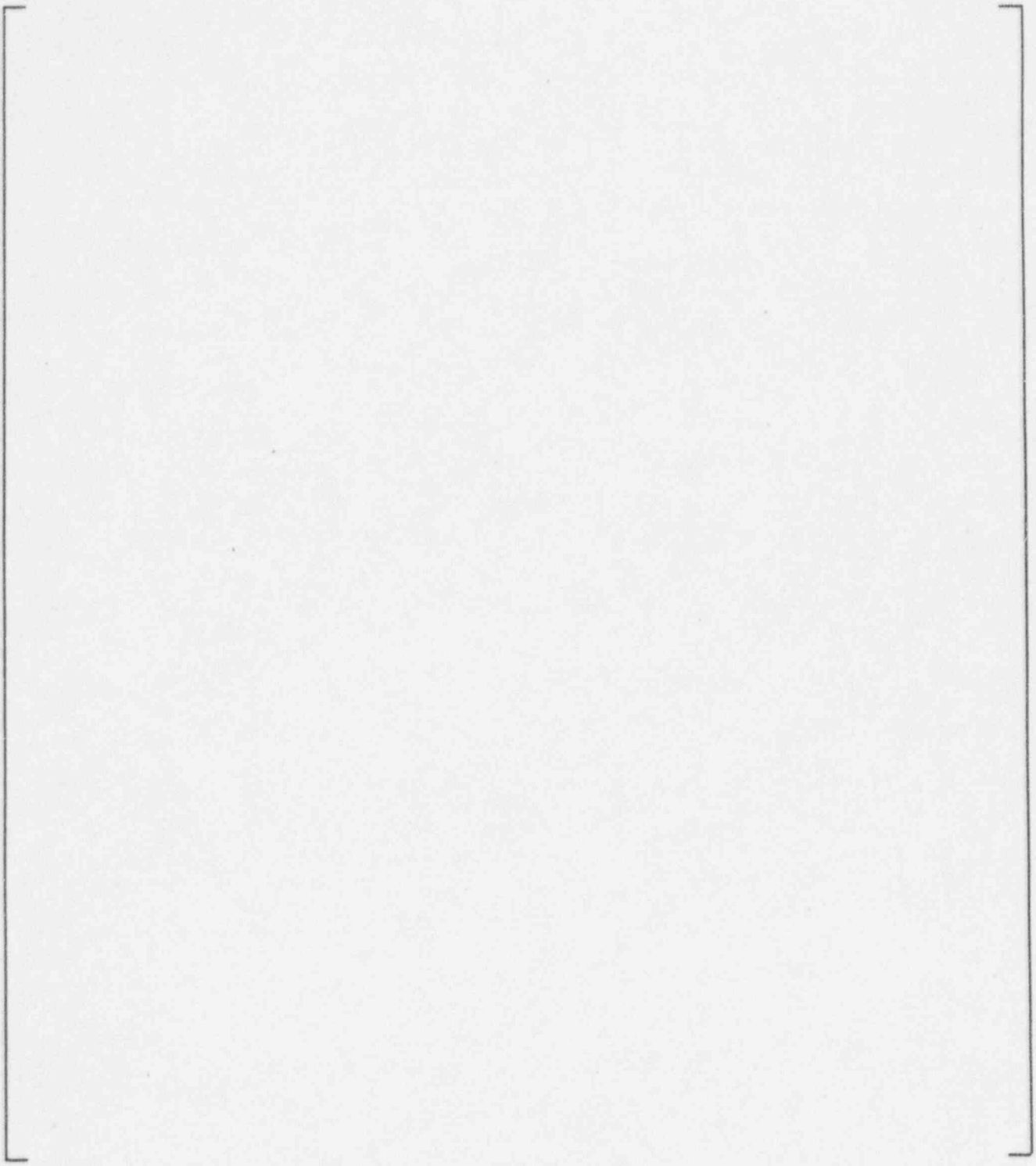

Figure 5.4-27 NOTRUMP Comparison to the Automatic Depressurization System Supply Tank (Pressurizer) Pressure for Test 250

a,b

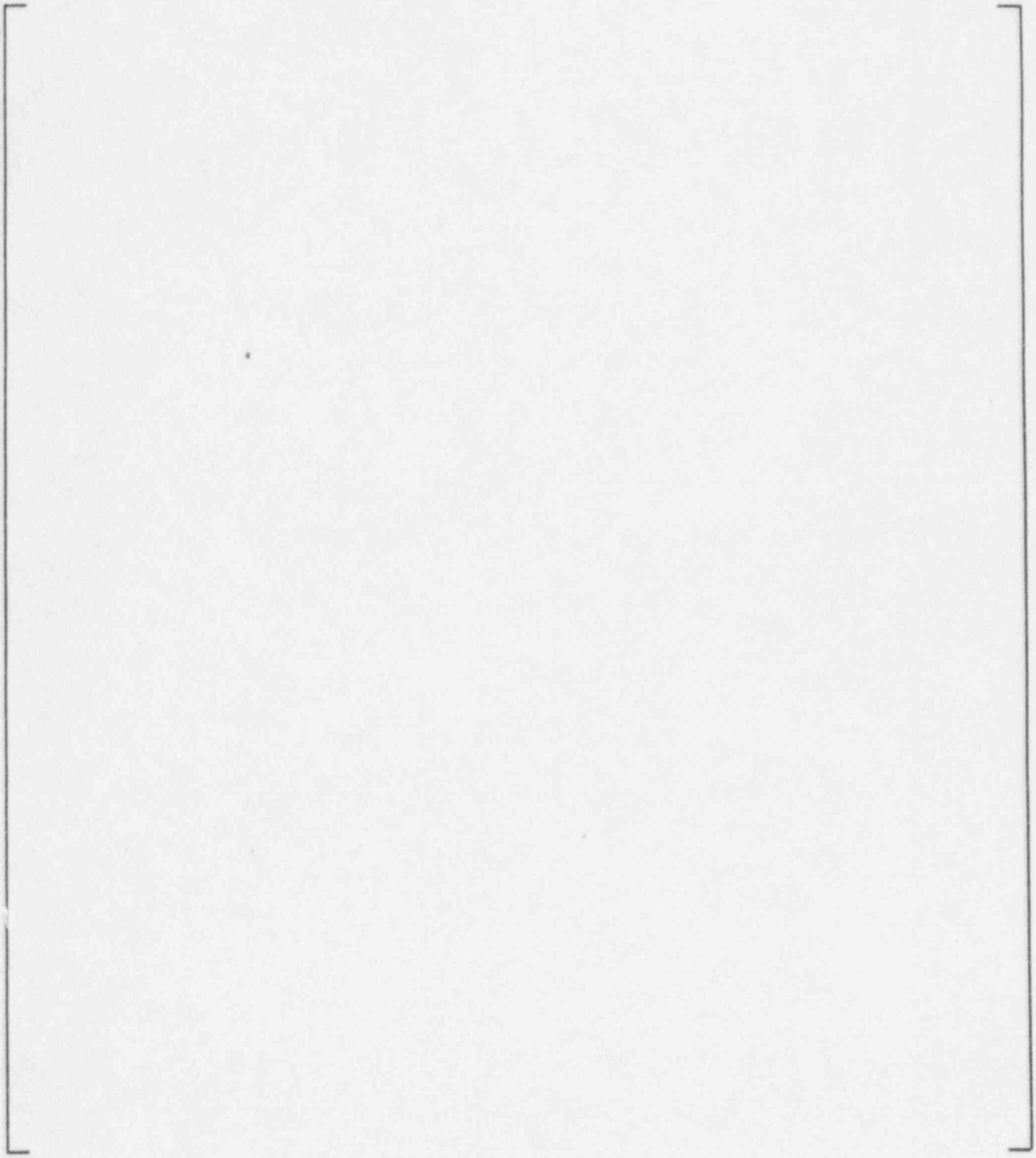

Figure 5.4-28 NOTRUMP Comparison to the Upstream and Downstream Pressures across Valve VLI-2 (A&M) for Test 250

a,b

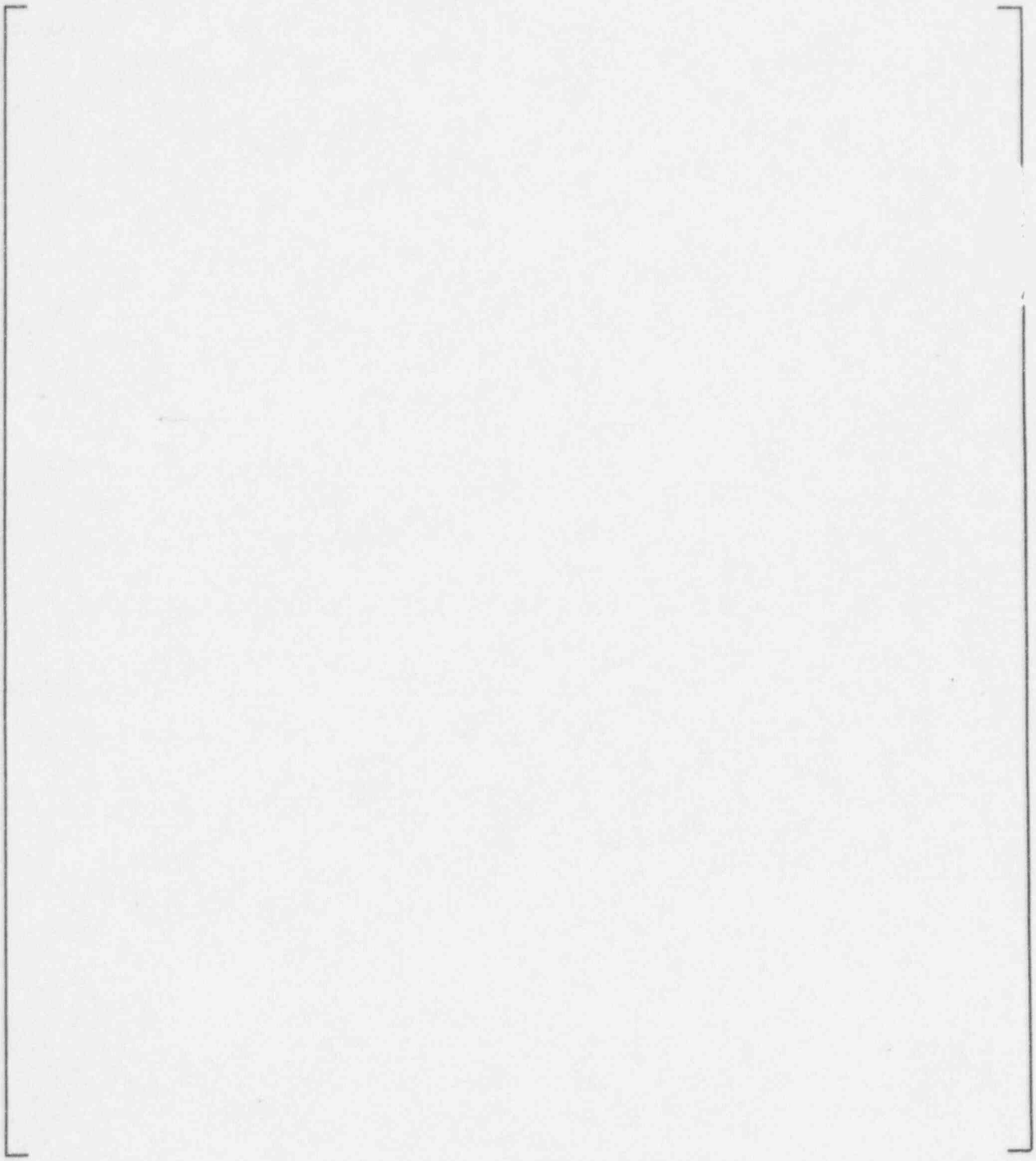

Figure 5.4-29 NOTRUMP Comparison to the Upstream and Downstream Pressures across the Automatic Depressurization System Valve Package for Test 250

a,b

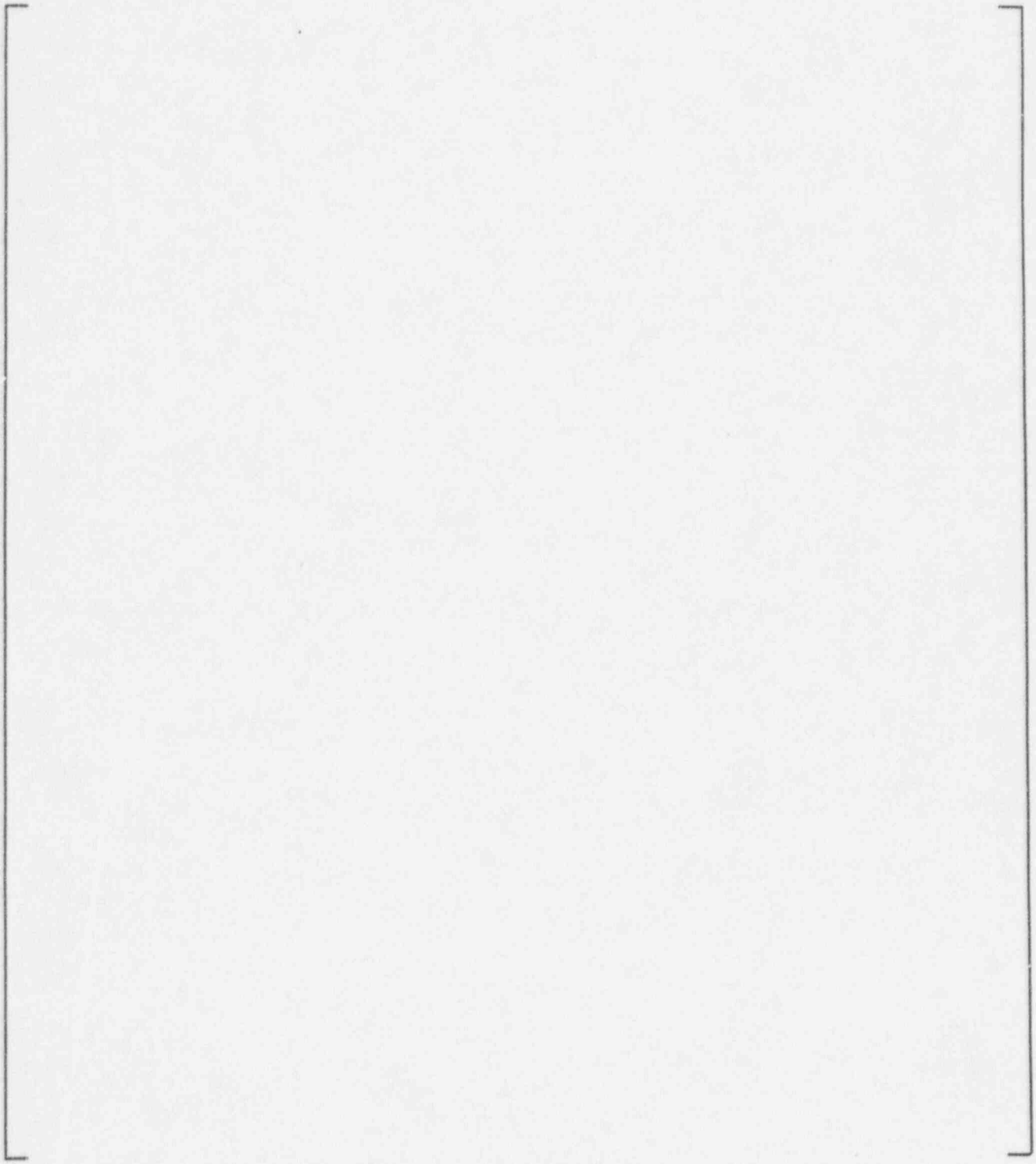

Figure 5.4-30 NOTRUMP Comparison to the Sparger Body and Sparger Arms Pressures for Test 250

a,b

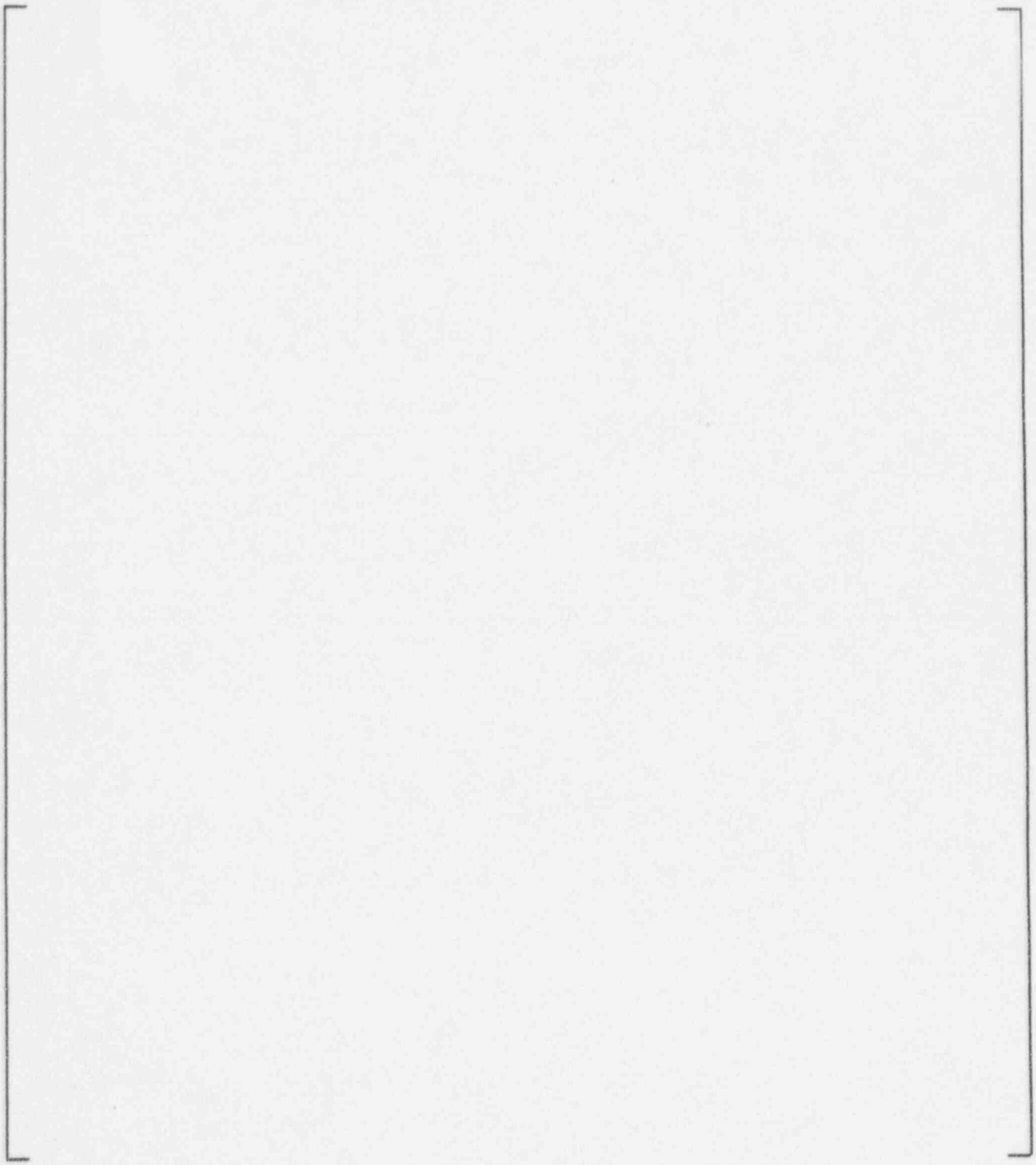

Figure 5.4-31 NOTRUMP Comparison to the Automatic Depressurization System Flow Rate for Test 320

a,b

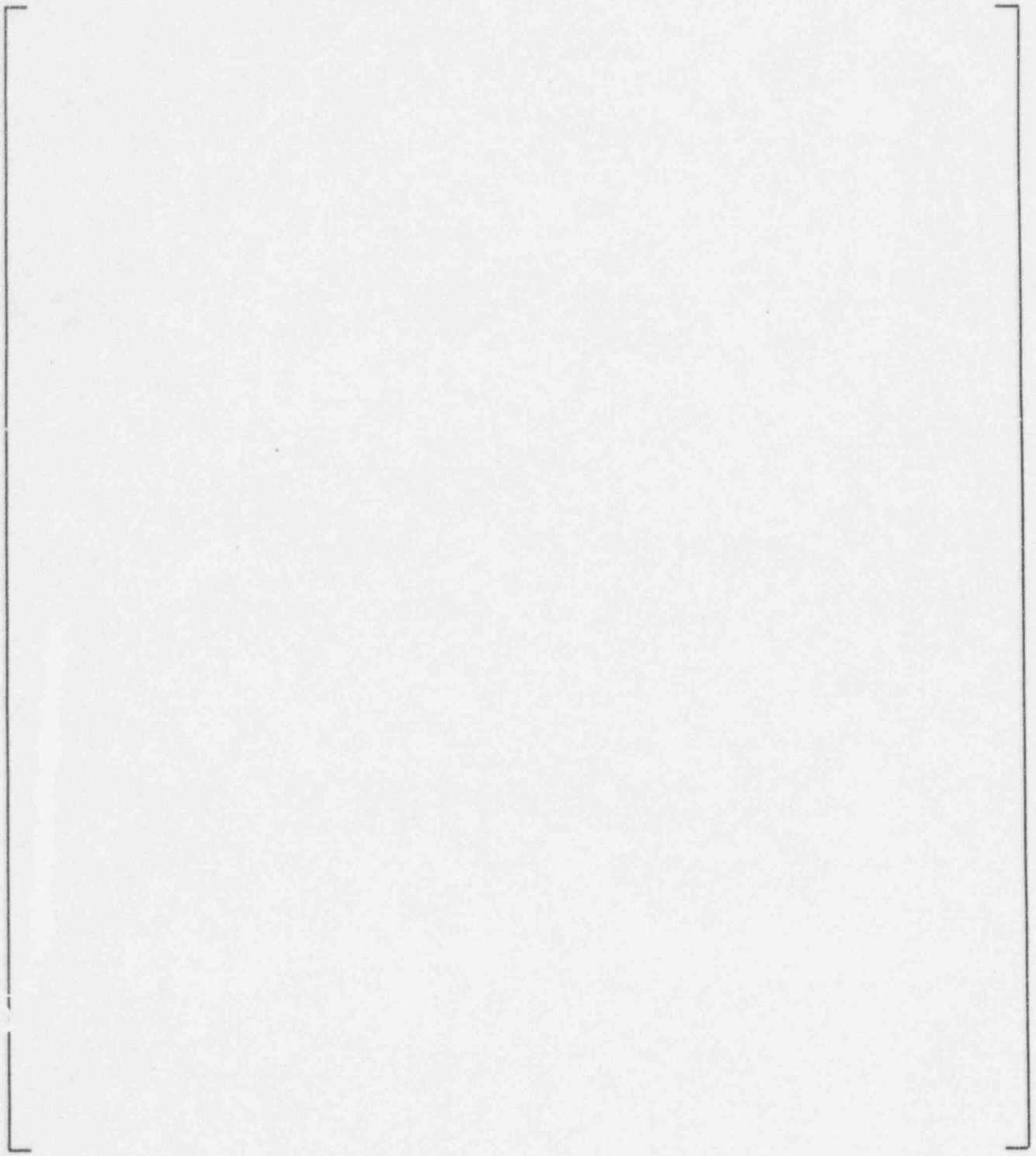

Figure 5.4-32 NOTRUMP Comparison to the Automatic Depressurization System Supply Tank (Pressurizer) Pressure for Test 320

a,b

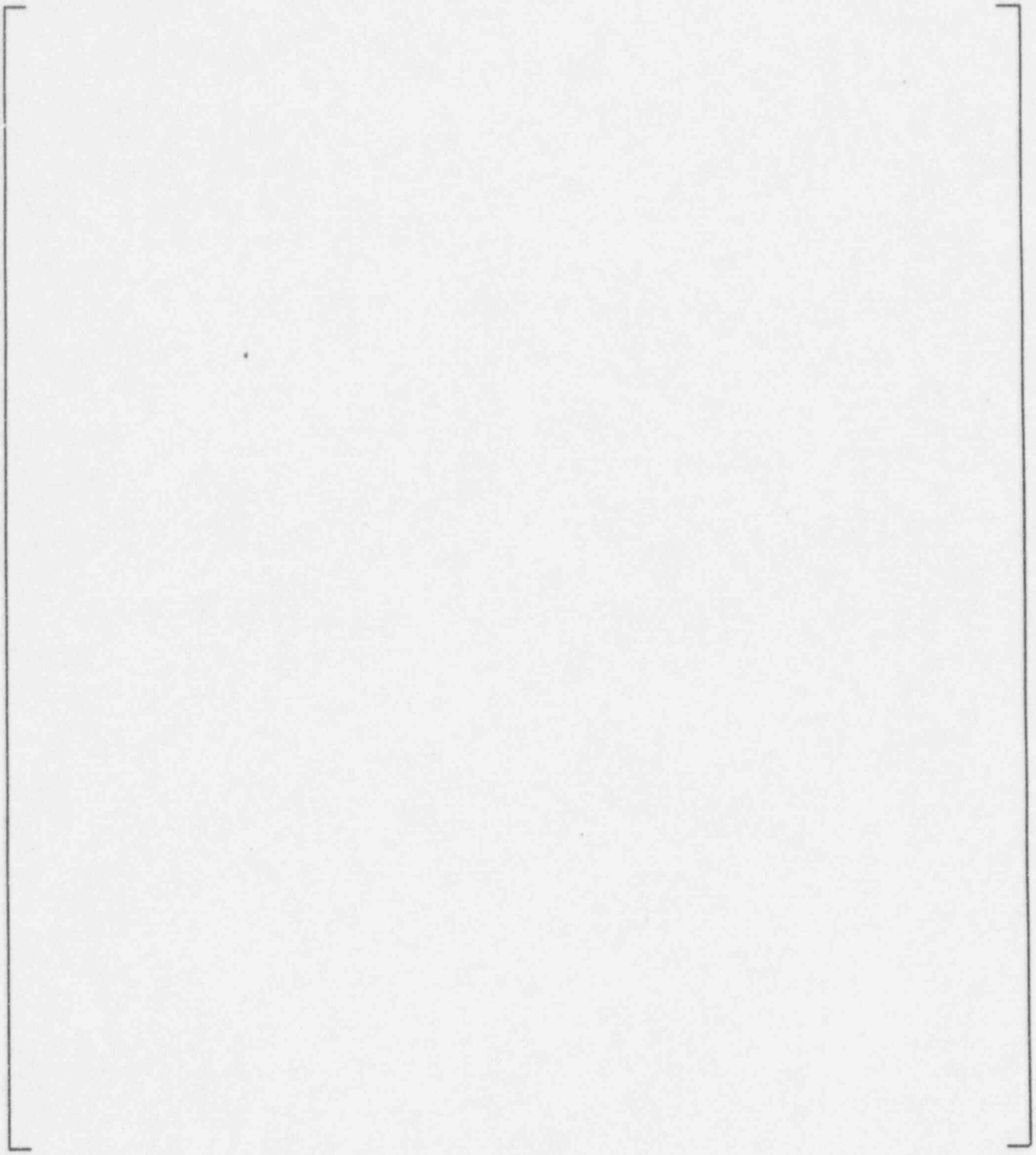

Figure 5.4-33 NOTRUMP Comparison to the Upstream and Downstream Pressures across Valve VLI-2 (A&M) for Test 320

a,b

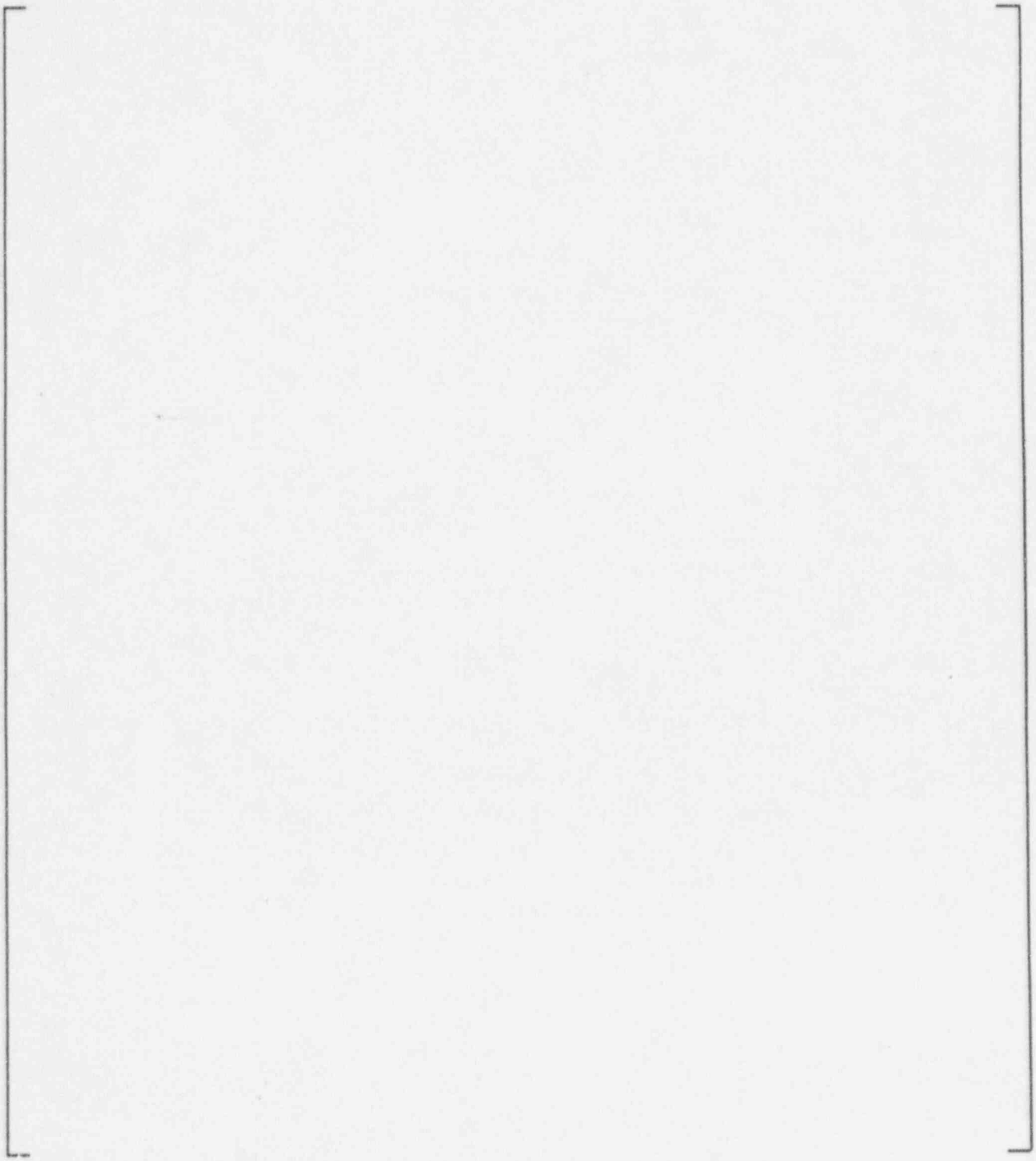

Figure 5.4-34 NOTRUMP Comparison to the Upstream and Downstream Pressures across the Automatic Depressurization System Valve Package for Test 320

a,b

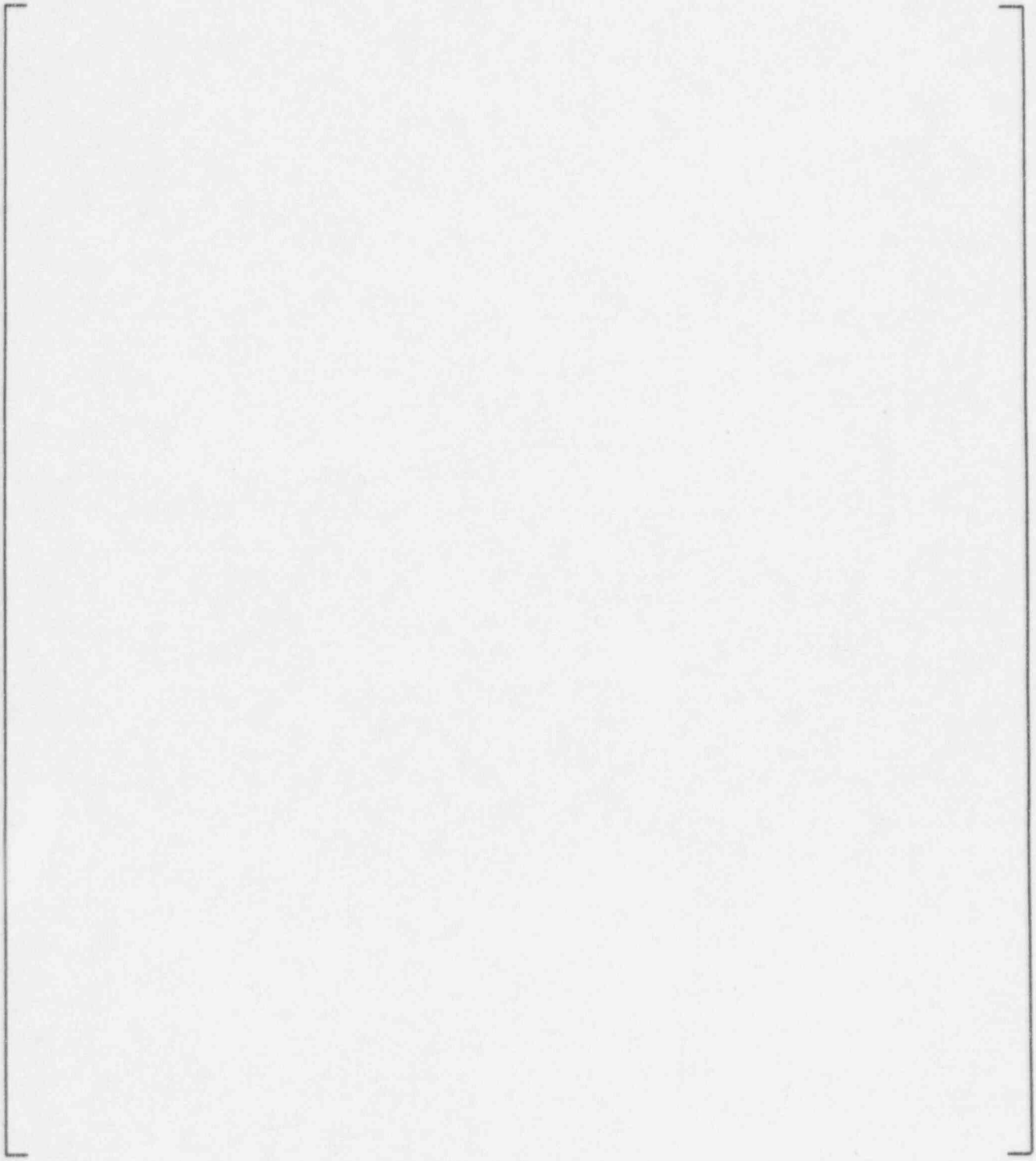

Figure 5.4-35 NOTRUMP Comparison to the Sparger Body and Sparger Arms Pressures for Test 320

a,b

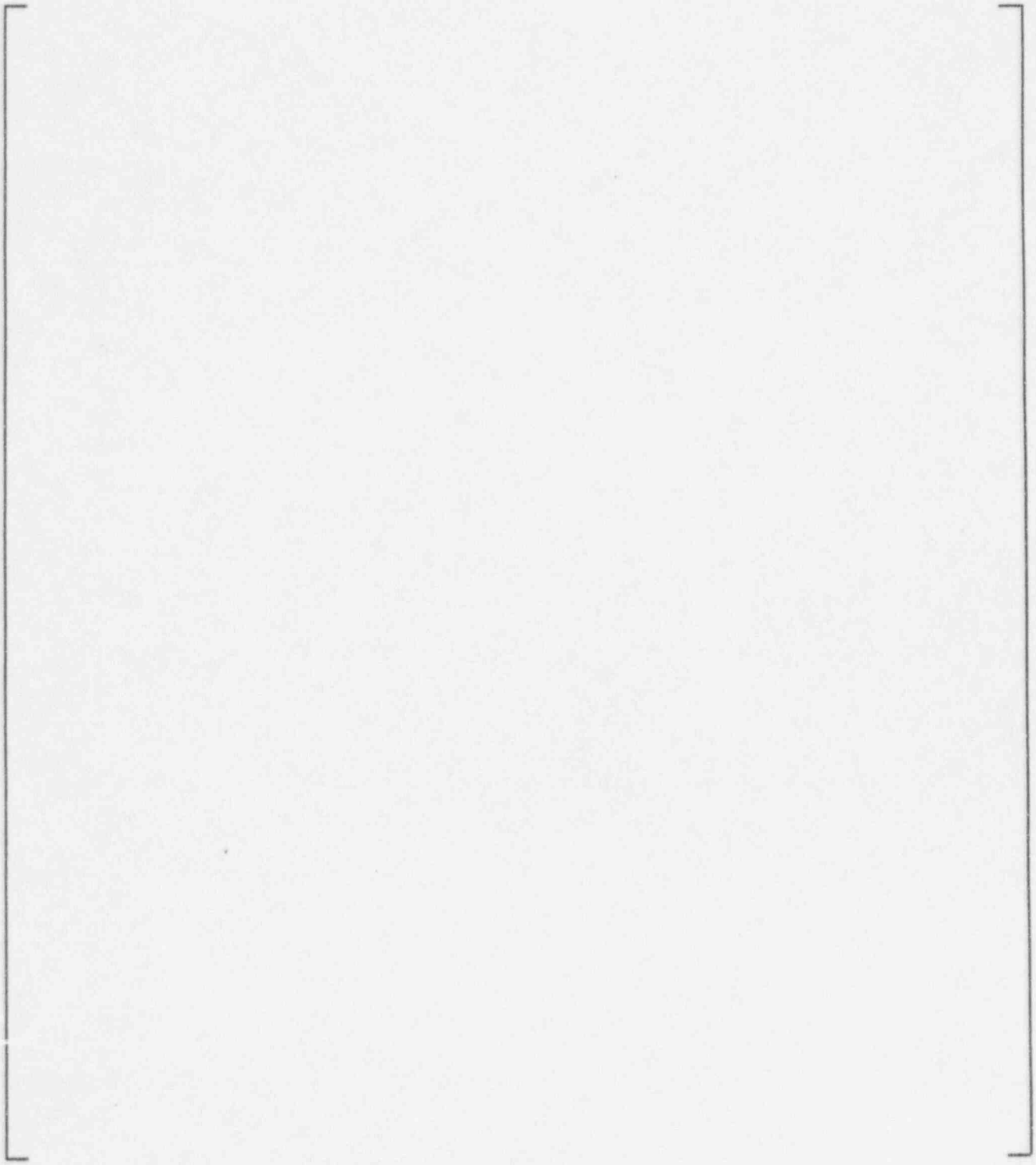

Figure 5.4-36 NOTRUMP Comparison to the Automatic Depressurization System Flow Rate for Test 340

a,b

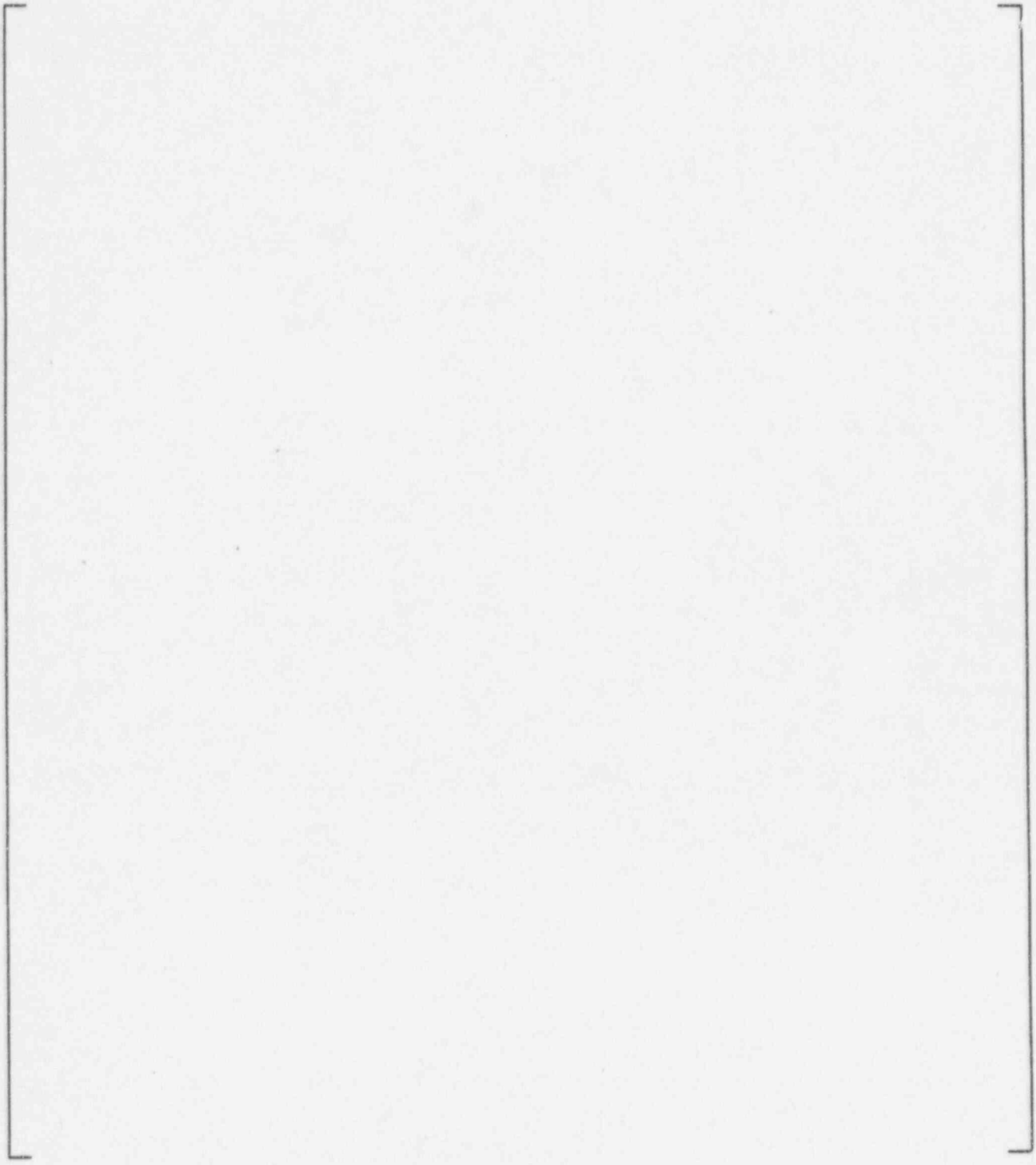

Figure 5.4-37 NOTRUMP Comparison to the Automatic Depressurization System Supply Tank (Pressurizer) Pressure for Test 340

a,b

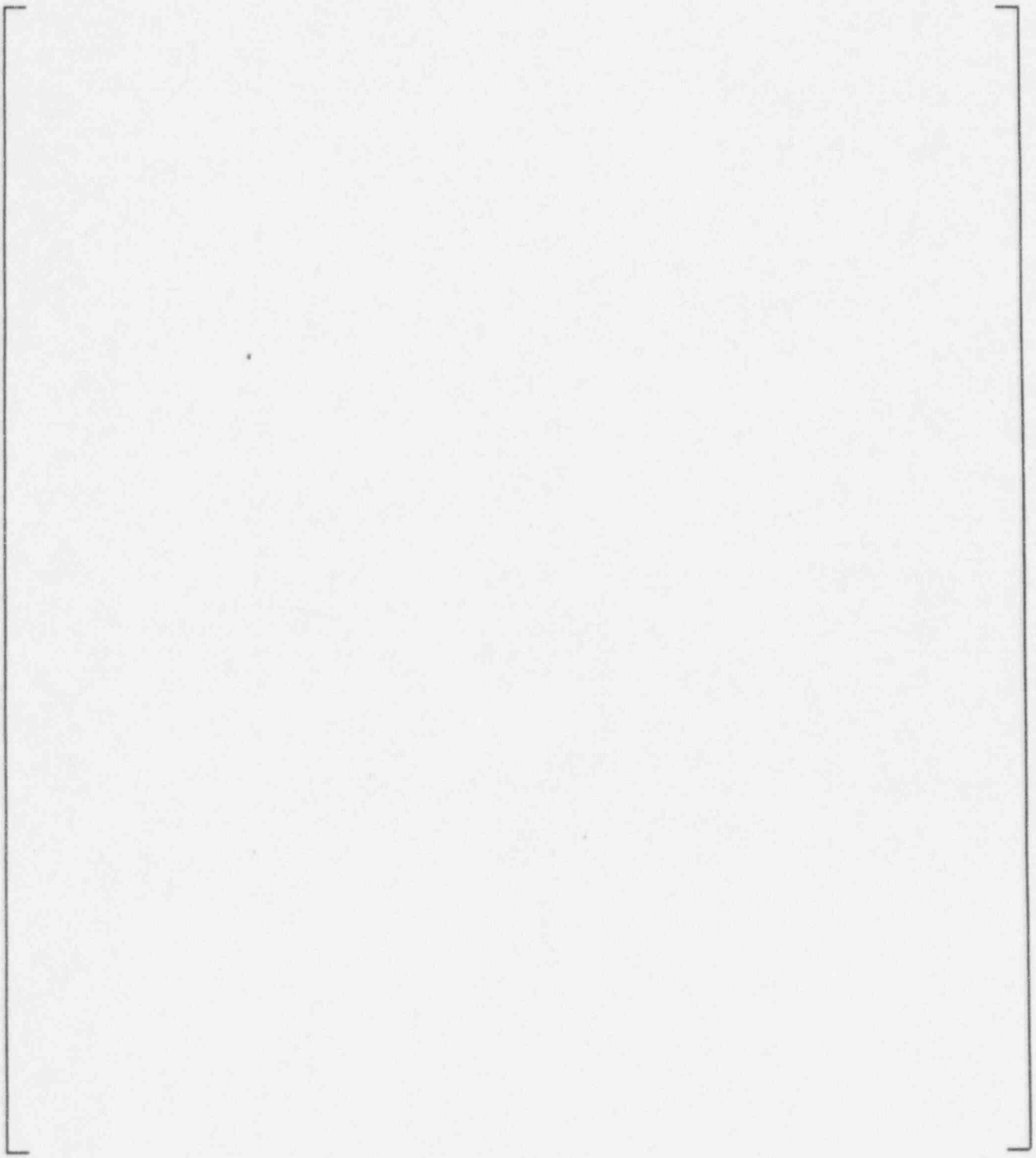

Figure 5.4-38 NOTRUMP Comparison to the Upstream and Downstream Pressures across Valve VLI-2 (A&M) for Test 340

a,b

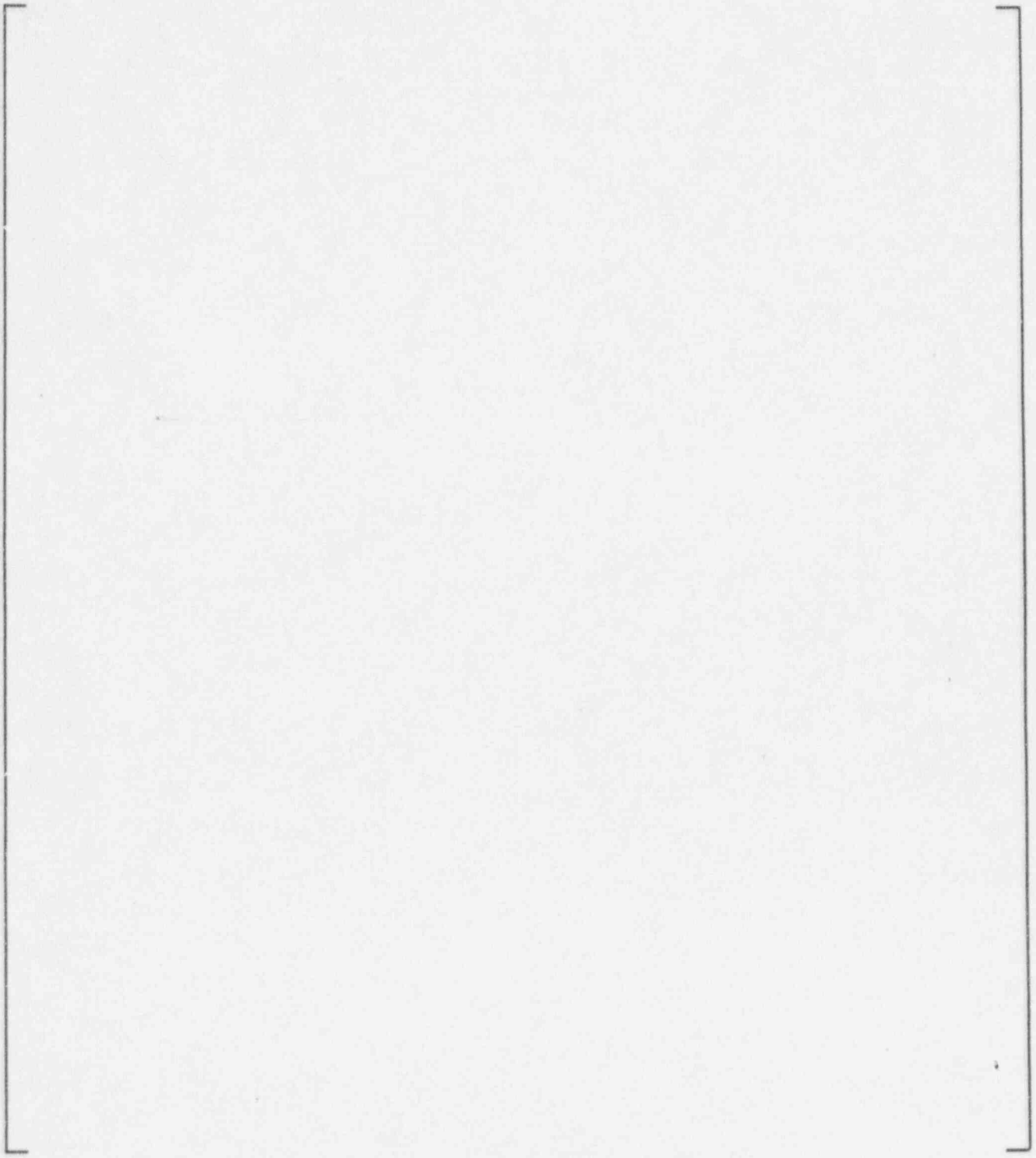

Figure 5.4-39 NOTRUMP Comparison to the Upstream and Downstream Pressures across the Automatic Depressurization System Valve Package for Test 340

a,b

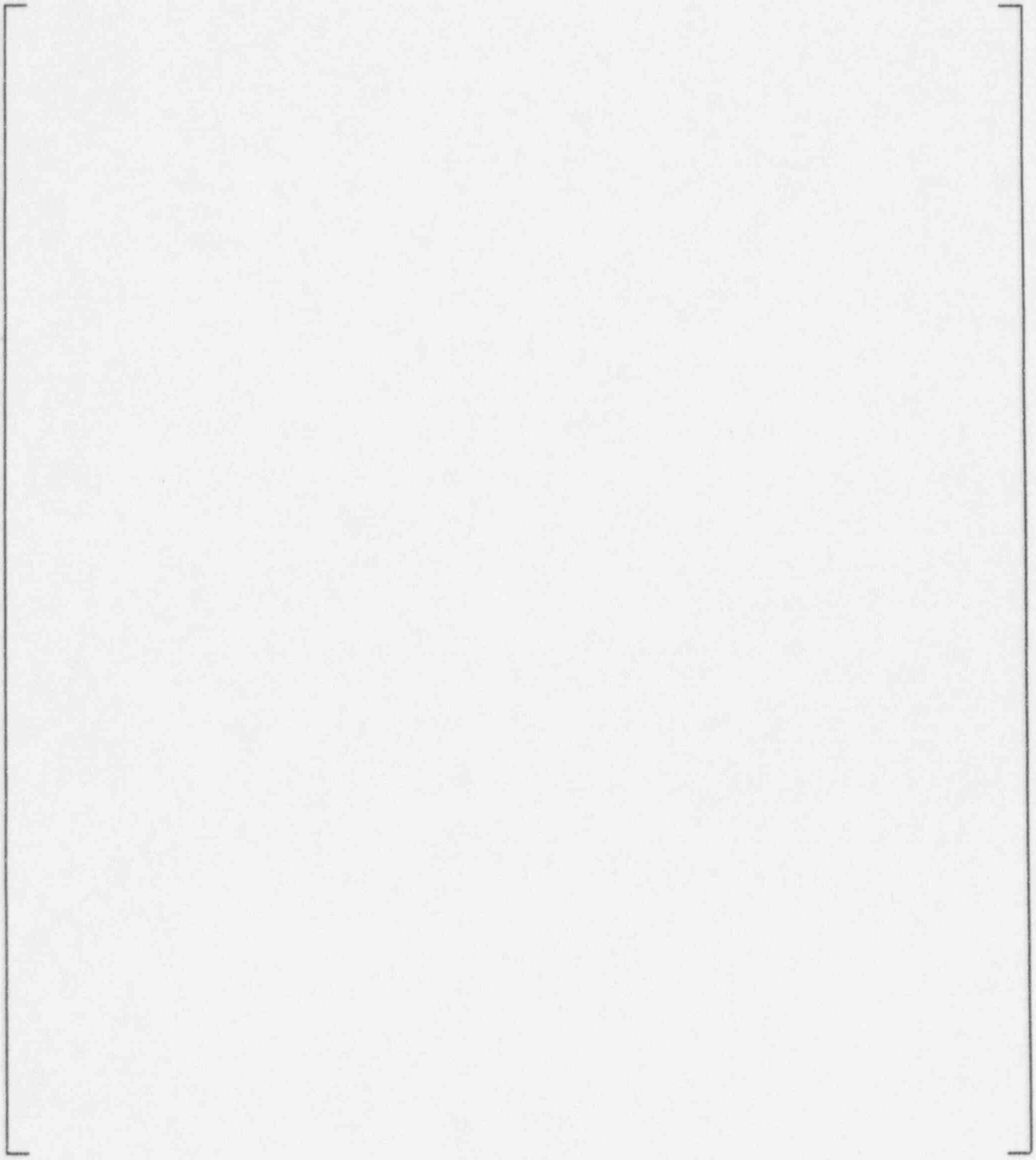

Figure 5.4-40 NOTRUMP Comparison to the Sparger Body and Sparger Arms Pressures for Test 340

5.5 Overall Comparison of NOTRUMP to the Tests

5.5.1 Critical Flow

The critical flow rate is accurately predicted by NOTRUMP at the choked locations. NOTRUMP tends to overpredict the pressure drops both at the choked locations and the unchoked valve location. Table 5.5-1 summarizes the locations of the occurrence of the critical flow for the eight tests investigated.

Figure 5.5-1 shows the composite plot of the predicted versus measured flow from the eight ADS Phase B1 tests. As the figure indicates, the NOTRUMP flow predictions are in excellent agreement with the test data. The calculation of the supply tank pressure is also in excellent agreement with the data, which agrees with the excellent flow predictions.

5.5.2 Pressure Drop Predictions

While NOTRUMP accurately predicts the flow through the ADS, the predictions of the VLI-2 valve and ADS valve package pressure drops are not as good. The code calculations follow the data trends but often lie outside the data uncertainty. Figure 5.5-2 shows the predicted and measured pressure drop for the VLI-2 valve (A&M), which indicate scatter, but most points indicate that NOTRUMP underpredicts this valve pressure drop.

The opposite is true for the ADS valve package as seen in Figure 5.5-3. In this case, NOTRUMP overpredicts the ADS valve package pressure drop for most cases. Since NOTRUMP underpredicts the upstream pressure drop, the inlet pressure with the ADS package is higher than the test data, which contributes to an overprediction of the ADS valve package. If the pressure drop is calculated from the inlet to the A&M valve, VLI-2, to downstream of the ADS valve package at PE16W and compared to the NOTRUMP prediction, the overall pressure drop is improved as shown in Figure 5.5-4. Note also, that since the NOTRUMP calculation agrees well with the upstream reservoir (pressurizer) pressure and the downstream reservoir pressure is fixed at a value slightly above atmospheric, NOTRUMP correctly predicts the overall pressure drop and the associated flow (see Figure 5.5-5), but is less accurate for the individual pressure drop across the components.

TABLE 5.5-1
OCCURRENCE OF CRITICAL FLOW

	VLI-2 Valve	ADS Valve
Test 210	No	Yes
Test 212	No	Yes
Test 220	Yes	
Test 240	Yes	No
Test 242	Yes	No
Test 250	No	
Test 320	Yes	No
Test 340	No	

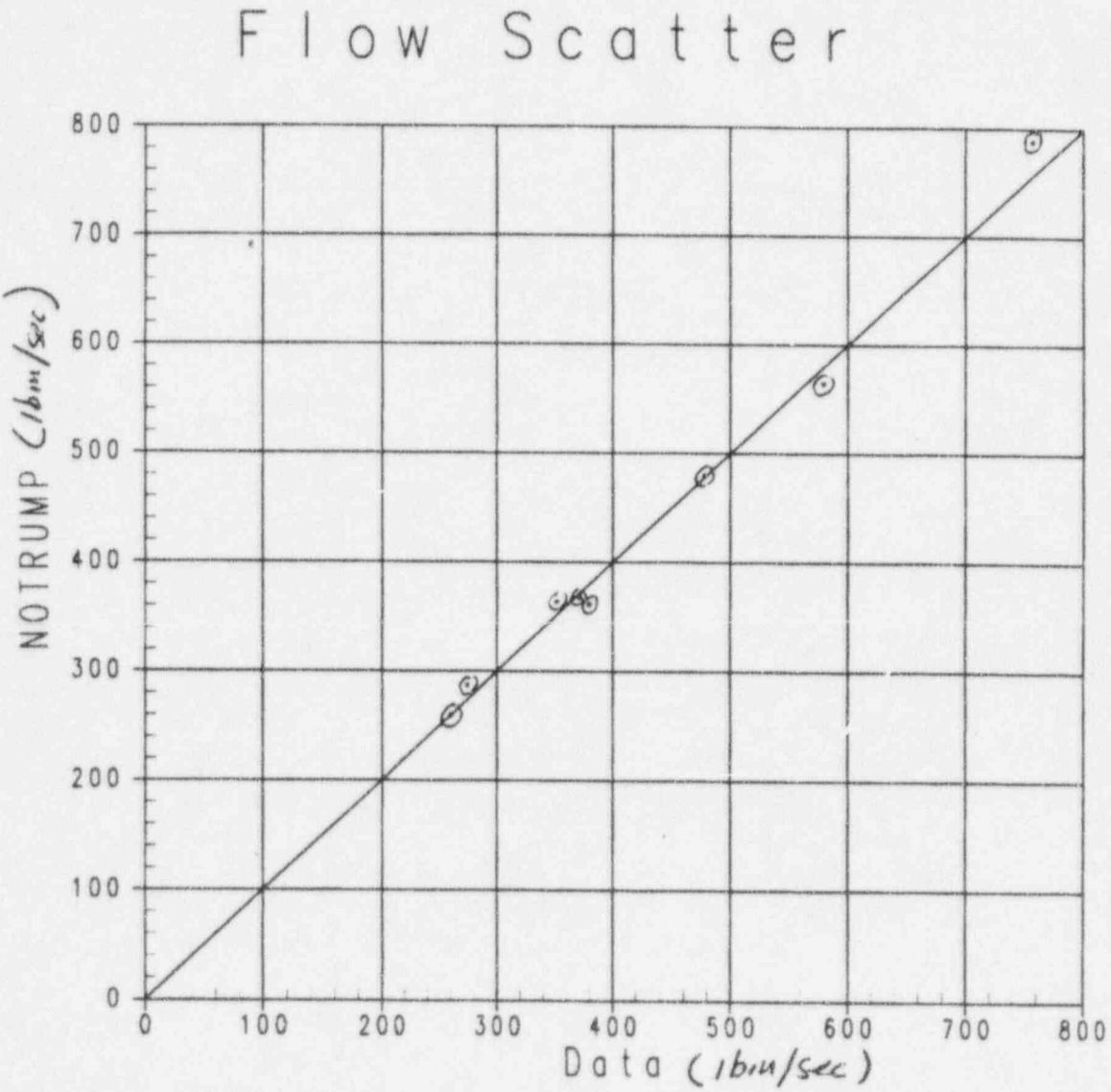

Figure 5.5-1 Overall Comparison of NOTRUMP-Predicted Automatic Depressurization System Flow with Automatic Depressurization System Test Data

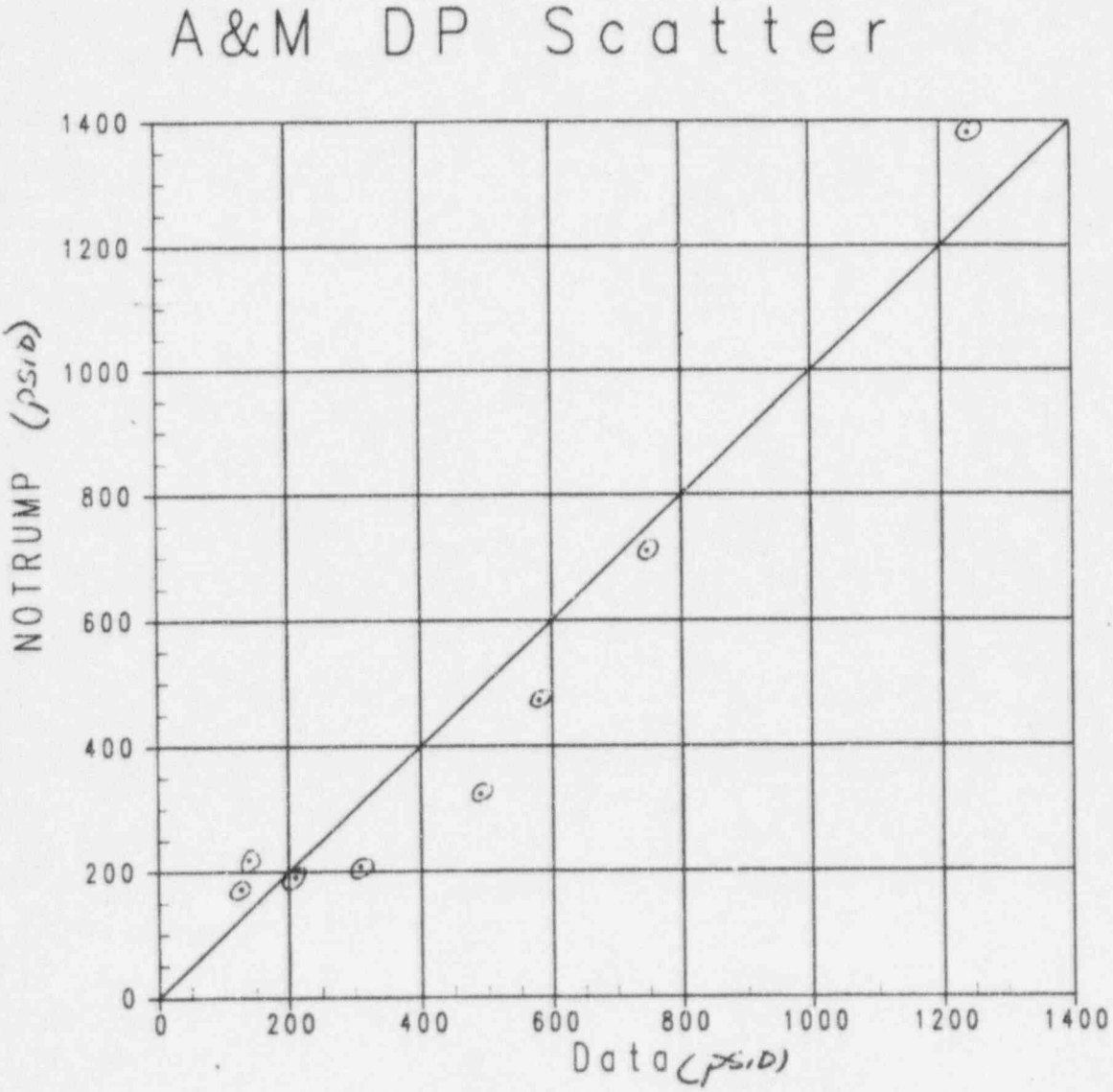

Figure 5.5-2 Overall Comparison of NOTRUMP-Predicted Valve VLI-2 (A&M) Pressure Drop

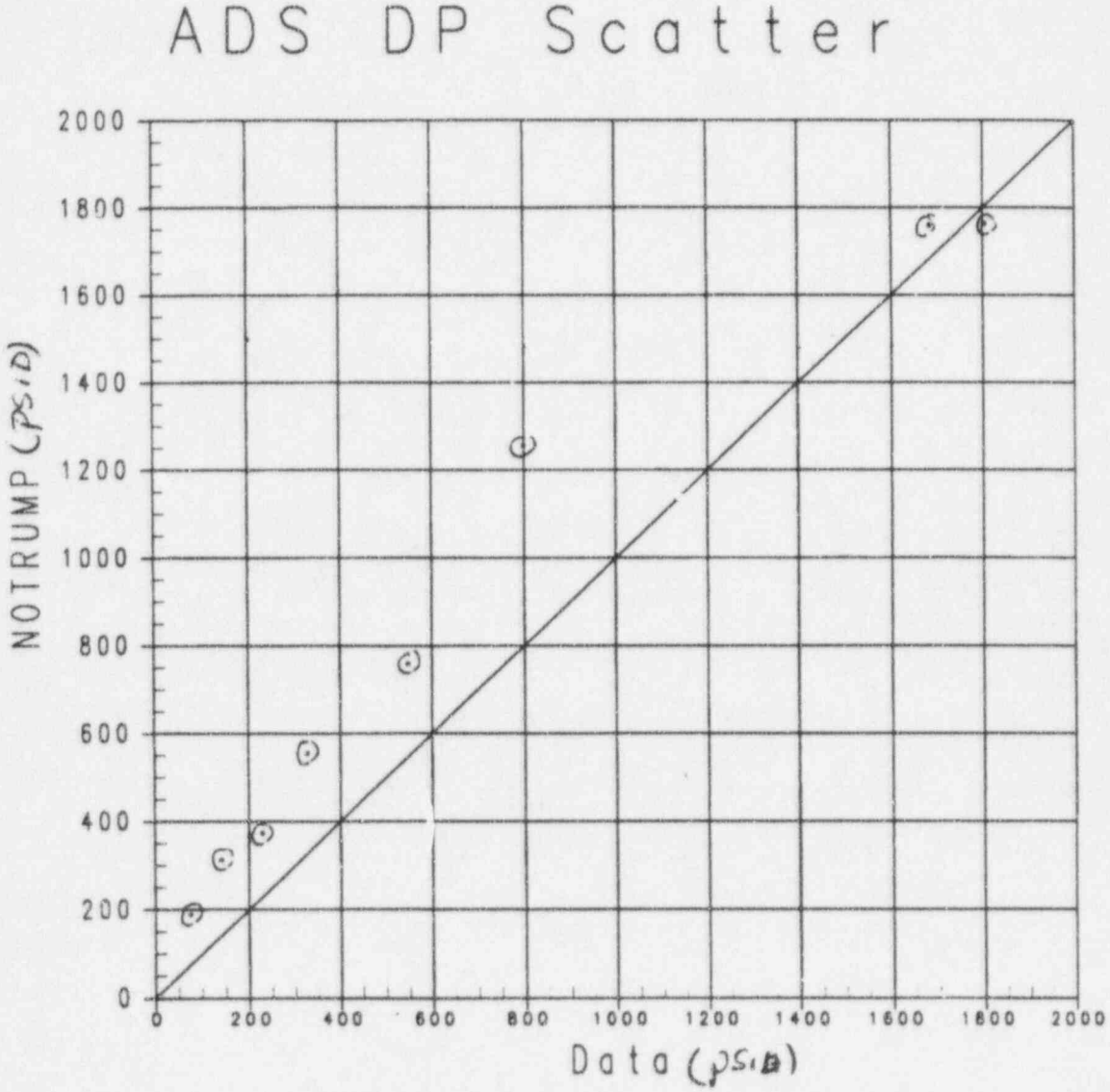

Figure 5.5-3 Overall Comparison of NOTRUMP-Predicted Automatic Depressurization System Valve Package Pressure Drop

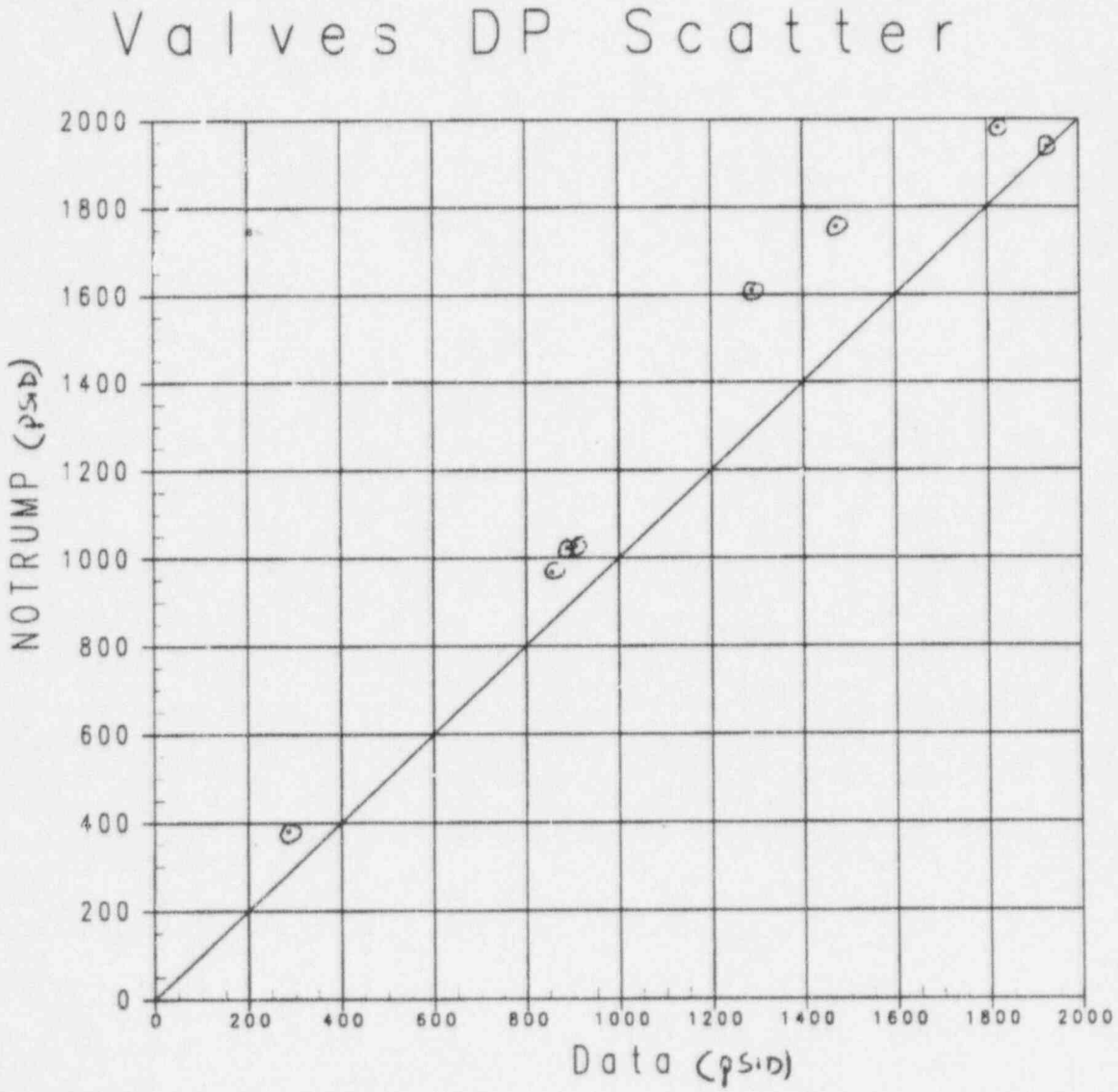

Figure 5.5-4 Overall Comparisons of NOTRUMP-Predicted Combined Valve VLI-2 and Automatic Depressurization System Valves Pressure Drop

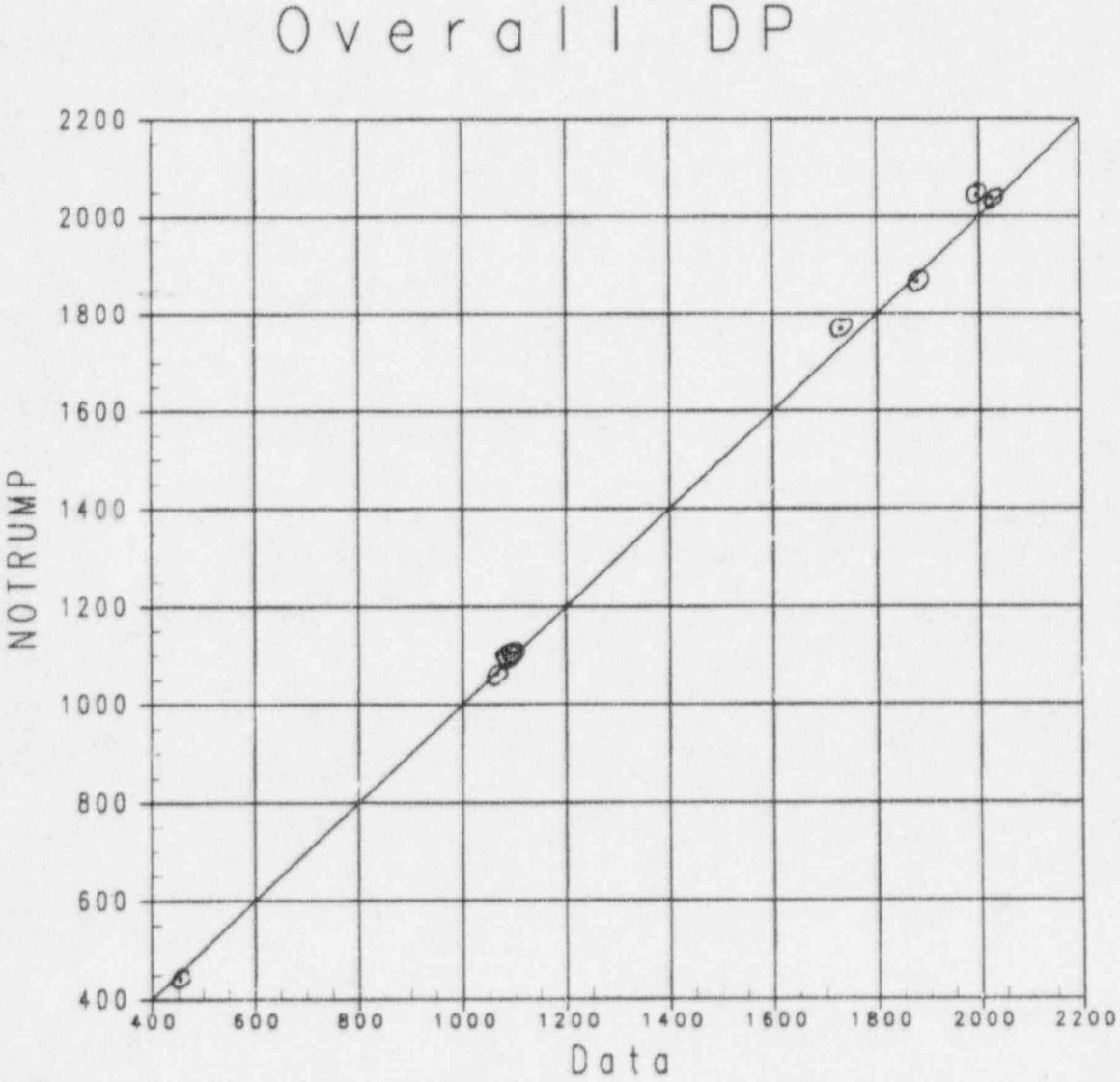

Figure 5.5-5 Overall Comparison of NOTRUMP-Predicted Total Pressure Drop

5.6 Assessment of the Automatic Depressurization System Phenomena Identification and Ranking Table

The small-break LOCA PIRT is given in Table 1-1 and indicates that the ADS 1-3 high ranked items include: ADS critical flow, two-phase pressure drop, and valve loss coefficients for the ADS blowdown period. The valve loss coefficients have been determined from the single-phase water and steam flow tests as well as from manufacturer's data for the particular valves. This parameter is an input condition to the analysis and reflects the specific valve design.

The ADS critical flow was measured in the tests over a range of conditions that bracket the AP600 ADS transient at full scale. The NOTRUMP comparisons to the flow data from the ADS tests is excellent, indicating that the critical flow models in NOTRUMP are appropriate for the calculation of flow through the ADS. This highly ranked PIRT item is fully addressed by the NOTRUMP analysis of the ADS tests.

The NOTRUMP two-phase pressure drop calculations for the ADS piping components are not as precise as the overall system pressure drop. There is underprediction of the upstream control valve and system piping pressure drop, and an overprediction of the pressure drop of the ADS valve package. When the flow is choked in the upstream control valve, the measured and predicted pressure drops across the control valve are larger. NOTRUMP underpredicts the upstream valve and piping pressure drop by 5 percent for pressure drops greater than 500 psid. When the flow in the ADS valve package is choked, the measured and predicted pressure drop are also large. In this case, NOTRUMP overpredicts the pressure drop by 23 percent for pressure drops greater than 500 psid. The overprediction in this case is caused primarily by one test, as seen in Figure 5.5-3. The overall pressure drop is predicted well, as seen in Figure 5.5-5, indicating that NOTRUMP is calculating the correct ADS flow and system pressure drop.

The test data from the ADS 1-3 tests and the analysis of these tests using the NOTRUMP code indicate that these highly ranked ADS items in the PIRT have been addressed for the AP600.

5.7 Conclusions

The NOTRUMP computer code has been compared to six of the 200-series tests and two of the 300-series tests from the ADS Phase B test data. The critical flow model used in NOTRUMP accurately predicts the critical flow at these locations where the flow is observed to be choked within the data uncertainty. The total overall pressure drop is correctly predicted, but the individual component pressure drops are not as accurately predicted by the code. Prediction of the overall pressure drop correctly is consistent with the excellent predictions of the ADS flows.

5.8 References

5-1 Miselis, V. V., A. J. Brockie and J. S. Nitkiewicz, *Facility Description Report AP600 Automatic Depressurization System Phase B1 Tests*, WCAP-14303 (Proprietary), March 1995.

5-2 Zaloudek, F. R., "Steam-Water Critical Flow From High Pressure Systems Interim Report," HW-80535, UC-38, TID-4500 (January 1964).

5-3 Henry, R. E. and H. K. Fauske, "The Two-Phase Critical Flow of One-Component Mixtures in Nozzles, Orifices, and Short Tubes," *Journal of Heat Transfer*, May 1971.

5-4 Yeh, H. C. and L. E. Hochreiter, "AP600 NOTRUMP Automatic Depressurization System Preliminary Validation Report," RCS-GSR-003, April 1995.

5-5 Wallis, G. B., *One-Dimensional Two-Phase Flow*, Chap. 2, McGraw-Hill, New York, 1969a.

5-6 Yeh, H.C., M. J. Loftus, L. E. Hochreiter, A. J. Brockie, *ADS Phase B1 Test Analysis Report*, WCAP-14305 (Proprietary), April 1995.

5-7 Peters, F. W., *Final Data Report for ADS Phase B1 Tests*, WCAP-14324, April 1995.

TABLE OF CONTENTS

LIST OF TABLES

LIST OF FIGURES

LIST OF FIGURES

LIST OF FIGURES

LIST OF FIGURES

LIST OF FIGURES

LIST OF FIGURES

6 NOTRUMP ANALYSIS OF THE CORE MAKEUP TANK TESTS

6.1 Introduction

This section provides the comparisons of the NOTRUMP code calculations for the CMT test data during the circulation period of CMT operation, which is examined in the 500-series (Reference 6-1) CMT tests. In addition, limited comparisons to the 300-series tests are also shown, which are used to confirm the preliminary validation report results. The 300-series tests were analyzed in Reference 6-2 and address the majority of the phenomena identified in the PIRT given as Table 1-1. Comparisons to the 500-series tests complete the analysis of the thermal-hydraulic phenomena, as identified in the CMT phenomena identification ranking table (PIRT) given in Table 6.1-1.

There are two modes of operation for the CMTs: circulation and draining. During the initial phase of a small-break LOCA, steam line break, or steam generator tube rupture event (SGTR), the RCS inventory is still at or near its steady-state value. When an S signal occurs (typically low pressurizer pressure), the reactor coolant pumps trip, and the CMT isolation valves open. With the valves open, there is gravity-driven flow from the CMT to the reactor vessel and a return flow from the cold leg balance line to the top of the CMT. This cycle is the circulation phase of the CMTs. The colder, denser CMT water drives flow into the reactor vessel because of the density difference between the CMT water and the cold leg balance line (approximately 30 percent with T_{cold} at 550°F and CMT water at 120°F). Figure 6.1-1, from the AP600 SSAR calculations (Reference 6-3), shows the calculated CMT draining flow during the circulation period for a 2-in. diameter cold leg break. The flow steadily decreases as the cold CMT water is replaced by hot water from the balance line, thereby decreasing the gravity draining head.

As the break continues to drain the RCS, the cold leg balance line begins to void (see Figure 6.1-2), the circulation flow path is broken, and the CMT drains as the water volume is replaced by steam from the cold leg. This cycle begins the draining mode of the CMT. The CMT injection flow rate is larger in this mode because of the greater density difference between the colder CMT water and the steam or two-phase mixture in the balance line.

Depending on how long the CMT is in the circulation mode, there is a potential for a thick, hot liquid layer to form at the top of the CMT. This layer reduces steam condensation when the CMT transitions into the draining mode. The hot liquid layer can flash as the RCS depressurizes, causing mixing and reducing the effects of condensation in the CMT.

If the break is larger, the circulation period is reduced because the cold leg balance line voids sooner, breaking natural circulation. In this case, the hot liquid layer in the CMT will be thinner or may not exist.

The potential for steam to interact with cold CMT liquid is minimized because the top of the CMT is connected to the cold leg. Some cold leg circulation occurs for nearly all cases during the mode of

operation for the CMT, which heats the liquid at the top of the CMT. Hot water at the top of the CMT reduces the rapid condensation, and the CMT drains more easily.

The CMT scaling report (Reference 6-5) evaluates the key thermal-hydraulic phenomena that are required to be modeled for each type of transient. Table 1-1, taken from that report, indicates the key CMT thermal-hydraulic phenomena that should be modeled for the small-break LOCA. Draining and circulation phases of CMT operation require safety analysis computer code validation. The NOTRUMP analysis of the 500-series CMT tests validates the code for the CMT circulation behavior.

TABLE 6.1-1
PHENOMENA IDENTIFICATION AND RANKING TABLE FOR THE AP600 CORE MAKEUP TANK

Phenomena	Large-Break LOCA	Small-Break LOCA	Main Steam Line Break	Steam Generator Tube Rupture
1) CMT Draining Effects				
– Condensation on cold thick steel surfaces	H	H	L	L
– Transient conduction in CMT walls	H	H	L	L
– Interfacial condensation on CMT water surface	H	H	M	M
– Dynamic effects of steam injection and mixing with CMT liquid and condensate	H	H	M	M
– Thermal stratification and mixing of warmer condensate with cold... CMT water	M	M	M	M
2) CMT Circulation				
– Natural circulation of CMT and cold leg balance line liquid	L	H	H	H
– Liquid mixing of cold leg balance line, condensate, and CMT liquid	L	M	M	M
– Flashing effects of hot CMT liquid layer	L	H	L	L
– CMT wall heat transfer	L	M	M	M

L = Low importance
M = Medium importance
H = High importance

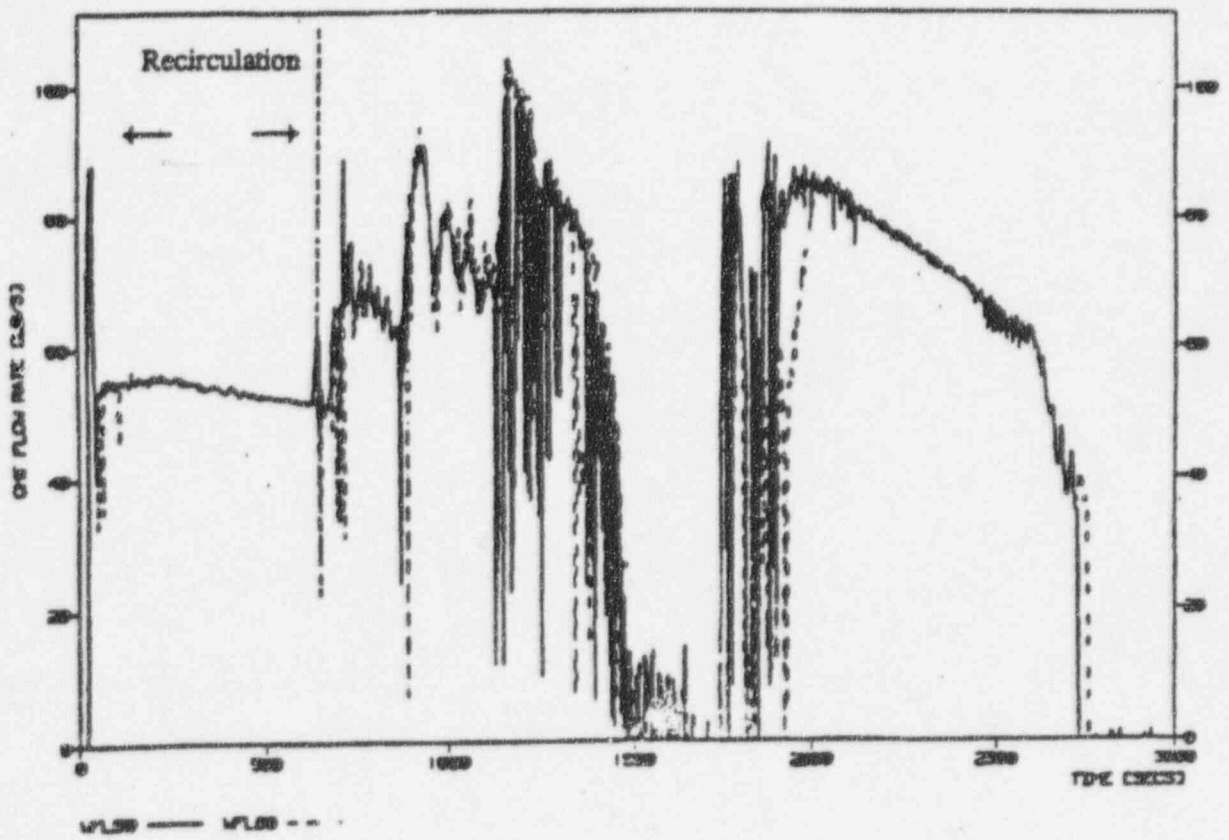

Figure 6.1-1 AP600 SSAR Calculation of Core Makeup Tank Draining Flow for 2-In. Cold Leg Break

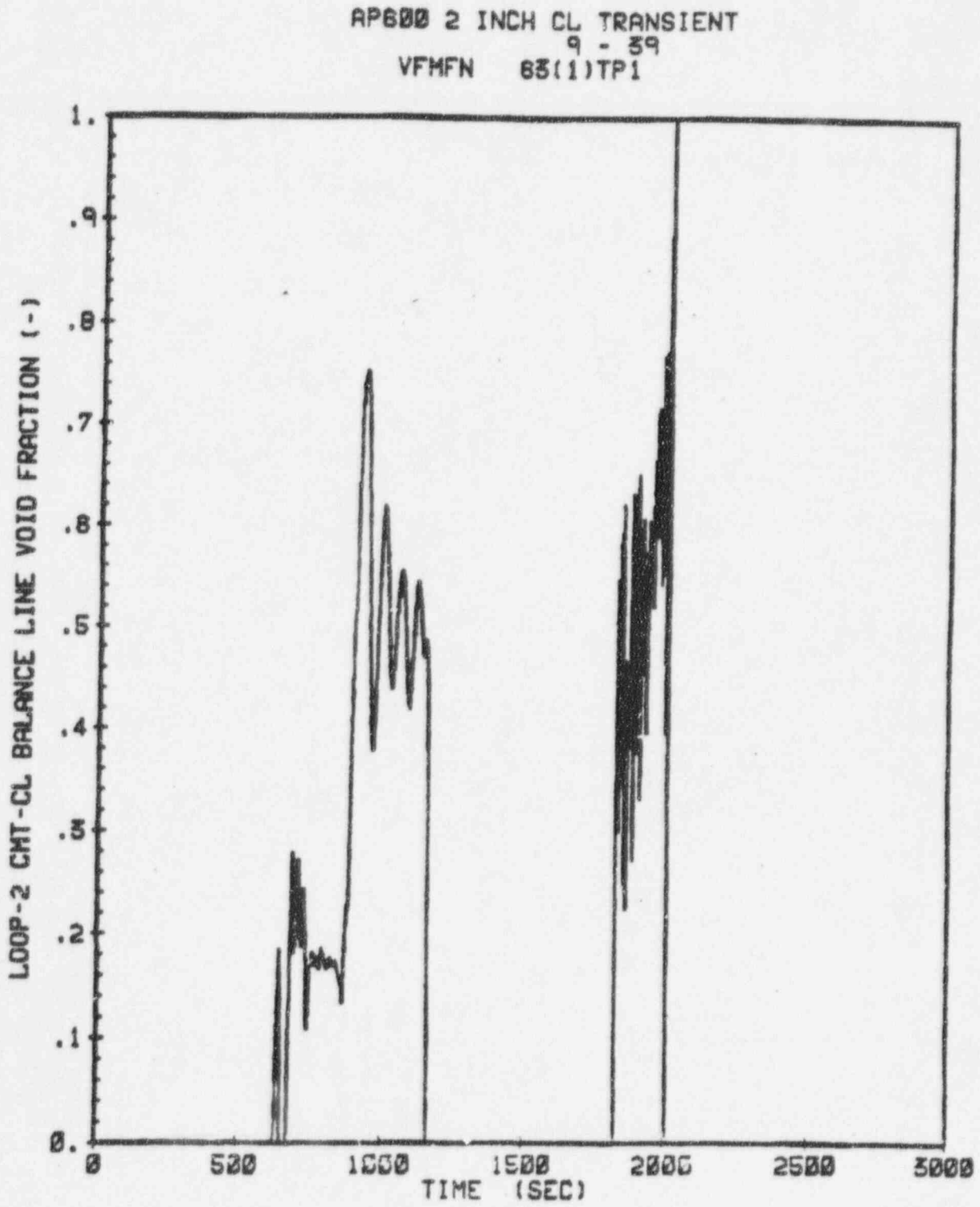

Figure 6.1-2 AP600 SSAR Cold Leg Balance Line Void Fraction for 2-In. Cold Leg Break

6.2 AP600 NOTRUMP Core Makeup Tank Model for 500-Series Tests

6.2.1 Core Makeup Tank Noding Description

The AP600 CMT is modeled using four fluid nodes, (Reference 6-5) as shown in Figure 6.2-1 taken from the AP600 SSAR (Reference 6-3). The volume split between the nodes is: the top node has 10 percent of the CMT volume, the next two nodes each contain 15 percent of the CMT volume, and the last node contains 60 percent of the CMT volume. The cold leg balance line is connected to the top node of the CMT, and the CMT drain line is connected to the bottom-most CMT node. The basis for the noding is to preserve a small volume at the top of the CMT so the water displacement during the circulation phase can be accurately modeled, as well as to retain the coarse noding in regions of the CMT, such as the bottom, where little change occurs. The above four-node CMT was found to give reasonably good comparisons to the 300-series CMT tests in the preliminary report (Reference 6-2). Using four CMT nodes results in a coarse representation of the axial fluid gradient within the CMT.

6.2.2 NOTRUMP Representation of the Core Makeup Tank

The fluid volume is modeled as interior fluid nodes that are connected to the balance line and the drain through flowlinks. The interior fluid node is defined as a fixed-control volume that consists of two regions: a lower mixture region that can contain liquid or a two-phase mixture and an upper region that contains vapor. Thermal equilibrium and spatial uniformity exist within each region, but not necessarily between the two regions. No flow (only mass and energy inventory) is associated with a fluid node. An interior fluid node may be connected with other fluid nodes via flowlinks and with metal nodes via heatlinks, as shown in Figure 6.2-2.

Heatlinks also connect fluid nodes to the CMT. An interior metal node is a fixed control volume containing metal at a uniform temperature and one conservation equation for total internal energy, which is written in terms of the metal temperature. An interior metal node may be connected with fluid nodes via heatlinks. A schematic diagram of an interior metal node is presented in Figure 6.2-3.

6.2.3 NOTRUMP Modeling of Core Makeup Tank Operation

Figure 6.2-4 shows the noding used to model the CMT for the CMT test simulation. The CMT noding used is similar to the SSAR, shown in Figure 6.2-1, with the same percentages used for the test as for the SSAR; however, since the test CMT is 10-ft. high, relative elevations of different nodes in the test are different than in the AP600 plant.

The NOTRUMP model used for the final validation report is different from that used for the preliminary NOTRUMP report for the analysis of the 500-series CMT tests. In the original model, shown in Figure 6.2-4, the full CMT loop was modeled including the steam/water reservoir (S/WR), which was modeled as a single node. It was observed that in the preliminary NOTRUMP calculations, the single-node steam/water reservoir fluid was calculated to mix uniformly with the cold CMT flow

that enters the hot steam/water reservoir as the CMT circulates. As a result of the perfect mixing in the reservoir, the liquid enthalpy flowing into the CMT balance line is lower than the measured value. In reality, as the CMT circulates, cold water from the CMT displaces the hot water in the reservoir and fills the lower portion of the vessel. A steep thermal gradient exists and the flow to the balance line remains hot for a much longer time period. Having a lower circulating temperature flowing into the CMT alters the buoyancy difference between the CMT and the reservoir and affects the predicted CMT circulating flow.

The improved CMT system modeling replaces the junction of the simulated cold leg balance line with a pressure, enthalpy boundary node that is maintained at a constant value at the measured conditions for the duration of the tests. This modeling scheme is shown in Figure 6.2-5. The as-measured system pressure and enthalpy in the steam/water reservoir (S/WR) are used as boundary conditions for the cold leg balance line as a normal boundary node for each test. The as-measured initial liquid temperatures are also used in the CMT, as well as the liquid temperature and pressure in the S/WR. The CMT fluid temperature data are grouped and averaged to establish the condition for each NOTRUMP fluid node in the tank. The measured data are also used to initialize wall temperatures for the CMT and the S/WR.

The test calculation is initialized by programming the drain valve in the CMT drain line and the isolation valve in steam line no. 2 to open. As the valves open and the CMT begins to circulate, hot water from the S/WR flows into the top of the CMT where it displaces the initially cold CMT liquid. The hot water enters the liquid at the top of the tank through the CMT steam distributor in the testing. In the NOTRUMP model, the mixing effect of the diffuser is accomplished by the fluid mixing in the first cell. The CMT diffuser is not explicitly modeled, but it is submerged in the fluid volume of the top cell in the NOTRUMP model. The hot liquid that would enter through the diffuser would mix with the colder liquid present at the top of the CMT. NOTRUMP calculates perfect mixing of the hot liquid from the cold leg pressure balance line, which is similar to what occurs with the diffuser at the top of the CMT.

Since the CMT liquid is initially highly subcooled, the hotter cold leg balance line liquid mixes and displaces the colder water. As the test proceeds, the hot water flows into the CMT remain high, and the volume rate of discharge flow out of the tank equals the volume of the hot water flow from the balance line into the CMT. When the CMT is in the circulation mode, hot water entering the CMT from the cold leg balance line mixes with cold water in the first cell, and a new fluid temperature is calculated. As the circulation and CMT draining process continues, hotter water from the top of the CMT node is transported downward to the nodes below. This fluid mixes with the fluid initially in the node, and a new temperature is calculated. In this process, there is a numerical diffusion of hotter fluid into lower CMT nodes, and any distinct thermal interface between the hotter liquid from the cold leg balance line and initially cold liquid in the CMT is smeared. This effect could be reduced by using more CMT nodes in the model, but it cannot be totally eliminated. The NOTRUMP comparisons to the CMT test data indicate that the calculated thermal diffusion does not have a

significant effect on the CMT circulation flow. The test and analysis proceeds until the thermal diving heads are reduced and the CMT drain rate decreases.

6.2.4 Specific NOTRUMP Models to be Verified

The specific NOTRUMP heat transfer models that are to be verified using the CMT tests include:

- The development of the water temperatures in the CMT
- The circulation behavior of the CMT and prediction of the flows
- The modeling of the hydraulic resistances in the CMT circulation system so the CMT drain flow can be calculated

The circulation behavior of the CMT is compared to the test data to examine the drain flow rate, the development of the CMT heated liquid layers, and the liquid level behavior as the CMT circulates. The CMT fluid thermocouples are grouped and averaged according to the CMT test noding sizes chosen and are compared to the calculated CMT liquid temperature for the specific node. The drain flow from the CMT tests is compared to the measured drain flow, using the pretest system resistance data. Drain flow comparisons indicate the effects of the different thermal centers on the circulation behavior of the NOTRUMP CMT predictions relative to the test data and any effects of the thermal mixing in the CMT.

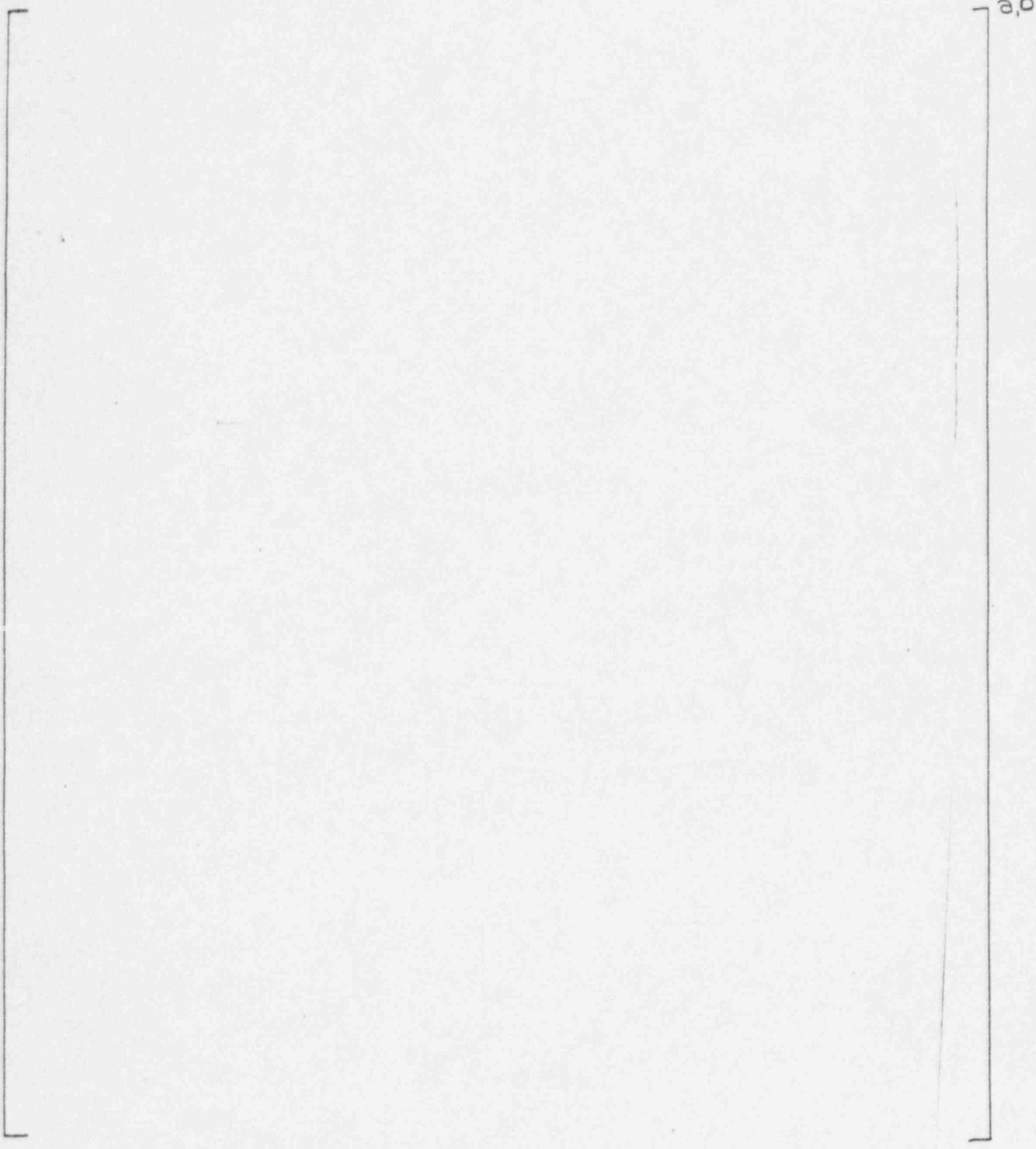

Figure 6.2-1 Detail of NOTRUMP Core Makeup Tank Noding (SSAR)

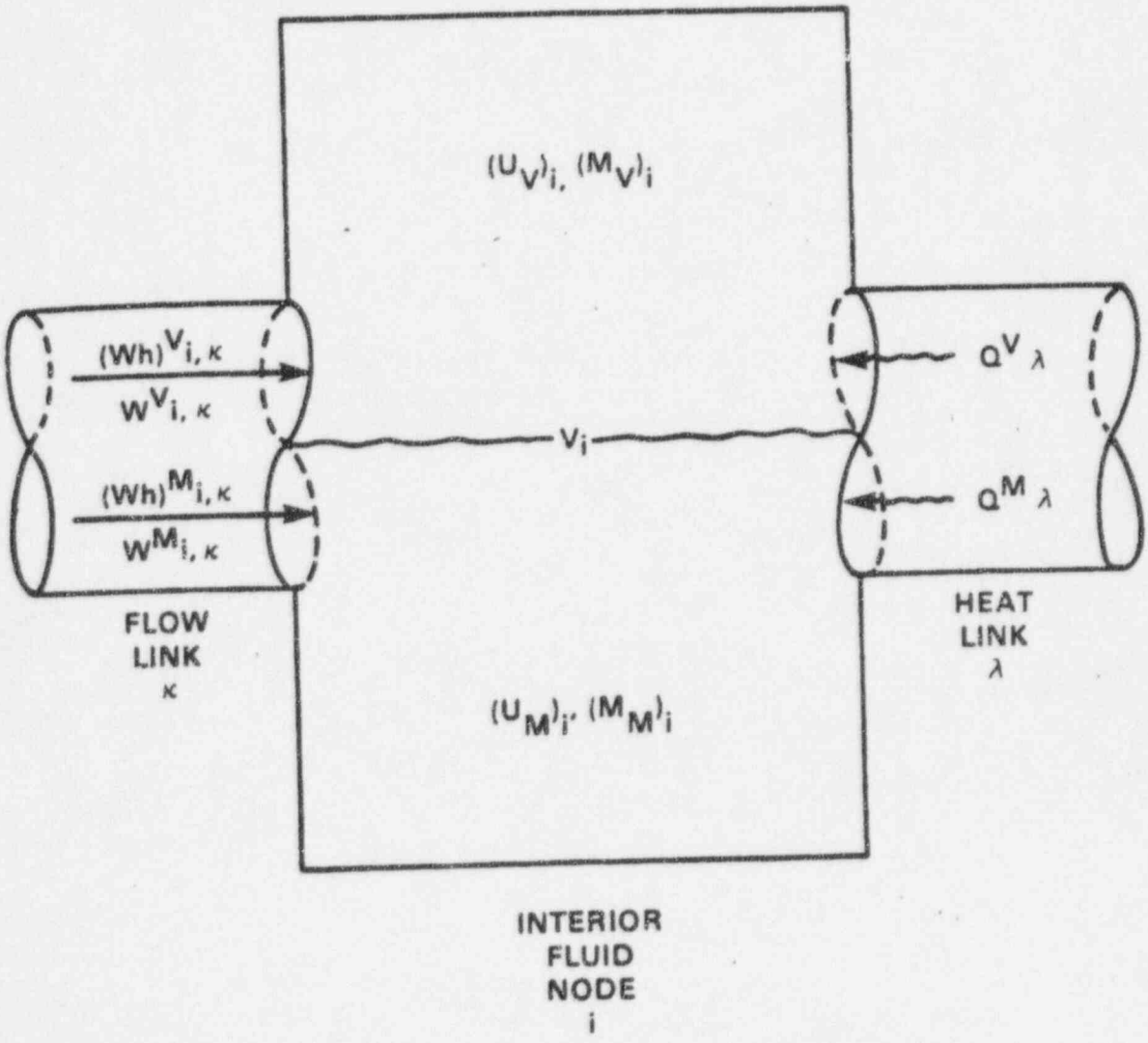

Figure 6.2-2 NOTRUMP Interior Fluid Node

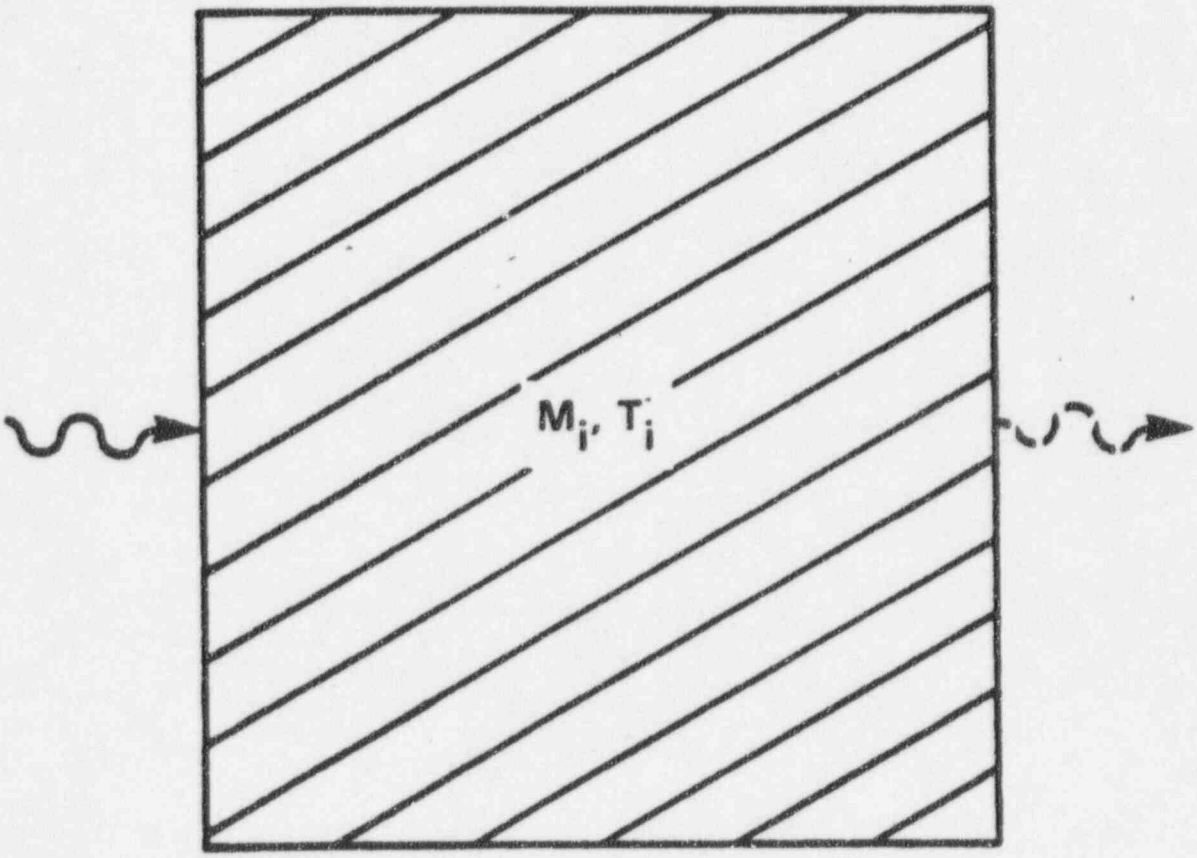

Figure 6.2-3 NOTRUMP Interior Metal Node

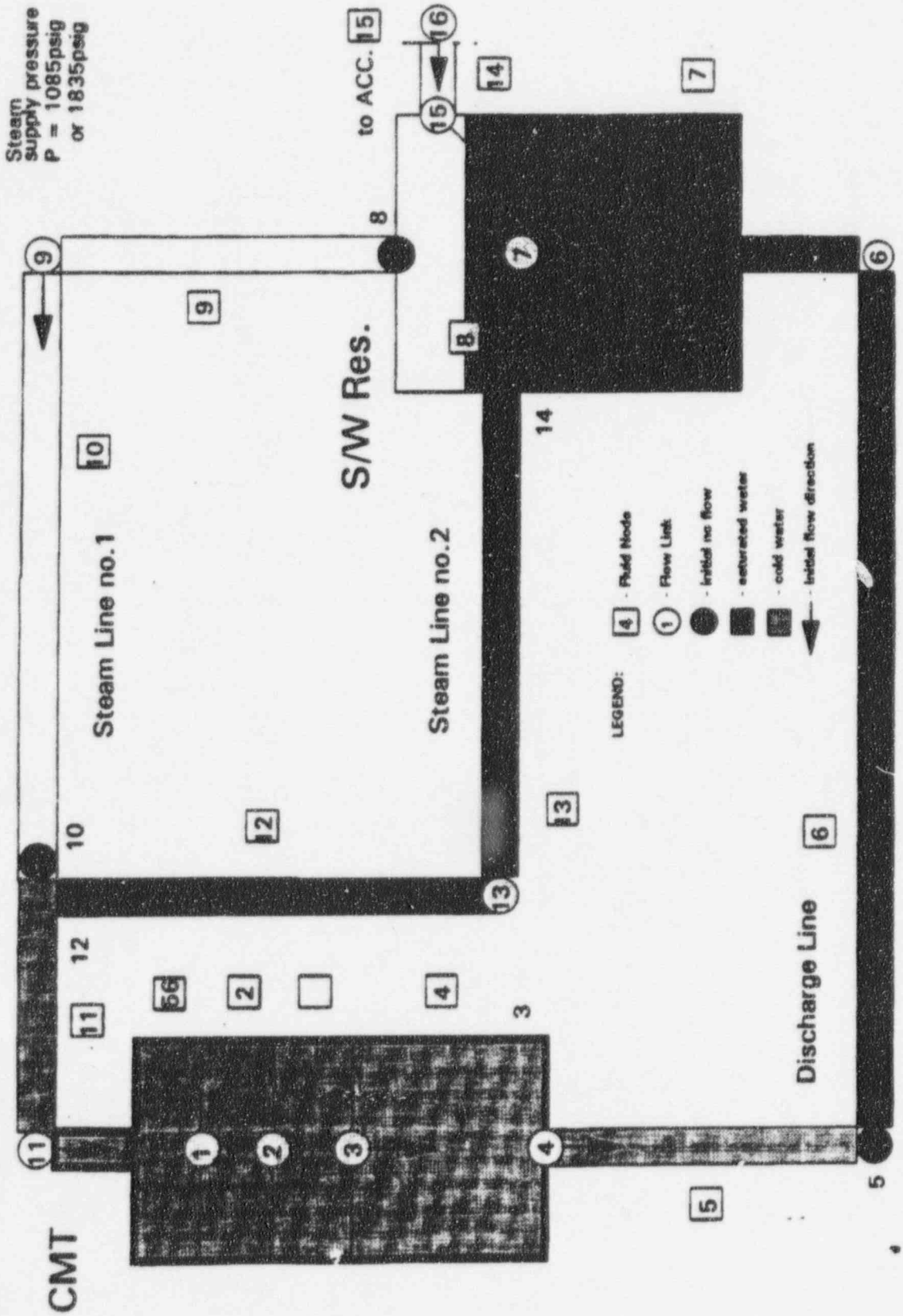

Figure 6.2-4 Core Makeup Tank Test Facility – NOTRUMP Noding Scheme for 500-Series Tests from the Preliminary Validation Report

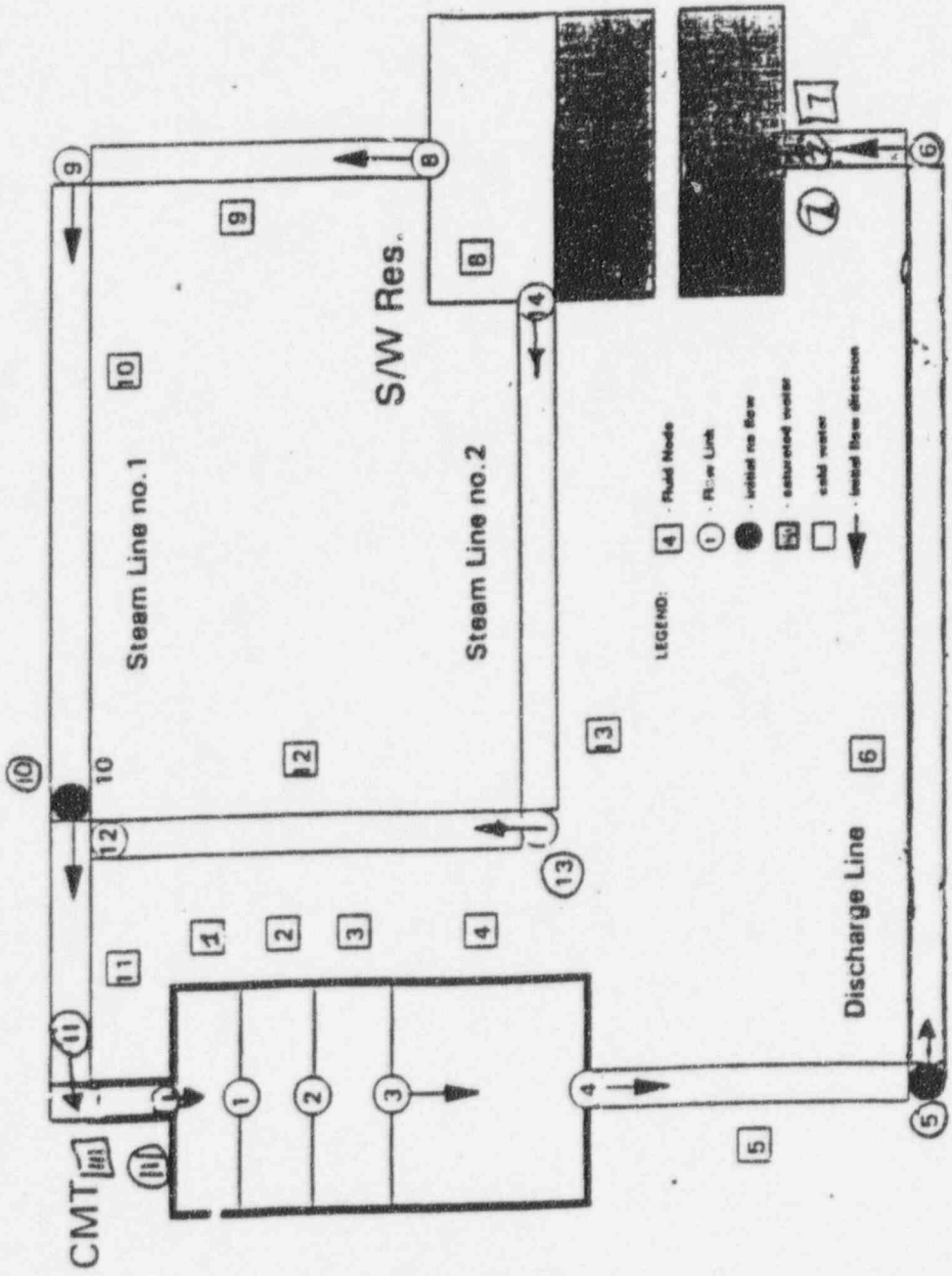

Figure 6.2-5 Final Validation Report NOTRUMP Core Makeup Tank Test Noding

6.3 NOTRUMP Comparisons to the 500-Series Core Makeup Tank Tests

6.3.1 Introduction

The 500-series CMT tests simulated CMT circulation behavior at two different pressures, 1085 psig (1100 psia) and 1835 psig (1850 psia). The tests were performed until a specified portion of the CMT was heated to the inlet steam/water reservoir temperature. The tests were then depressurized at a relatively constant rate to simulate the ADS valve opening. The NOTRUMP simulations concentrate on the circulation period of the tests to examine the development of the hot thermal layers in the CMT and the circulating flow rate between the CMT and the steam/water reservoir. The conditions for the 500-series CMT tests are shown in Table 6.3-1.

When comparing the NOTRUMP calculations to the test data, the uncertainties on the data are either specified on the plot or shown as uncertainty bars. An uncertainty value of two sigma (2σ) is used for the data uncertainty, as determined from the measurement uncertainties specified in the *Core Makeup Tank Final Data Report* (Reference 6-1).

If the core prediction lies within the measurement uncertainties, the agreement is regarded as being "excellent." If the data uncertainty bands are large, then there is less confidence in the code prediction. If the code prediction sometimes lies within the uncertainty bands and follows the same trends as the data, the agreement is regarded as "reasonable." If the data trends are not captured by the prediction and the prediction always lies outside of the data uncertainty, the agreement is regarded as "minimal."

If the code does not have the models to predict the phenomena, this becomes a limitation of the code that must be addressed to determine if the inability to predict the phenomena invalidates the analysis.

TABLE 6.3-1 CORE MAKEUP TANK MATRIX TEST PROGRAM – 500 SERIES				
Test Run Number	**Test Type**	**Approximate CMT Drain Rate (gpm)**	**Steam Supply Pressure (psig)**	**Conditions**
C059502	Natural circ.	16	1085	Natural circ. until 1/5 CMT heated
C061504	Natural circ.	16	1085	Natural circ. until 1/2 CMT heated
C064506	Natural circ.	16	1085	Natural circ. until CMT fully heated
C065506	Drain/depress.	16	1085 followed by depress. to 20	1.5/0.5 psi/sec nominal depress. rate
C066501	Natural circ.	6	1085	Natural circ. until 1/5 CMT heated
C067501	Drain/depress.	6	1085 followed by depress. to 20	1.5/0.5 psi/sec nominal depress. rate
C068503	Natural circ.	6	1085	Natural circ. until 1/2 CMT heated
C069503	Drain/depress.	6	1085 followed by depress. to 20	1.5/0.5 psi/sec nominal depress. rate
C070505	Natural circ.	6	1085	Natural circ. until CMT fully heated
C071505	Drain/depress.	6	1085 followed by depress. to 20	1.5/0.5 psi/sec nominal depress. rate
C072509	Natural circ.	16	1835	Natural circ. until CMT fully heated
C073509	Drain/depress.	16	1835 followed by depress. to 20	1.5/0.5 psi/sec nominal depress. rate
C074508	Natural circ.	16	1835	Natural circ. until 1/2 CMT heated
C075508	Drain/depress.	16	1835 followed by depress. to 20	1.5/0.5 psi/sec nominal depress. rate
C076507	Natural circ.	16	1835	Natural circ. until 1/5 CMT heated
C077507	Drain/depress.	16	1835 followed by depress. to 20	1.5/0.5 psi/sec nominal depress. rate

6.4 NOTRUMP Circulation Behavior Comparisons with the 500-Series Core Makeup Tank Tests

6.4.1 NOTRUMP Comparisons to Core Makeup Tank Tests C059502 and C066501

These are natural circulation tests that were conducted at a system pressure of 1085 psig. The drain valve was assumed to be fully opened, and the tests were terminated when the CMT water was heated so that the top 20 percent of the tank was hot. The drain line resistance was adjusted to give approximately 6 gpm (test C066501) or 16 gpm (test C059502). While the initial drain resistance was set so that the drain flow for test C059502 would have been 16 gpm, the actual flow was lower. Test C059502 is discussed first, followed by test C066501.

Figure 6.4-1 shows the measured system pressure and the pressure used in the NOTRUMP calculation as a boundary condition for test C059502. After the first 500 seconds, the two curves agree within the data uncertainty. The NOTRUMP calculations are shown as dashed lines, and the data are solid lines.

Figure 6.4-2 shows the calculated NOTRUMP CMT liquid temperature in different nodes. There is not a sharp interface in the CMT water temperature due to the numerical diffusion caused by the flow at one temperature in the top cell moving down to the cell below and mixing. Figure 6.4-3 from the *Core Makeup Tank Test and Analysis Report* (Reference 6-6) shows the axial plot of the CMT thermocouples for this test. Early in time there is a definite thermal front that moves down the CMT. This effect is smeared in the NOTRUMP calculation since the higher-temperature liquid appears in the NOTRUMP lower fluid cells earlier than indicated by the data.

Figures 6.4-4 to 6.4-7 show the comparison of the NOTRUMP individual fluid node temperature to the average of the CMT fluid thermocouples contained within that particular node. As these figures indicate, the agreement is good for the top-most node, which is also the smallest node in the model. As the node size increases, the NOTRUMP-calculated fluid temperature increases faster than the average measured temperature for the node due to the numerical diffusion of the hotter CMT water. This increase is particularly true of the bottom-most nodes in the NOTRUMP model, where the liquid in the NOTRUMP nodes heats up at a much faster rate compared to the data. The temperature uncertainty is small (less than 1°F) and is not plotted on the figures. The calculated NOTRUMP temperatures do not agree with the data, but the trends are consistent.

Measured and calculated drain flow comparisons from the CMT are shown in Figure 6.4-8. The test data and NOTRUMP calculations indicate a nearly constant drain flow, and the NOTRUMP calculation is within the data uncertainties for all but the beginning of the test. The integrated drain flow for test C059502 is shown in Figure 6.4-9 and is compared to the integrated NOTRUMP drain flow. As the figure indicates, the NOTRUMP integrated flow is within the uncertainty of the integrated flow rate so that the agreement is excellent.

6.4 NOTRUMP Circulation Behavior Comparisons with the 500-Series Core Makeup Tank Tests

6.4.1 NOTRUMP Comparisons to Core Makeup Tank Tests C059502 and C066501

These are natural circulation tests that were conducted at a system pressure of 1085 psig. The drain valve was assumed to be fully opened, and the tests were terminated when the CMT water was heated so that the top 20 percent of the tank was hot. The drain line resistance was adjusted to give approximately 6 gpm (test C066501) or 16 gpm (test C059502). While the initial drain resistance was set so that the drain flow for test C059502 would have been 16 gpm, the actual flow was lower. Test C059502 is discussed first, followed by test C066501.

Figure 6.4-1 shows the measured system pressure and the pressure used in the NOTRUMP calculation as a boundary condition for test C059502. After the first 500 seconds, the two curves agree within the data uncertainty. The NOTRUMP calculations are shown as dashed lines, and the data are solid lines.

Figure 6.4-2 shows the calculated NOTRUMP CMT liquid temperature in different nodes. There is not a sharp interface in the CMT water temperature due to the numerical diffusion caused by the flow at one temperature in the top cell moving down to the cell below and mixing. Figure 6.4-3 from the *Core Makeup Tank Test and Analysis Report* (Reference 6-6) shows the axial plot of the CMT thermocouples for this test. Early in time there is a definite thermal front that moves down the CMT. This effect is smeared in the NOTRUMP calculation since the higher-temperature liquid appears in the NOTRUMP lower fluid cells earlier than indicated by the data.

Figures 6.4-4 to 6.4-7 show the comparison of the NOTRUMP individual fluid node temperature to the average of the CMT fluid thermocouples contained within that particular node. As these figures indicate, the agreement is good for the top-most node, which is also the smallest node in the model. As the node size increases, the NOTRUMP-calculated fluid temperature increases faster than the average measured temperature for the node due to the numerical diffusion of the hotter CMT water. This increase is particularly true of the bottom-most nodes in the NOTRUMP model, where the liquid in the NOTRUMP nodes heats up at a much faster rate compared to the data. The temperature uncertainty is small (less than 1°F) and is not plotted on the figures. The calculated NOTRUMP temperatures do not agree with the data, but the trends are consistent.

Measured and calculated drain flow comparisons from the CMT are shown in Figure 6.4-8. The test data and NOTRUMP calculations indicate a nearly constant drain flow, and the NOTRUMP calculation is within the data uncertainties for all but the beginning of the test. The integrated drain flow for test C059502 is shown in Figure 6.4-9 and is compared to the integrated NOTRUMP drain flow. As the figure indicates, the NOTRUMP integrated flow is within the uncertainty of the integrated flow rate so that the agreement is excellent.

A similar set of plots (see Figures 6.4-10 to 6.4-18) are shown for test C066501, which is a 1085-psig circulation test but with a different flow resistance in the CMT discharge line. The same behavior is observed for this test as for test C059502. The NOTRUMP-predicted temperatures do not agree well with the data except the top node in the CMT; this nodal temperature is outside the temperature uncertainty. The NOTRUMP calculations do agree with the data trends and behavior, thus they are considered to be reasonable.

The NOTRUMP comparisons to the CMT drain flow are shown in Figure 6.4-17 and indicate a higher predicted flow rate, which lies above the data uncertainty until the end of the test. The same behavior is seen in Figure 6.4-18 for the integrated flow rate for the test as compared to the NOTRUMP calculation. Since the code predictions and the data trends are similar, this agreement is reasonable.

6.4.2 NOTRUMP Comparisons to Core Makeup Tank Tests C061504 and C068503

Test C068503 and C061504 are similar to tests C066501 and C059502, with the exception that the CMT was allowed to recirculate until the water in the CMT was approximately one-half heated. Pressure for this test was 1085 psig (1100 psia). Test C068503 had the CMT discharge line resistance set so that the circulating flow would be approximately 6 gpm, while in test C061504, the resistance was set for 16 gpm. Test C061504 is discussed first, followed by test C068503.

Pressure at the top of the CMT is shown in Figure 6.4-19 for test C061504 and indicates that the NOTRUMP code remains at the fixed initial pressure while the test drifted slightly higher (approximately 50 psia) toward the end of the test. The upward drift results in the NOTRUMP calculation being outside of the test pressure uncertainty.

The NOTRUMP-calculated axial temperature distribution for the different fluid nodes is shown in Figure 6.4-20 and indicates that numerical diffusion is causing heating of the fluid in the lower computational cells similar to the other tests. The measured fluid temperature distribution for this test is shown in Figure 6.4-21, which indicates less diffusion and more of a thermal front moving through the CMT.

The individual calculated NOTRUMP CMT fluid temperatures for each hydraulic cell are shown in Figures 6.4-22 to 6.4-25. The comparison of the upper two NOTRUMP hydraulic cells is good. The lower two hydraulic cells have higher temperatures, early in time, due to the numerical diffusion caused by the numerical diffusion in the code. The NOTRUMP temperature predictions are outside the temperature uncertainty (~1°F); however, the predictions do follow the data trends and are reasonable.

The comparisons of the calculated CMT drain flow and the measured CMT drain flow are shown in Figure 6.4-26. NOTRUMP correctly calculates the measured initial drain flow value, then shows a gradual decrease as the CMT heats up and the initially colder water is gradually displaced by the hot water from the simulated cold leg balance line. The NOTRUMP calculation lies within the flow rate

uncertainty and is considered to be in excellent agreement with the test data. The integrated flow is shown in Figure 6.4-27 and is also seen to be in excellent agreement.

A similar set of comparisons for test C068503 are shown in Figures 6.4-28 to 6.4-36. The pressure agreement for this test is excellent as shown in Figure 6.4-28. The temperature behavior predicted by NOTRUMP shows the same behavior as the tests and the agreement is the best for the top node of the CMT. The lower-most two nodes show the effects of the numerical thermal diffusion.

The circulating flow rate comparison is shown in Figure 6.4-35 and indicates that the NOTRUMP-calculated value lies below the data, within the uncertainties, then crosses the data. It should be noted that the flowmeter was initially not functioning at the beginning of the test. The calculation and data trends are similar, therefore, the comparison is reasonable. The same behavior is seen in the integrated flow comparison in Figure 6.4-36. The integrated flow values agree better, indicating that the NOTRUMP calculation agrees with the data trend.

6.4.3 NOTRUMP Comparisons to Core Makeup Tank Tests C064506 and C070505

These CMT tests were performed at 1085 psig (1100 psia), and the CMT was allowed to recirculate until the tank was fully heated. Test C070505 had the discharge line resistance set so that the nominal circulating flow would be 6 gpm, while test C064506 had the line resistance set for a nominal 16 gpm. Test C064506 is discussed first, followed by test C070505.

Pressure at the top of the tank for test C064506 is shown in Figure 6.4-37 and indicates good agreement between the code and the data.

The calculated NOTRUMP fluid temperatures are shown in Figure 6.4-38 and indicate that the tank heatup and numerical thermal diffusion effects are similar to that seen in other tests. The axial distribution of the measured fluid temperatures is shown in Figure 6.4-39 and indicates that there is a thermal front moving down the tank as it heats up.

The individual fluid temperatures for the different hydraulic cells is shown in Figures 6.4-40 to 6.4-43 for each cell. The calculated NOTRUMP fluid temperatures reasonably agree, and the tank heats completely. Only the lower-most node in the NOTRUMP calculation indicates a difference at the end of the test.

Comparisons of the NOTRUMP-calculated drain flow and the measured drain flow from the CMT are shown in Figure 6.4-44. As this figure indicates, the NOTRUMP calculation agrees with the measured drain flow within the test data uncertainty.

The change in the slope of the data drain flow at approximately 700 seconds is due to the penetration of the CMT thermal front to the bottom of the CMT. This can be confirmed by examining Figure 6.4-39, the third plot down from the top, which shows that at approximately 680 seconds, the

hot water reaches the bottom of the tank. Since NOTRUMP smears the temperatures in the CMT, this inflection in the drain flow is not observed in the calculation. The integrated drain flow agrees well between the NOTRUMP calculation and the integral of the drain flow measurement, as seen in Figure 6.4-45.

A similar set of comparison plots for test C070505 are shown in Figures 6.4-46 to 6.4-54. The NOTRUMP calculation agrees well with the circulating flow data as seen in Figure 6.4-53 and lies within the data uncertainty. A similar behavior is seen for the integral flow comparison in Figure 6.4-54. Again, the agreement is excellent.

6.4.4 Comparisons of the NOTRUMP Circulation Behavior with the 500-Series CMT Tests at 1835 psig (1850 psia)

The 1835-psig CMT circulation tests were performed in the same manner as the 1085-psig tests. The CMT was allowed to recirculate until it was heated to 20 percent in test C076507, 50 percent in test C074508, and the CMT was fully heated in test C072509. The same set of figures are shown for each of the 1835-psig cases as were shown for the 1085-psig cases.

Figures 6.4-55 to 6.4-63 show the comparisons for test C076507. The flow comparisons in Figure 6.4-62 indicate that the NOTRUMP prediction agrees well with the CMT circulation flow and lies within the data uncertainty. Similar behavior is seen in tests C074508 and C072509 (see Figures 6.4-64 to 6.4-82). The NOTRUMP calculation for the drain flow lies within the data uncertainty for test C074508 and outside of the test data at the end of the test for test C072509. The inflection observed in the data circulating flow rate is due to the hot water reaching the bottom of the CMT.

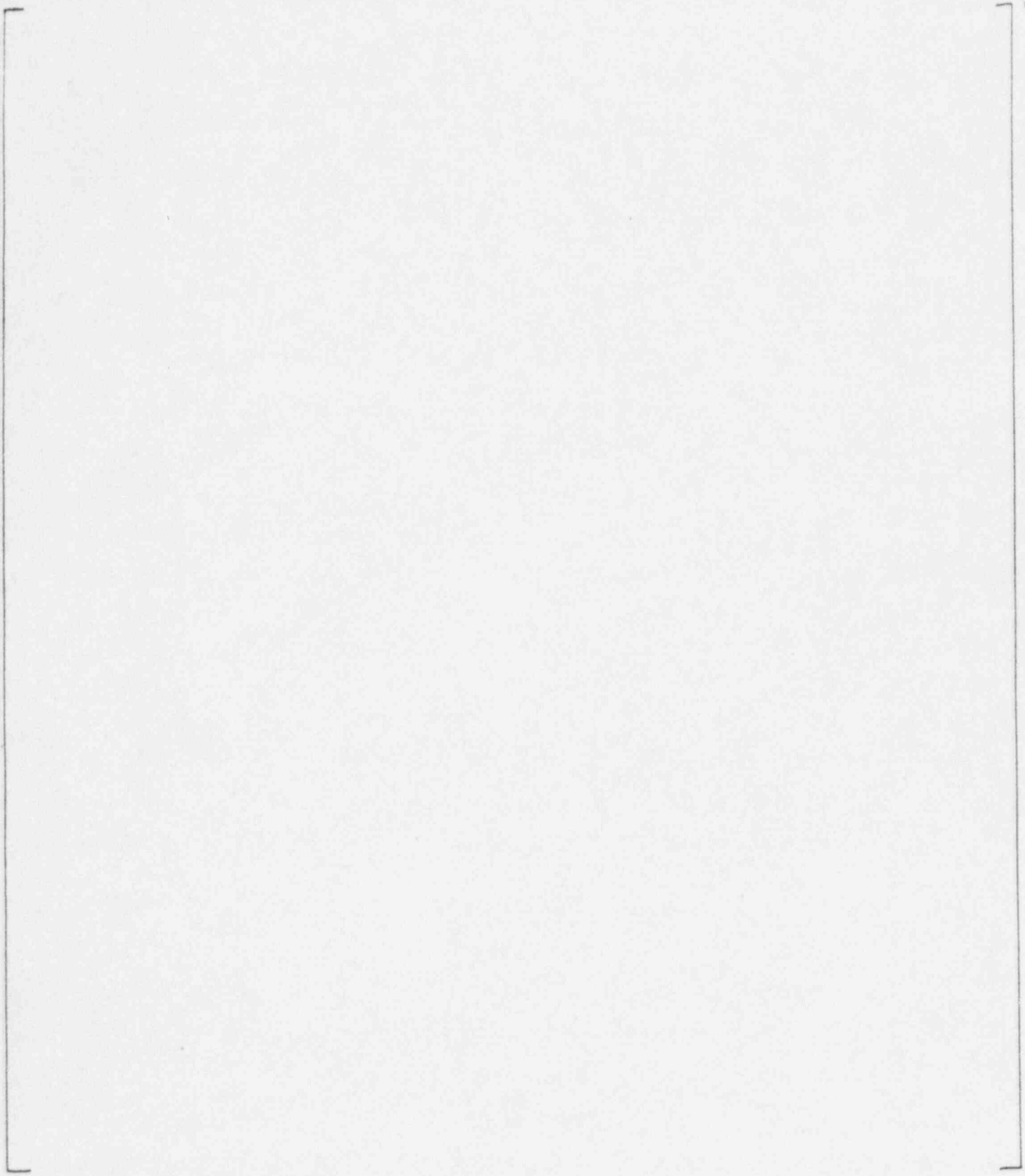

Figure 6.4-1 NOTRUMP Comparisons to Core Makeup Tank Pressure for Test C059502

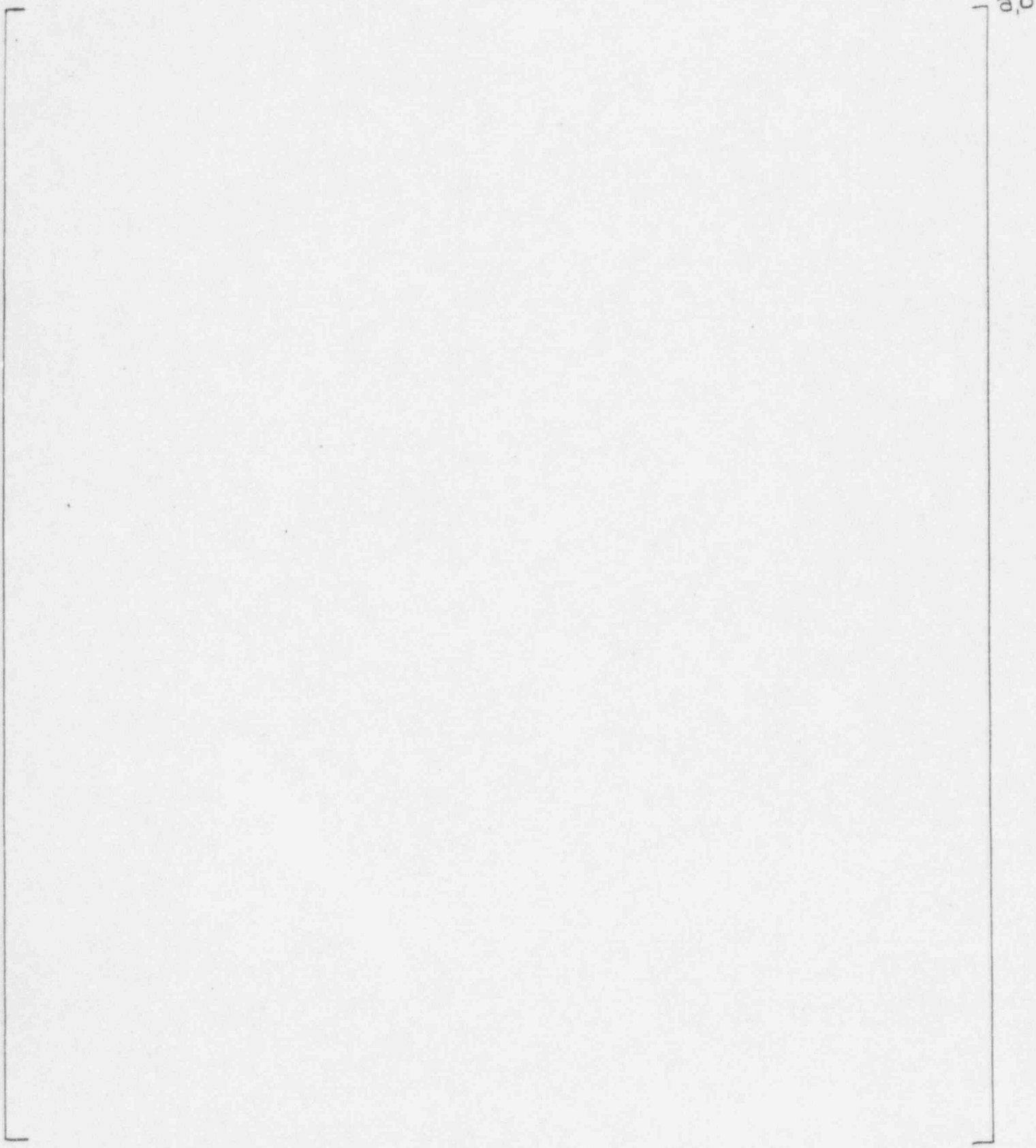

Figure 6.4-2 NOTRUMP-Calculated Core Makeup Tank Fluid Node Temperatures for Test C059502

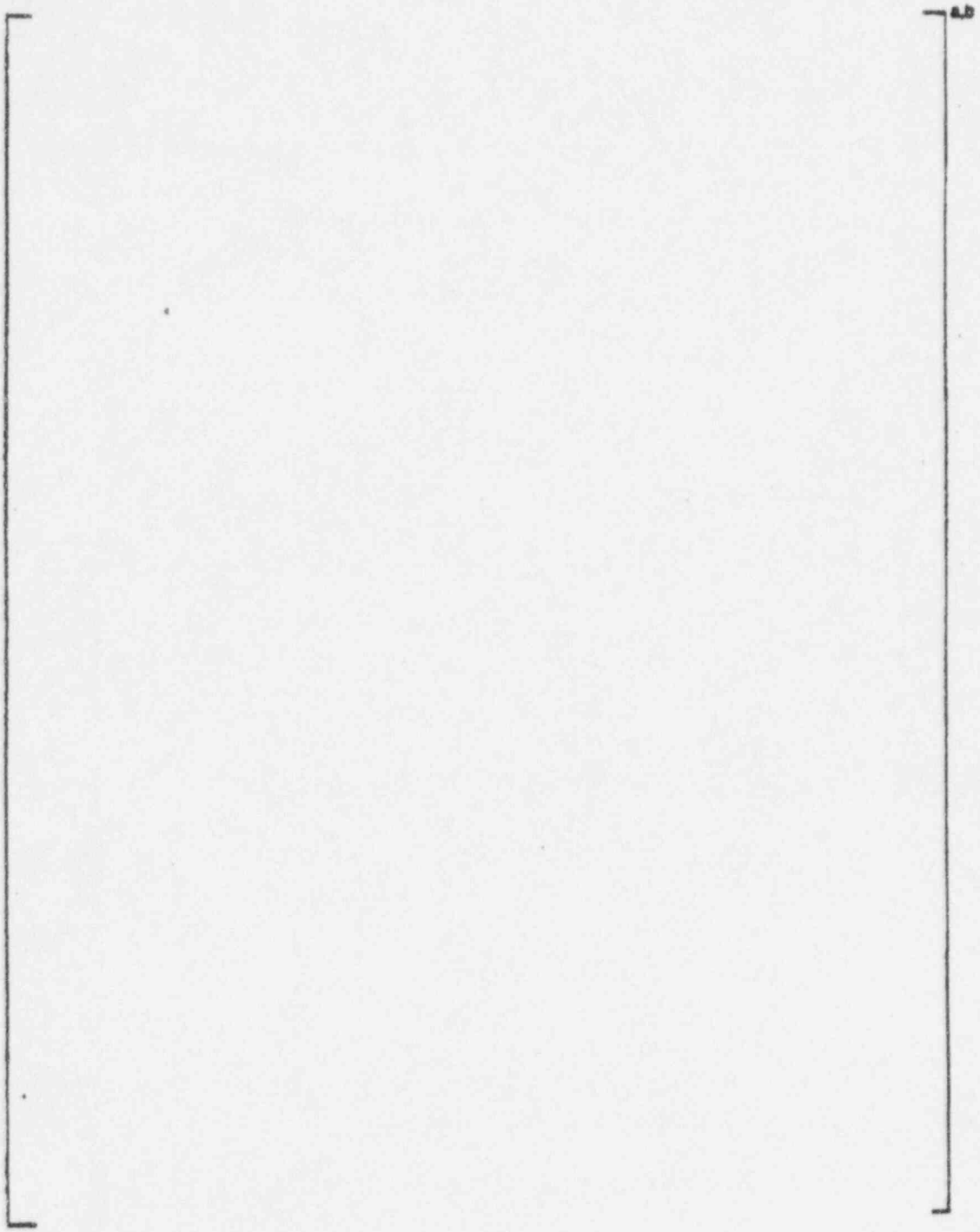

Figure 6.4-3 Core Makeup Tank Axial Fluid Temperatures for Test C059502

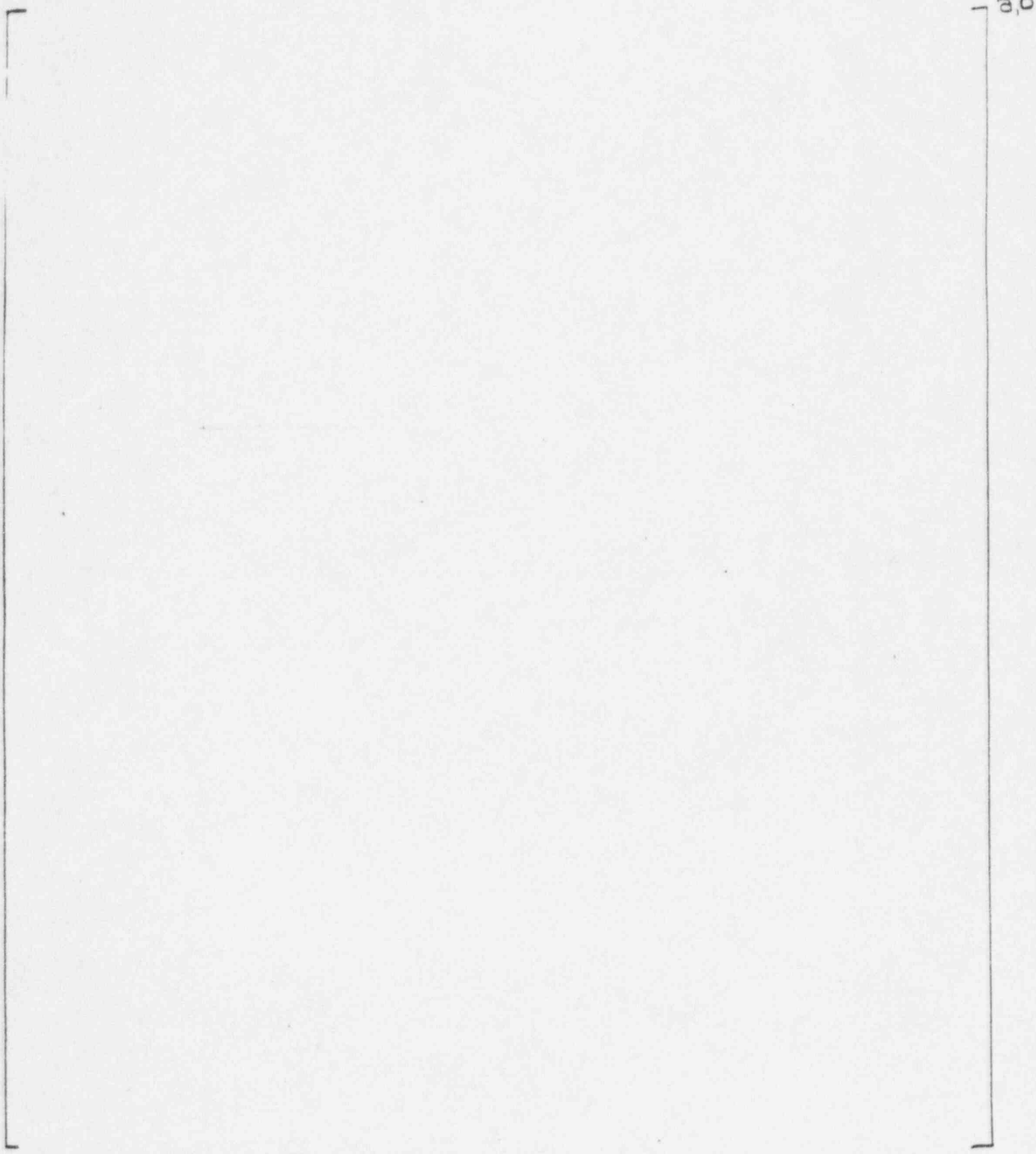

Figure 6.4-4 NOTRUMP Comparisons to Core Makeup Tank Top Node for Test C059502

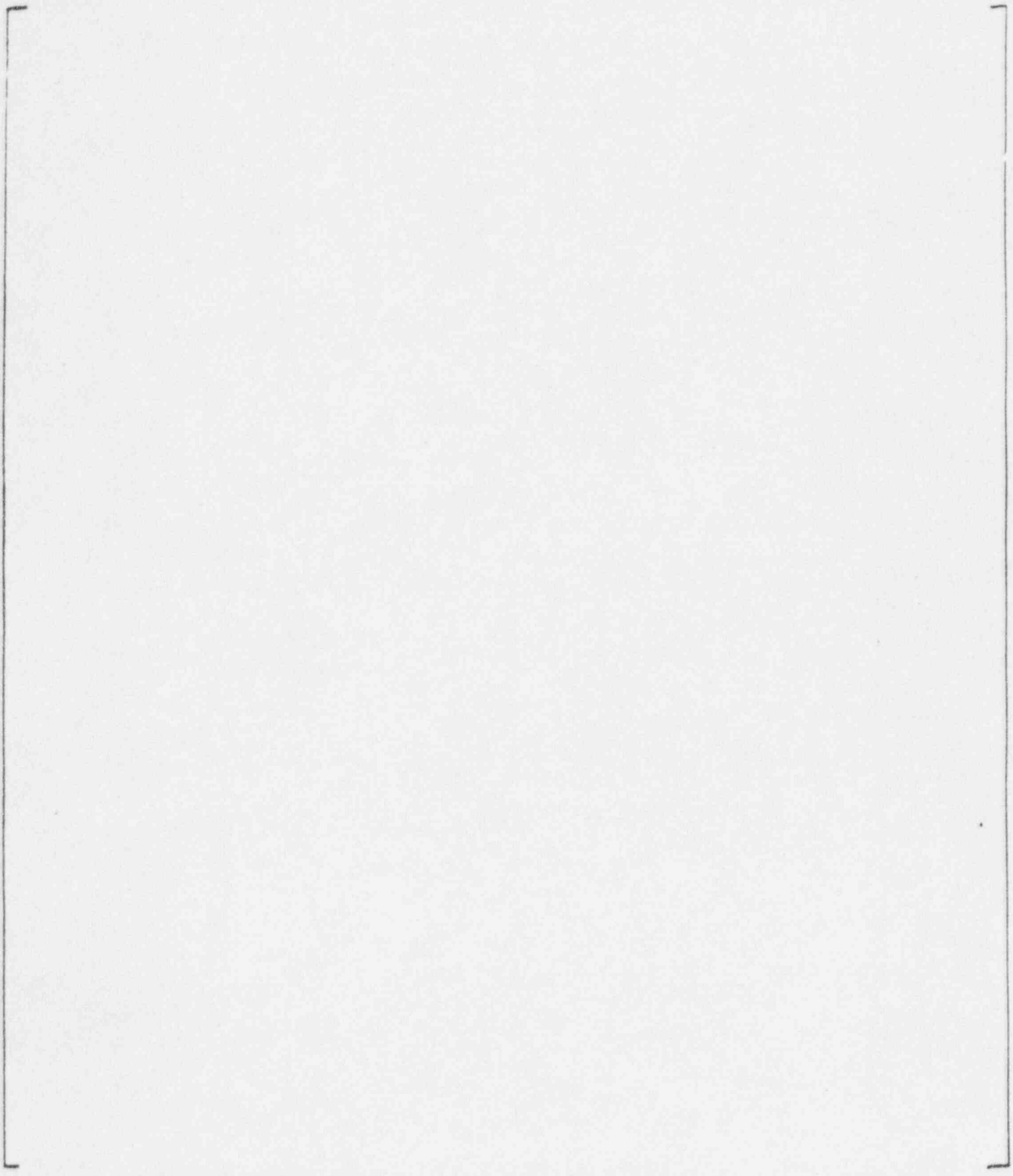

Figure 6.4-5 NOTRUMP Comparisons to Core Makeup Tank Top Cylindrical Node for Test C059502

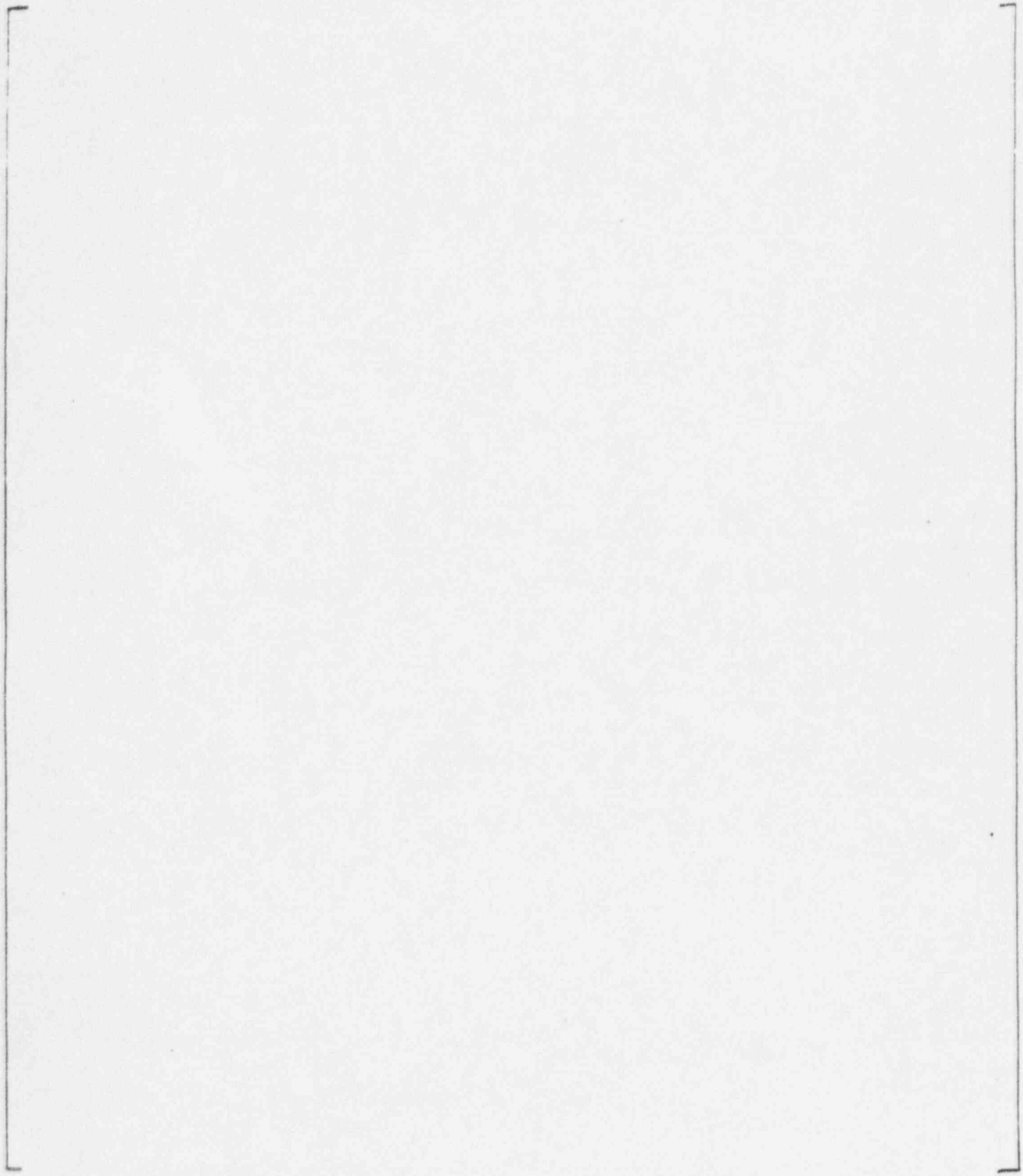

Figure 6.4-6 NOTRUMP Comparisons to Core Makeup Tank Bottom Cylindrical Node for Test C059502

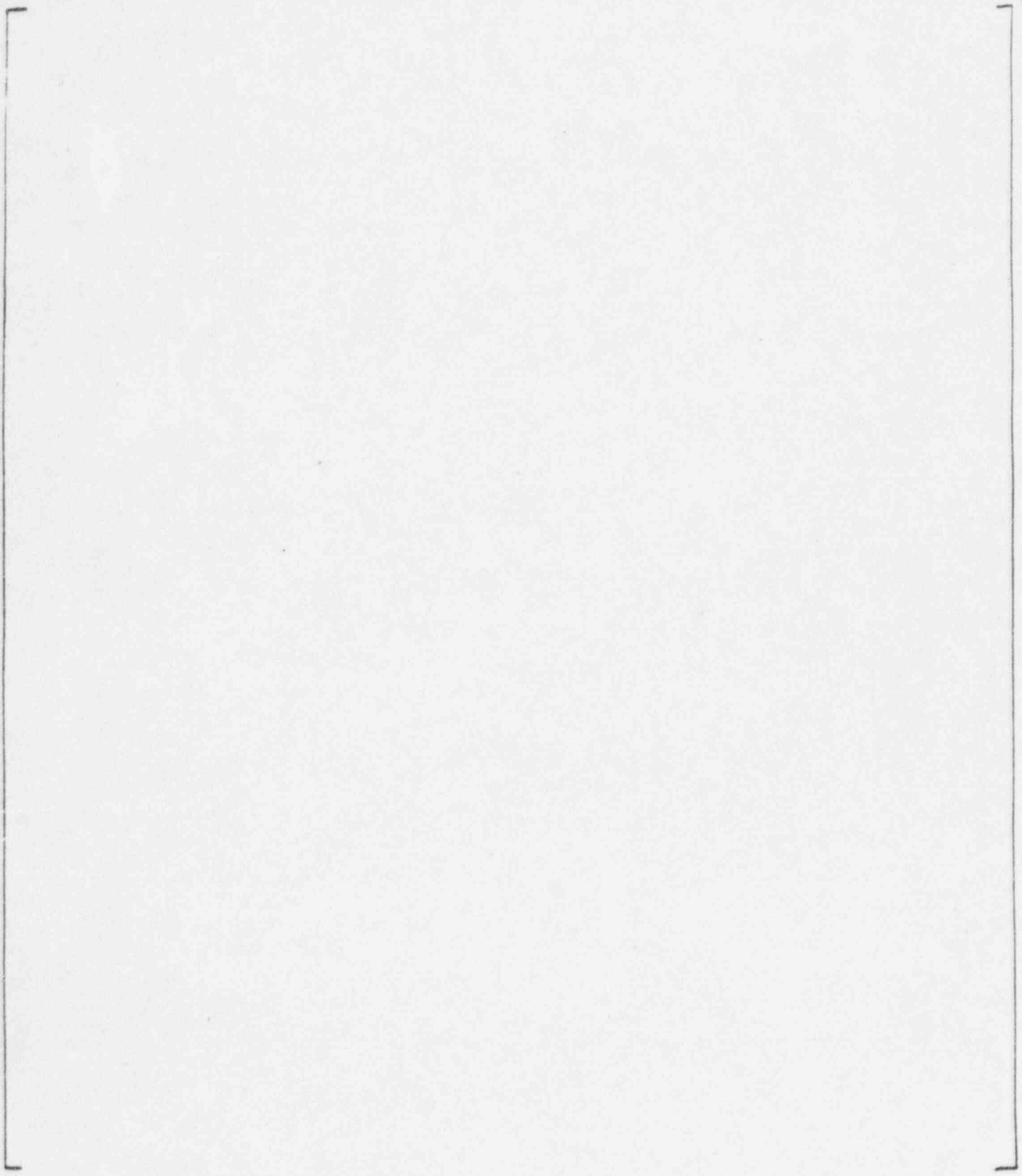

Figure 6.4-7 NOTRUMP Comparisons to Core Makeup Tank Bottom-Most Node for Test C059502

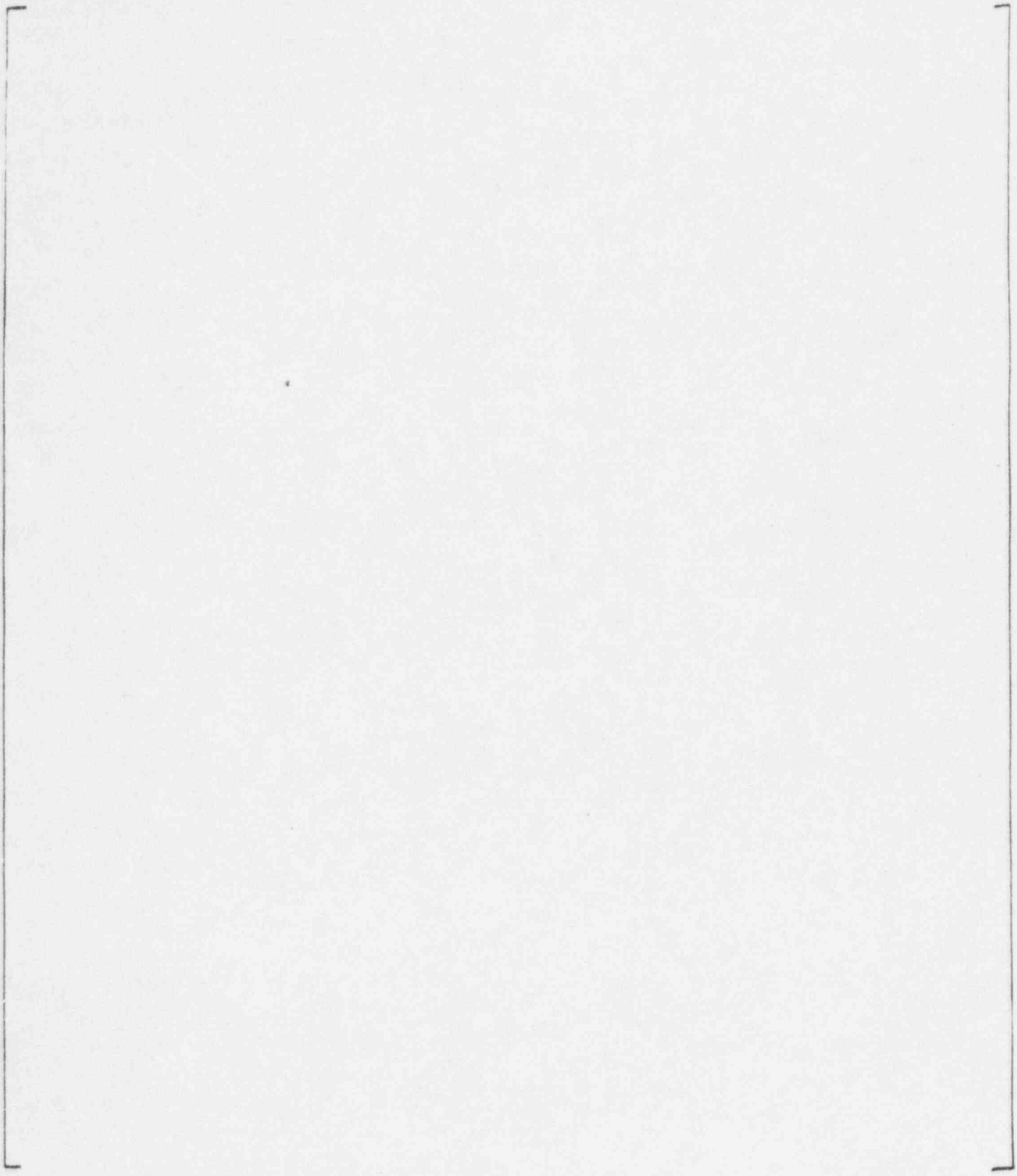

Figure 6.4-8 NOTRUMP Comparisons for Core Makeup Tank Drain Flow for Test C059502

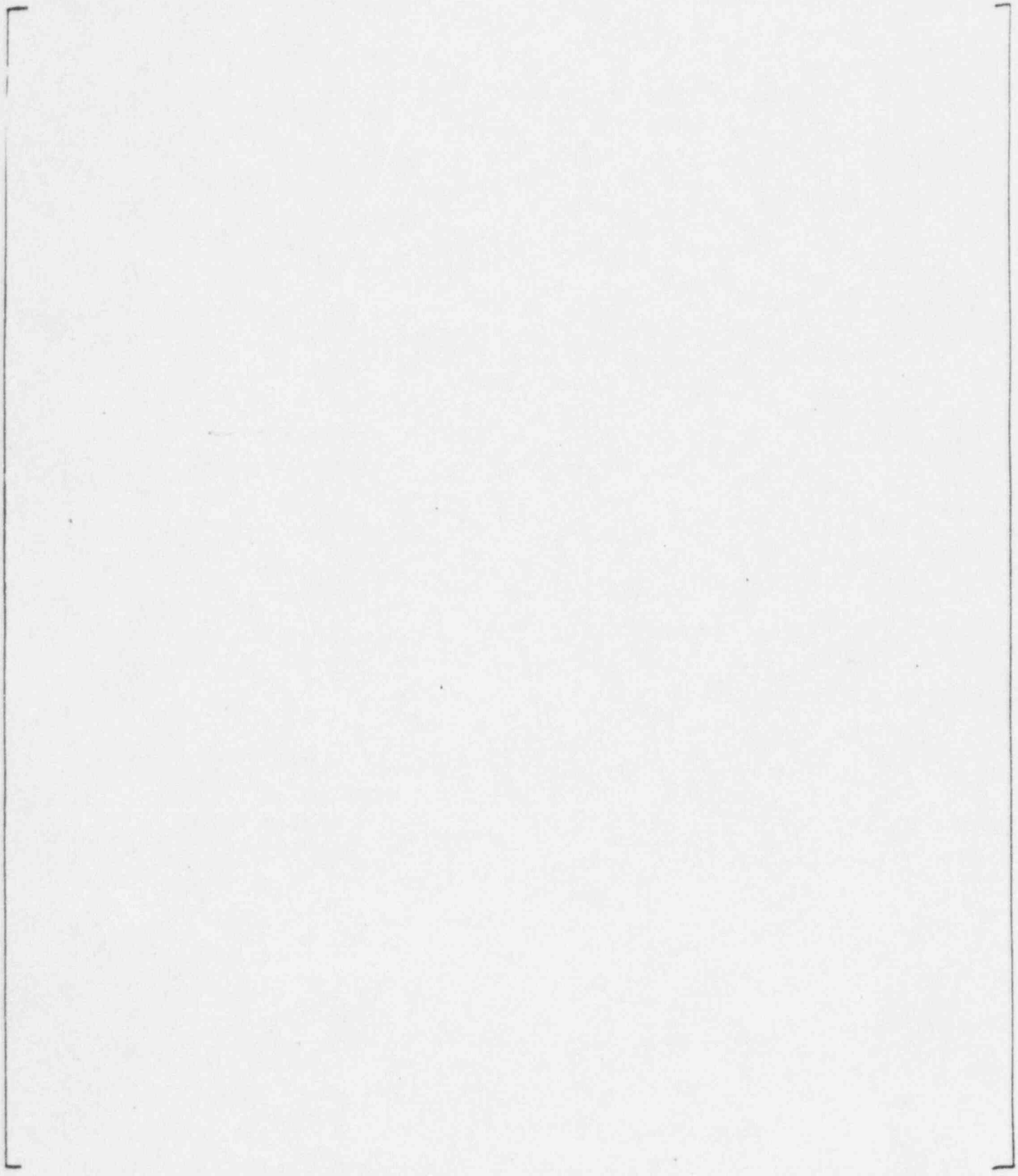

Figure 6.4-9 NOTRUMP Comparisons for Core Makeup Tank Integrated Drain Flow for Test C059502

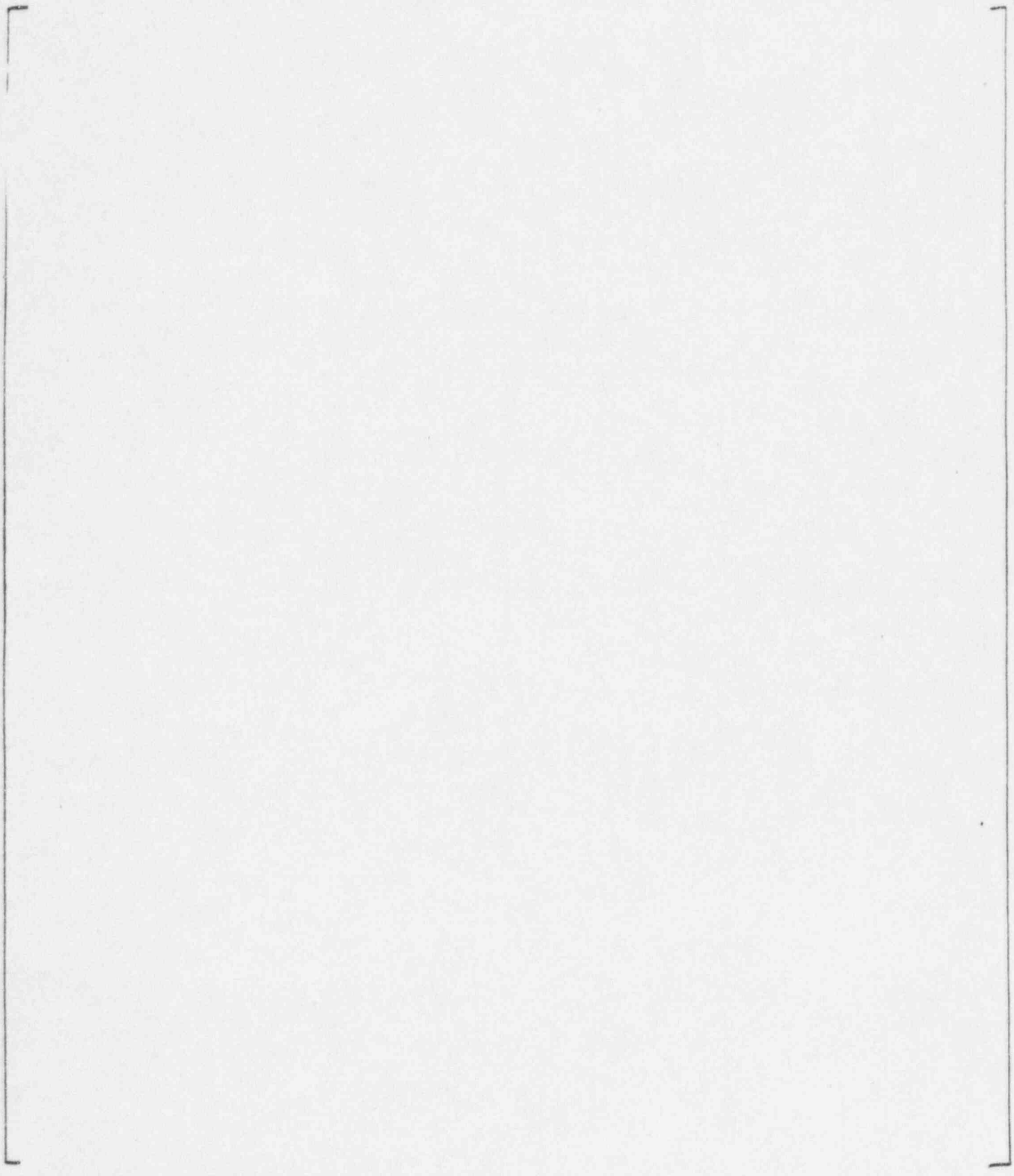

Figure 6.4-10 NOTRUMP Comparisons to Core Makeup Tank Pressure for Test C066501

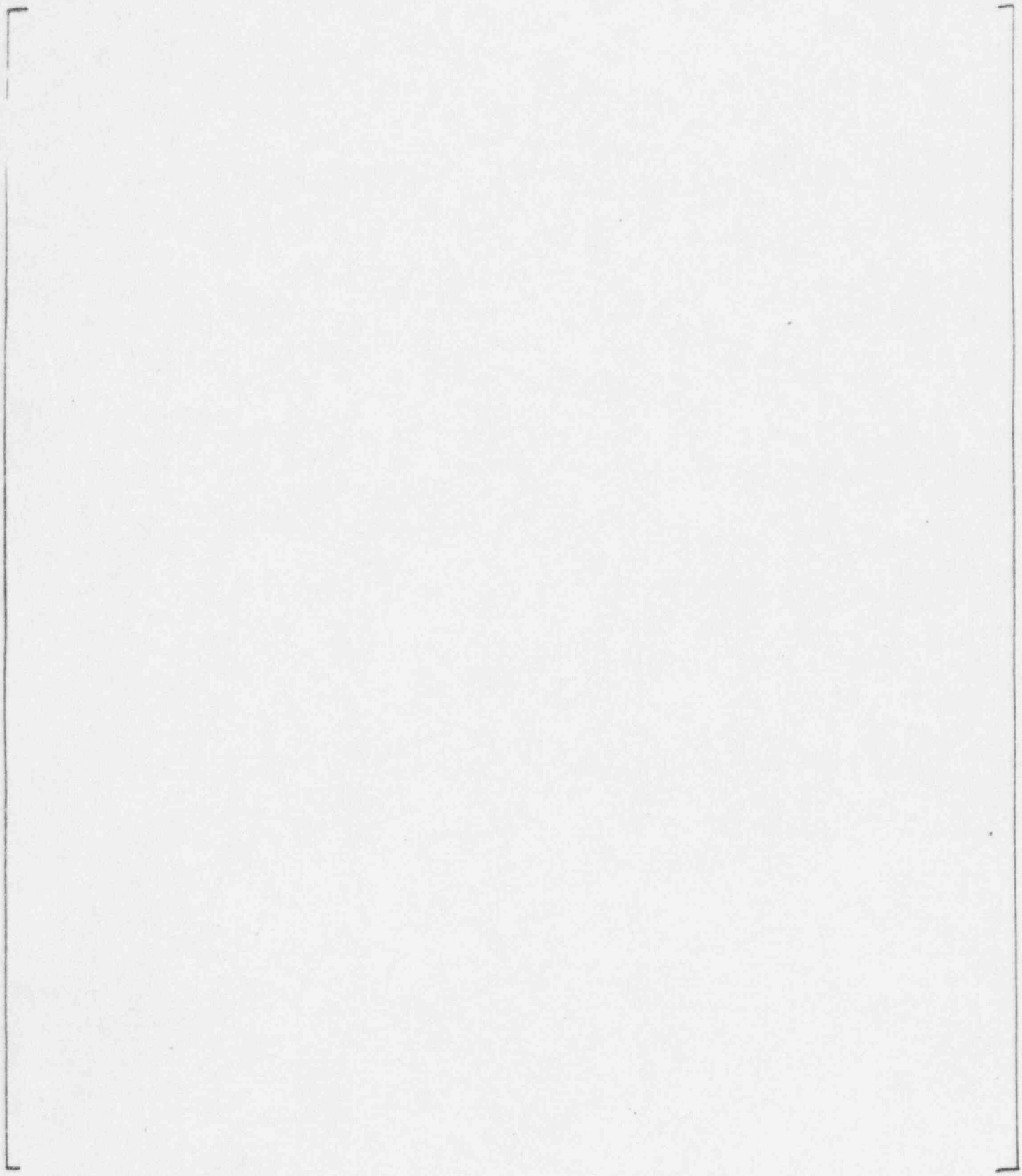

Figure 6.4-11 NOTRUMP-Calculated Core Makeup Tank Fluid Node Temperatures for Test C066501

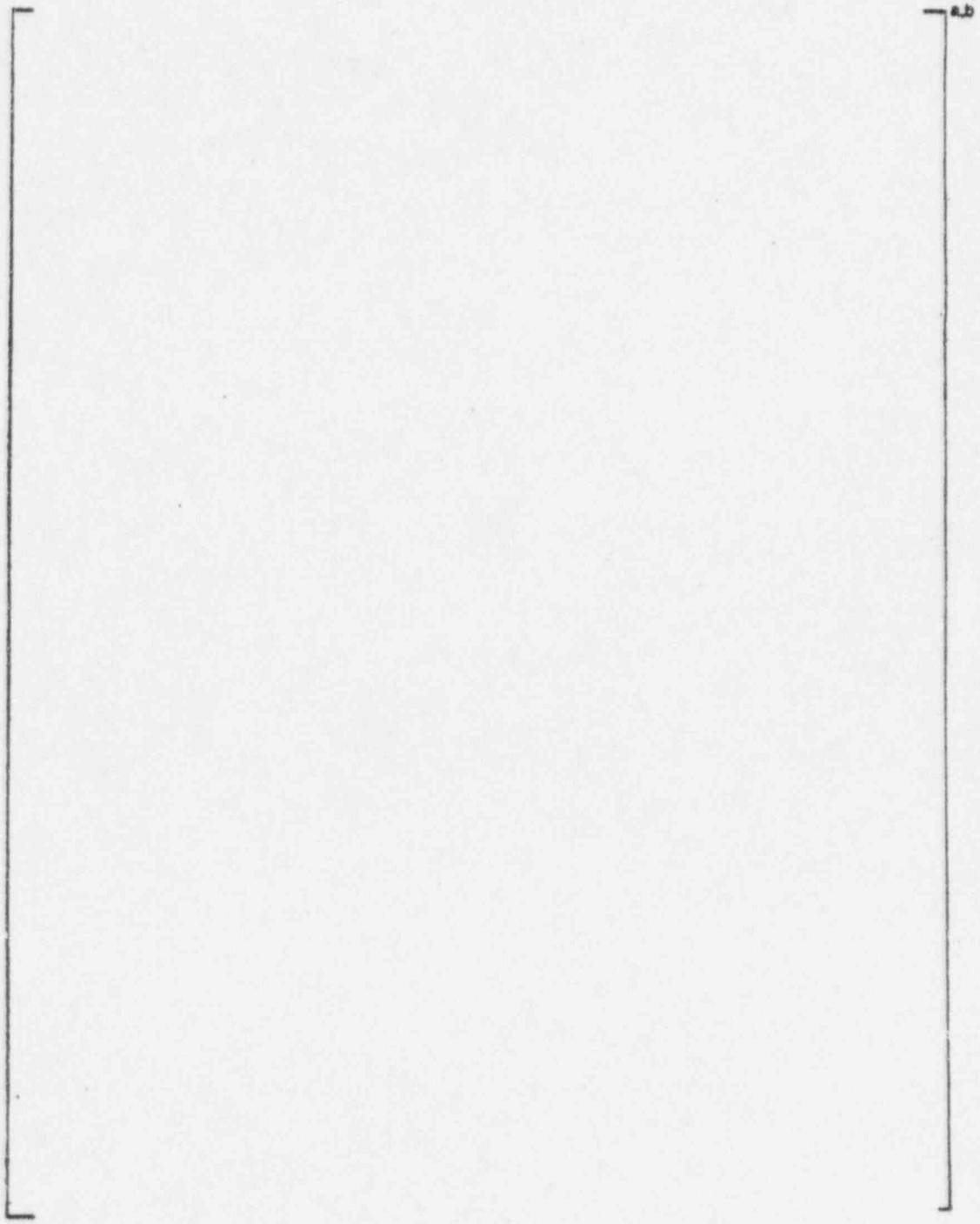

Figure 6.4-12 Core Makeup Tank Axial Fluid Temperatures for Test C066501

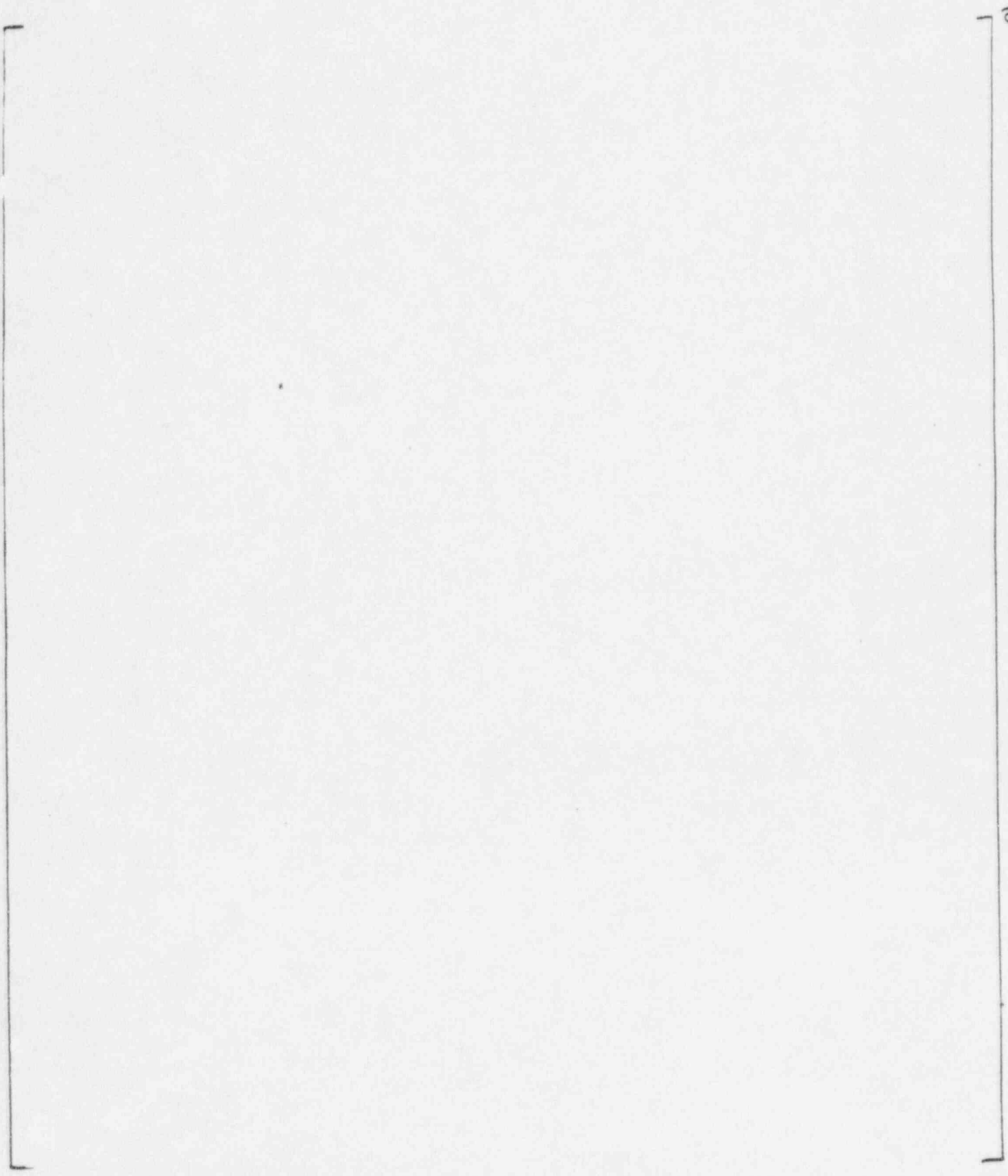

Figure 6.4-13 NOTRUMP Comparisons for Core Makeup Tank Top Node for Test C066501

a,b

Figure 6.4-14 NOTRUMP Comparisons for Core Makeup Tank Top Cylindrical Node for Test C066501

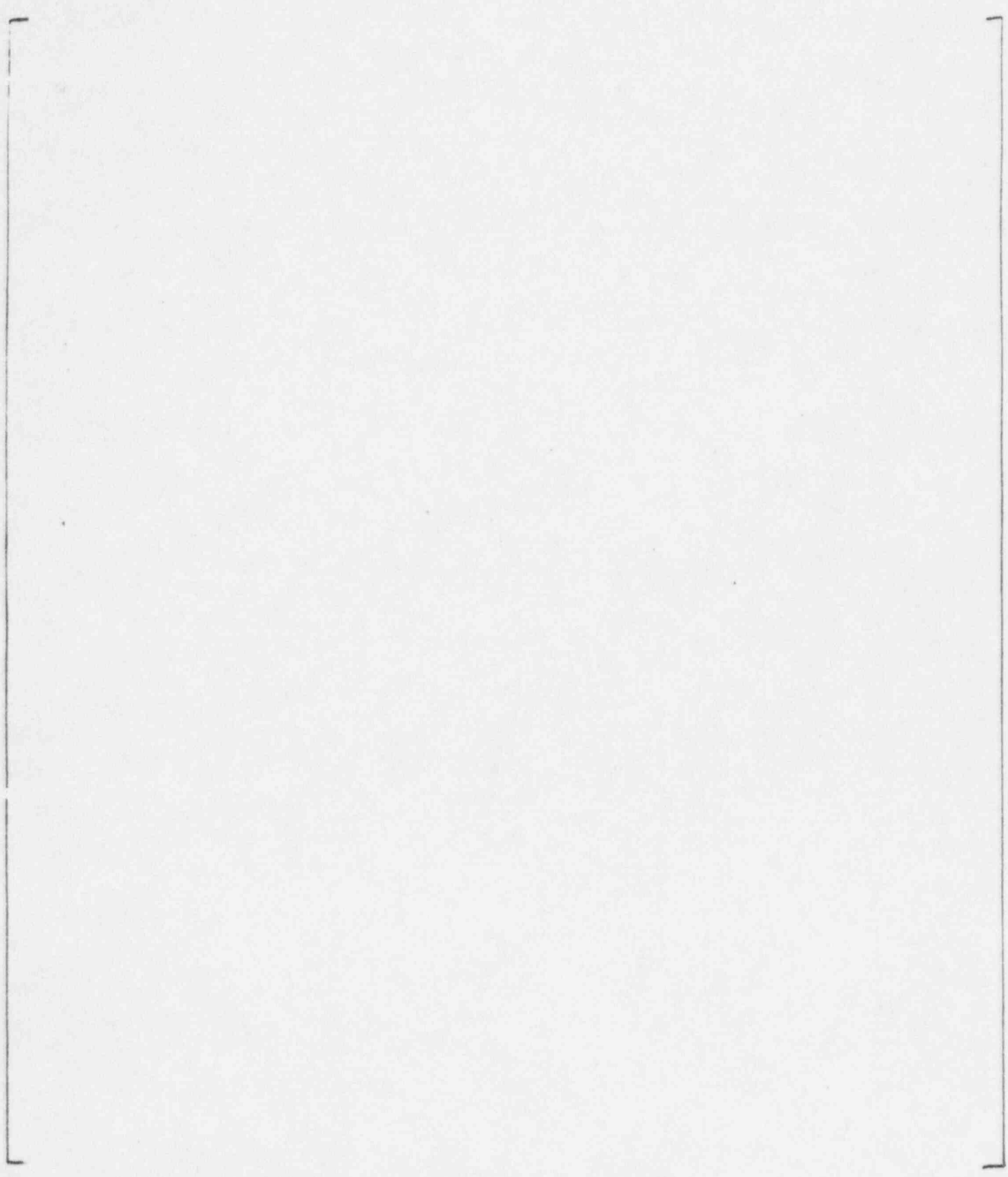

Figure 6.4-15 NOTRUMP Comparisons for Core Makeup Tank Bottom Cylindrical Node for Test C066501

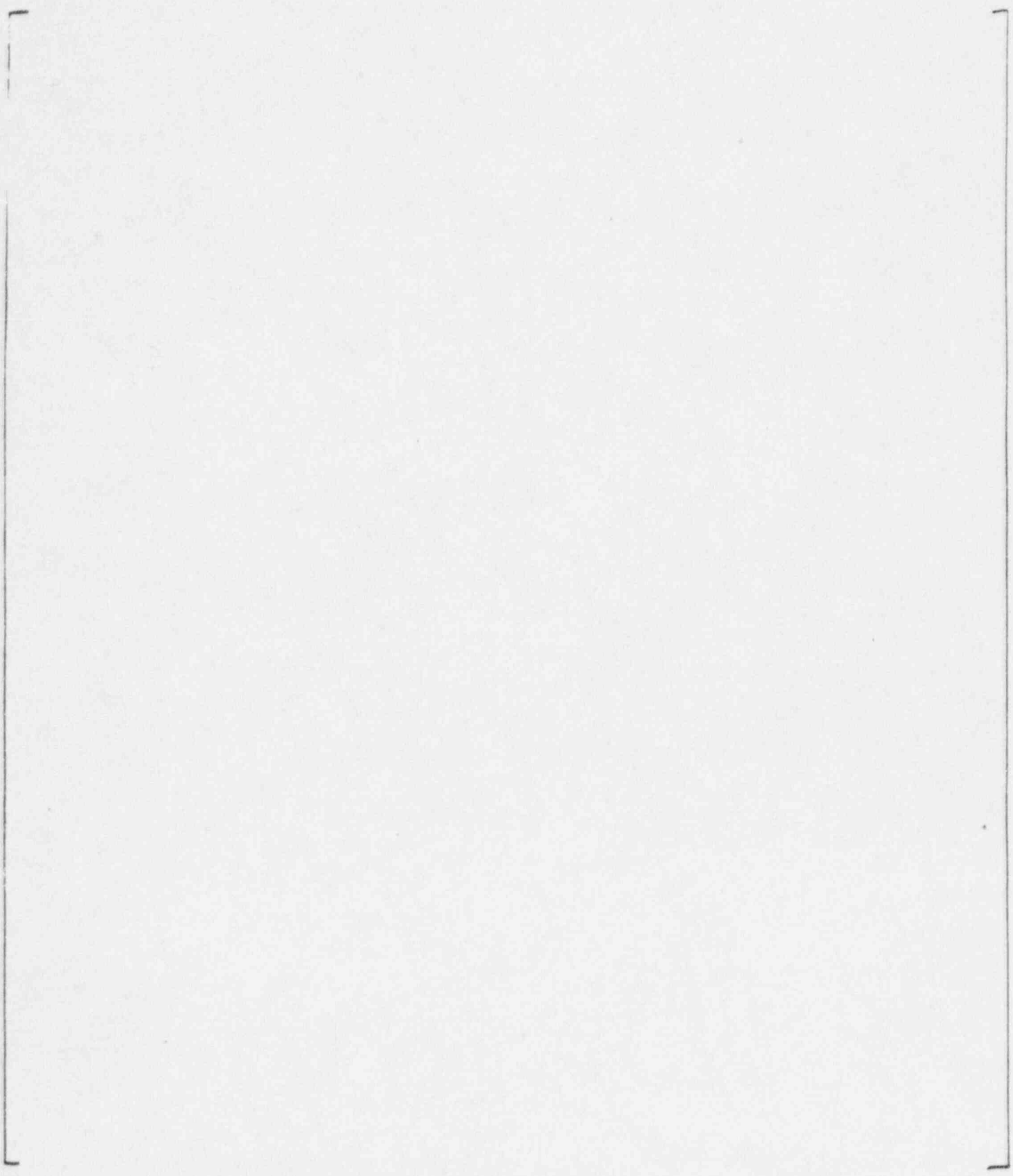

Figure 6.4-16 NOTRUMP Comparisons for Core Makeup Tank Bottom-Most Node for Test C066501

[a,b

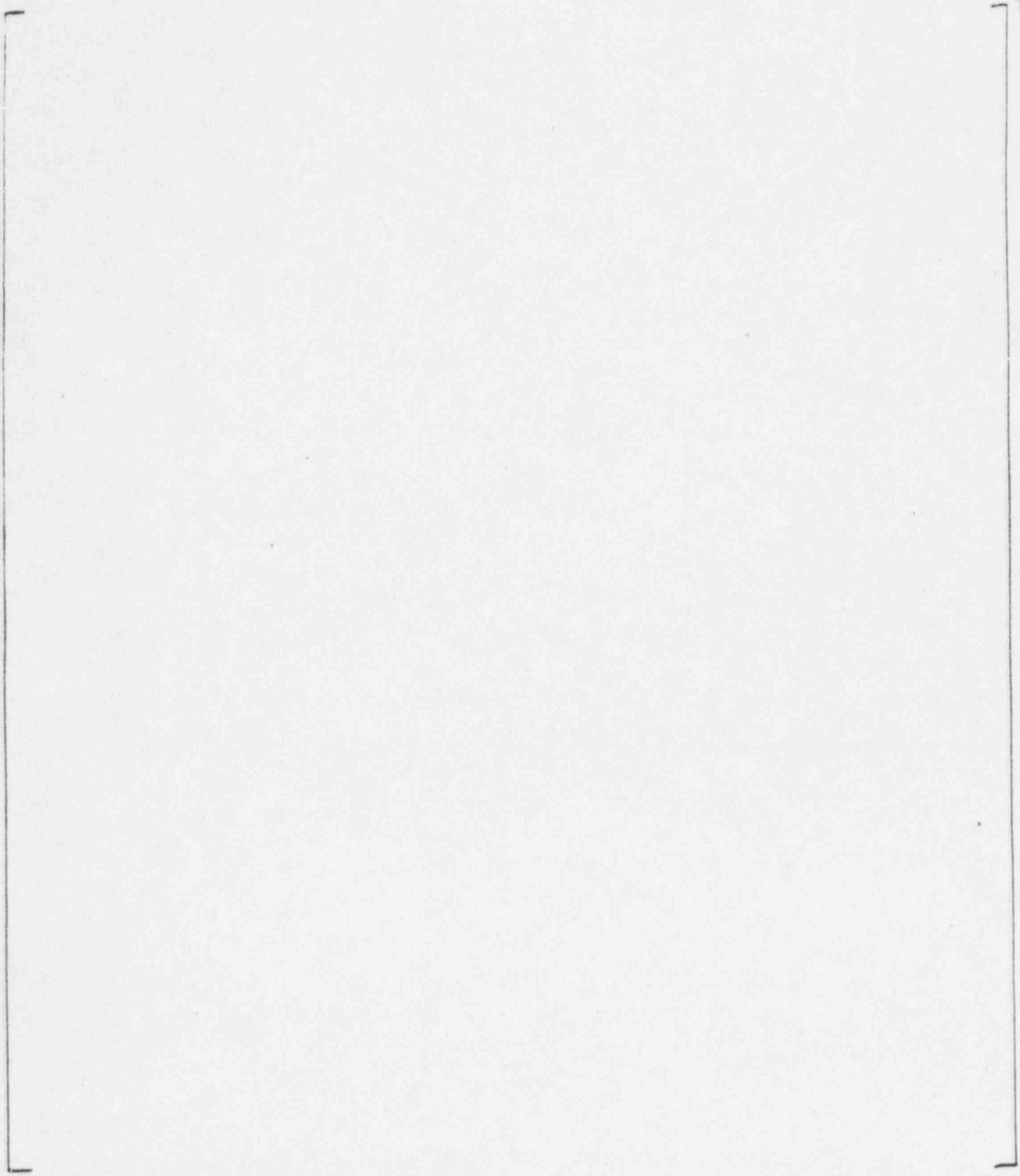

]

Figure 6.4-17 NOTRUMP Comparisons for Core Makeup Tank Drain Flow for Test C066501

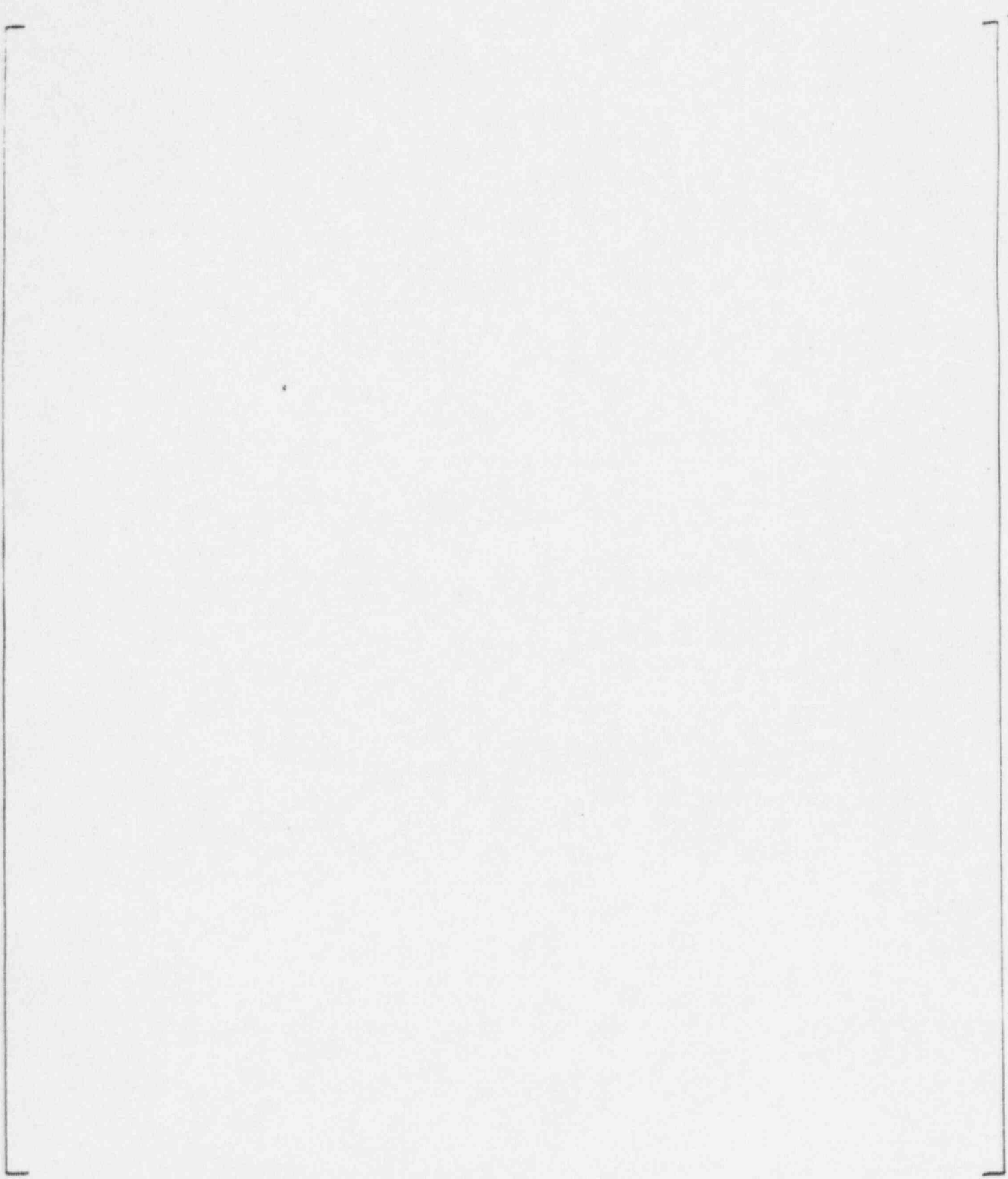

Figure 6.4-18 NOTRUMP Comparisons for Core Makeup Tank Integrated Drain Flow for Test C066501

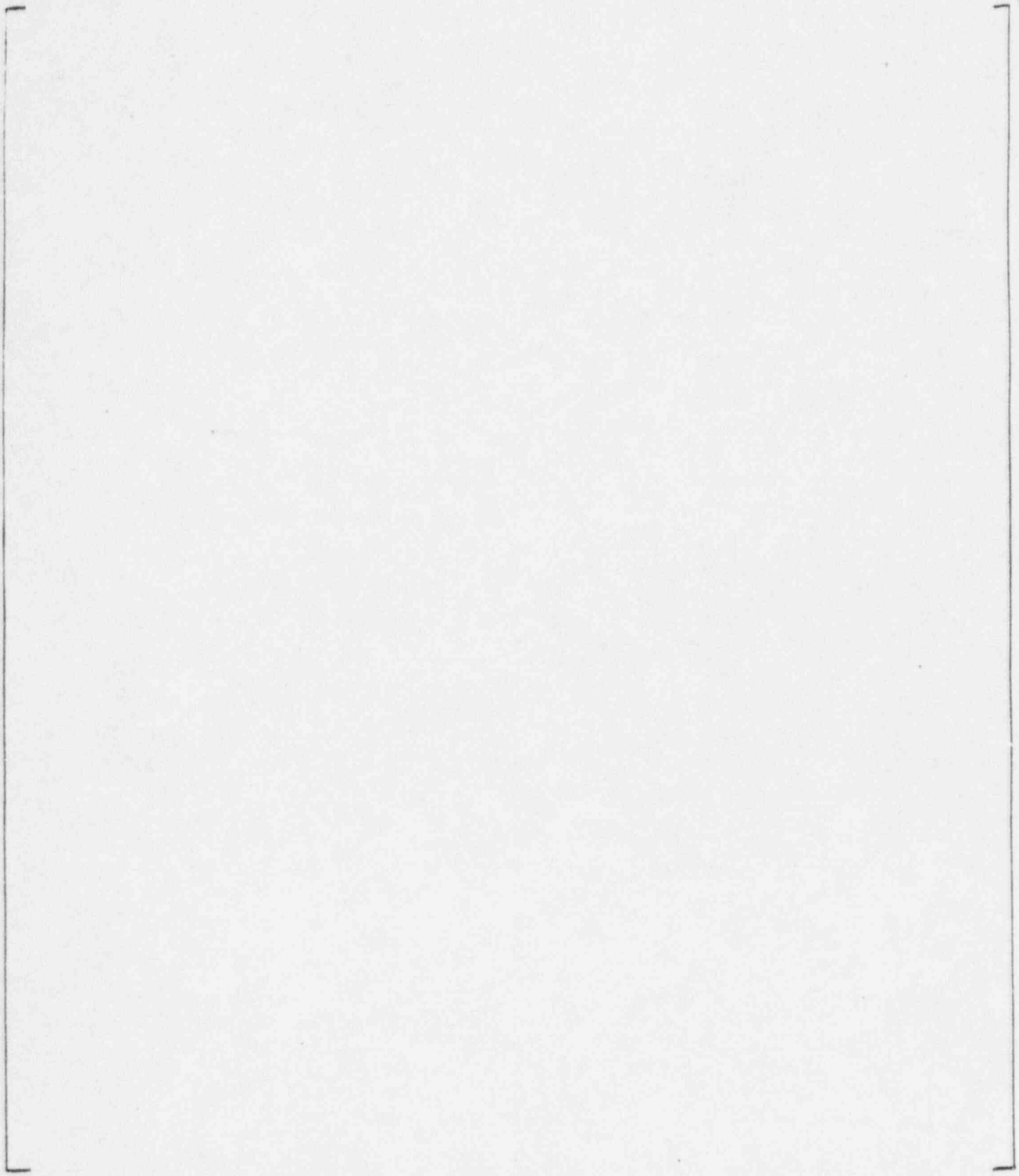

Figure 6.4-19 NOTRUMP Comparisons to Core Makeup Tank Pressure for Test C061504

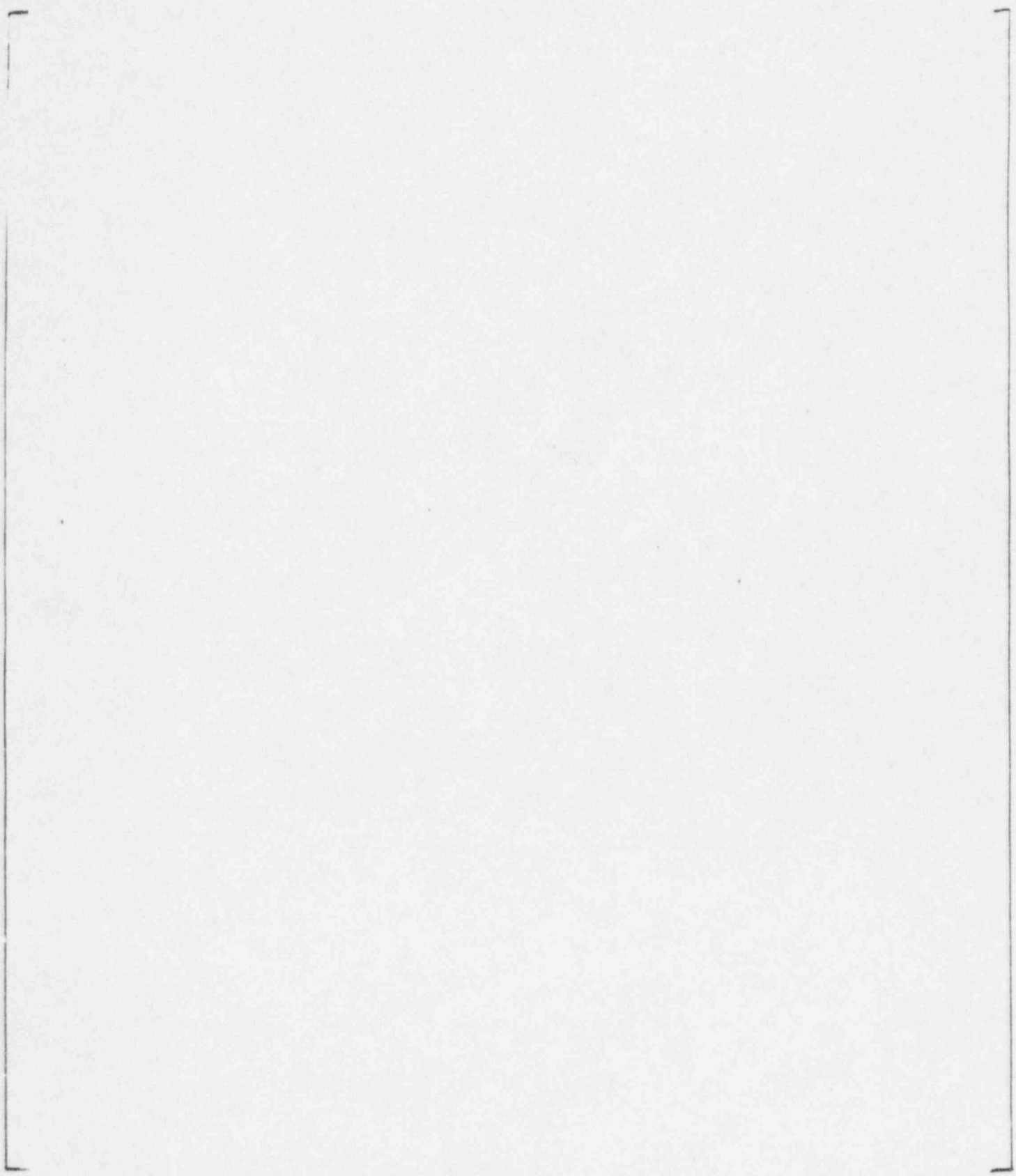

Figure 6.4-20 NOTRUMP-Calculated Core Makeup Tank Fluid Node Temperatures for Test C061504

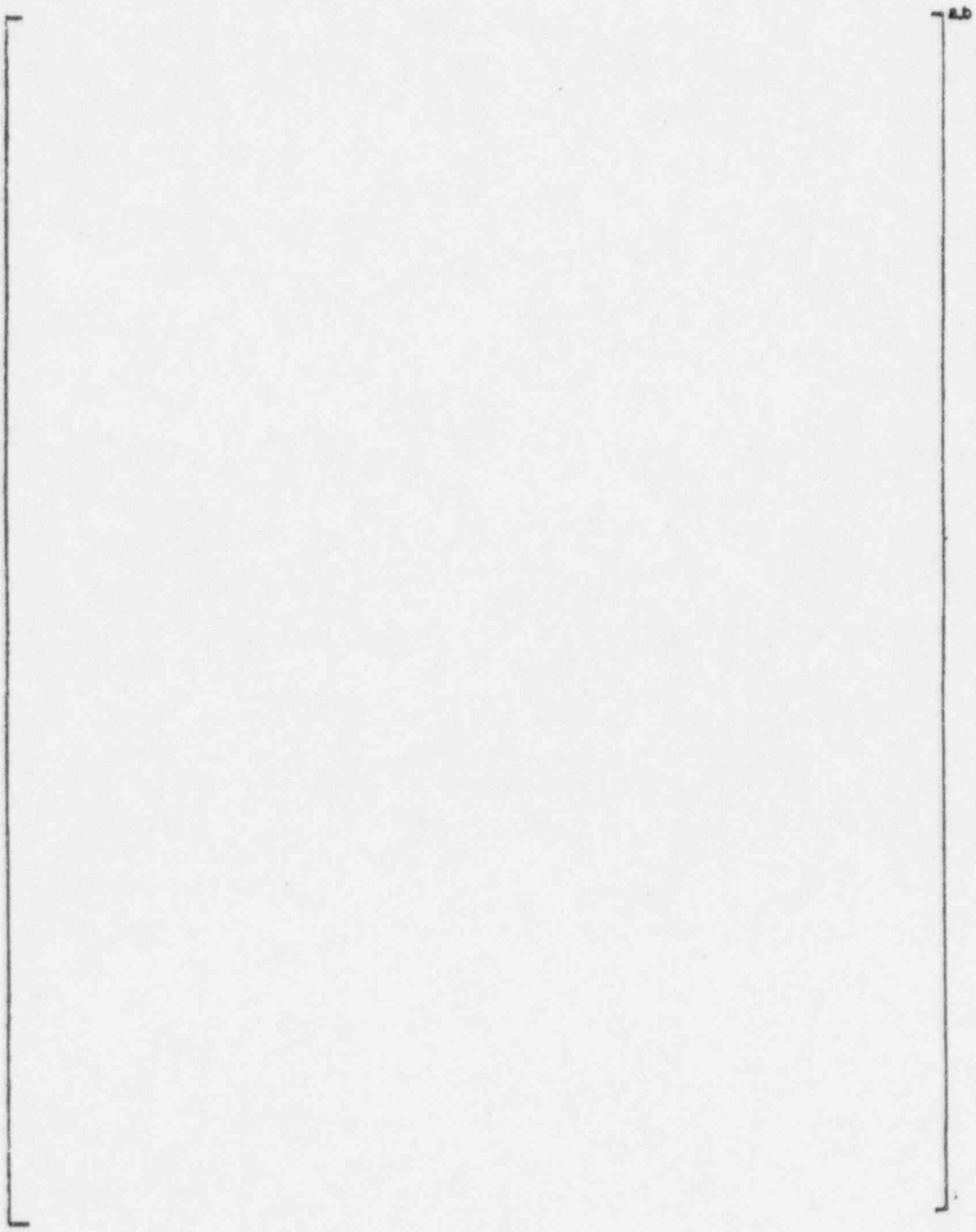

Figure 6.4-21 Core Makeup Tank Axial Fluid Temperatures for Test C061504

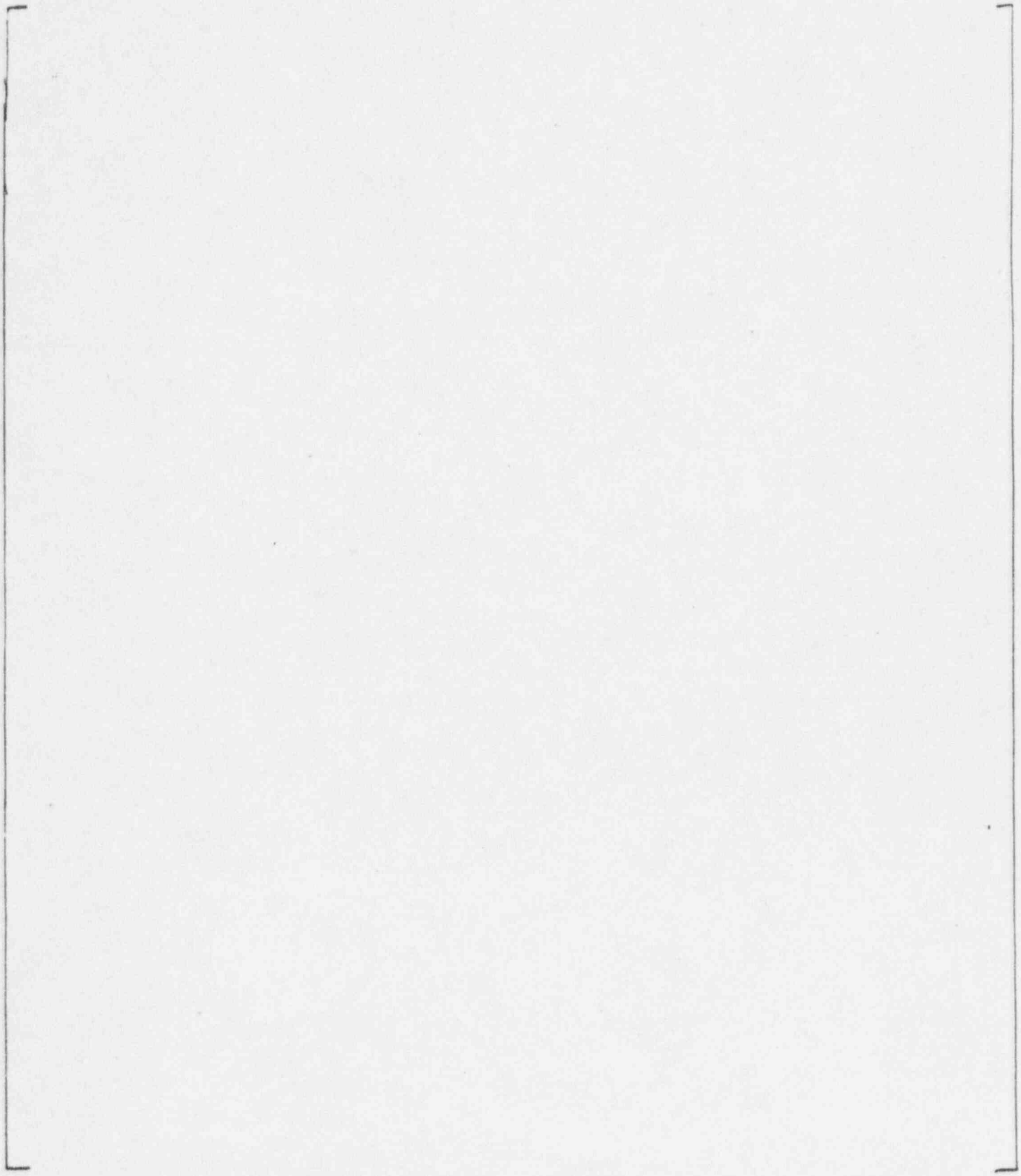

Figure 6.4-22 NOTRUMP Comparisons for Core Makeup Tank Top Node for Test C061504

[a,b]

Figure 6.4-23 NOTRUMP Comparisons for Core Makeup Tank Top Cylindrical Node for Test C061504

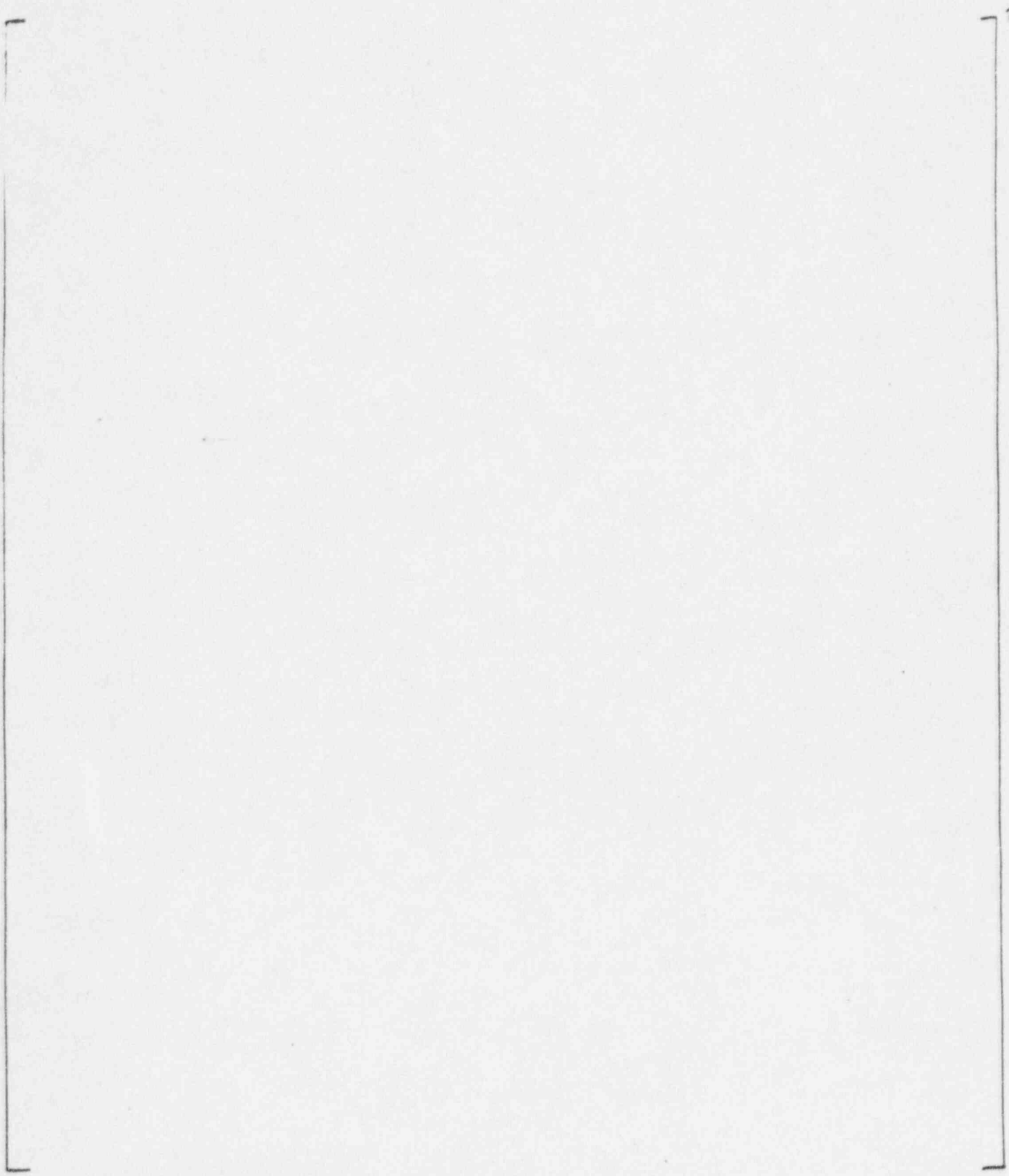

Figure 6.4-24 NOTRUMP Comparisons for Core Makeup Tank Bottom Cylindrical Node for Test C061504

a,b

Figure 6.4-25 NOTRUMP Comparisons for Core Makeup Tank Bottom-Most Node for Test C061504

[ ] a,b

Figure 6.4-26 NOTRUMP Comparisons for Core Makeup Tank Drain Flow for Test C061504

a,b

Figure 6.4-27 NOTRUMP Comparisons for Core Makeup Tank Integrated Drain Flow for Test C061504

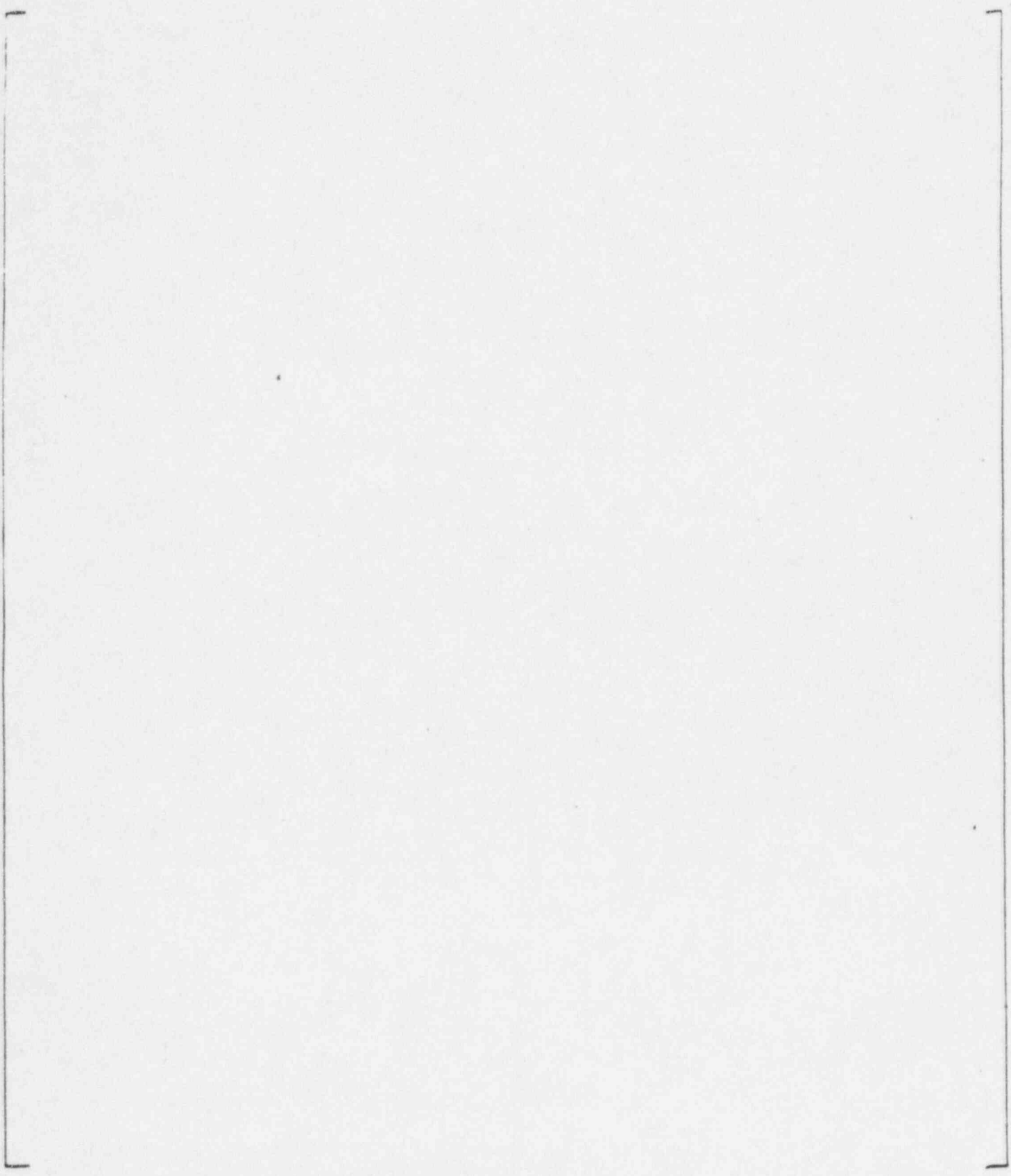

Figure 6.4-28 NOTRUMP Comparisons to Core Makeup Tank Pressure for Test C068503

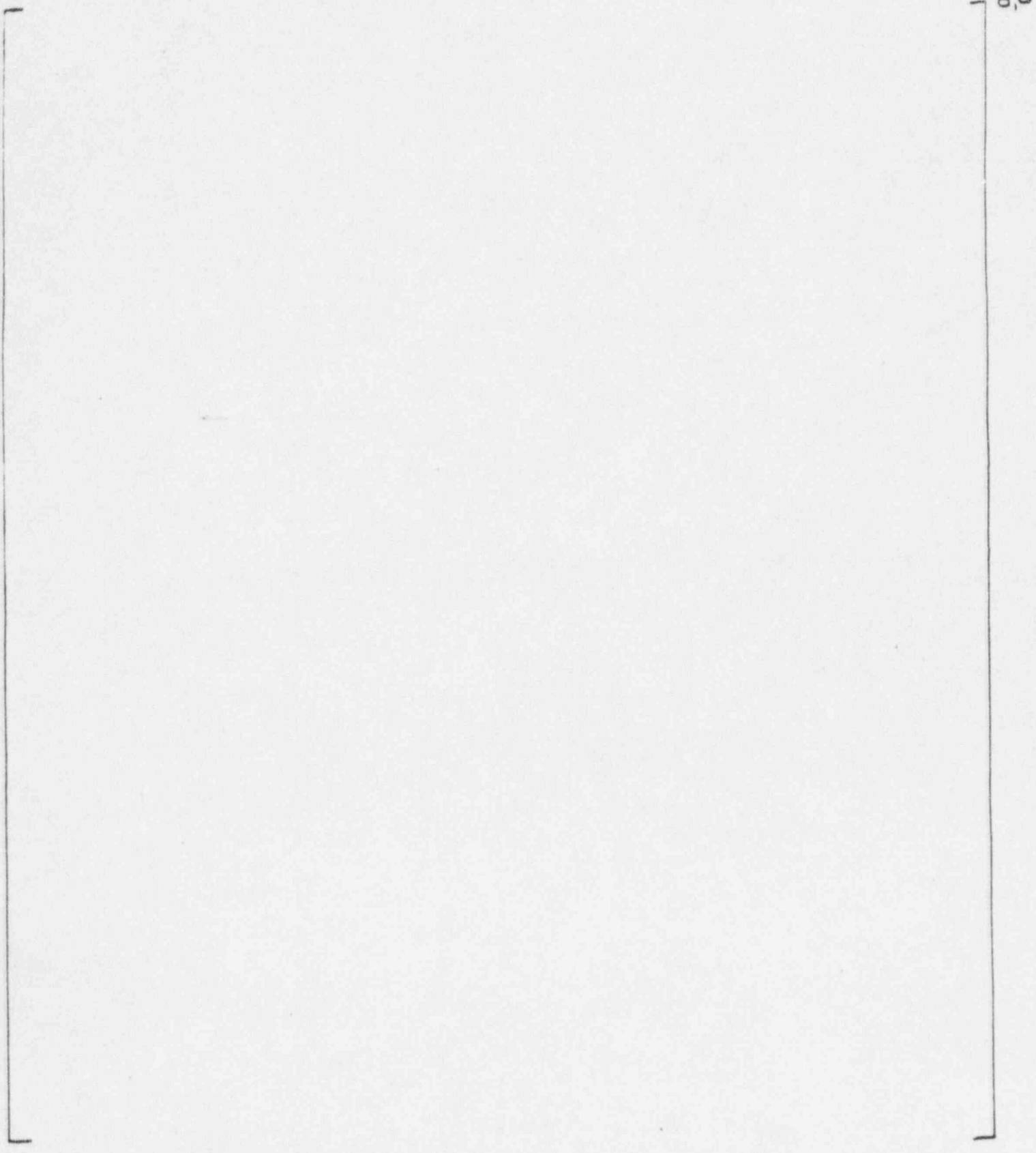

Figure 6.4-29 NOTRUMP-Calculated Core Makeup Tank Fluid Node Temperatures for Test C068503

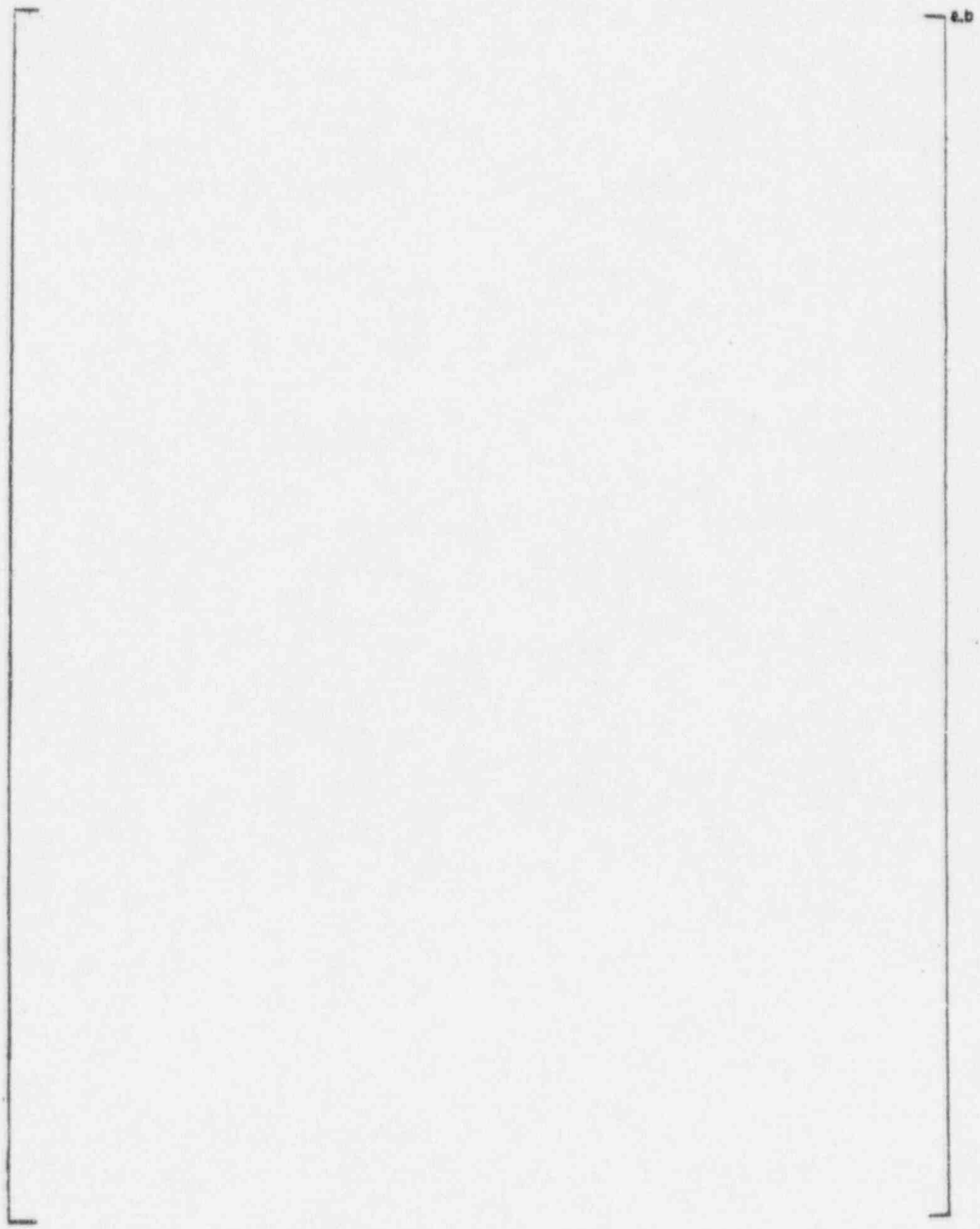

Figure 6.4-30 Core Makeup Tank Axial Fluid Temperatures for Test C068503

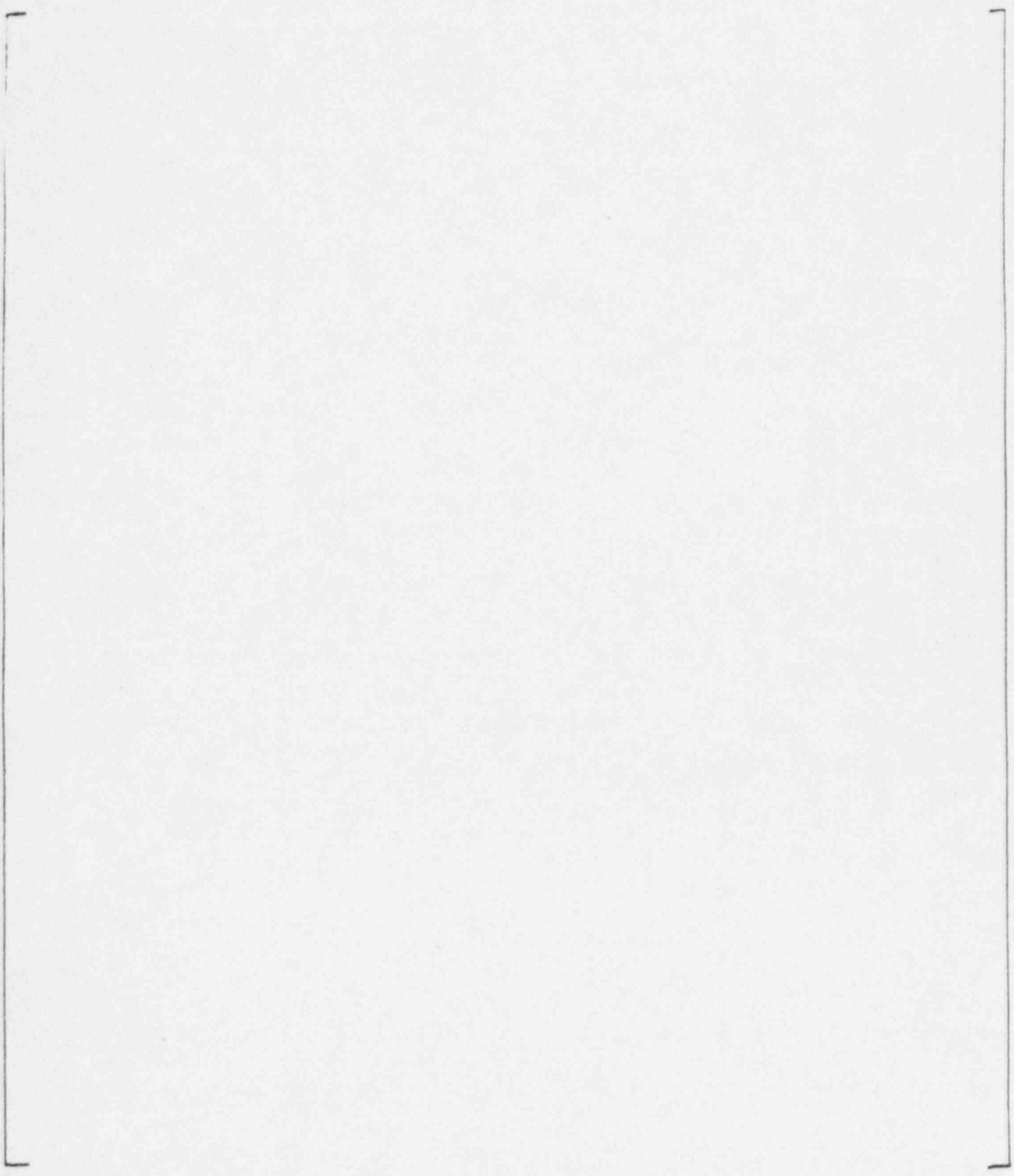

Figure 6.4-31 NOTRUMP Comparisons for Core Makeup Tank Top Node for Test C068503

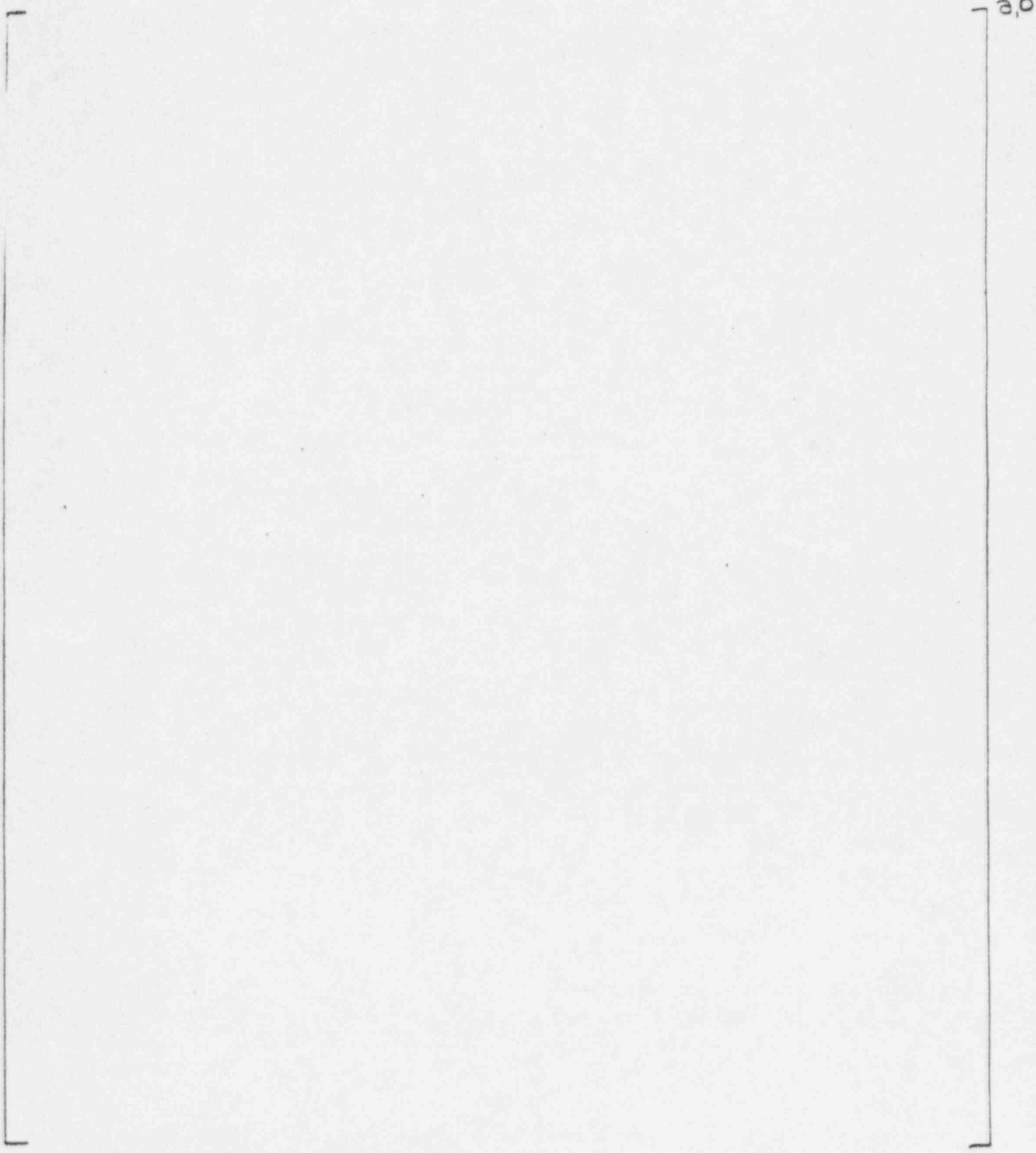

Figure 6.4-32 NOTRUMP Comparisons for Core Makeup Tank Top Cylindrical Node for Test C068503

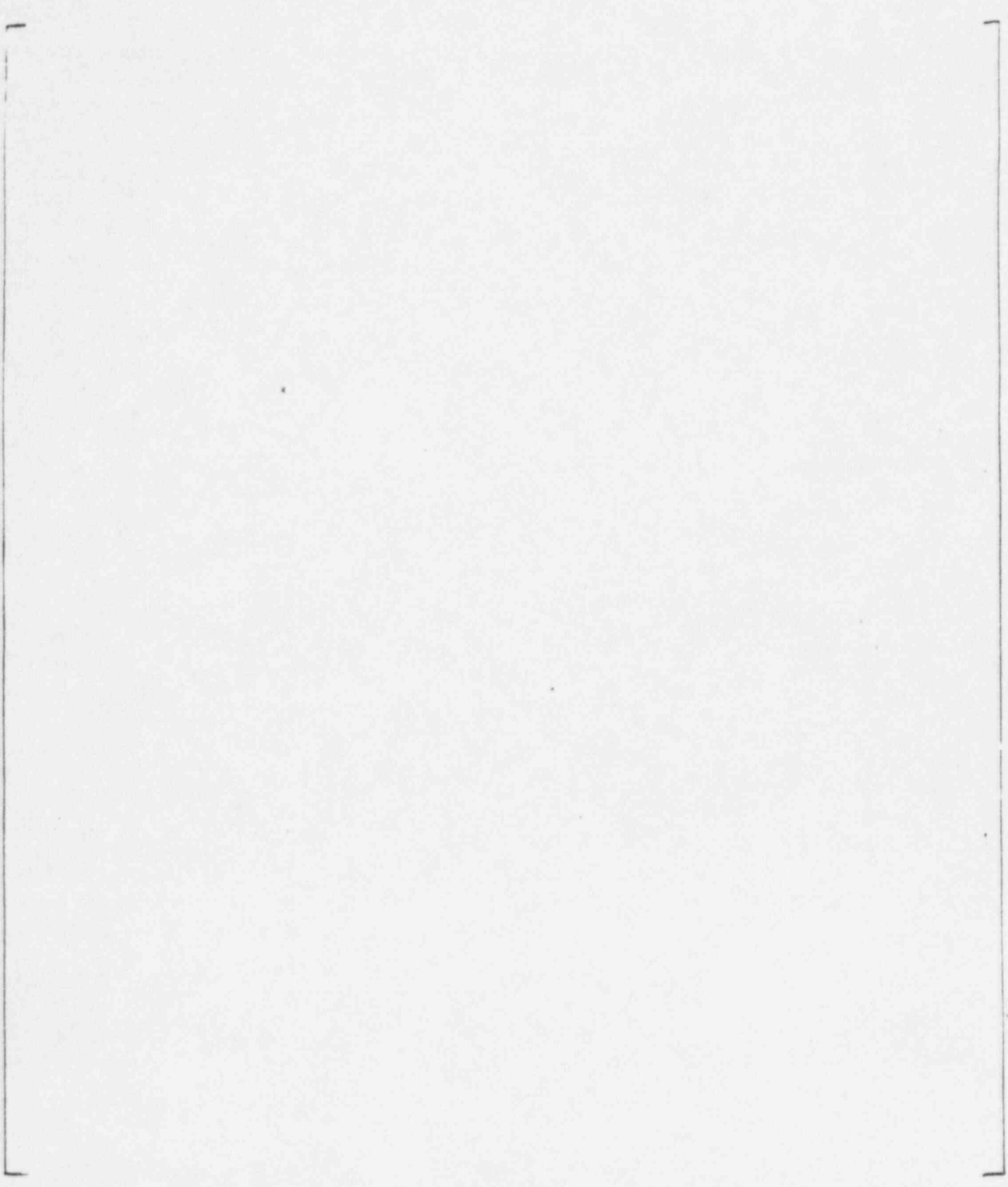

Figure 6.4-33 NOTRUMP Comparisons for Core Makeup Tank Bottom Cylindrical Node for Test C068503

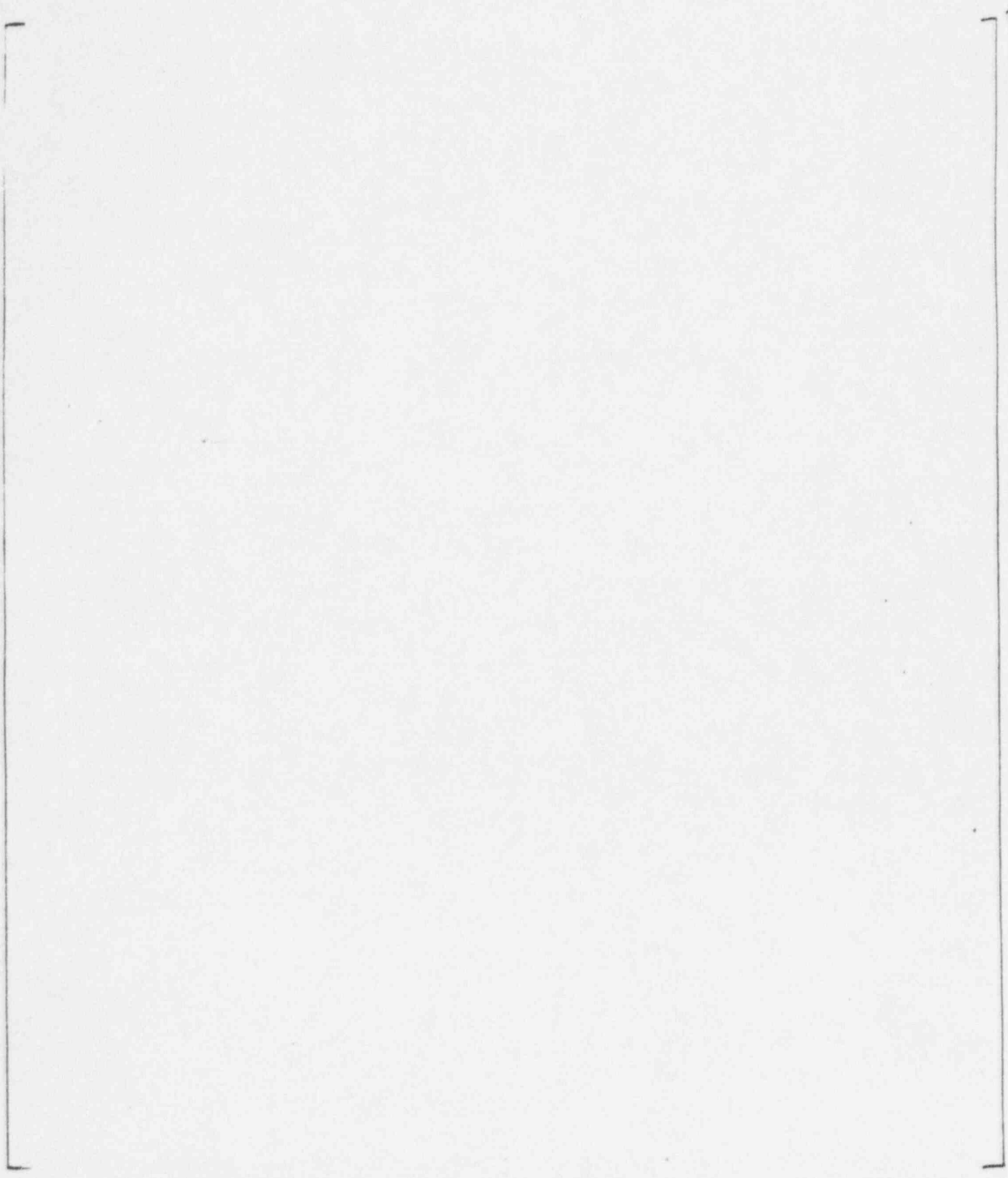

Figure 6.4-34 NOTRUMP Comparisons for Core Makeup Tank Bottom-Most Node for Test C068503

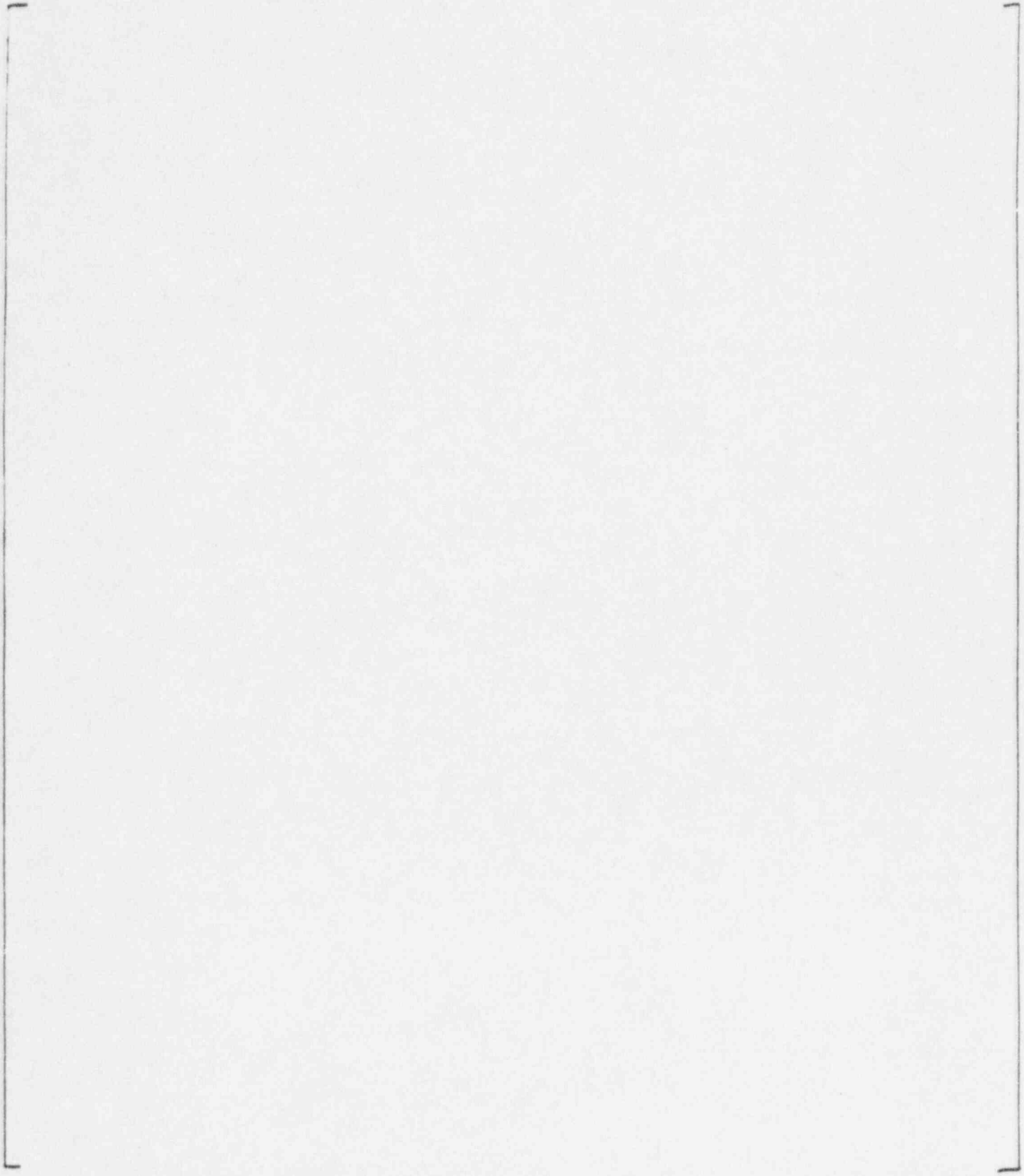

Figure 6.4-35 NOTRUMP Comparisons for Core Makeup Tank Drain Flow for Test C068503

[ ] a,b

Figure 6.4-36 NOTRUMP Comparisons for Core Makeup Tank Integrated Drain Flow for Test C068503

a,b

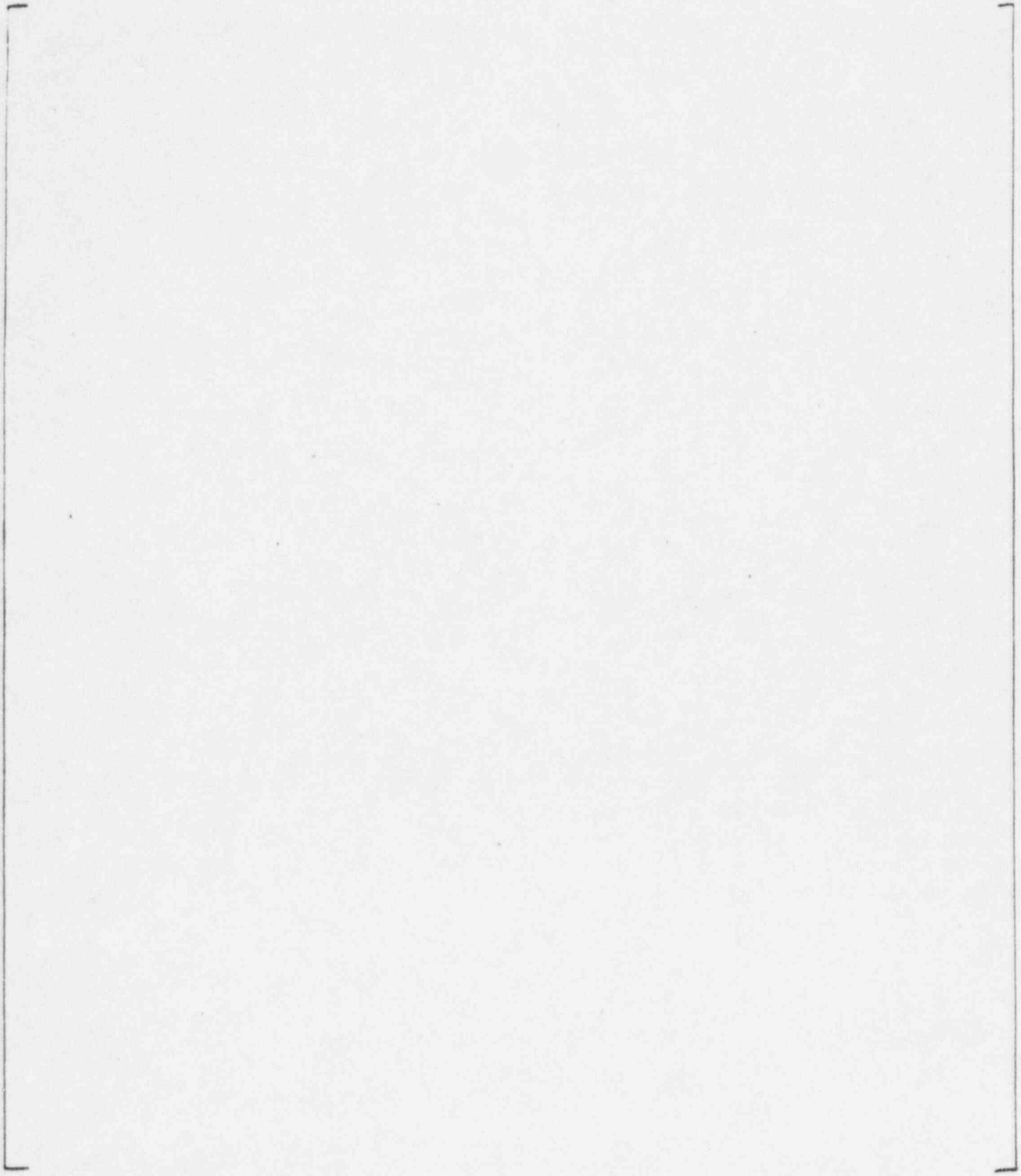

Figure 6.4-37 NOTRUMP Comparisons to Core Makeup Tank Pressure for Test C064506

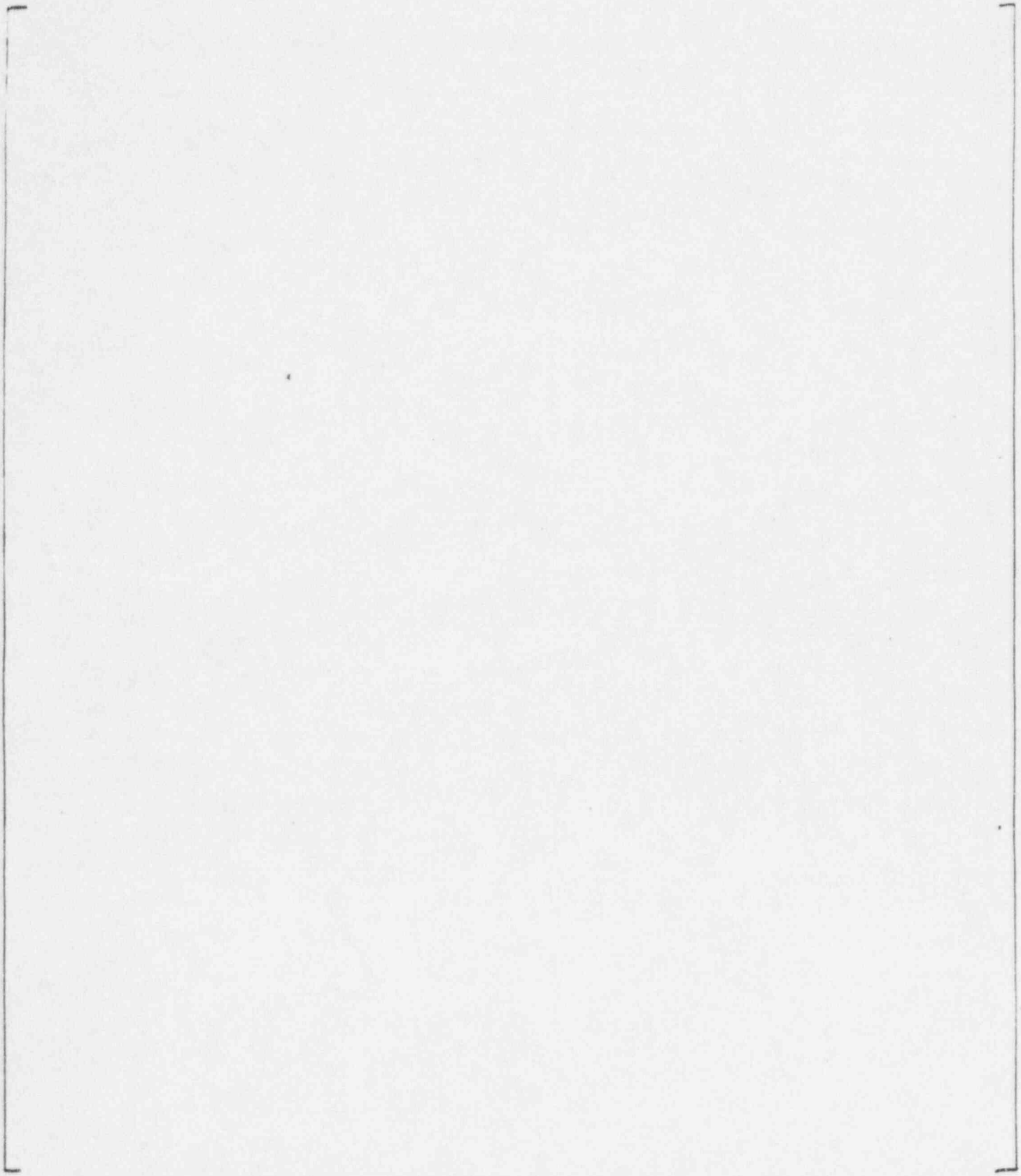

Figure 6.4-38 NOTRUMP-Calculated Core Makeup Tank Fluid Node Temperatures for Test C064506

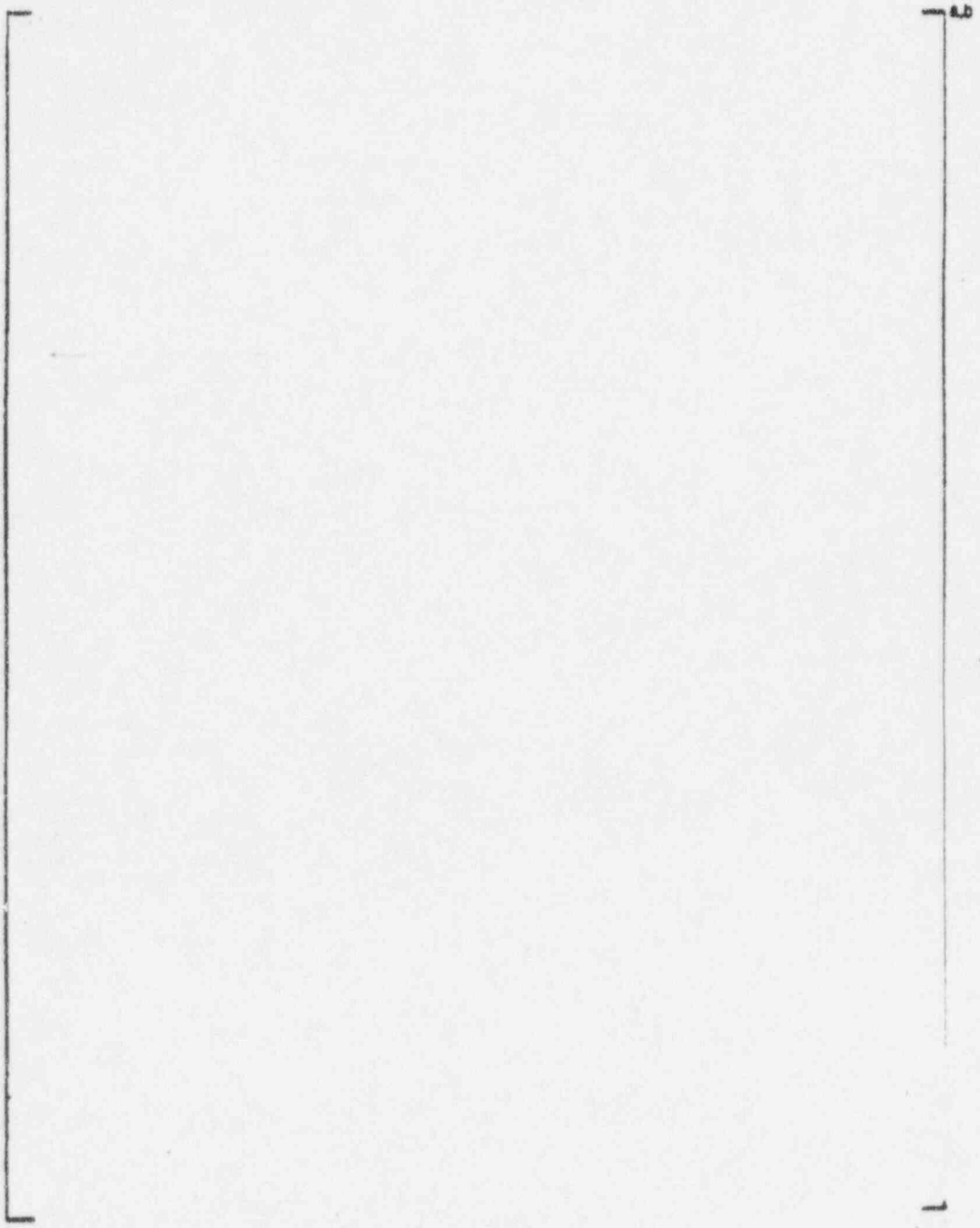

Figure 6.4-39 Core Makeup Tank Axial Fluid Temperatures for Test C064506

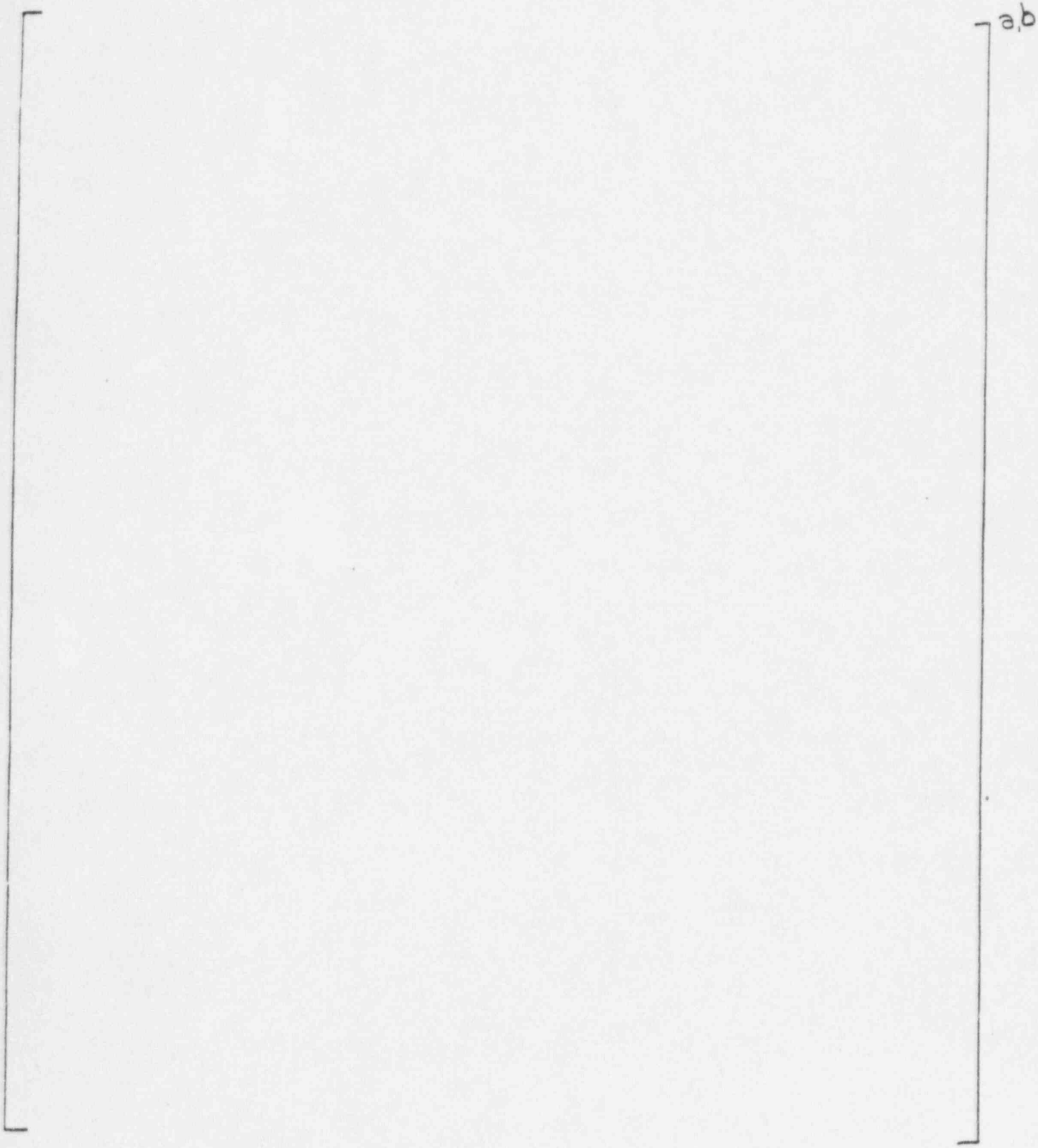

Figure 6.4-40 NOTRUMP Comparisons for Core Makeup Tank Top Node for Test C064506

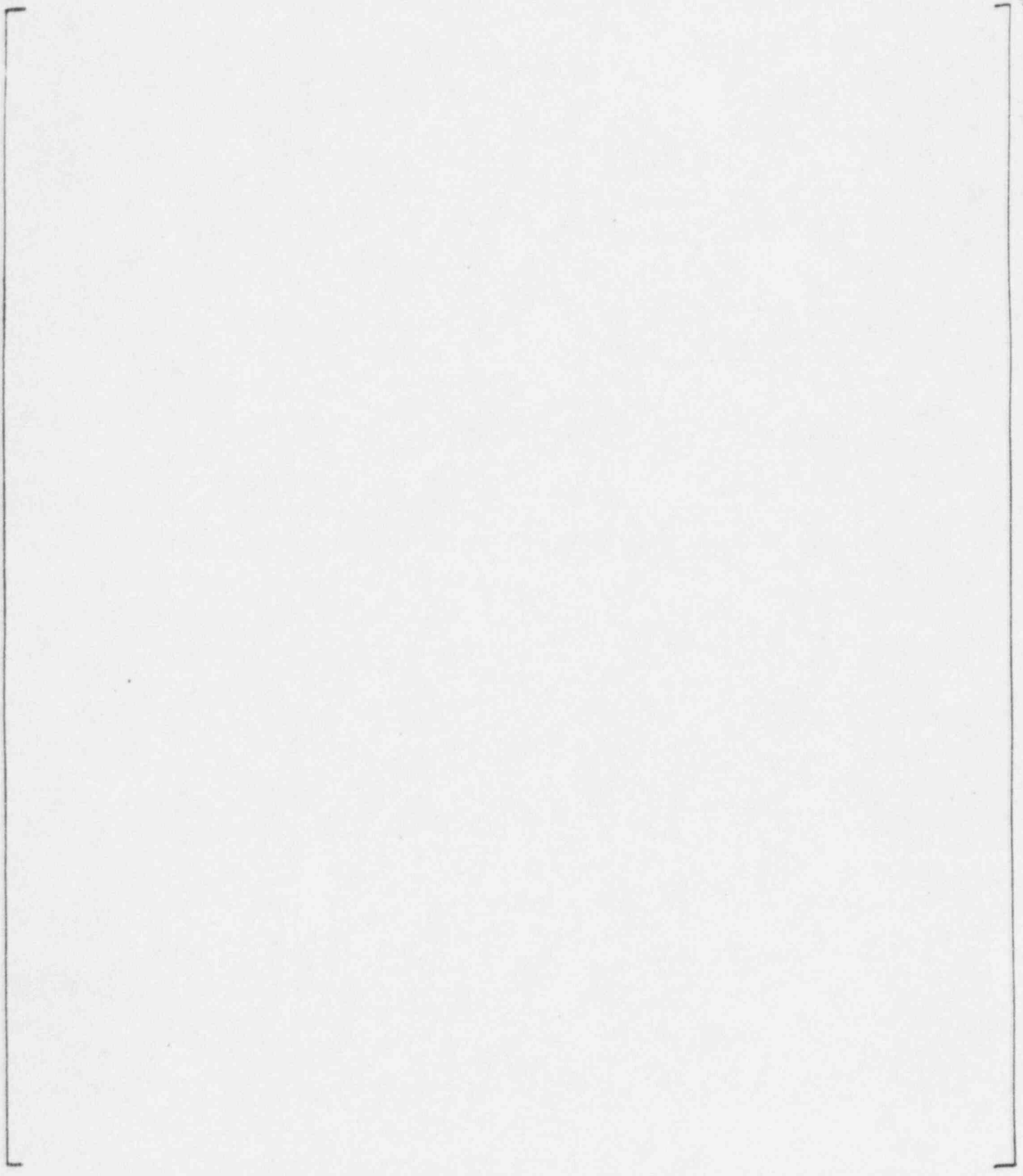

Figure 6.4-41 NOTRUMP Comparisons for Core Makeup Tank Top Cylindrical Node for Test C064506

[a,b]

Figure 6.4-42 NOTRUMP Comparisons for Core Makeup Tank Bottom Cylindrical Node for Test C064506

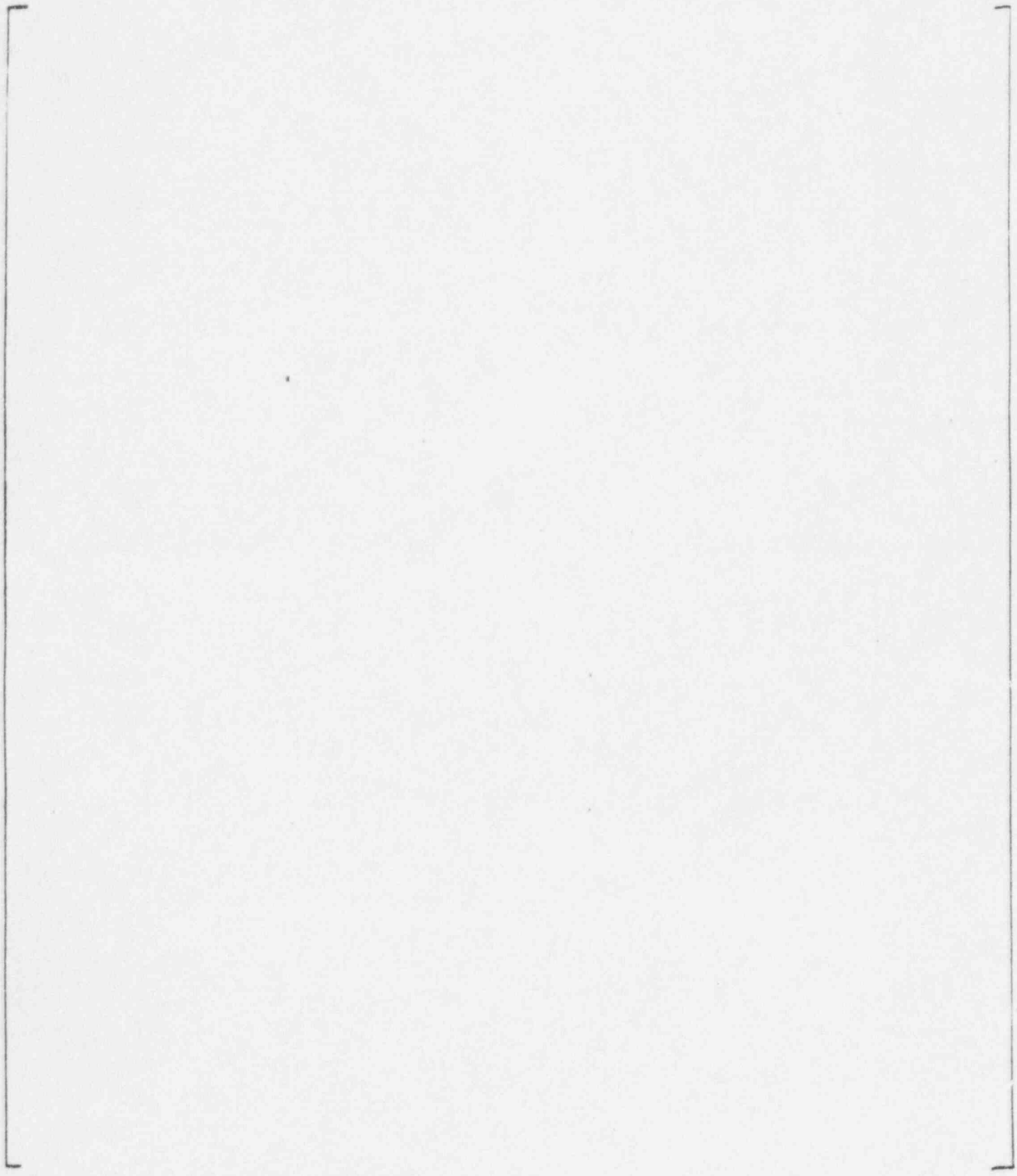

Figure 6.4-43 NOTRUMP Comparisons for Core Makeup Tank Bottom-Most Node for Test C064506

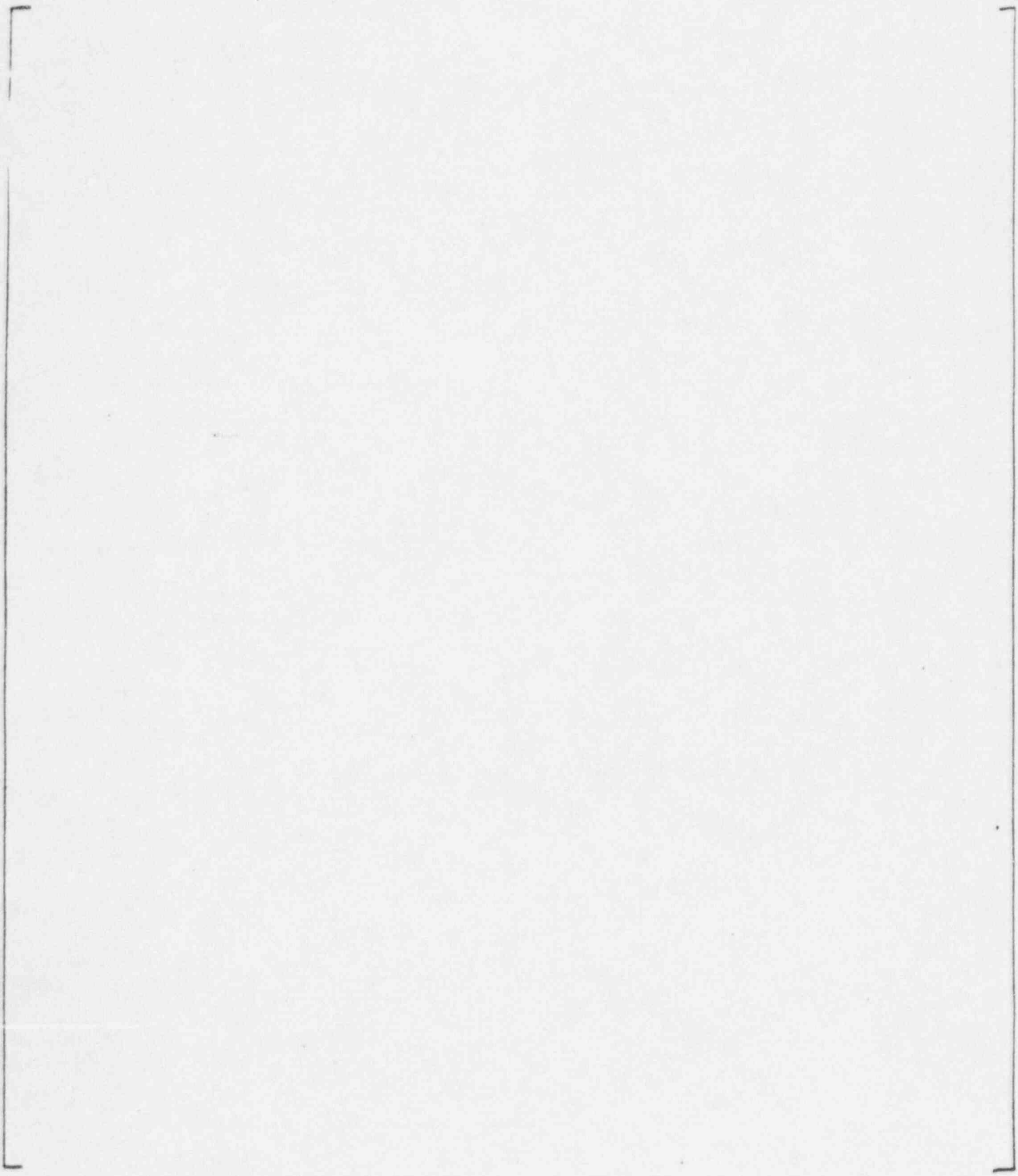

Figure 6.4-44 NOTRUMP Comparisons for Core Makeup Tank Drain Flow for Test C064506

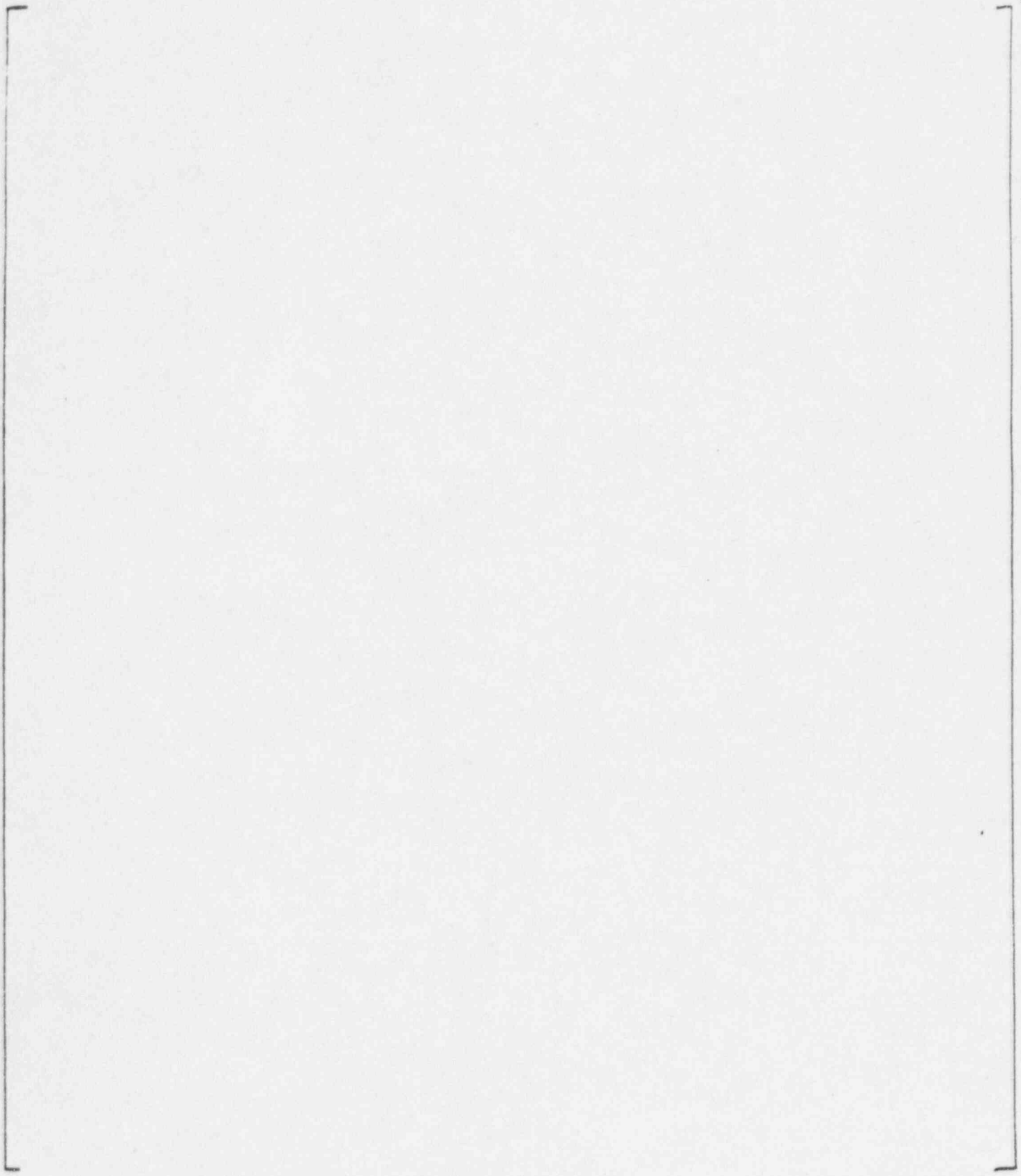

Figure 6.4-45 NOTRUMP Comparisons for Core Makeup Tank Integrated Drain Flow for Test C064506

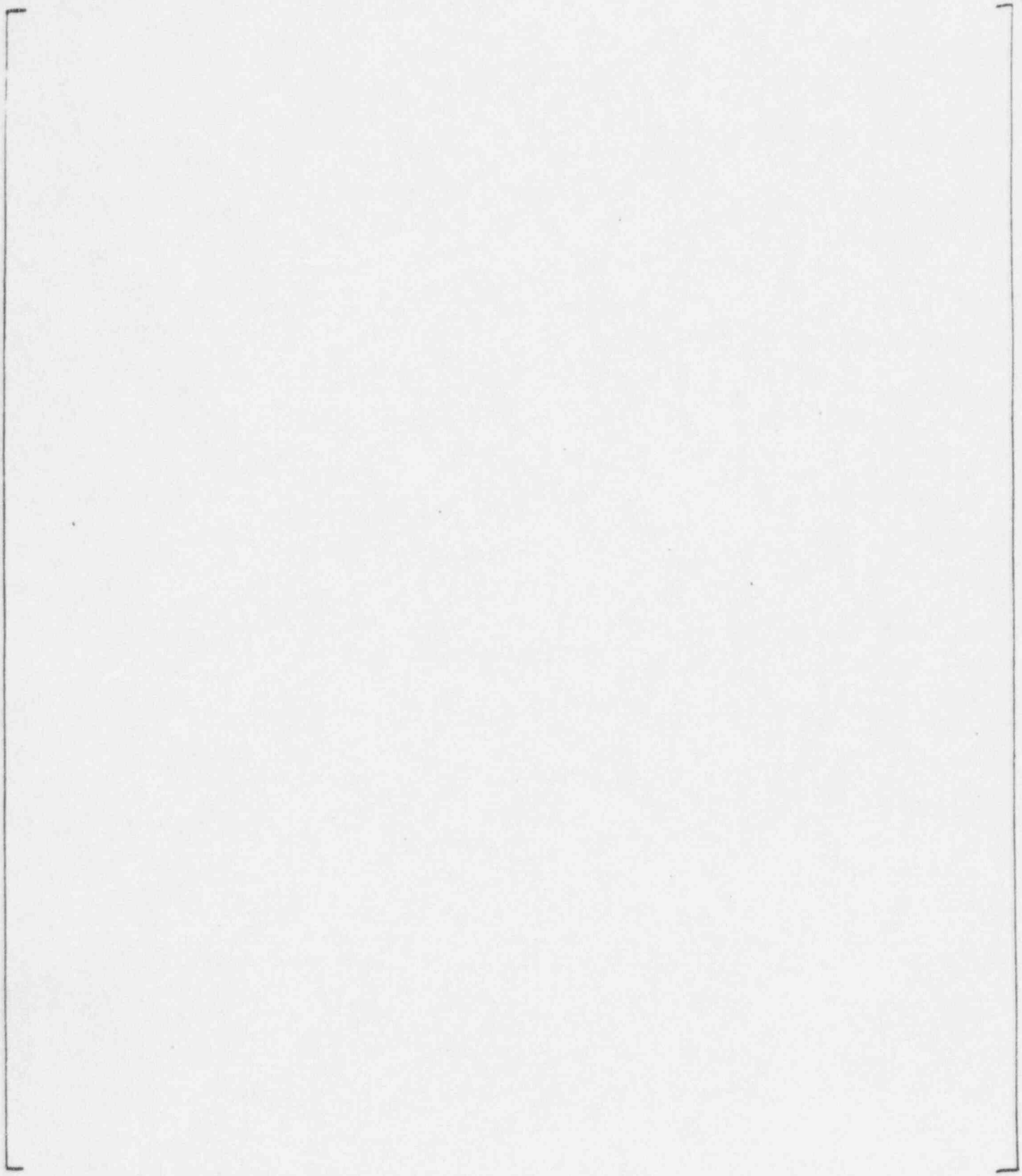

Figure 6.4-46 NOTRUMP Comparisons to Core Makeup Tank Pressure for Test C070505

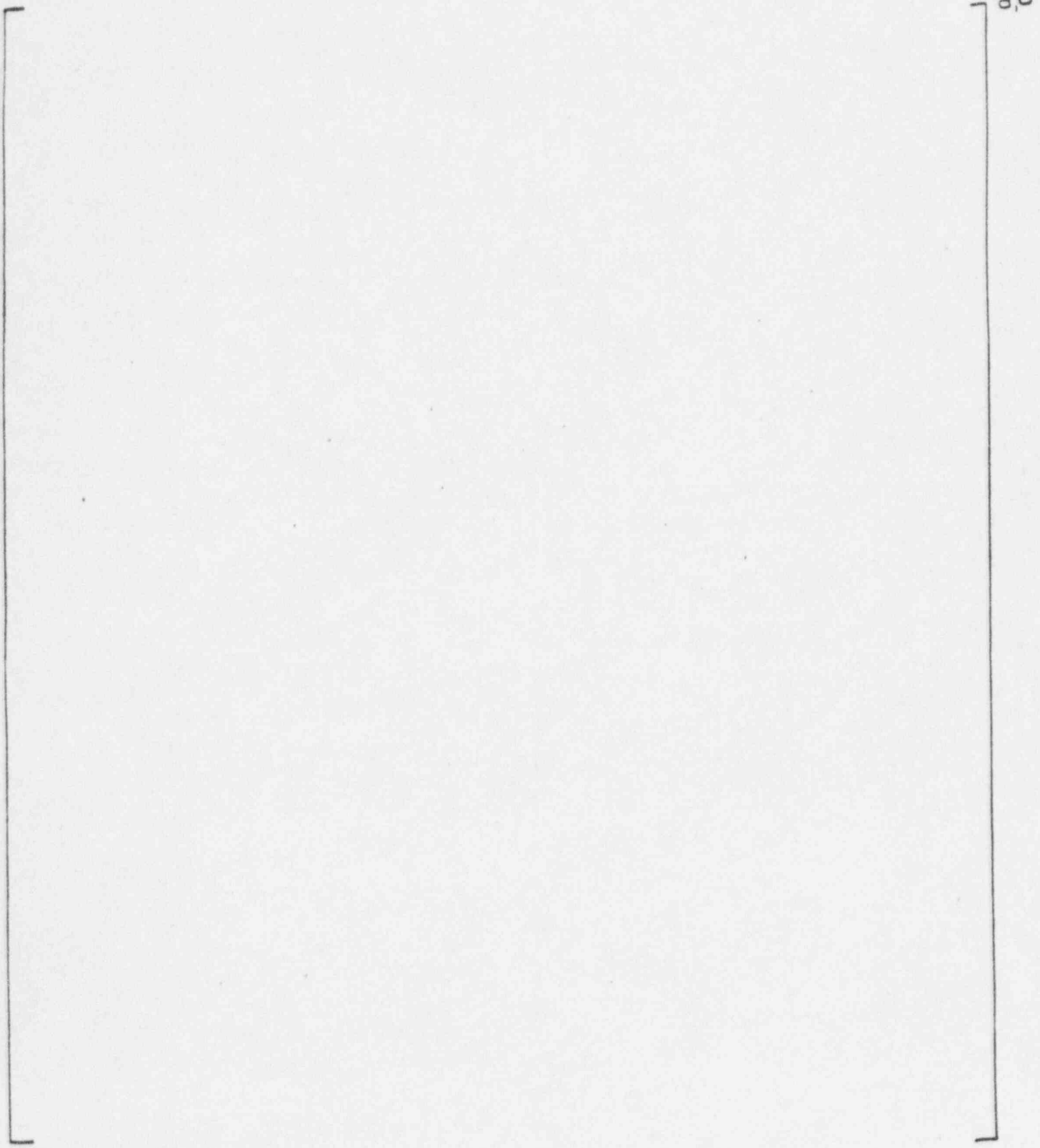

Figure 6.4-47 NOTRUMP-Calculated Core Makeup Tank Fluid Node Temperatures for Test C070505

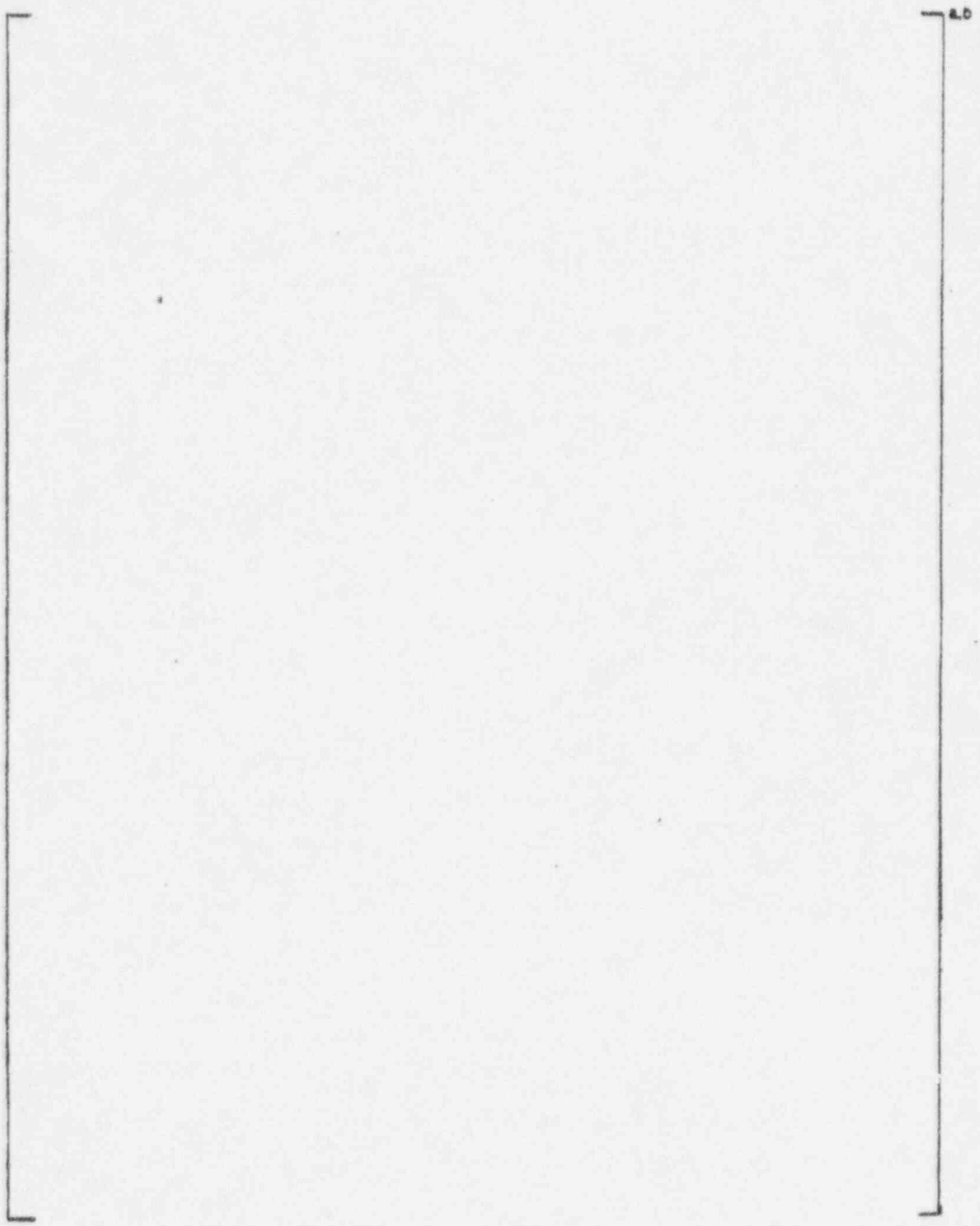

Figure 6.4-48 Core Makeup Tank Axial Fluid Temperatures for Test C070505

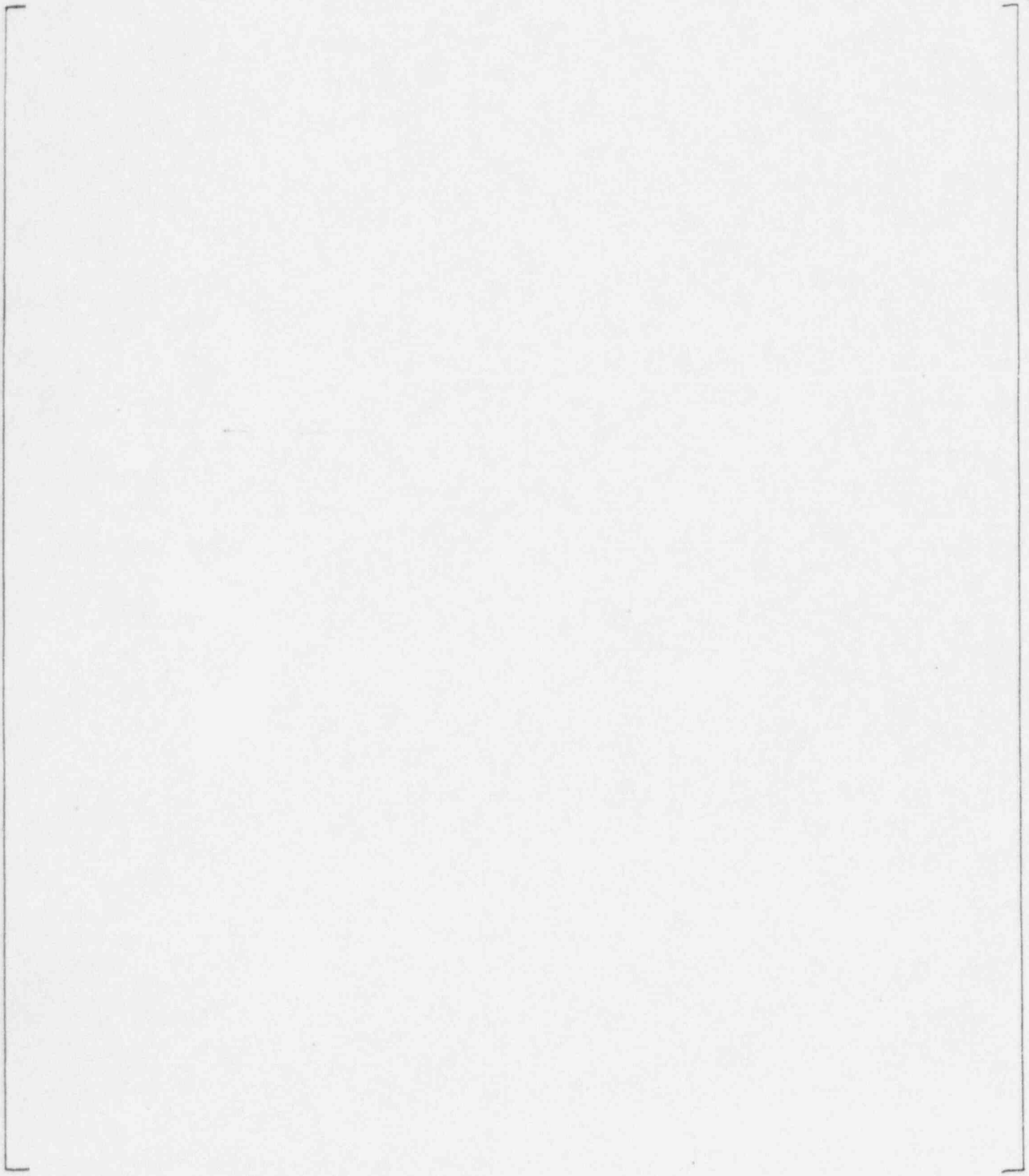

Figure 6.4-49 NOTRUMP Comparisons for Core Makeup Tank Top Node for Test C070505

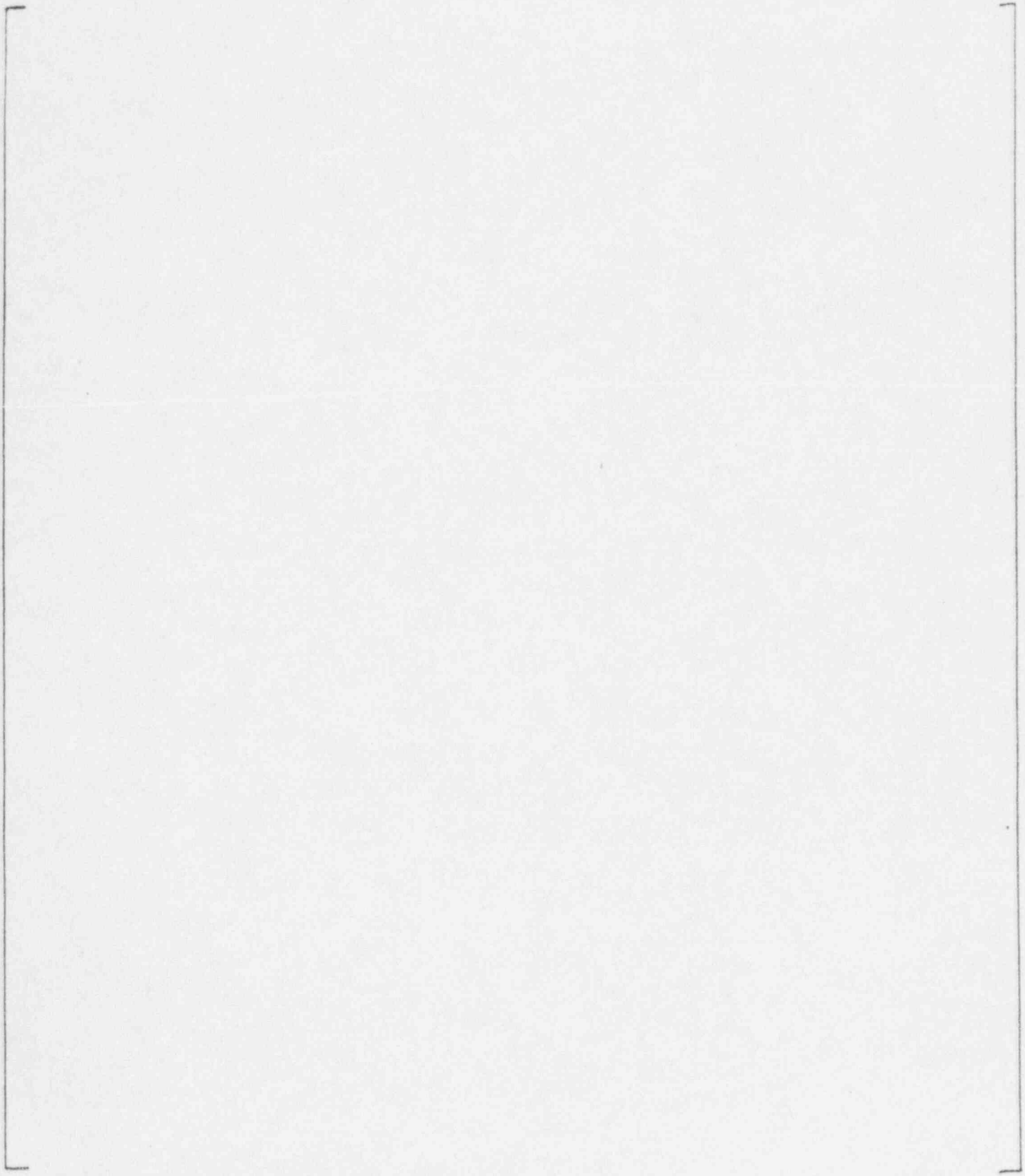

Figure 6.4-50 NOTRUMP Comparisons for Core Makeup Tank Top Cylindrical Node for Test C070505

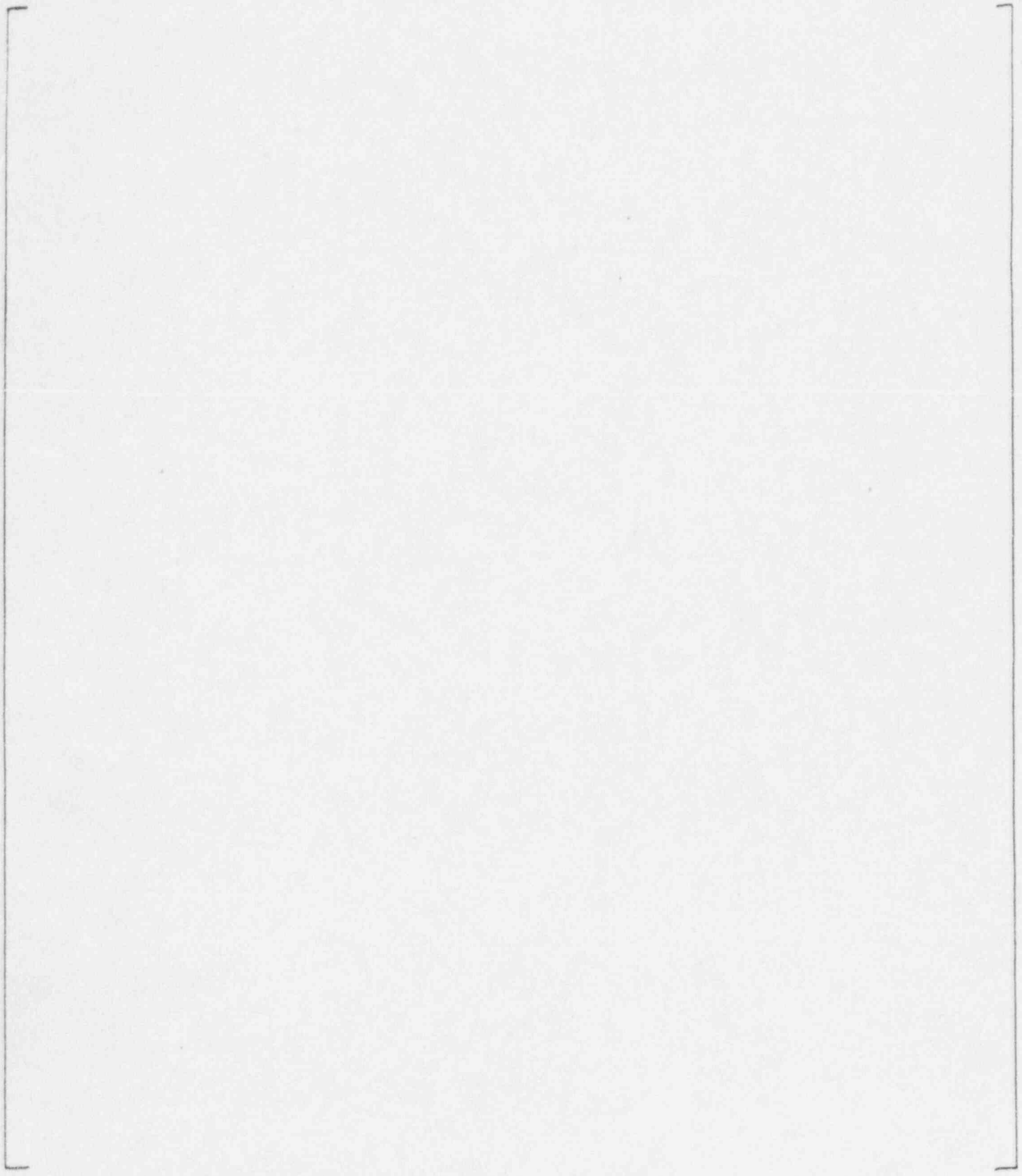

Figure 6.4-51 NOTRUMP Comparisons for Core Makeup Tank Bottom Cylindrical Node for Test C070505

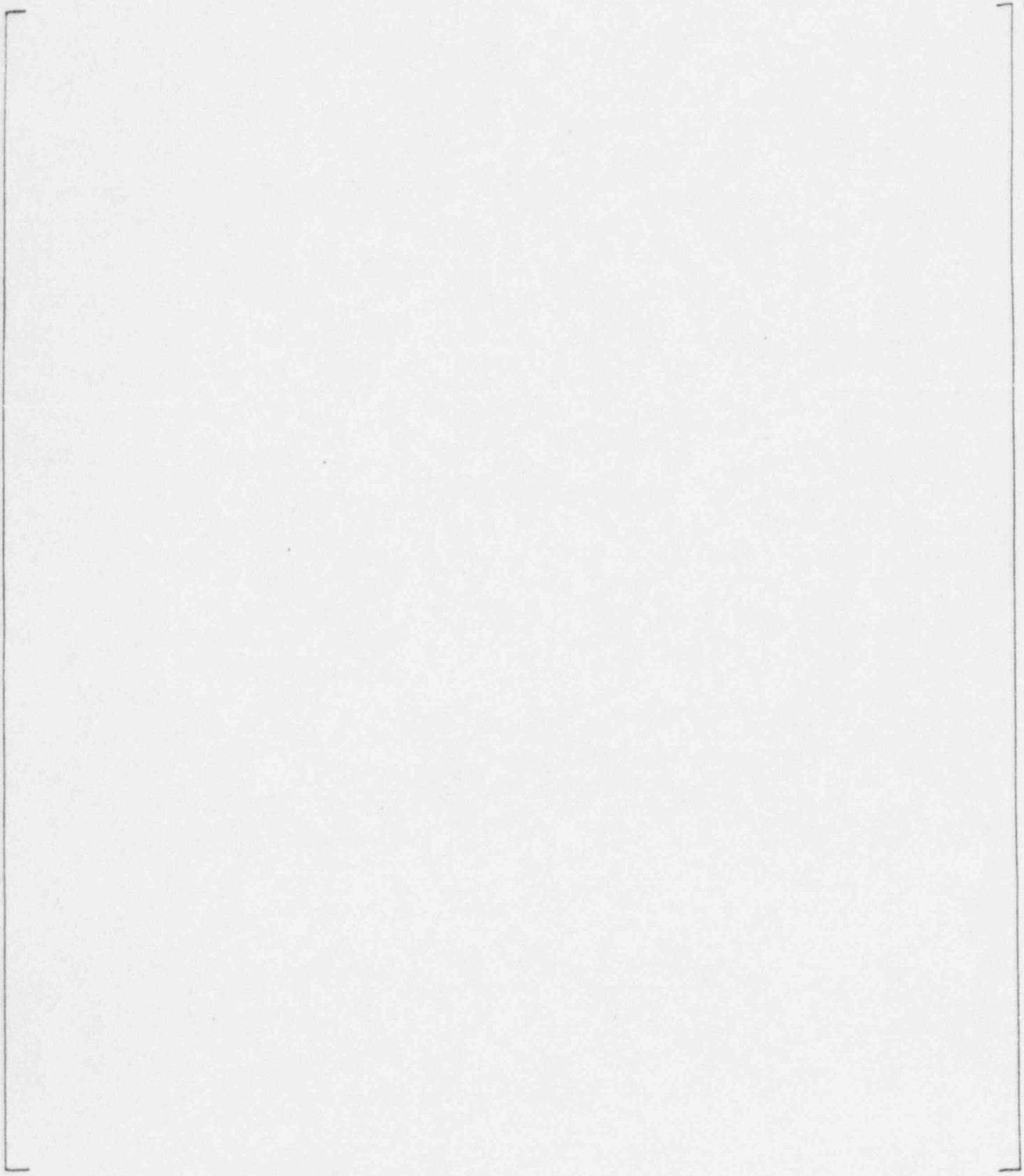

Figure 6.4-52 NOTRUMP Comparisons for Core Makeup Tank Bottom-Most Node for Test C070505

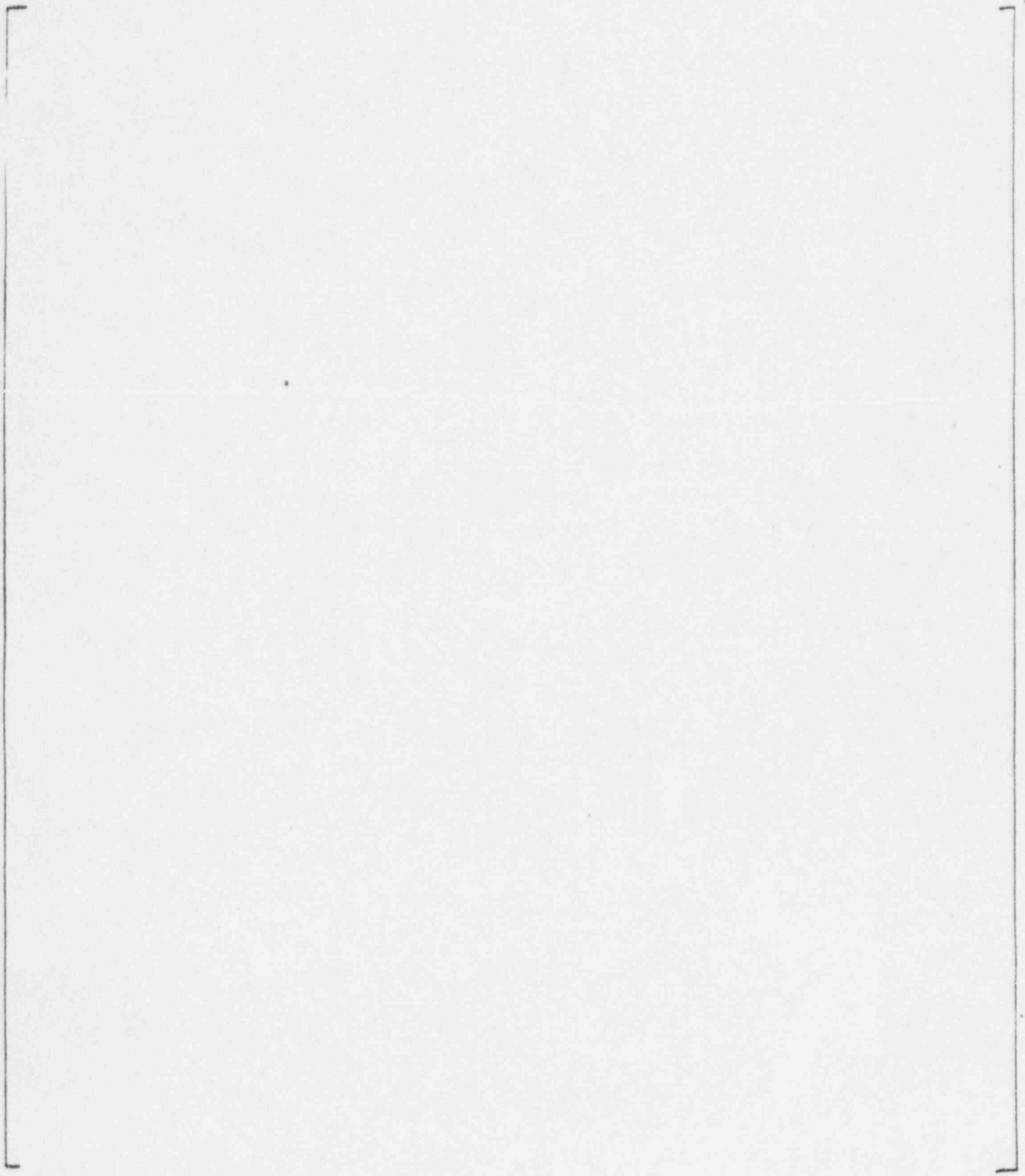

Figure 6.4-53 NOTRUMP Comparisons for Core Makeup Tank Drain Flow for Test C070505

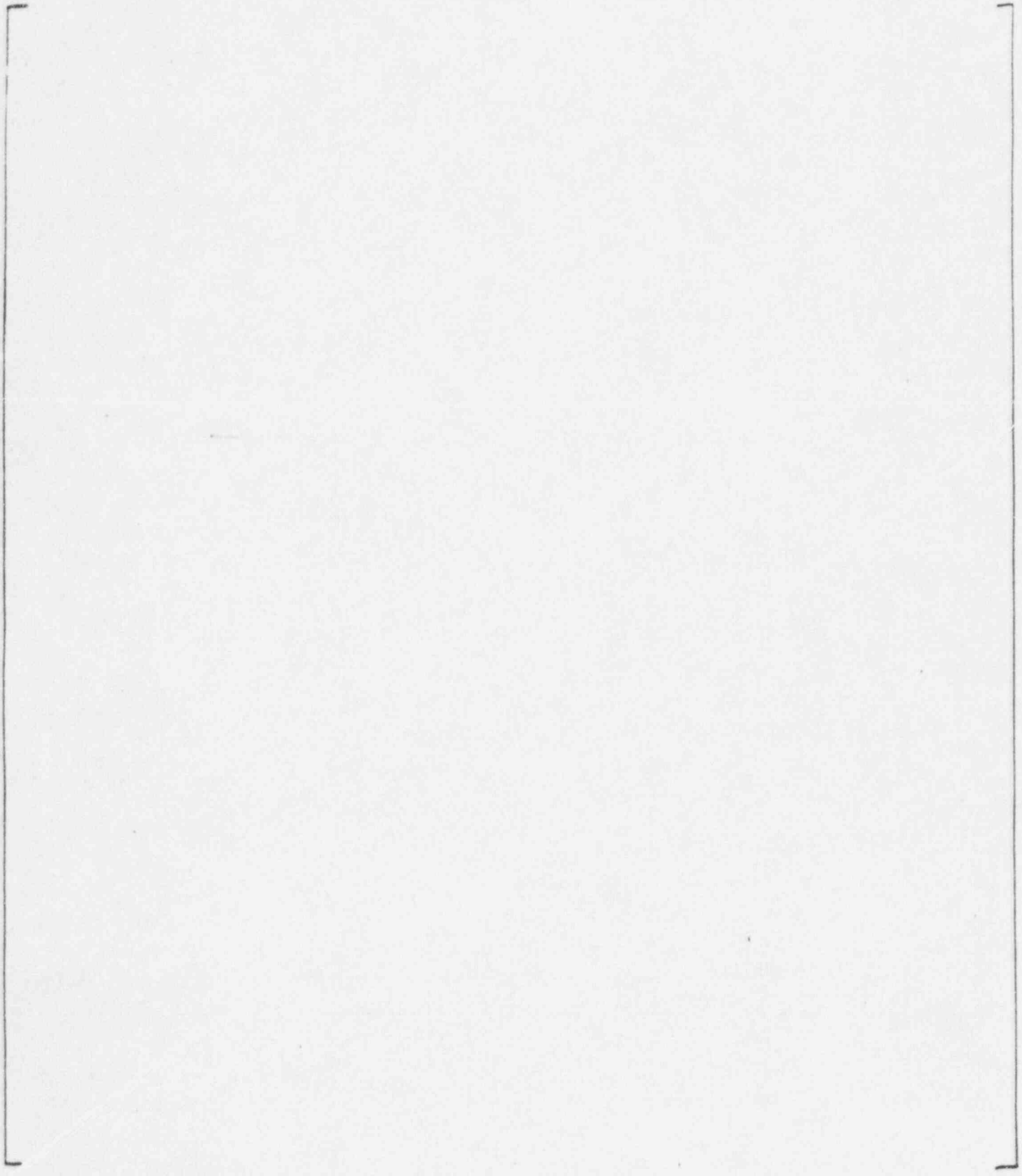

Figure 6.4-54 NOTRUMP Comparisons for Core Makeup Tank Integrated Drain Flow for Test C070505

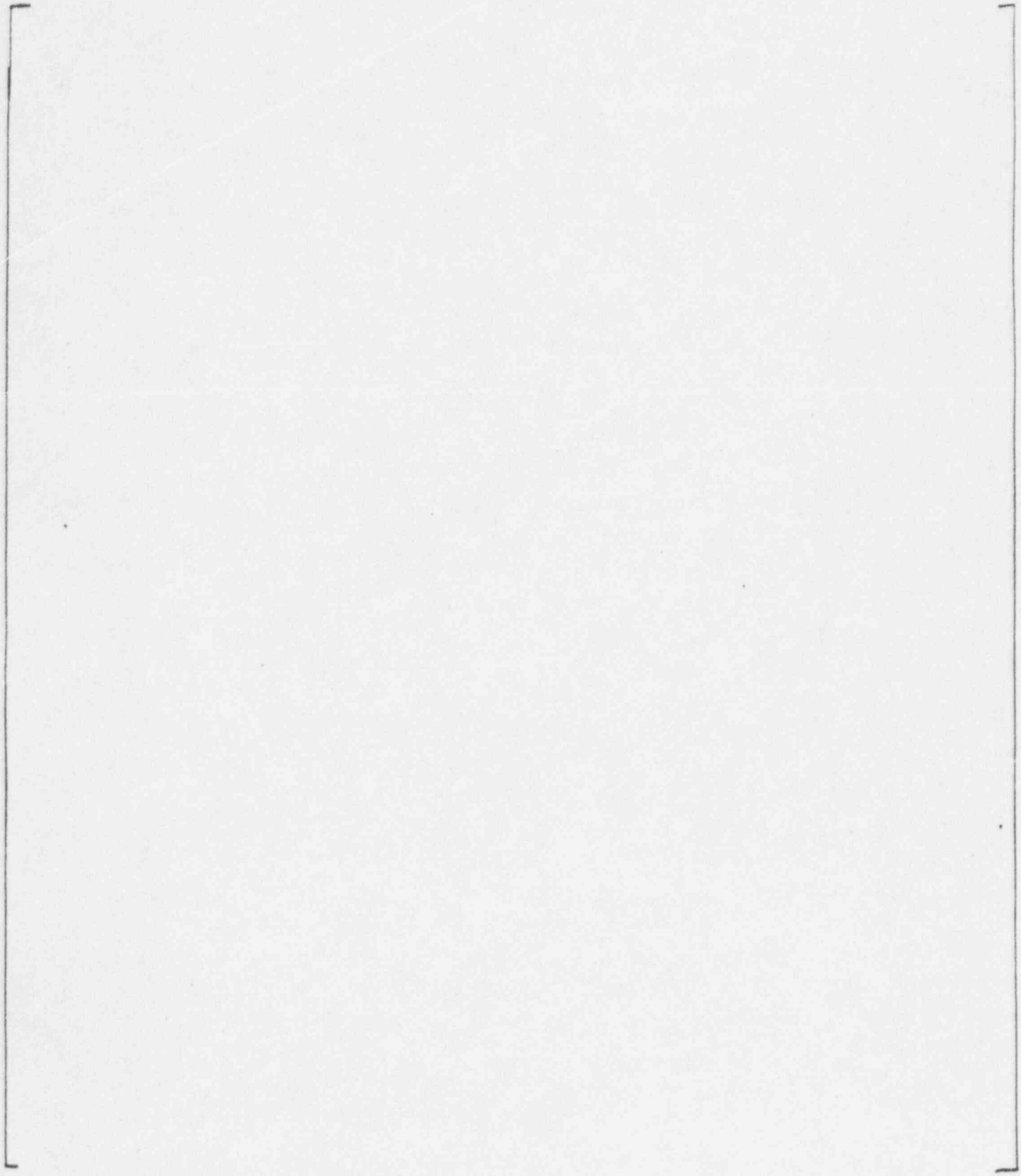

Figure 6.4-55 NOTRUMP Comparisons to Core Makeup Tank Pressure for Test C076507

a,b

Figure 6.4-56 NOTRUMP-Calculated Core Makeup Tank Fluid Node Temperatures for Test C076507

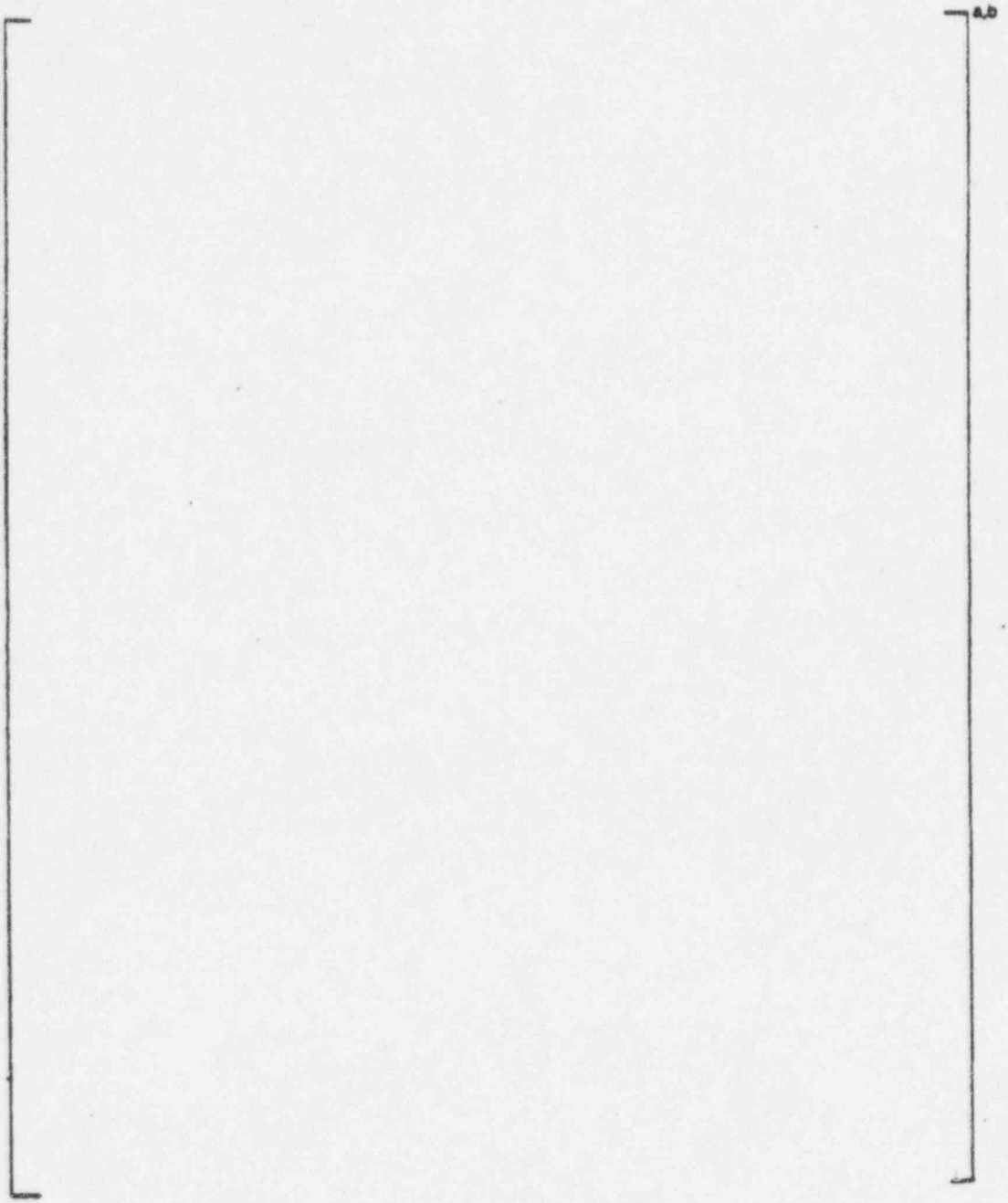

Figure 6.4-57 Core Makeup Tank Axial Fluid Temperatures for Test C076507

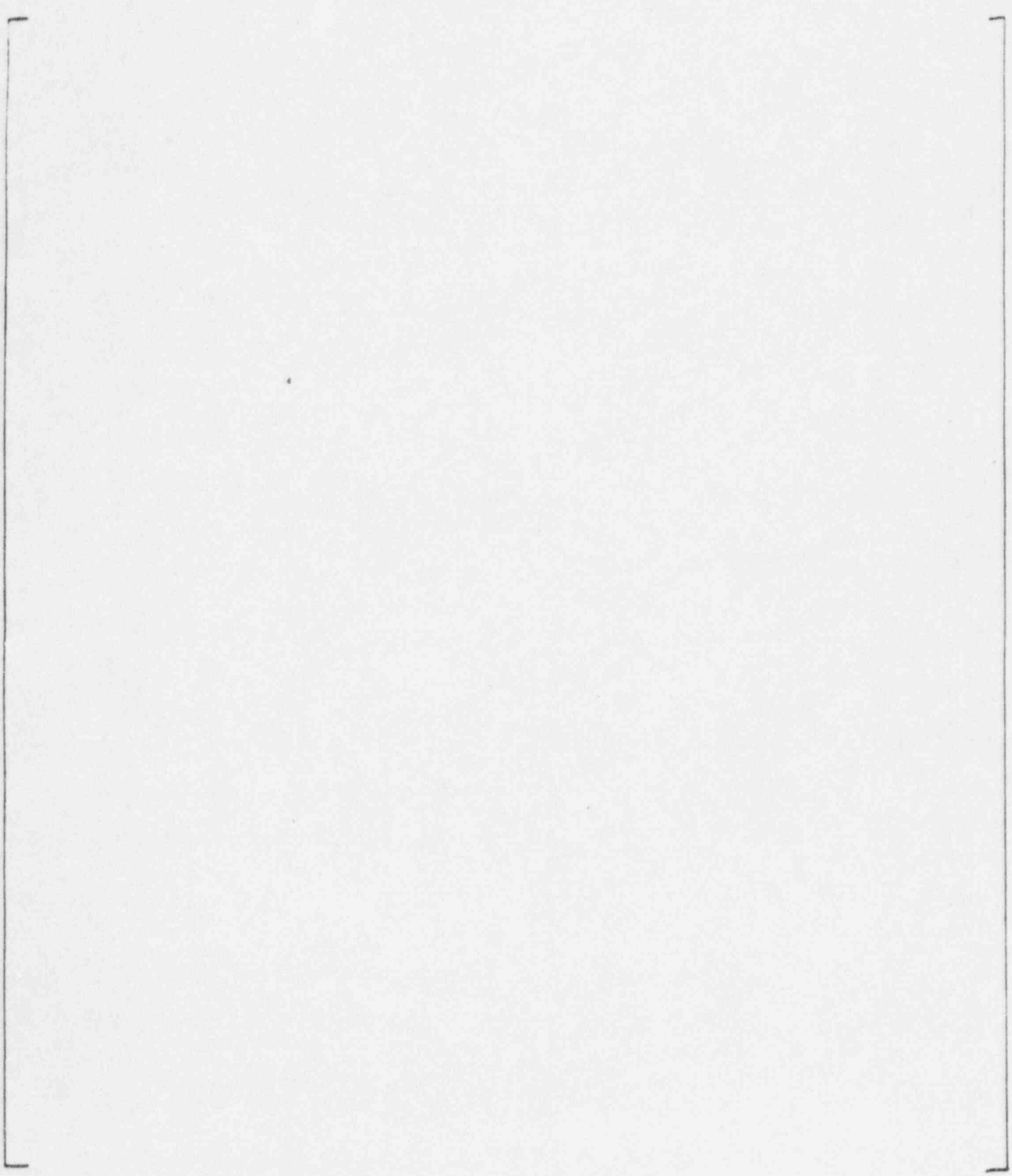

Figure 6.4-58 NOTRUMP Comparisons for Core Makeup Tank Top Node for Test C07[illegible]07

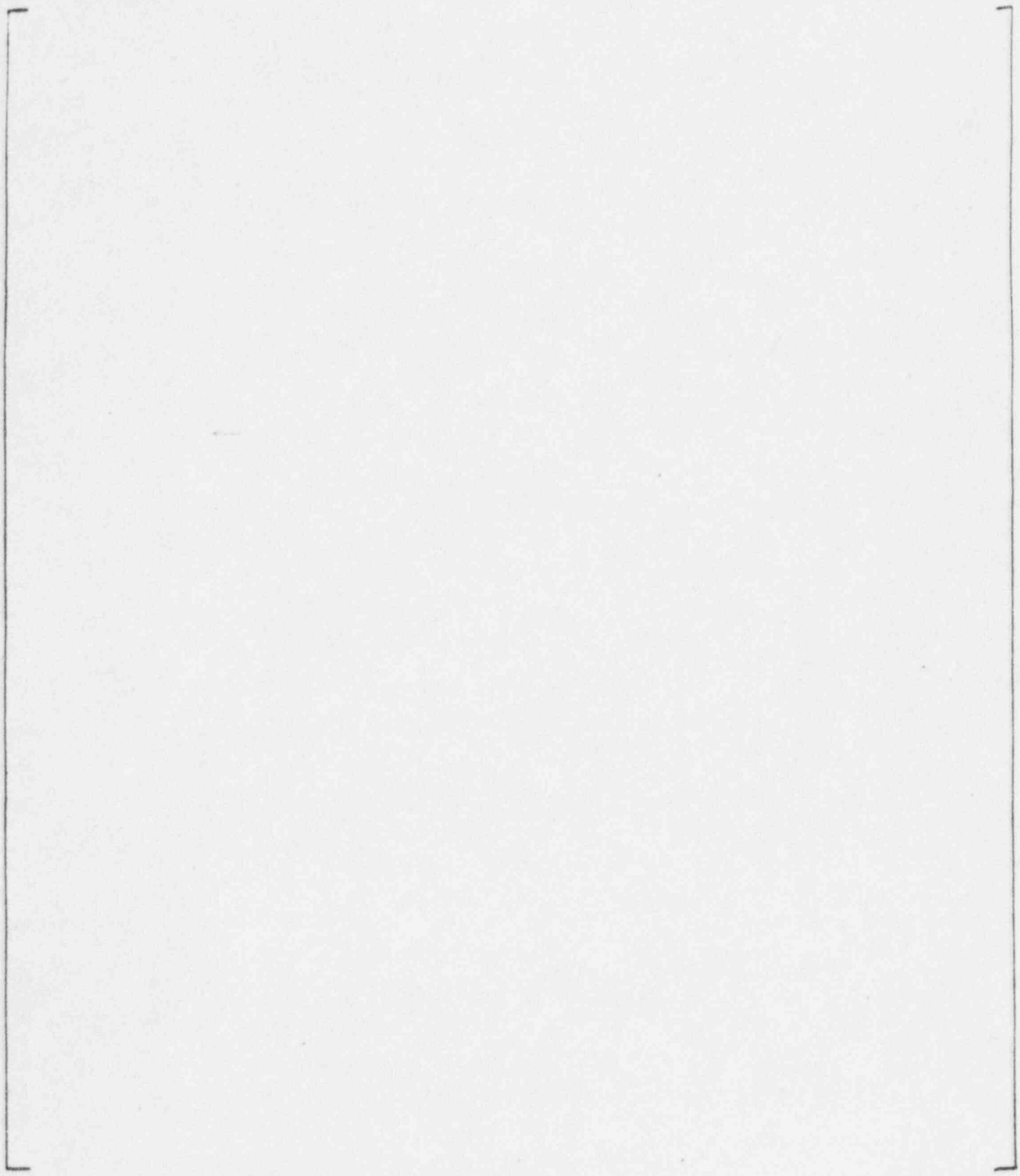

Figure 6.4-59 NOTRUMP Comparisons for Core Makeup Tank Top Cylindrical Node for Test C076507

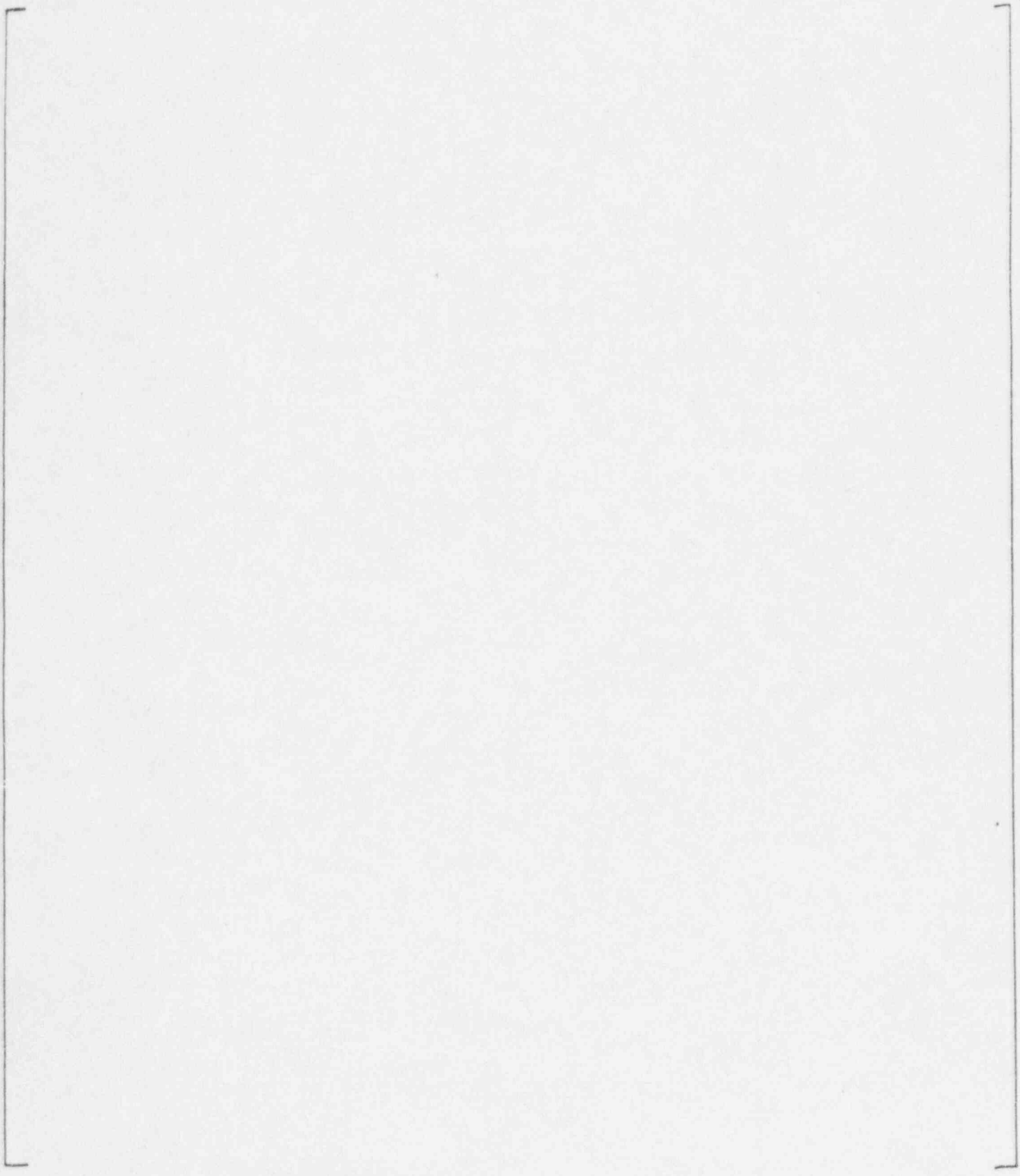

Figure 6.4-60 NOTRUMP Comparisons for Core Makeup Tank Bottom Cylindrical Node for Test C076507

a,b

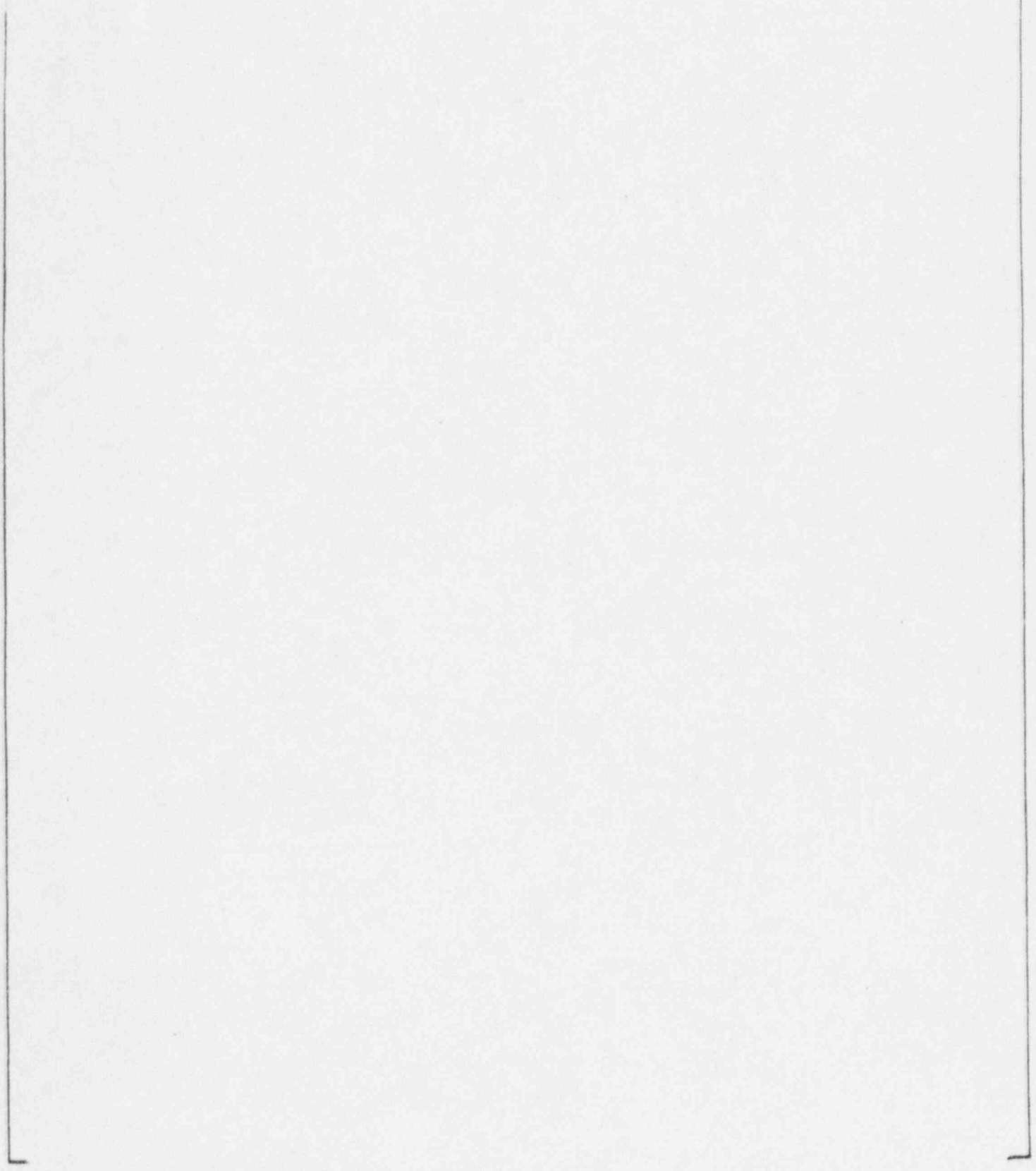

Figure 6.4-61 NOTRUMP Comparisons for Core Makeup Tank Bottom-Most Node for Test C076507

a,b

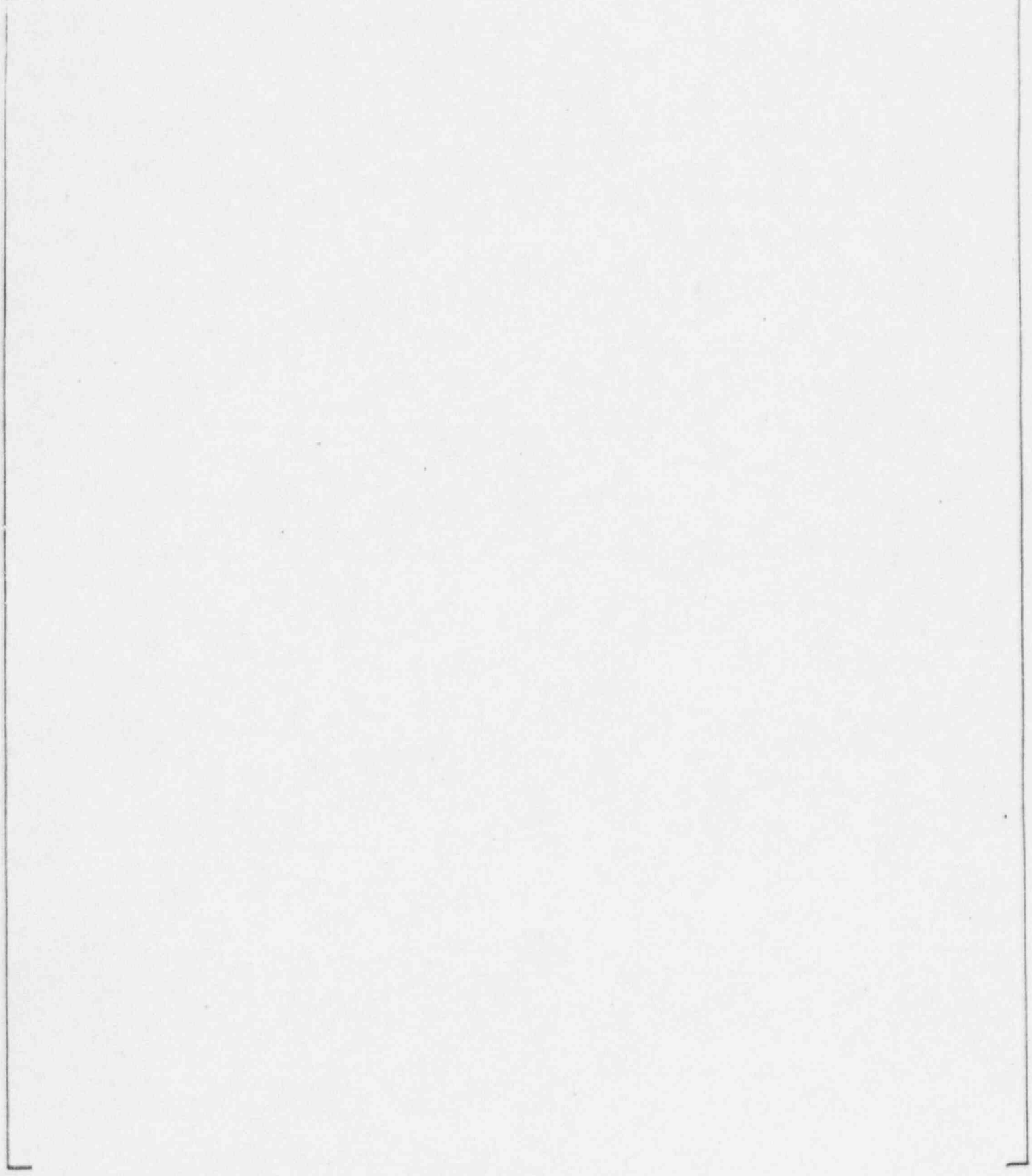

Figure 6.4-62 NOTRUMP Comparisons for Core Makeup Tank Drain Flow for Test C076507

[ ] a,b

Figure 6.4-63 NOTRUMP Comparisons for Core Makeup Tank Integrated Drain Flow for Test C076507

[a,b]

Figure 6.4-64 NOTRUMP Comparisons to Core Makeup Tank Pressure for Test C074508

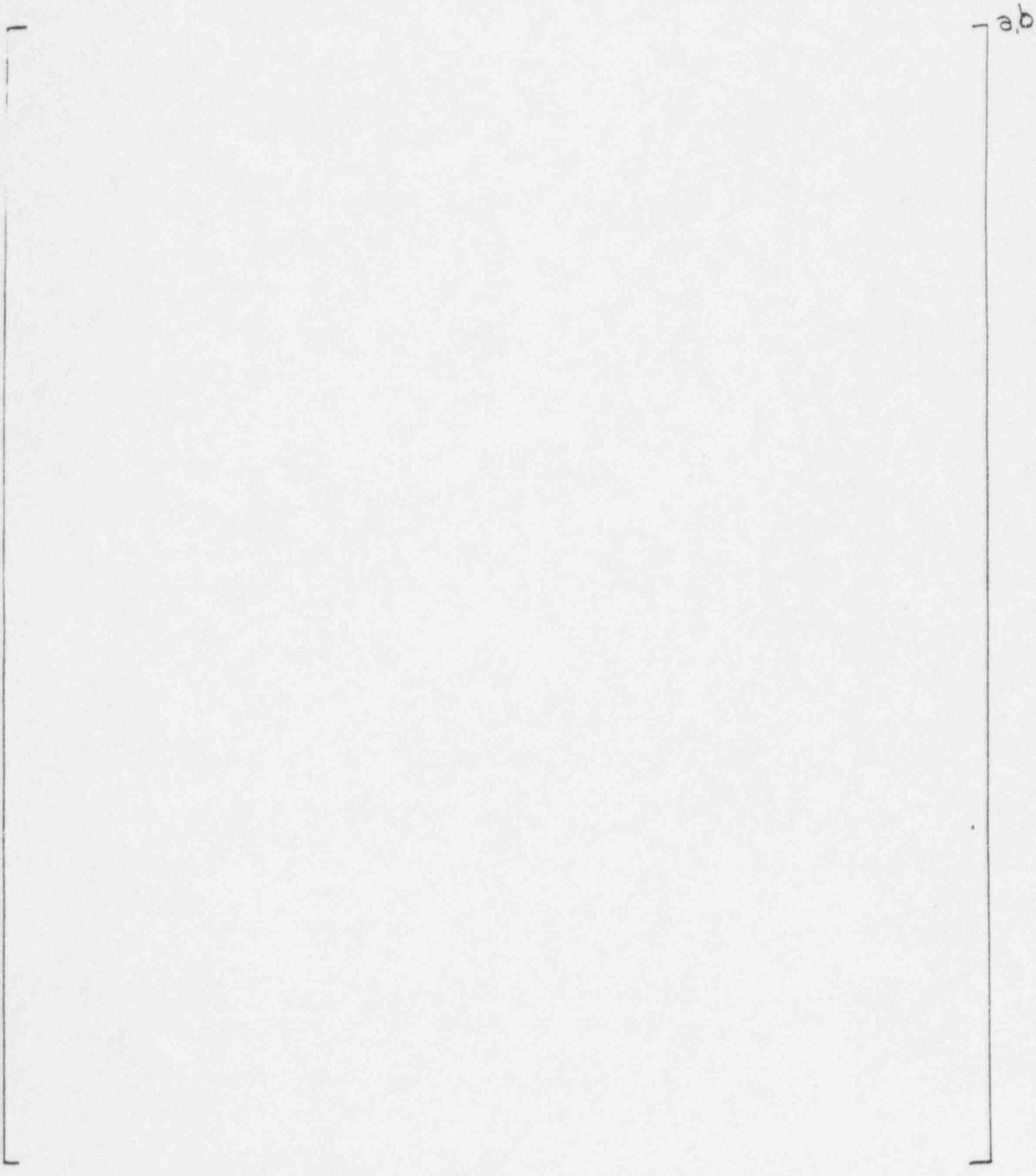

Figure 6.4-65 NOTRUMP-Calculated Core Makeup Tank Fluid Node Temperatures for Test C074508

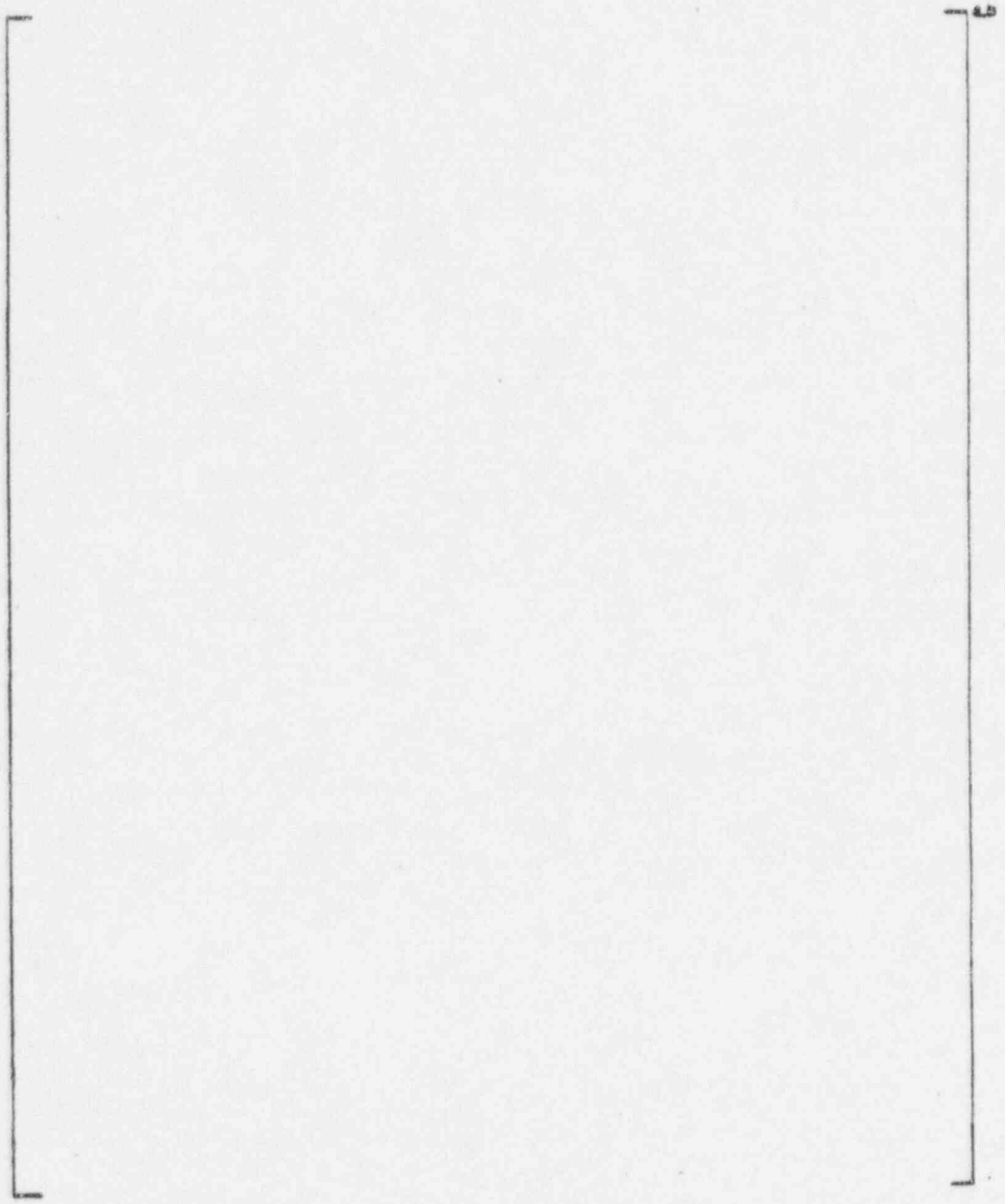

Figure 6.4-66 Core Makeup Tank Axial Fluid Temperatures for Test C074508

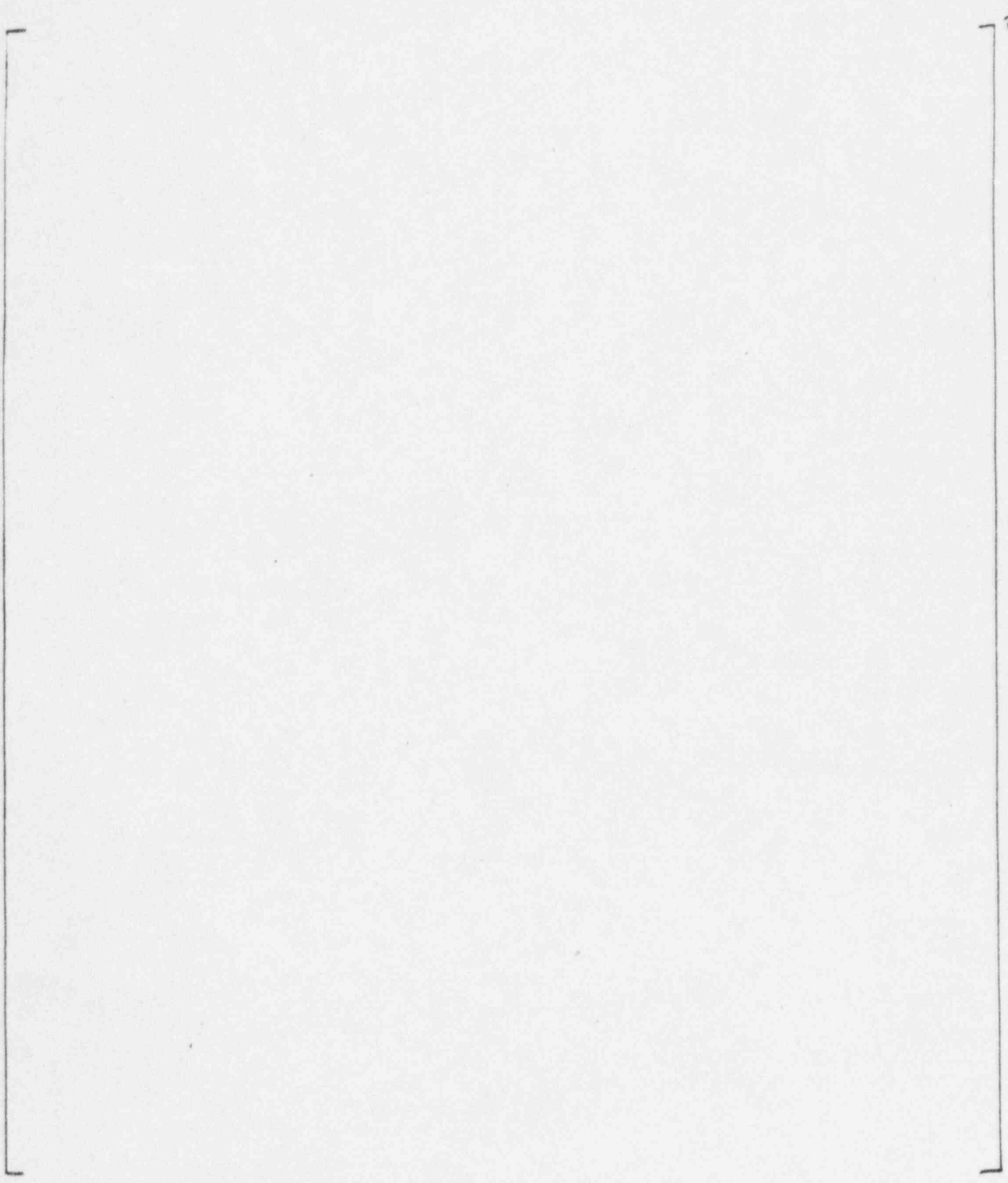

Figure 6.4-67 NOTRUMP Comparisons for Core Makeup Tank Top Node for Test C074508

a,b

Figure 6.4-68 NOTRUMP Comparisons for Core Makeup Tank Top Cylindrical Node for Test C074508

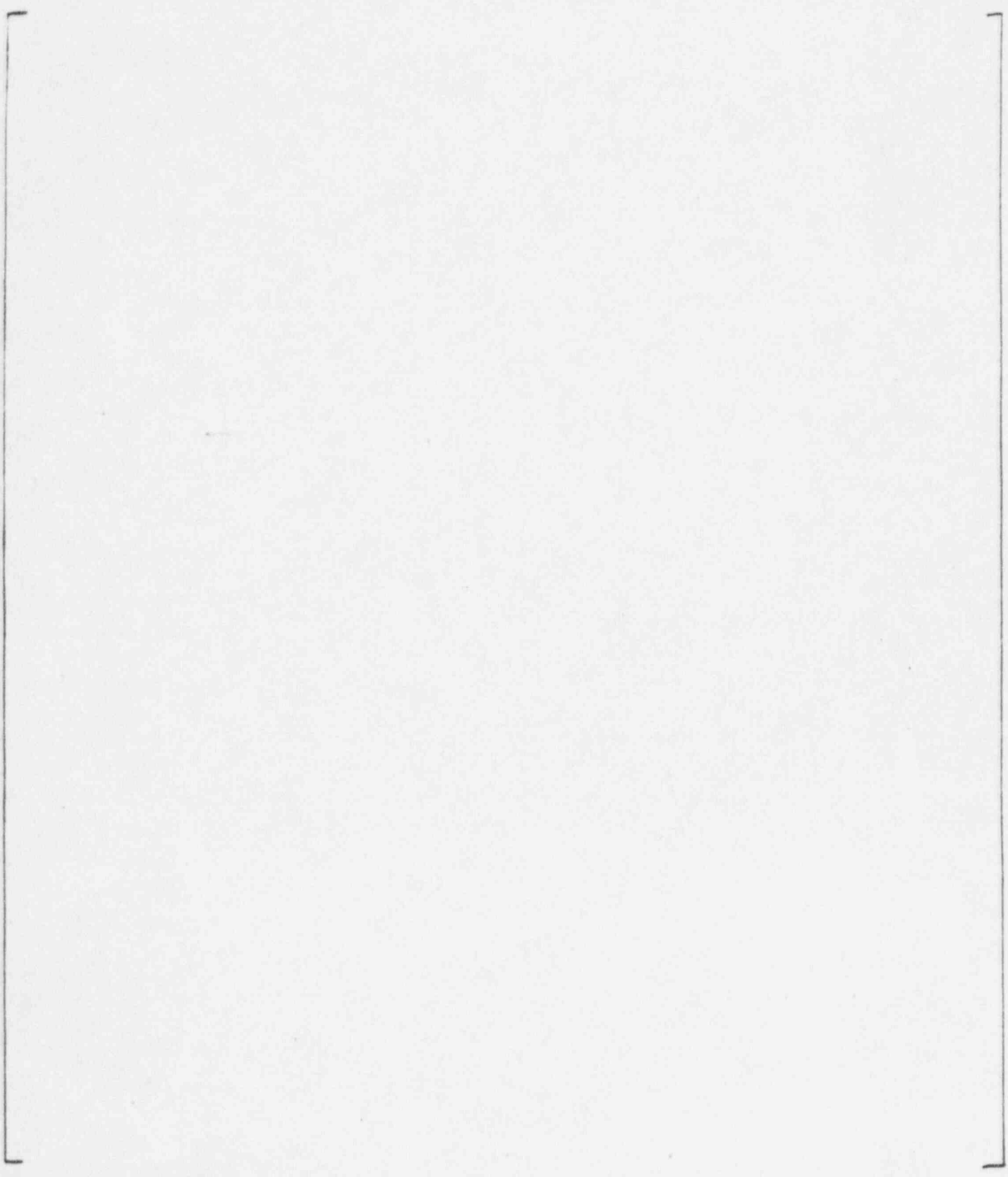

Figure 6.4-69 NOTRUMP Comparisons for Core Makeup Tank Bottom Cylindrical Node for Test C074508

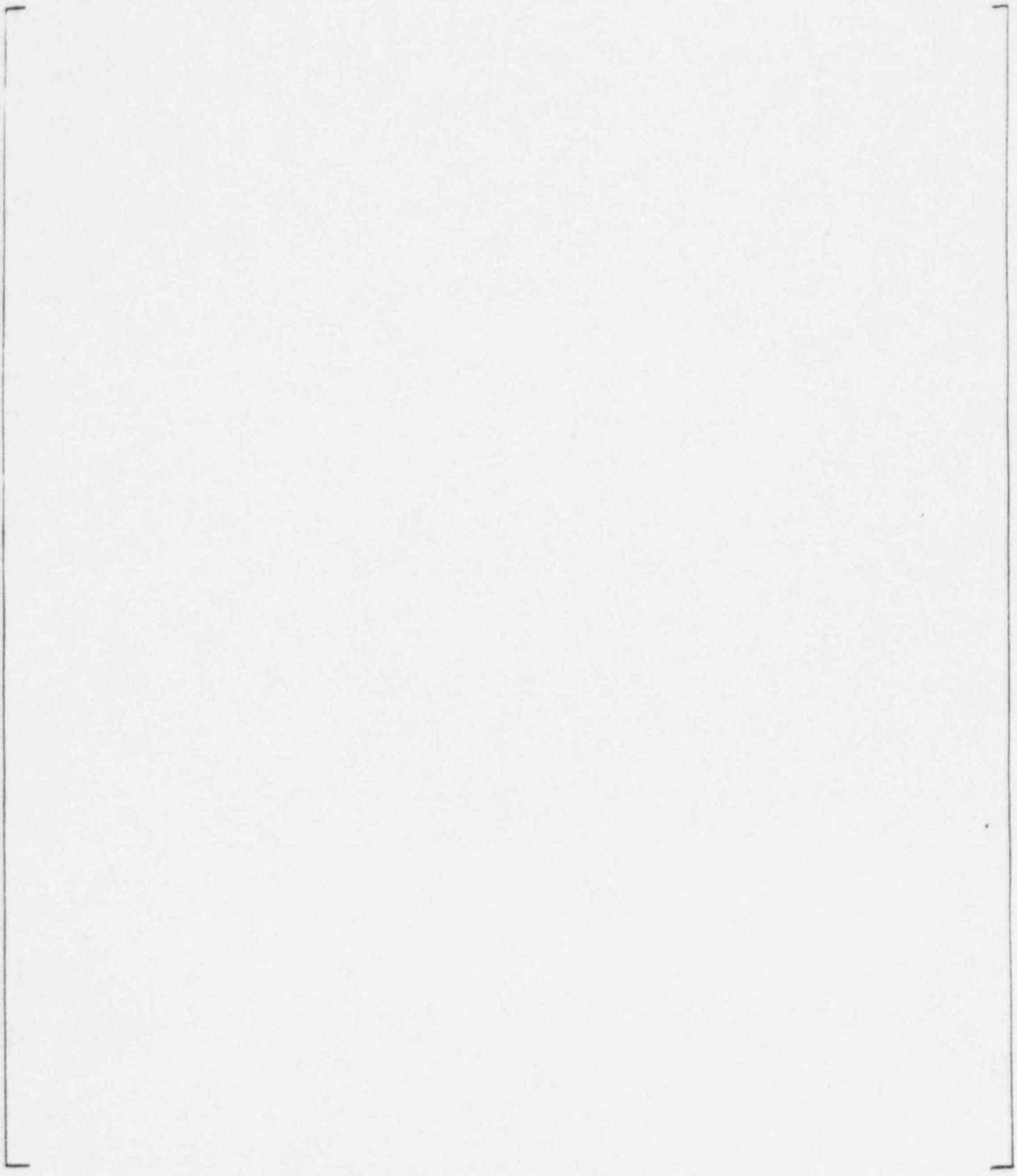

Figure 6.4-70 NOTRUMP Comparisons for Core Makeup Tank Bottom-Most Node for Test C074508

[ ]a,c

Figure 6.4-71 NOTRUMP Comparisons for Core Makeup Tank Drain Flow for Test C074508

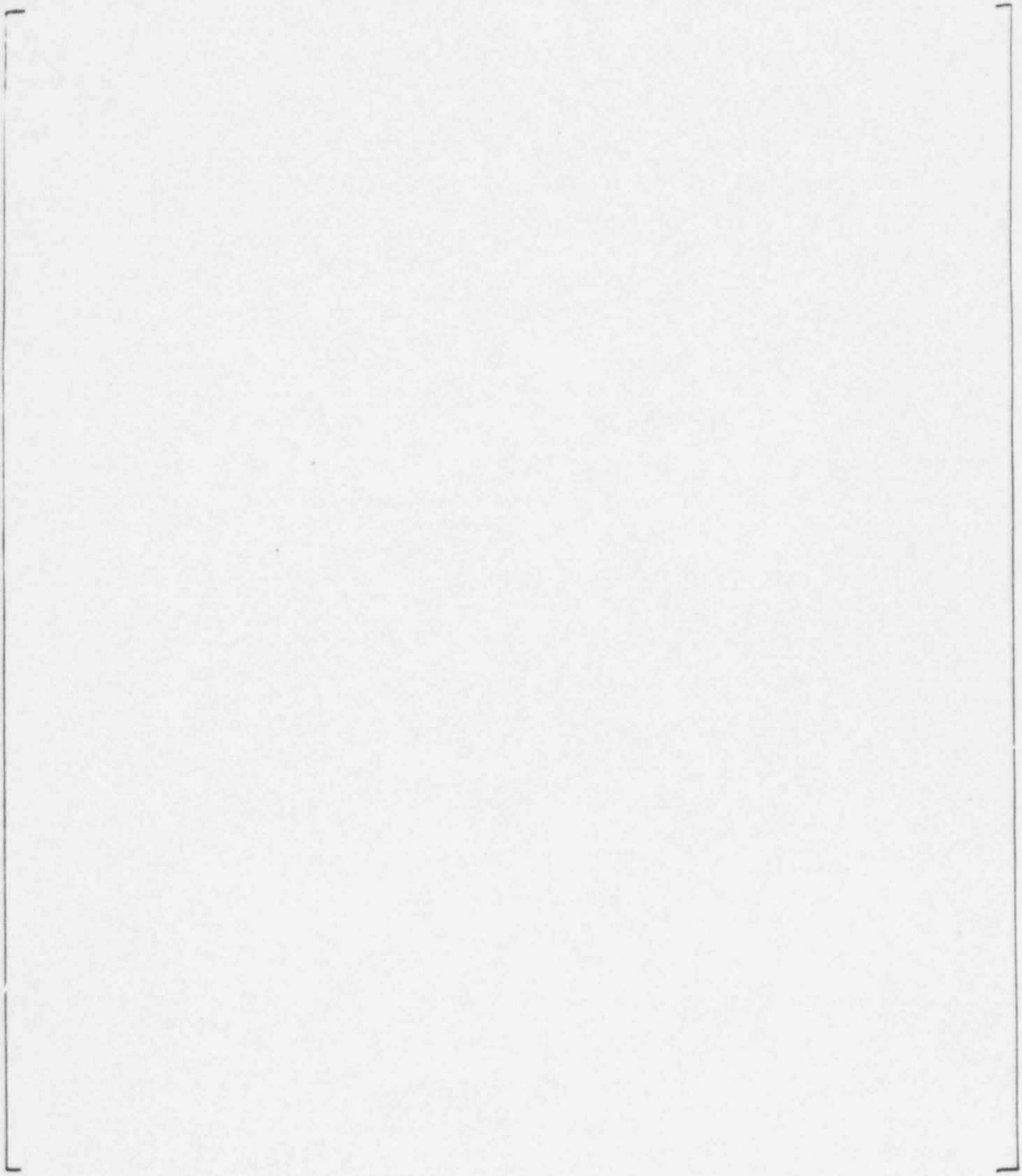

Figure 6.4-72 NOTRUMP Comparisons for Core Makeup Tank Integrated Drain Flow for Test C074508

a,b

Figure 6.4-73 NOTRUMP Comparisons to Core Makeup Tank Pressure for Test C072509

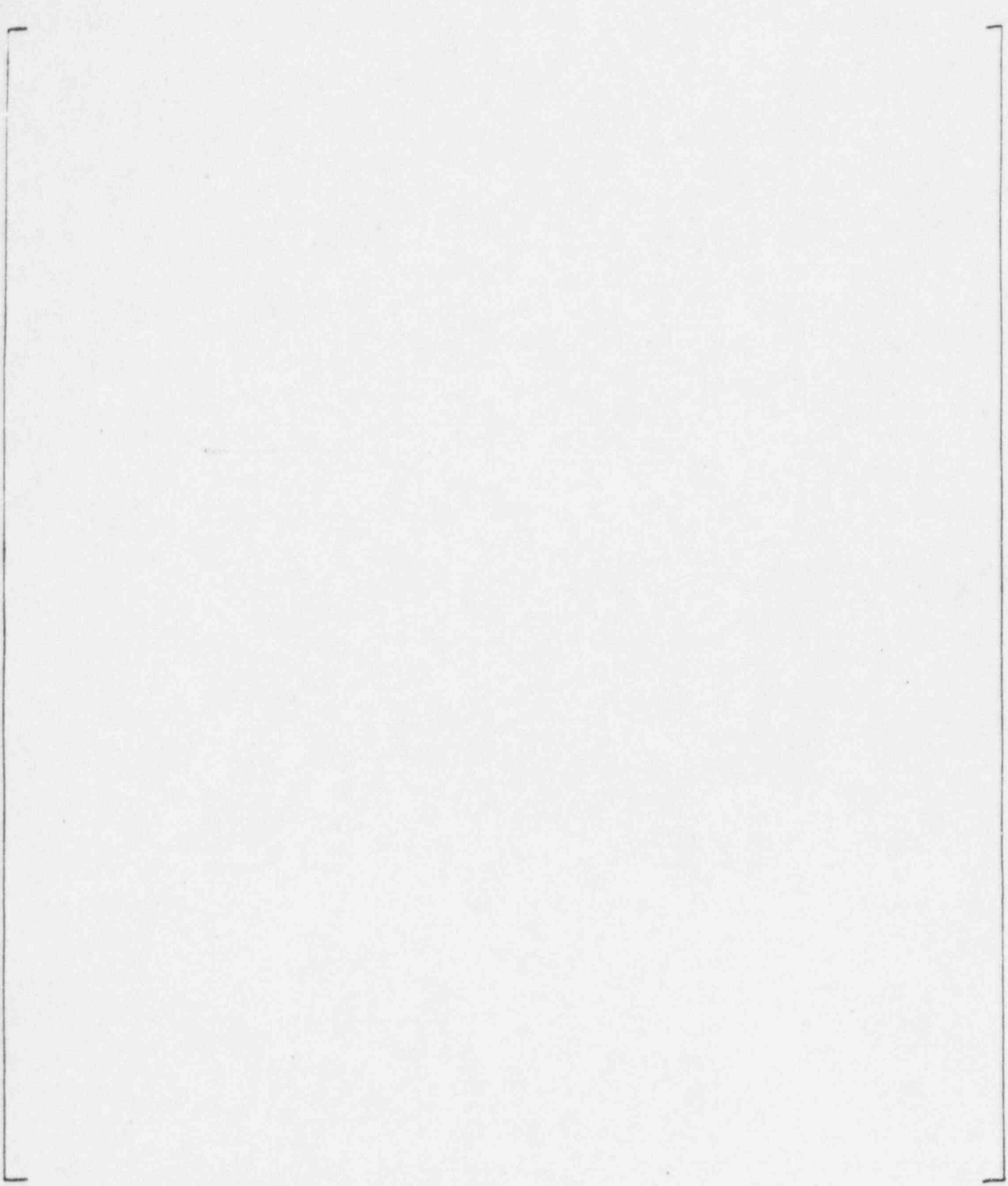

Figure 6.4-74 NOTRUMP-Calculated Core Makeup Tank Fluid Node Temperatures for Test C072509

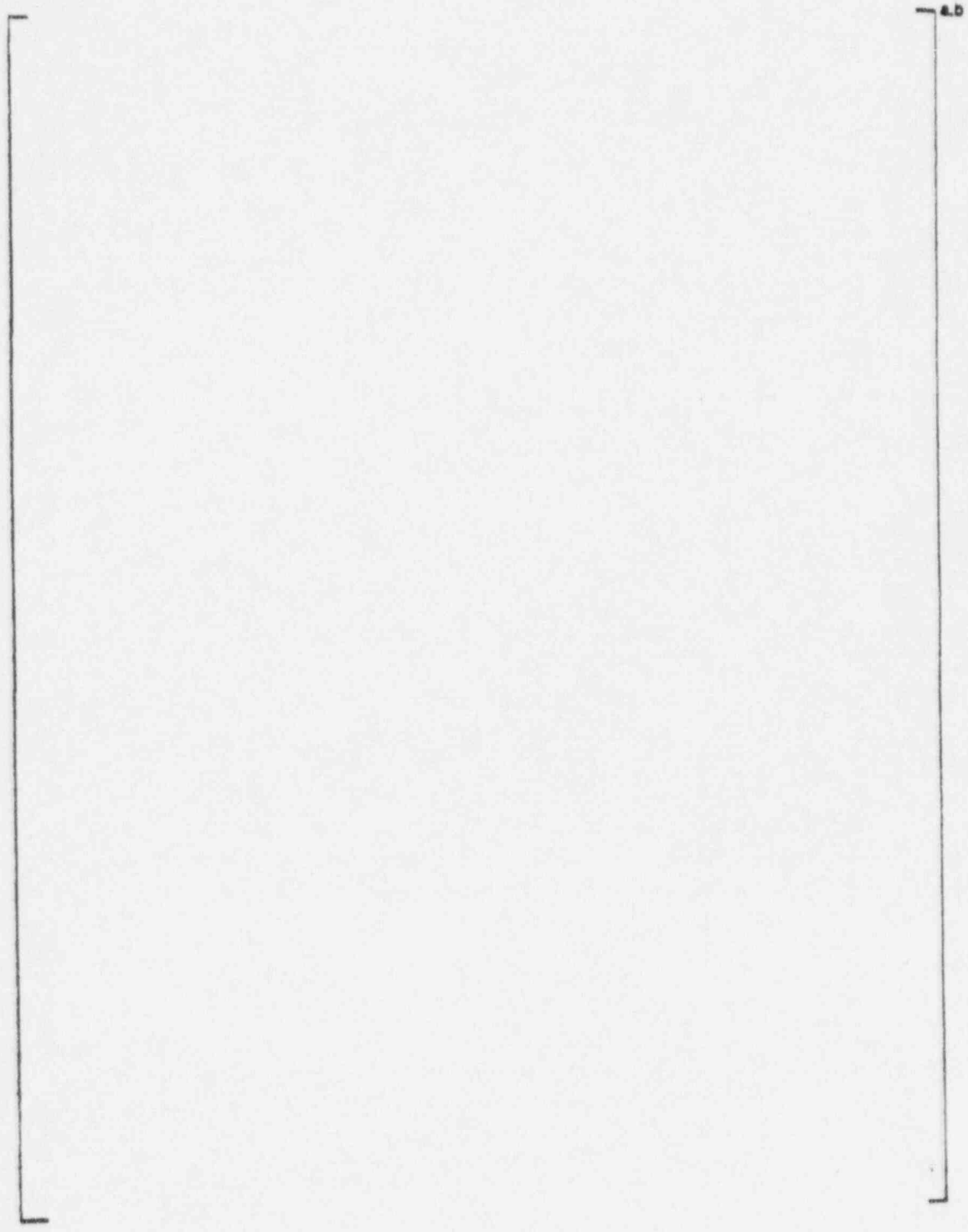

Figure 6.4-75 Core Makeup Tank Axial Fluid Temperatures for Test C072509

[ ] a,b

Figure 6.4-76 NOTRUMP Comparisons for Core Makeup Tank Top Node for Test C072509

a,b

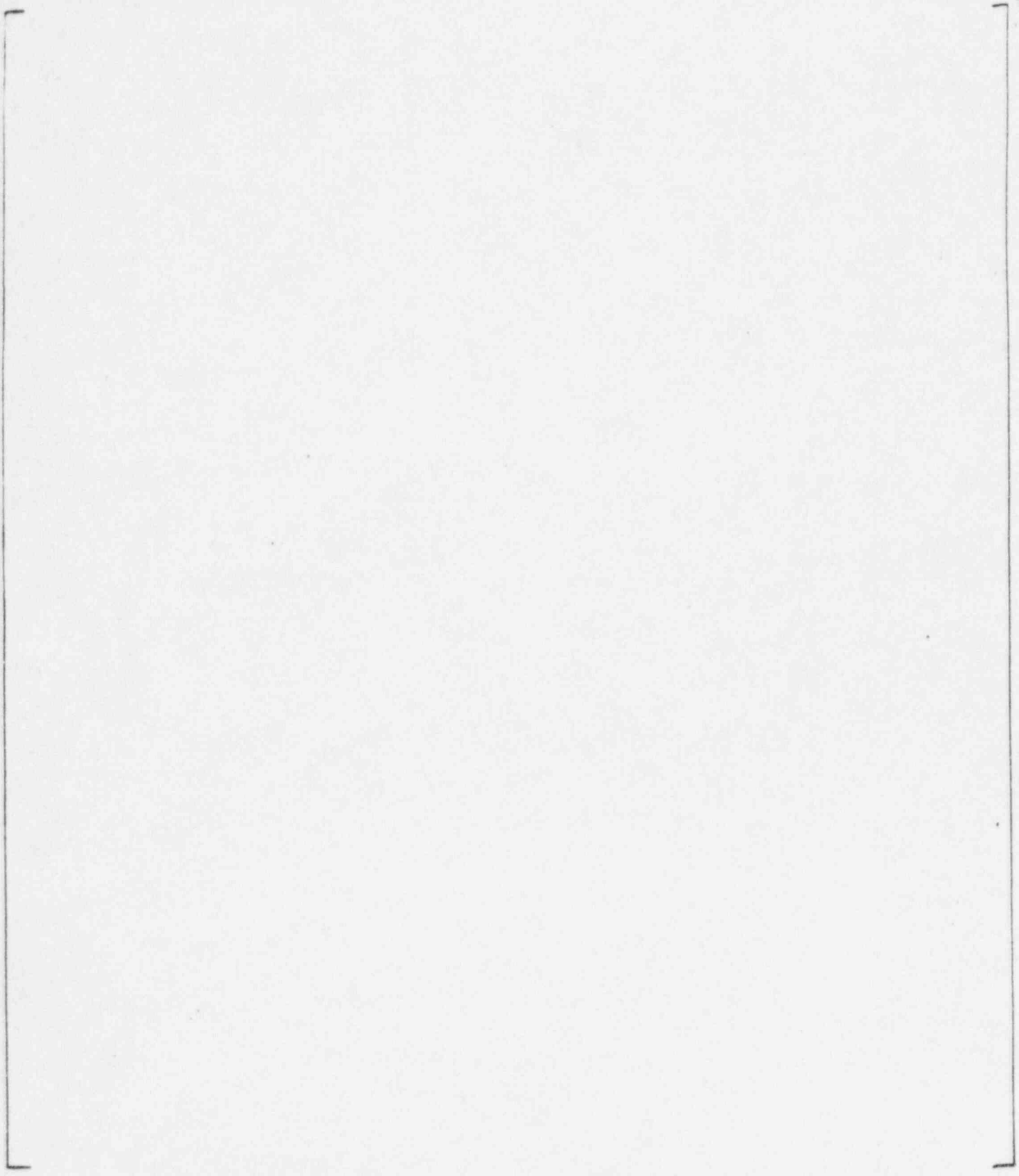

Figure 6.4-77 NOTRUMP Comparisons for Core Makeup Tank Top Cylindrical Node for Test C072509

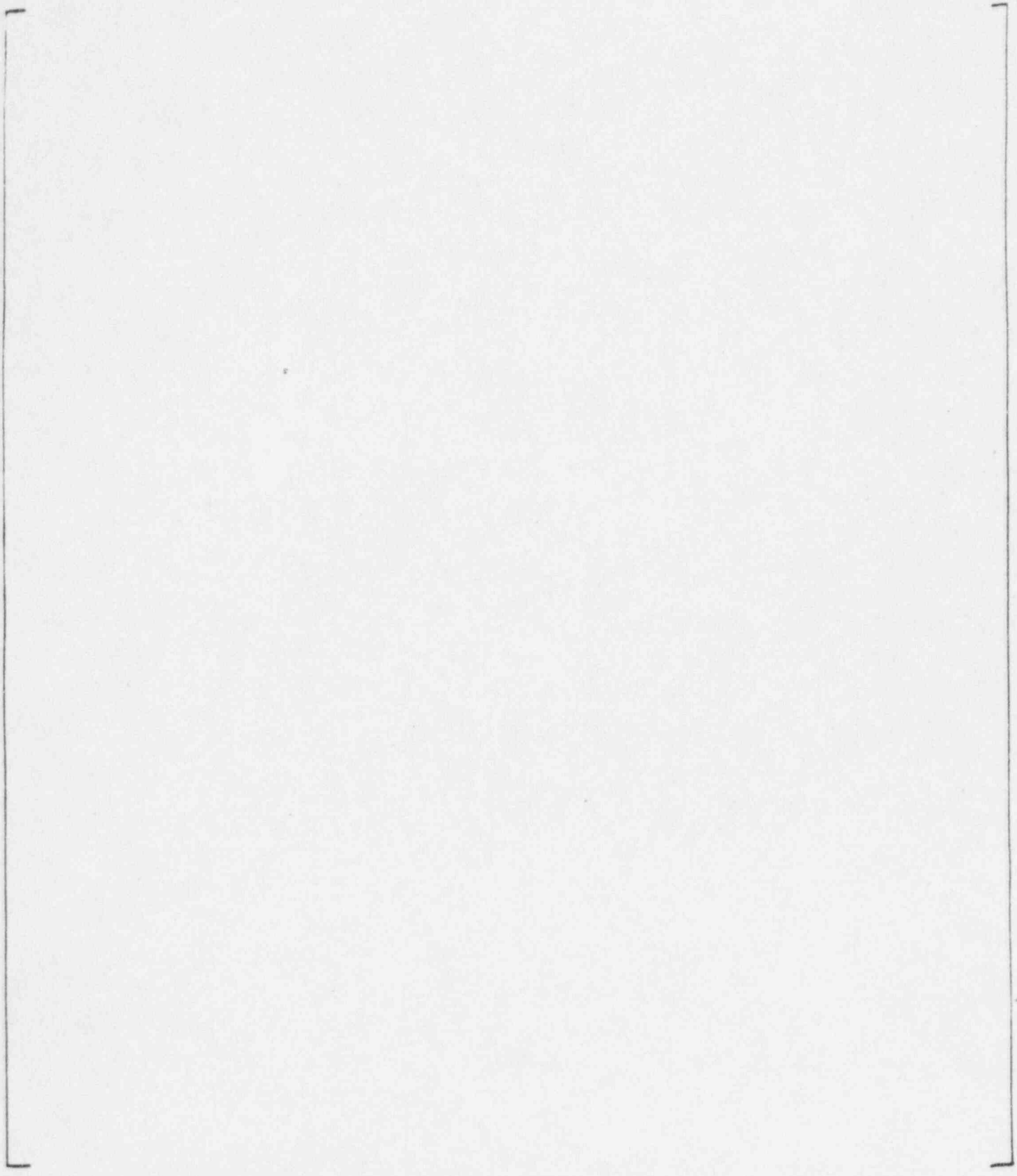

Figure 6.4-78 NOTRUMP Comparisons for Core Makeup Tank Bottom Cylindrical Node for Test C072509

[ ] a,b

Figure 6.4-79 NOTRUMP Comparisons for Core Makeup Tank Bottom-Most Node for Test C072509

[ ] a,b

Figure 6.4-80 NOTRUMP Comparisons for Core Makeup Tank Drain Flow for Test C072509

a,b

Figure 6.4-81 NOTRUMP Comparisons for Core Makeup Tank Integrated Drain Flow for Test C072509

6.5 Comparison of NOTRUMP to the 300-Series Core Makeup Tank Tests

6.5.1 Introduction

A limited number of CMT 300-series tests have been analyzed with the final version of the NOTRUMP code to confirm that the previous results of the preliminary validation report (Reference 6-2) for the 300-series tests remain valid. The extremes in the system pressure are examined. Test C039309, a 1100-psi test, and test C031307, a 25-psi test, are reanalyzed with the final version of NOTRUMP.

The 300-series CMT tests are separate effects tests that specifically examine the steam/water condensation and mixing that would be expected of the CMT performance following a postulated larger small-break LOCA in which there is almost no CMT circulation. This situation can only occur if the break is large and dominates the flow behavior of the primary system, so that the circulation behavior of the CMT is minimized, and the CMT water at the top of the CMT is cold. This situation could also occur for a large-break LOCA. For most small-break situations, there will be significant circulation to heat up the top water layer, which will reduce the rapid condensation.

The CMT facility is modeled using the same noding as for the 500-series test as shown in Figure 6.2-5. The test initial conditions are used as boundary conditions for the calculation. Also, the transient steam flow and enthalpy are input to better model the dynamic effects of the condensation and draining process. This minor change in the CMT test facility noding from the preliminary report has no difference in the results since the steam conditions are given from the test.

The tests revealed an initial surge of steam into the CMT as the steam was rapidly condensed by the subcooled water at the top of the tank. As the condensation progressed, the water layer at the top of the tank mixed with the steam, and the temperature of the layer approached the saturation temperature for the pressure in the tank. Once the temperature of the liquid layer at the top of the tank approached saturation, the steam was not fully condensed and a steam-water interface formed at the top of the tank. Once this interface formed, the tank drained as if there was air at the top of the tank. The observed drain flow increased to near the nominal value, which was determined by a free drain of the tank. The steam flow significantly decreased since the condensation was reduced to the liquid layer at the top of the CMT, and the wall condensation was also reduced since the hot liquid layer heated the CMT walls.

The results for the repeat calculations for the 300-series tests are described, and plots are provided comparing the NOTRUMP calculations to the CMT data. The CMT test has a large number of fluid thermocouples in the tank to measure the heat-up of the liquid as the steam enters the tank and mixes. The thermocouples that correspond to a NOTRUMP fluid node are combined and mass-enthalpy averaged to obtain the average temperature of the CMT water that corresponds to the NOTRUMP noding for the tank in a similar fashion as for the 500-series tests.

6.5.2 NOTRUMP Comparisons to the 10-psig (24.7-psia) Core Makeup Tank Tests

The comparisons of the NOTRUMP calculations to the 10-psig (24.7 psia) tests are shown in Figures 6.5-2 to 6.5-9. The calculated CMT fluid temperatures are compared to the average measured temperatures for each CMT node as shown in Figures 6.5-2 to 6.5-5. Figure 6.5-2 shows the top-most node and measured temperatures and shows that this node rapidly heats up due to the steam condensation at the top of the CMT. The uncertainty in the temperature measurements is small, ~2°F, so that NOTRUMP is outside the data range. However, the calculation follows the trends closely. The NOTRUMP-calculated temperature is delayed relative to the data in reaching saturation by approximately 25 seconds. As the CMT drains, the thermocouples in the lower nodes record the higher fluid temperatures as seen in Figures 6.5-3 to 6.5-5. The effect of numerical diffusion can also be seen in Figures 6.5-4 and 6.5-5 in which the calculated CMT fluid temperature is increasing before this is measured by the fluid thermocouples.

Figure 6.5-6 shows the calculated and measured pressure at the top of the CMT. The steam/water reservoir pressure was held at a constant 25 psia for this test. As the figure indicates, that is when the repeat condensation is occurring. The pressure at the top of the CMT is significantly lower. As a result there is a large pressure difference between the reservoir and the CMT, resulting in large steam flow into the CMT for this time period.

Figure 6.5-7 shows the comparisons of the steam flow into the top of the CMT. Since the test is conducted with pressure boundary conditions (as opposed to fixed-flow boundary conditions), the steam flow to the CMT is induced by condensation as well as the volume replacement as the tank drains. The high steam flow at the beginning of the test is caused by rapid, direct condensation of the steam as it exits the diffuser in the CMT nozzle. Once the liquid at the top of the CMT is near or at the saturation temperature, the rapid condensation ceases, and the steam flow into the tank decreases sharply. The steam flow into the tank now is due to: the volume replacement as the tank drains and the wall condensation effects. There may still be some direct contact condensation on the liquid surface; however, the magnitude of this condensation is small since the liquid is at or near the saturation temperature. One of the most important parameters for the code-to-data comparisons is the timing of when the CMT begins to rapidly drain. When the top liquid layer heats to near saturation, the steam from the CMT diffuser is no longer condensed and bubbles up to the top of the tank, allowing a water level to form. At this time, the pressure at the top of the CMT returns to near the pressure in the steam/water reservoir, and the CMT begins to drain freely.

The CMT drain flow is shown in Figure 6.5-8. The drain flow corresponds to the steam flow shown in Figure 6.5-7; that is, when the steam flow is large, indicating high condensation rates, the drain flow is small since the pressure at the top of the CMT is reduced due to the rapid condensation, as shown in Figure 6.5-6. Once the rapid condensation ceases, the level in the CMT decreases as the CMT drains. For this test, NOTRUMP predicts a longer delay in the CMT draining than observed in the data for this test. However, the thermal-hydraulic phenomena associated with the condensation and mixing at the top of the CMT are captured by NOTRUMP.

The NOTRUMP-predicted CMT drain flow is within the uncertainty of the drain flow measurement as shown in Figure 6.5-8 for the majority of the test, for both low flow and high flow periods. The NOTRUMP integrated drain flow and test integrated drain flows are shown in Figure 6.5-9, and the NOTRUMP comparison is within the data uncertainty.

6.5.3 NOTRUMP Comparisons to the 1085-psig (1100-psia) Core Makeup Tank Tests

The comparisons to the 1085-psig (1100-psia) test (C039309) are shown in Figures 6.5-10 to 6.5-17 and show similar behavior as the previous test; however, the higher pressure tests have shallow mixing and substantial top subcooling at the time free draining starts. Thus, while NOTRUMP predicts a more rapid heatup to the liquid in the top NOTRUMP cell relative to the data, the drain time predicted by NOTRUMP is delayed relative to the data. As a result, the steam flow into the CMT is larger for extended time in the NOTRUMP calculation relative to the test data, and the resulting agreement is poorer. However, the predicted drain flows shown in Figure 6.5-16 and 6.5-17 are accurately predicted by NOTRUMP.

6.5.4 Overall Comparisons of the NOTRUMP Core Makeup Tank Model to the Core Makeup Tank 300-Series Tests

The results of all the comparisons are shown on Figure 6.5-18 from the preliminary validation report as a comparison of the time at which rapid CMT draining was initiated during the test and from the NOTRUMP calculation. The two tests that are reanalyzed are shown in Figure 6.5-18. The delay in the drain time is chosen as the main parameter to assess the performance of the NOTRUMP CMT model and its capability. There is ample scatter of the NOTRUMP prediction relative to the test data; however, the overall trend is for the NOTRUMP calculation to predict longer delays in the rapid CMT delivery relative to the tests. The majority of the points on this figure are from the preliminary validation report. The recalculated tests are shown by the crosses and agree well with the original calculations. While the comparisons are not perfect between the NOTRUMP predictions and the CMT data, the NOTRUMP model does capture the key thermal-hydraulic effects observed in the tests. That is, there are delays due to the mixing of the steam coming into the CMT. The top liquid layer must heat up to near saturation before draining can occur. There is rapid condensation at the top of the CMT, and once the rapid condensation ceases, the tank drains freely. Therefore, the NOTRUMP CMT model, while crude in its number of computational cells, does capture and model the key thermal-hydraulic behavior observed in the CMT tests.

A comparison of the approximate average CMT discharge rate during the mixing phase and while rapid condensation is occurring before rapid draining starts is shown in Figure 6.5-19. The majority of the points on this figure are from the preliminary validation report. The recalculated points are shown as open circles. The agreement is good between the original calculations and the recalculated flows. The arrow with the point indicates that the new point would be on the original calculated point. NOTRUMP predicts the flow well during this period. This comparison is significant for high pressure conditions, because the drain rate during the condensation phase is a large fraction of the free draining

rate. Thus at high pressure, the importance of differences between calculated and actual delays in the drain initiation is minimized.

The transient comparisons already shown indicate that NOTRUMP agrees well with the actual drain rate after completion of the mixing phase. This is summarized in Figure 6.5-20, which compares the approximate maximum drain rates during that period. The recalculated points are shown on this figure and agree well with the original calculations.

Since the reanalysis of the selected 300-series tests shows essentially no difference from the original calculations performed in the preliminary validation report, the results of the preliminary validation report calculations for the 300-series are attached in Appendix 6A.

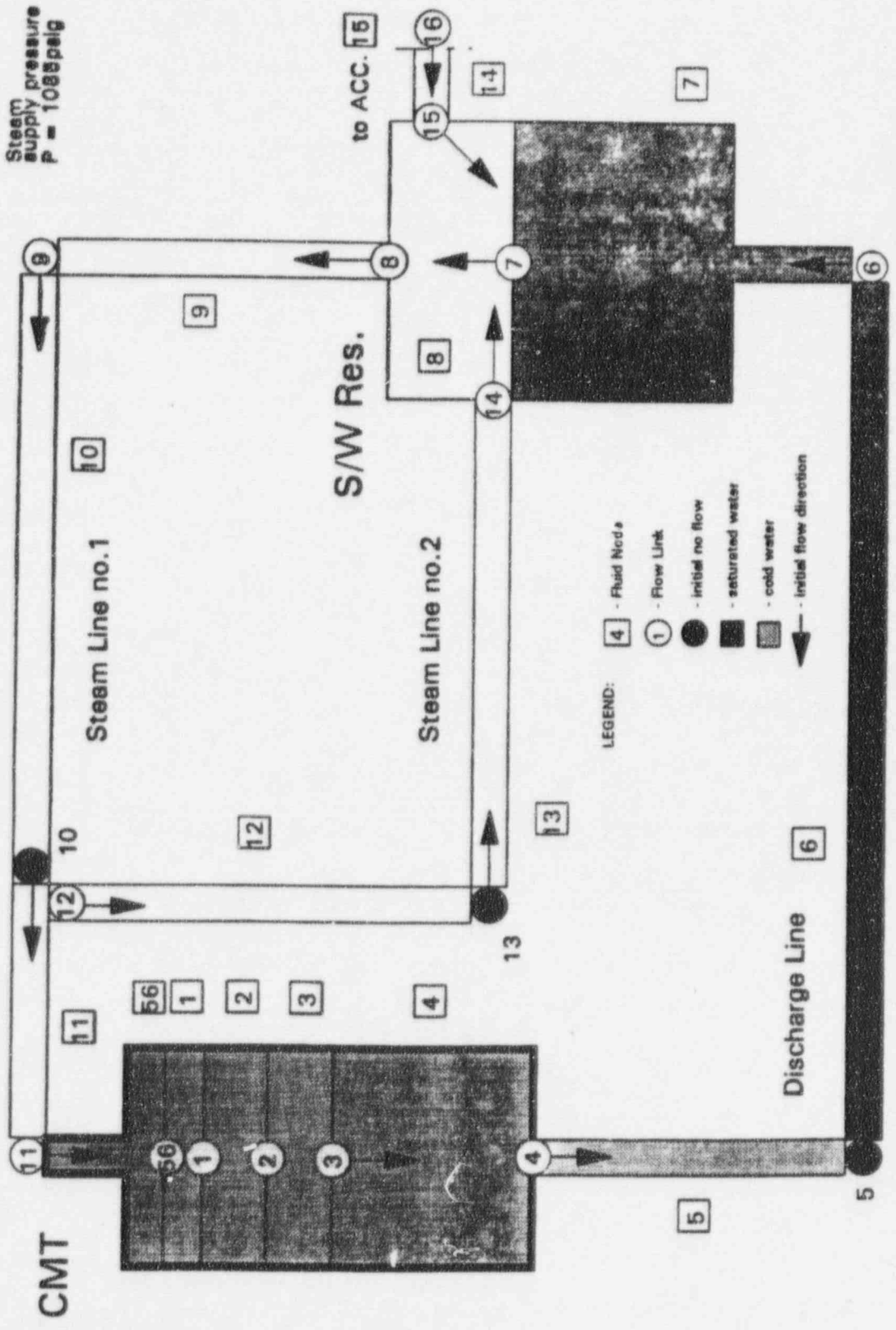

Figure 6.5-1 Core Makeup Tank Test Facility - NOTRUMP Noding Scheme for 300-Series Core Makeup Tank Test Analysis

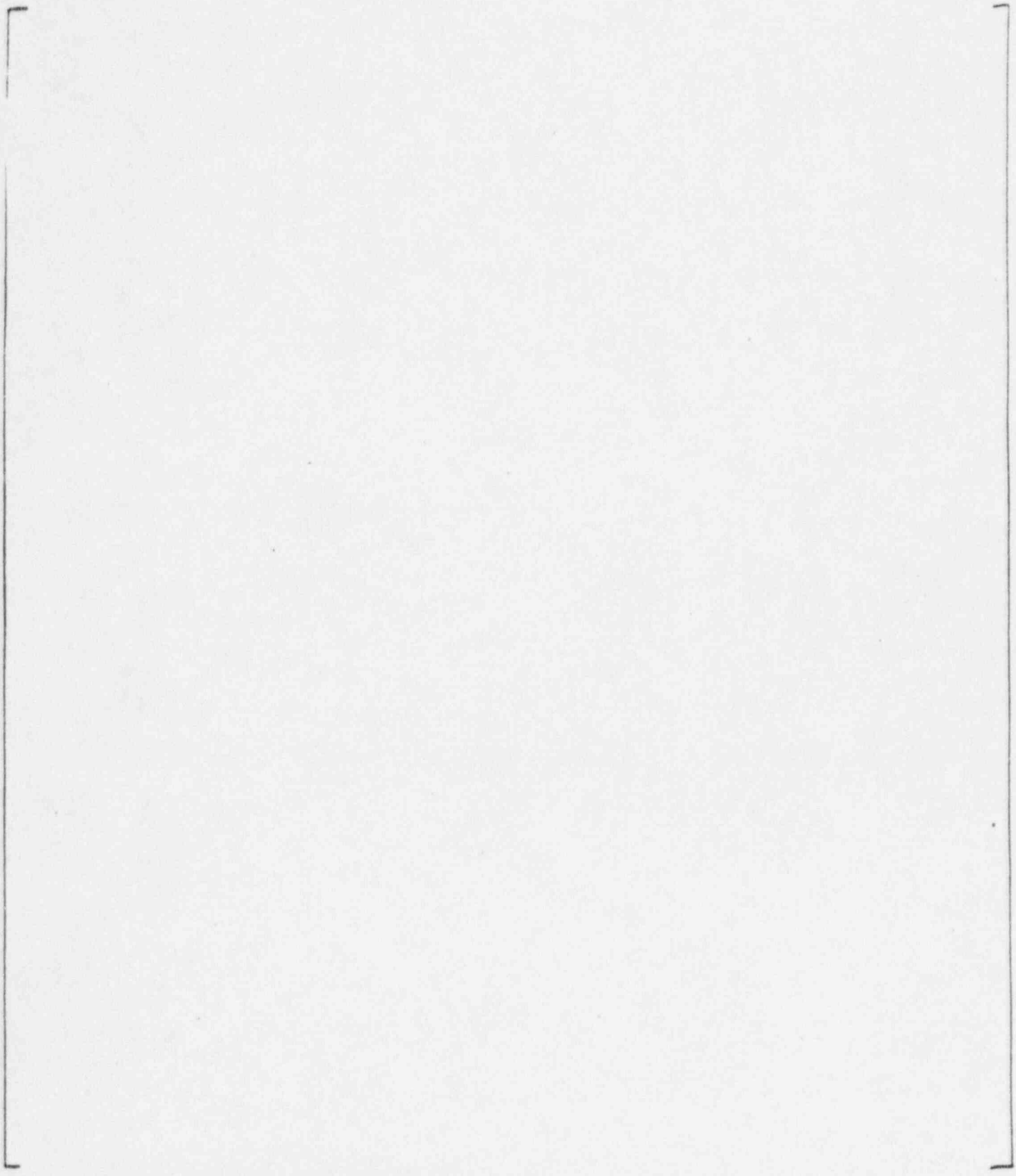

Figure 6.5-2 NOTRUMP Comparisons for Top Core Makeup Tank Node (Node 56) for Test C031307

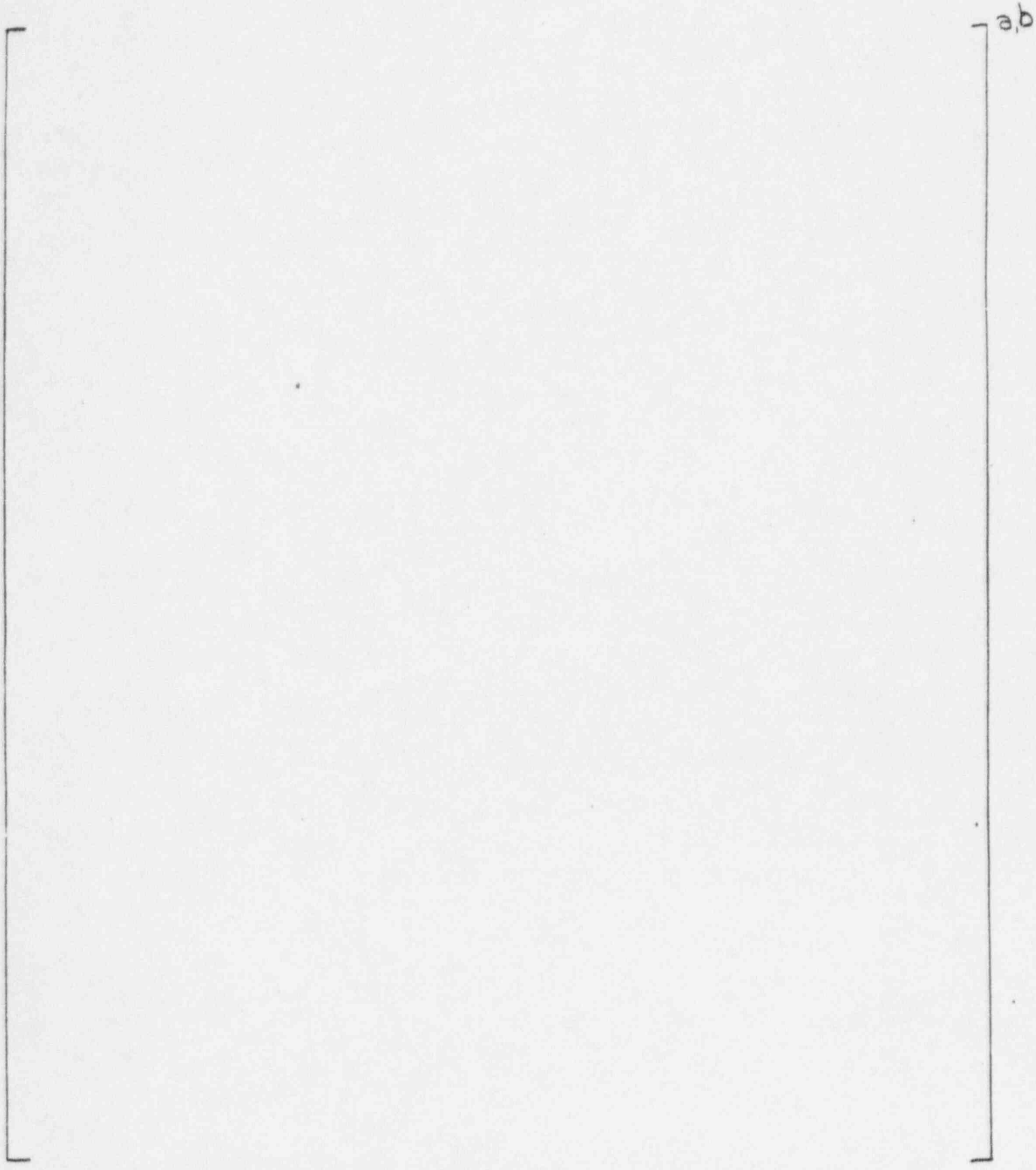

Figure 6.5-3 NOTRUMP Comparisons for Top Cylindrical Node (Node 2) for Test C031307

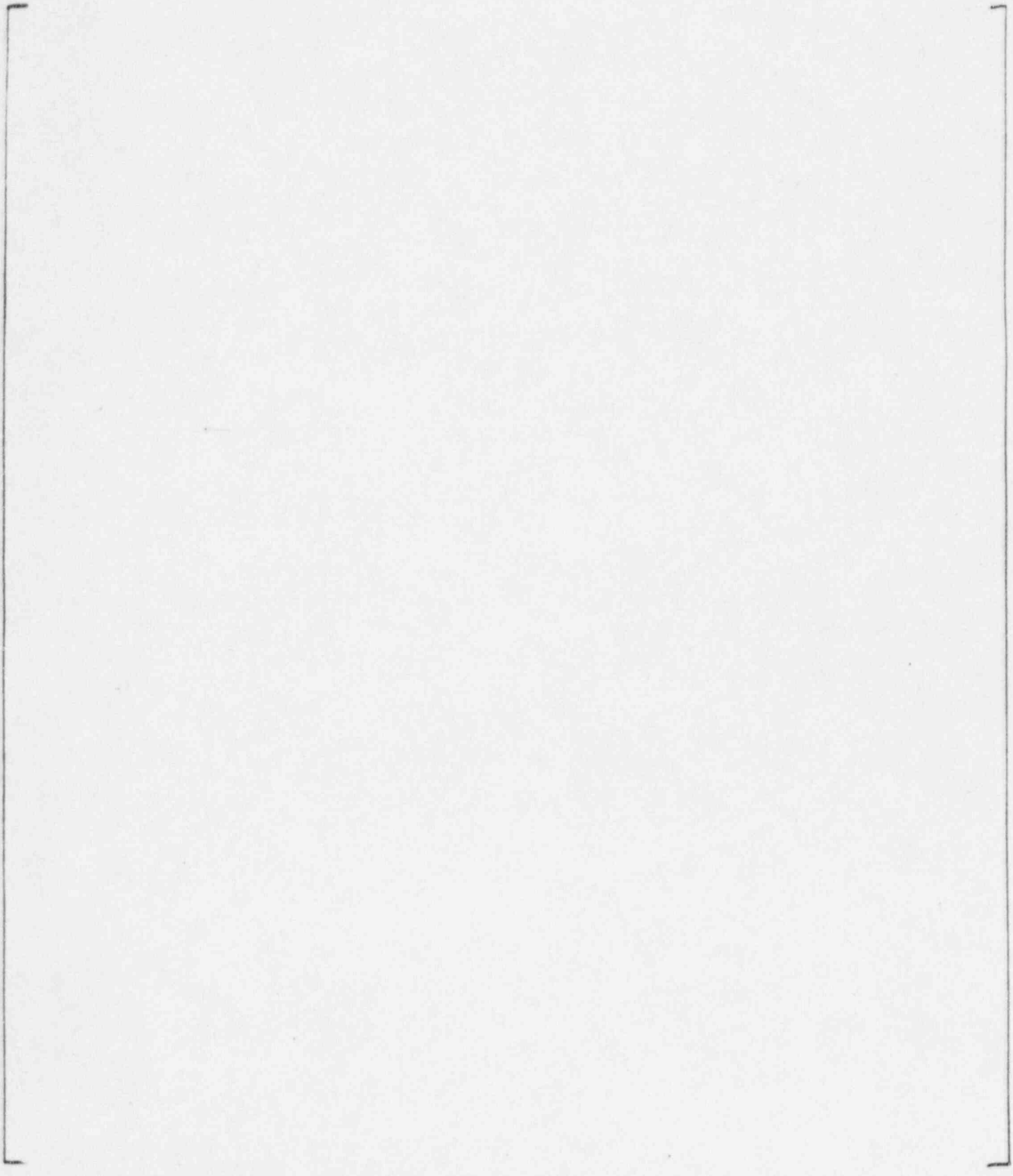

Figure 6.5-4 NOTRUMP Comparisons for Core Makeup Tank Node 3 for Test C031307

[ ] a,b

Figure 6.5-5 NOTRUMP Comparisons for Core Makeup Tank Node 4 for Test C031307

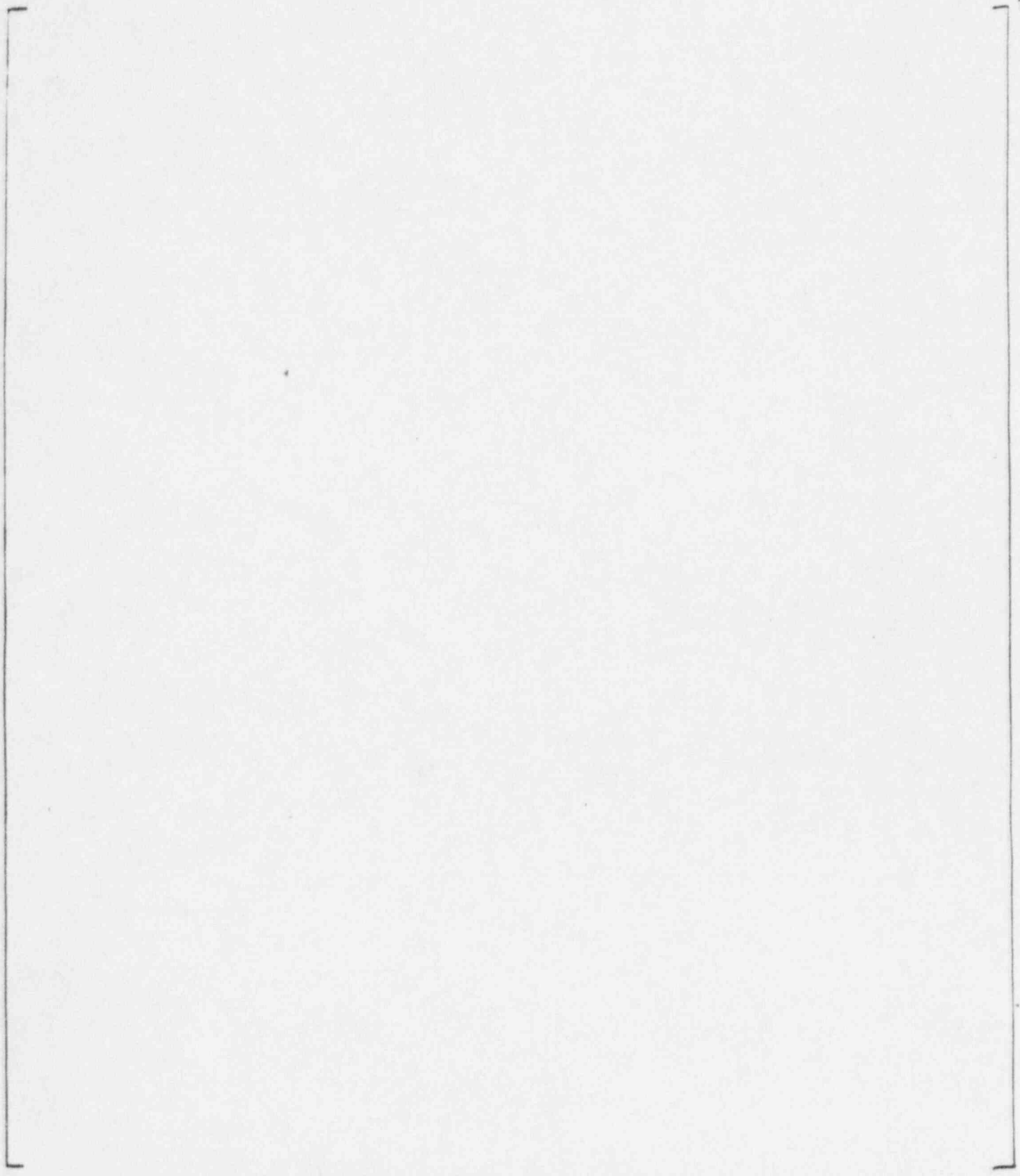

Figure 6.5-6 NOTRUMP Comparisons to Core Makeup Tank Pressure at Top of Core Makeup Tank for Test C031307

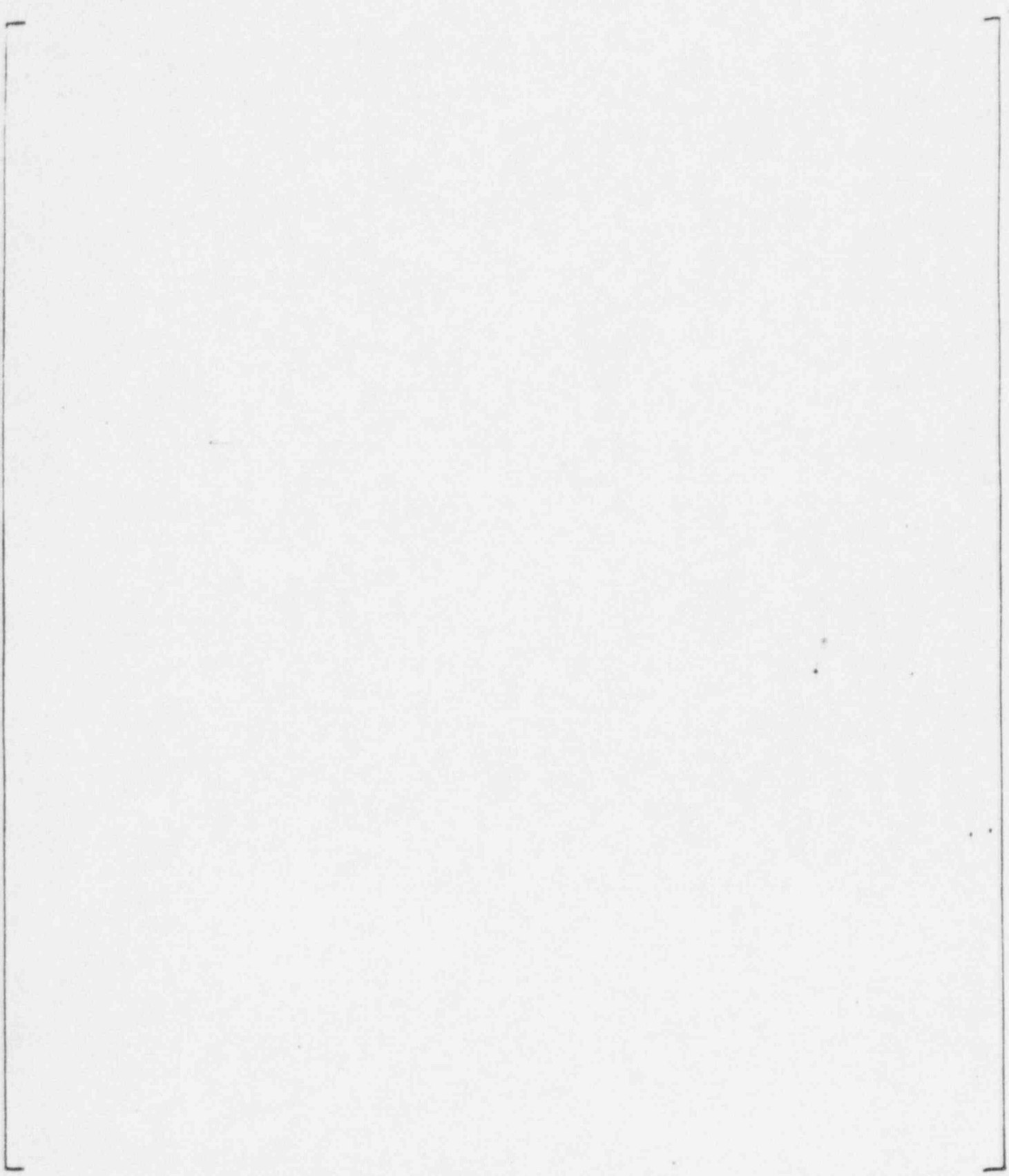

Figure 6.5-7 NOTRUMP Comparisons to Inlet Core Makeup Tank Steam Flow for Test C031307

[ ] a,b

Figure 6.5-8 NOTRUMP Comparisons to Core Makeup Tank Drain Flow for Test C031307

a,b

Figure 6.5-9 NOTRUMP Comparisons to Integrated Core Makeup Tank Drain Flow for Test C031307

a,b

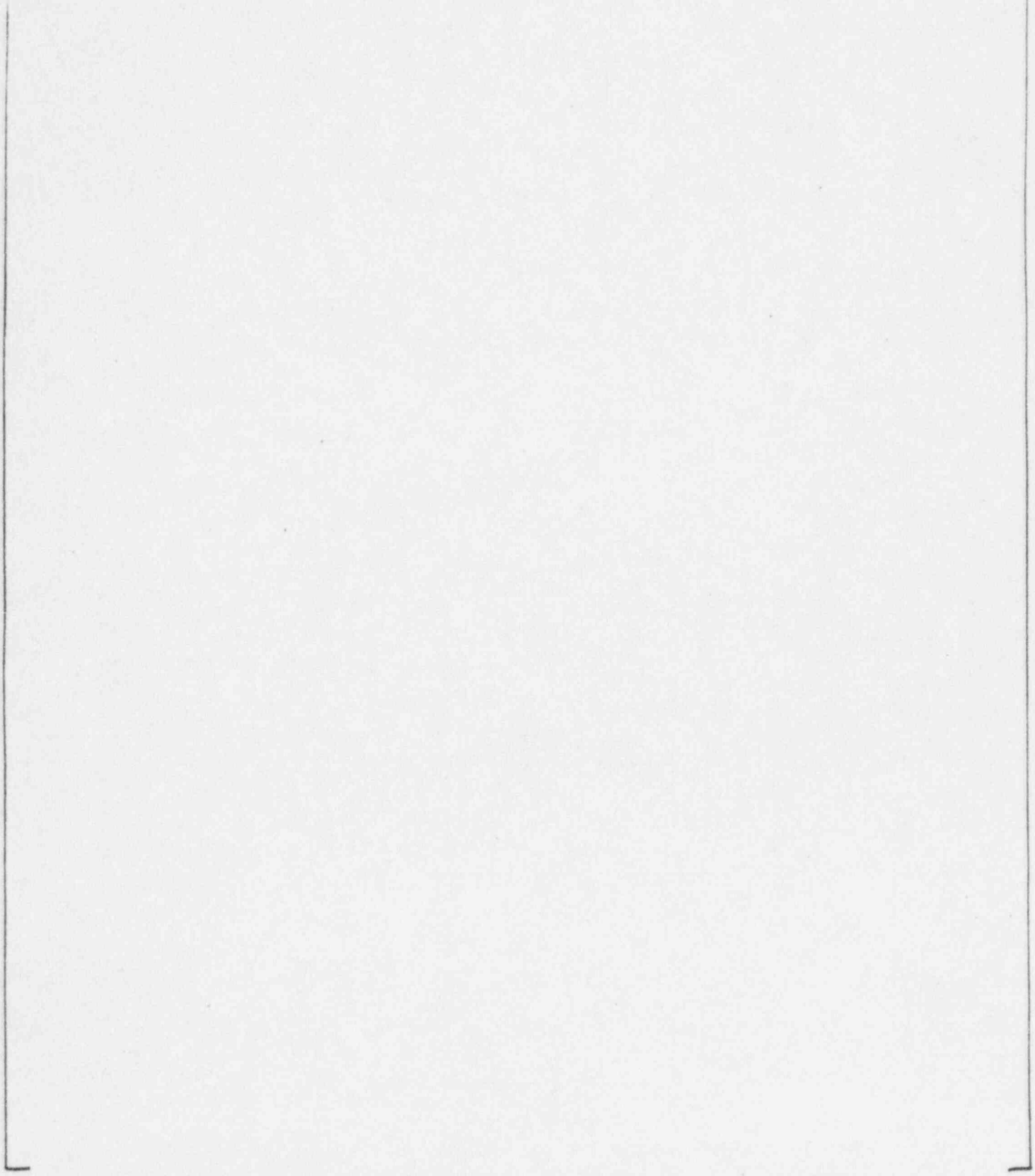

Figure 6.5-10 NOTRUMP Comparisons to Top Core Makeup Tank Node (Node 56) Temperatures for Test C039309

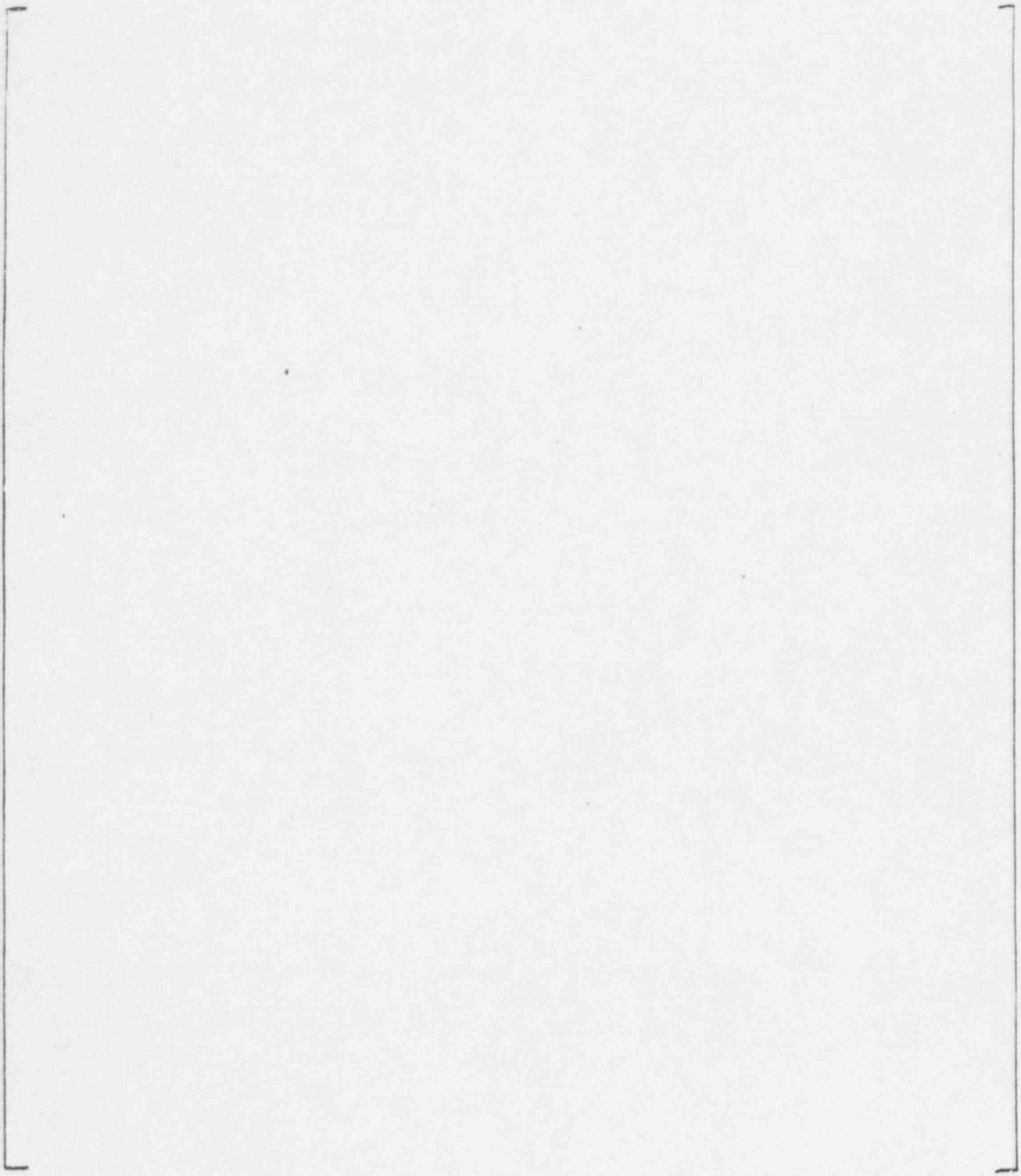

Figure 6.5-11 NOTRUMP Temperature Comparisons for Core Makeup Tank Node 2 for Test C039309

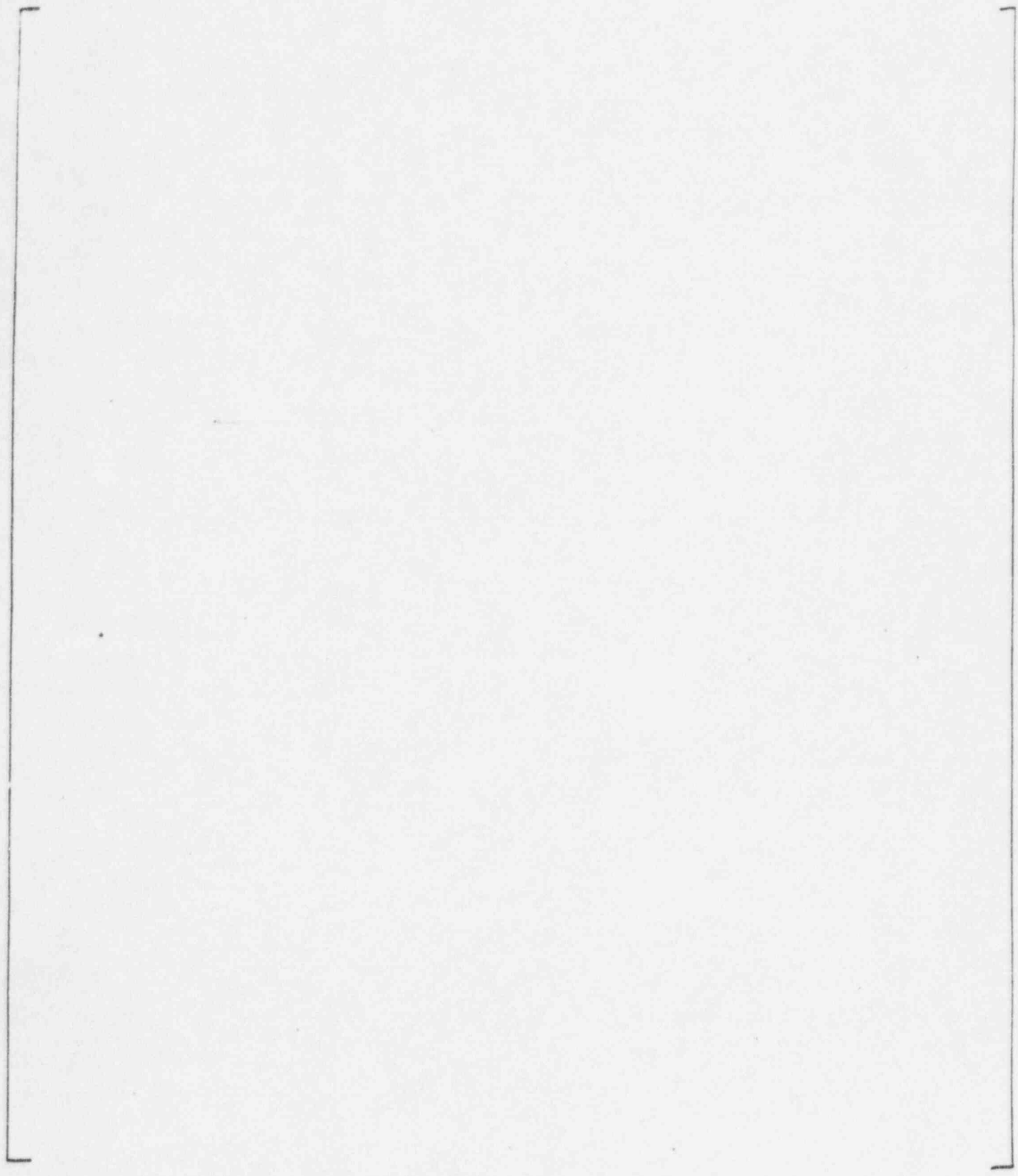

Figure 6.5-12 NOTRUMP Temperature Comparisons for Core Makeup Tank Node 3 for Test C039309

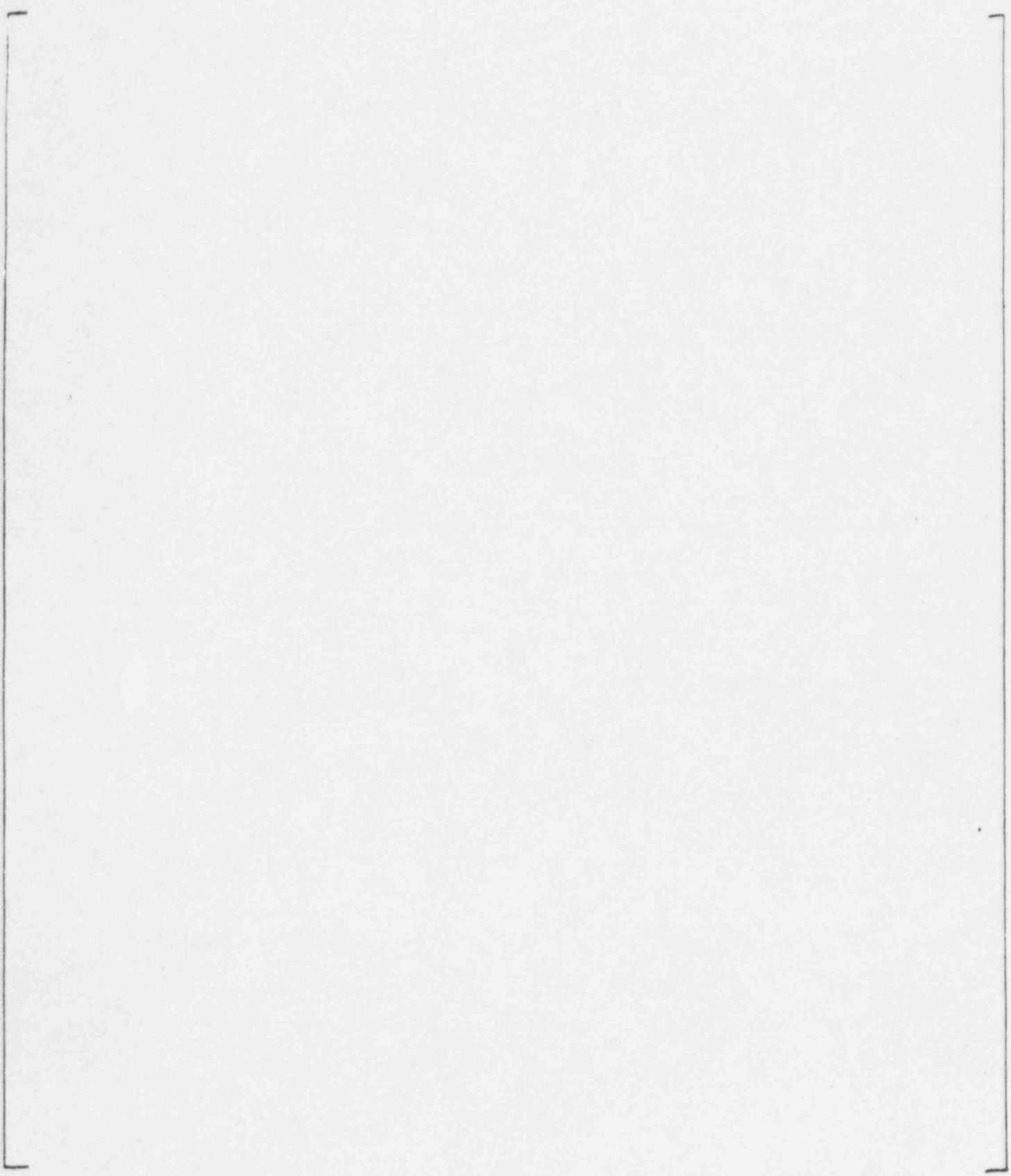

Figure 6.5-13 NOTRUMP Temperature Comparisons for Core Makeup Tank Node 4 for Test C039309

[ ] a,b

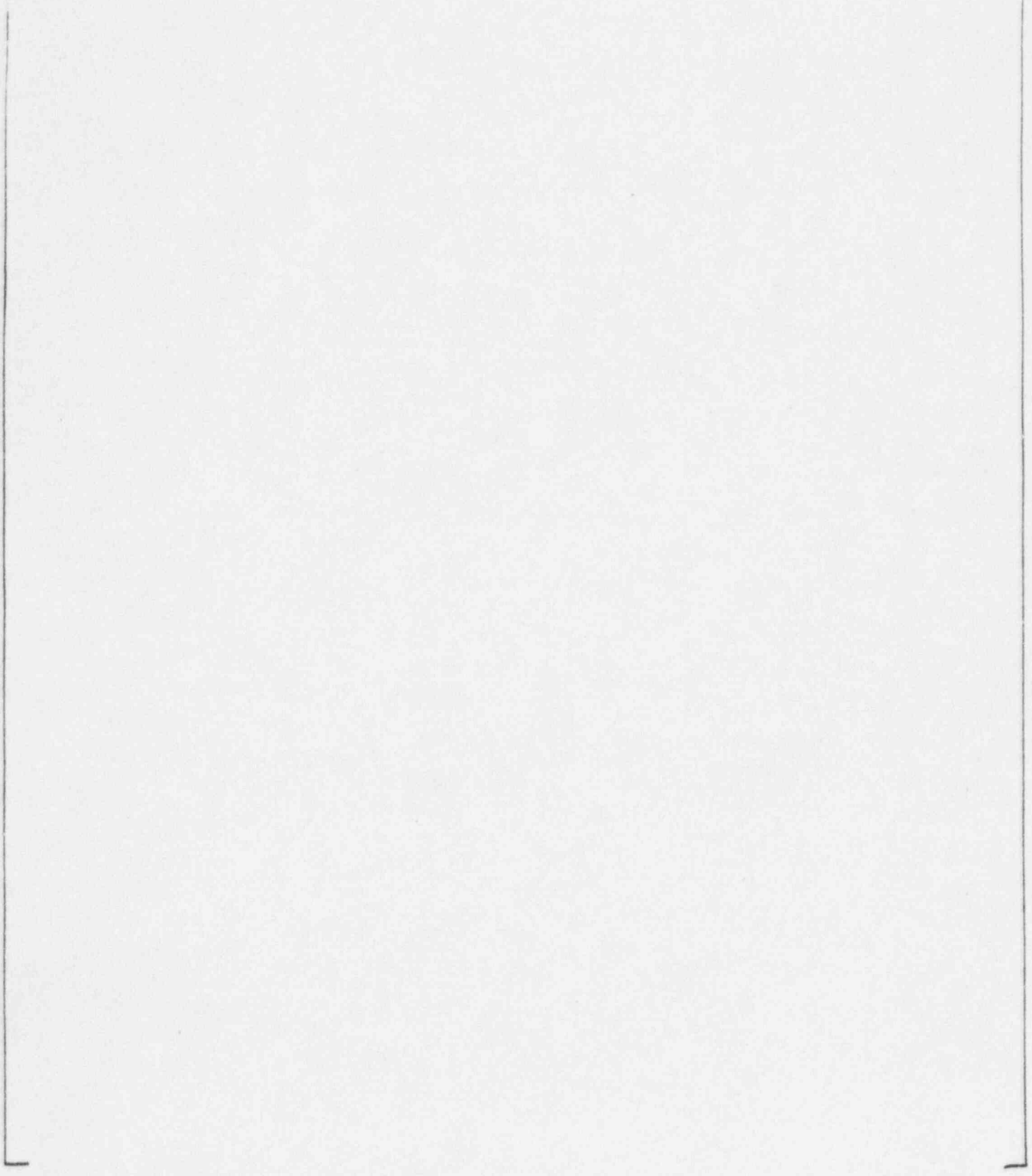

Figure 6.5-14 NOTRUMP Comparisons to Core Makeup Tank Pressure for Test CO39309

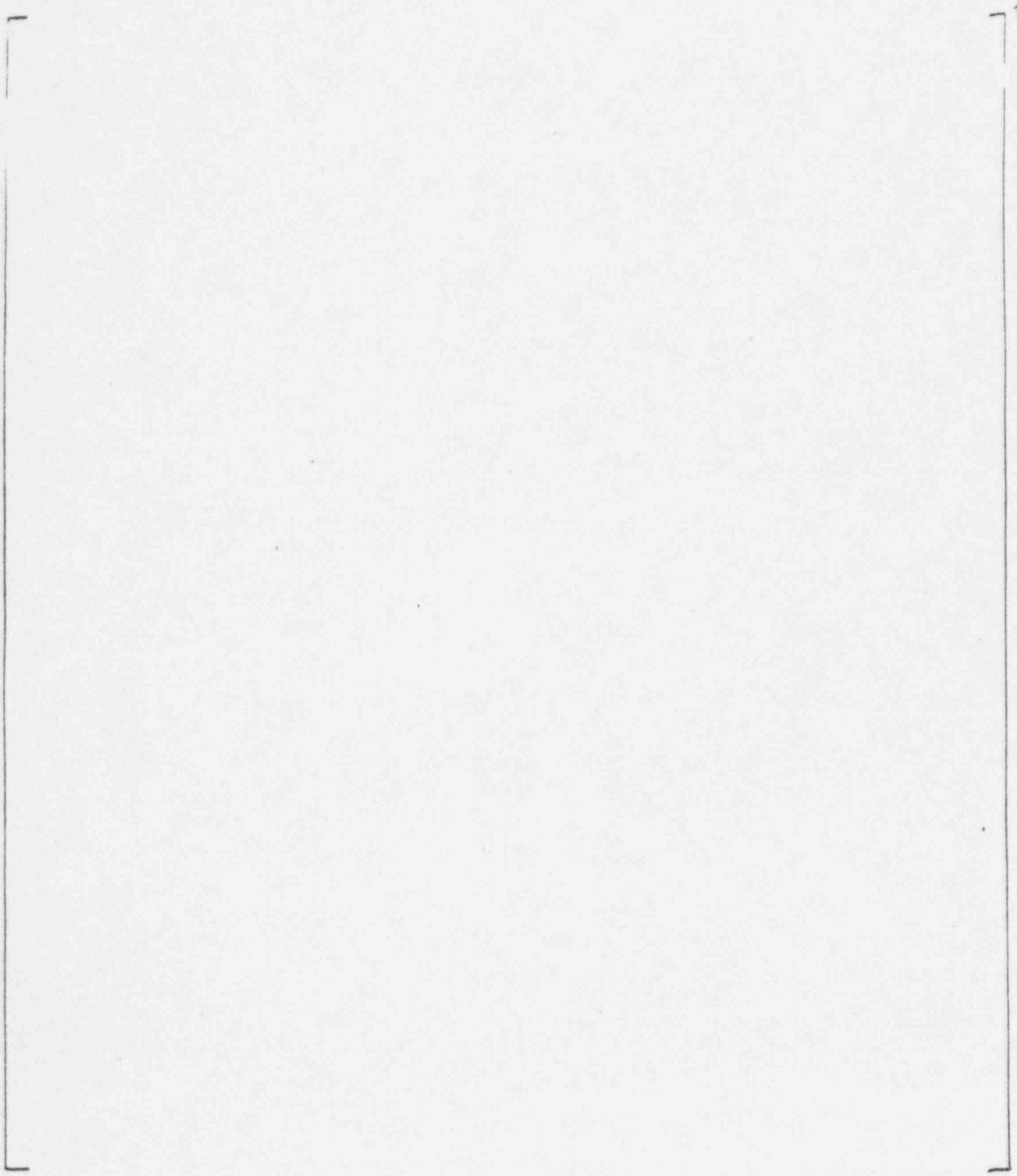

Figure 6.5-15 NOTRUMP Comparisons to Inlet Steam Flow for Test C039309

a,b

Figure 6.5-16 NOTRUMP Comparisons to Core Makeup Tank Drain Flow for Test C039309

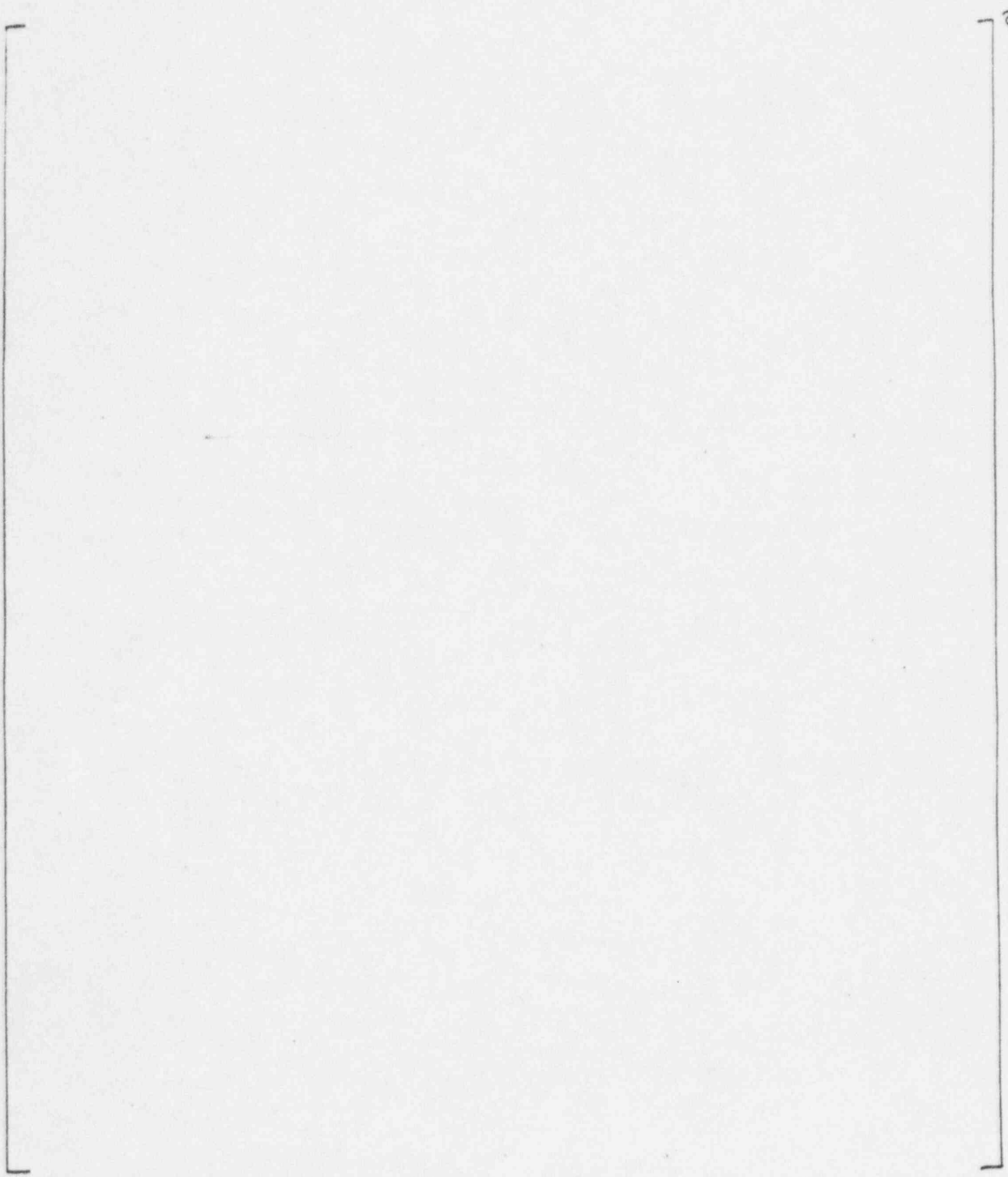

Figure 6.5-17 NOTRUMP Comparisons to Integrated Core Makeup Tank Drain Flow for Test C039309

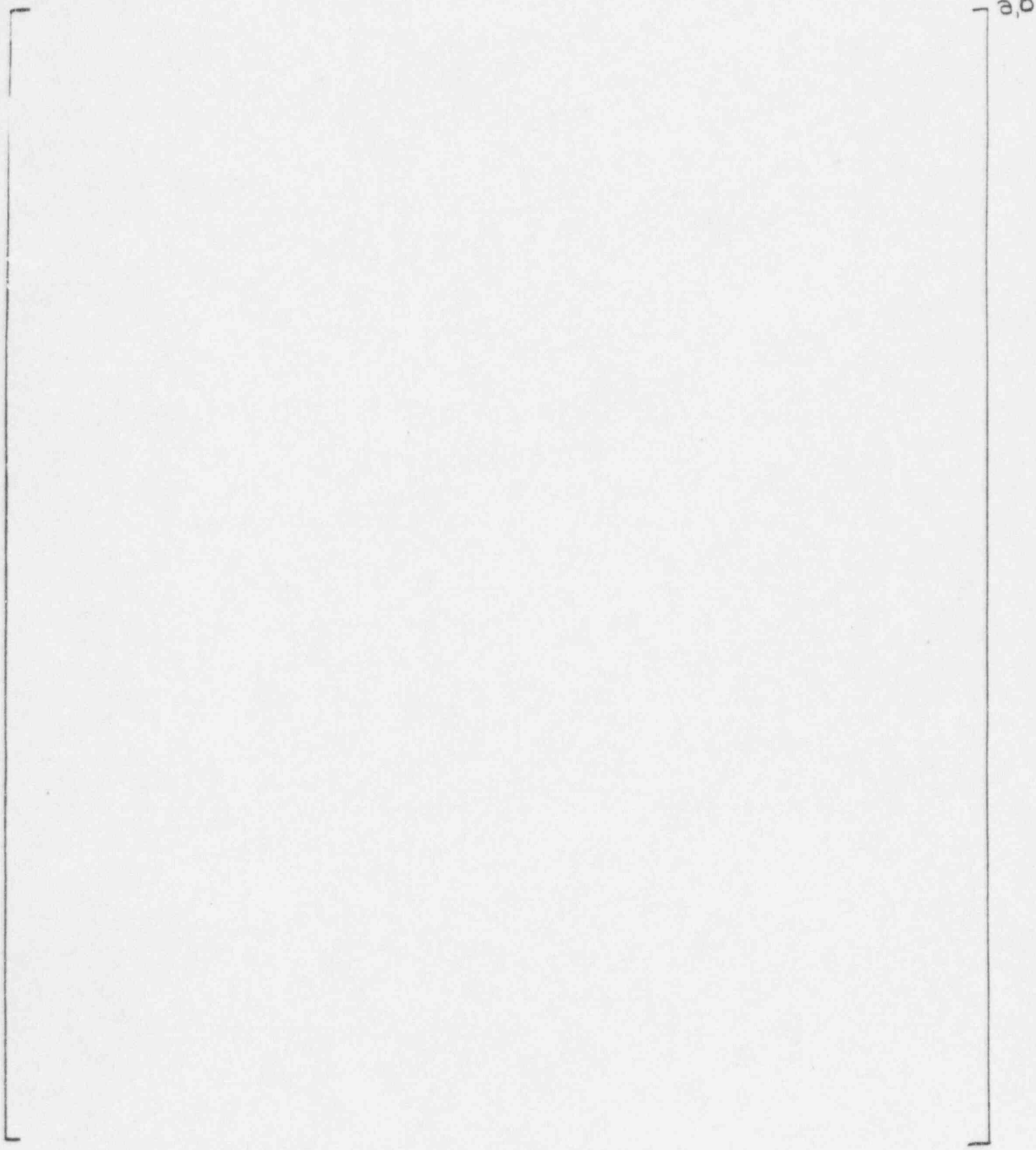

Figure 6.5-18 Comparison of the NOTRUMP Calculated Drain Time Delay to the Measured Core Makeup Tank Drain Delay

a,b

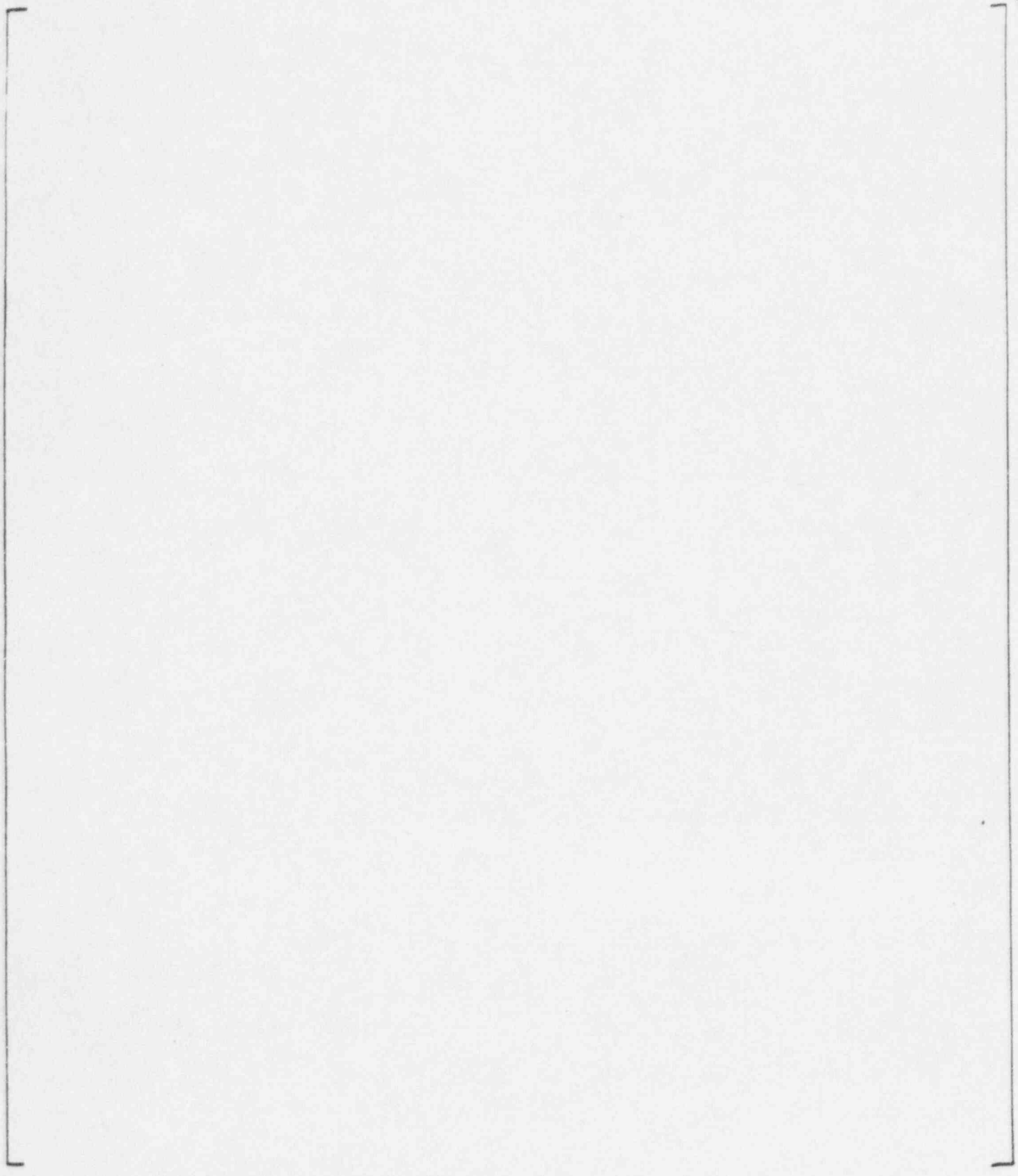

Figure 6.5-19 Comparison of NOTRUMP Average Calculated Core Makeup Tank Discharge Flow with Tests during the Mixing Period before Free Draining Starts

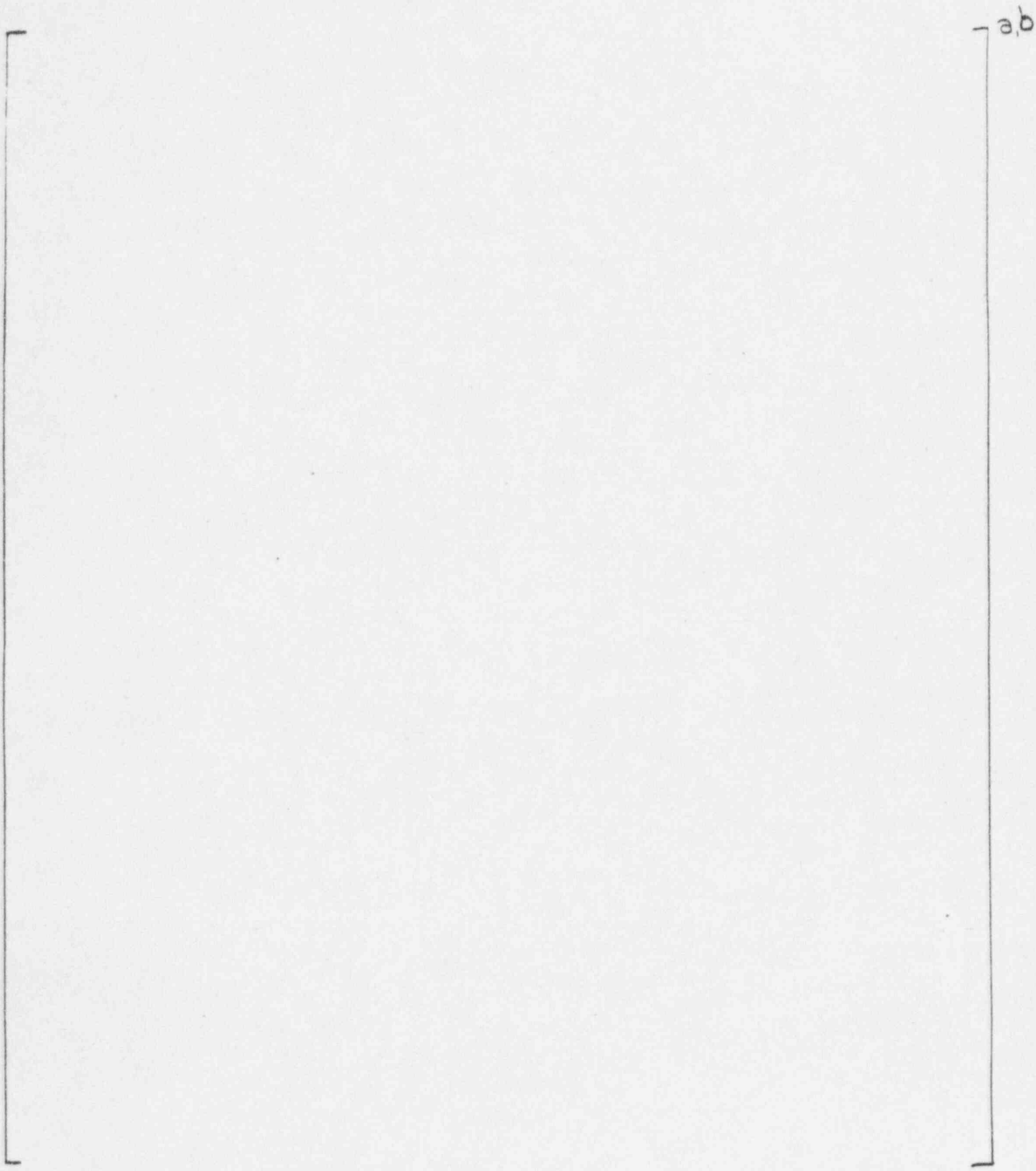

Figure 6.5-20 Comparison of NOTRUMP Calculated Maximum Free Drain Flow with Tests

6.6 Assessment of the NOTRUMP Comparison Results Against the AP600 PIRT

NOTRUMP provides reasonably good agreement for the CMT drain flow for the tests where the CMT could circulate and heat up to 20 percent and 50 percent. As the CMT continues to heat completely, the NOTRUMP comparisons show less agreement with the data trends, particularly at the end of the test.

The NOTRUMP calculations indicate a smooth decreasing discharge flow as the CMT heats up from the flow from the simulated balance line to the top of the CMT. This is the expected trend since the thermal center between the CMT and the steam/water reservoir is decreasing with time as the CMT is heated and the reservoir is cooled from the cold water from the draining CMT. The available cold flow test data for the line and valve resistances are used in the NOTRUMP model to reduce differences between the test and the simulation. The data show inflection points in the CMT circulation flow, which occur when the hot liquid layer reaches the bottom of the CMT. NOTRUMP does not predict this effect due to the numerical thermal diffusion.

The most important quantity is the time-averaged flow, which is delivered from the CMT to the steam/water reservoir. The average circulating flows calculated from the predictions and the measurements are shown in Figure 6.6-1. The average CMT circulating flow comparisons agree well between the NOTRUMP calculations and the test data. In most cases, the calculated circulating flow is within the uncertainty of the flow measurement, indicating excellent agreement.

The fluid temperature predicted by NOTRUMP indicates the presence of numerical diffusion so that a sharp thermal gradient is not predicted for the CMT 500-series tests. Since the circulating flows agree well between NOTRUMP and the test data, it is concluded that a lower level of accuracy is acceptable for the CMT fluid temperature distribution, and coarse noding such as that used in NOTRUMP is adequate to capture the thermal effects.

The analysis of the 300-series tests indicates that the NOTRUMP code will model and capture thermal-hydraulic behavior for situations in which steam enters the top of the CMT. There is rapid condensation and mixing of the initially subcooled CMT liquid with the steam as it enters the CMT through the steam diffuser at the top of the tank. The rapid condensation process continues until a liquid layer is formed at the top of the CMT, which is near the saturation temperature. At that time, the rapid condensation stops, and the CMT drains freely. NOTRUMP predicts the thermal-hydraulic effects observed in the tests. The code prediction of when the rapid draining of the tank would begin shows scatter, but is conservative, i.e., longer, than the tests. The repeat calculations agree well with the original CMT 300-series calculations performed in 1994. NOTRUMP captures the key thermal-hydraulic phenomena for CMT draining when condensation occurs at the top of the CMT.

If the PIRT is examined in Table 1-1 for the highly ranked CMT thermal-hydraulic phenomena during the CMT draindown period, items such as the condensation at the top of the CMT and the dynamic effects of the steam mixing with the CMT liquid are highly ranked. These phenomena are present in

the 300-series CMT tests. The NOTRUMP predictions for these tests are reasonably good. As noted above, the rapid condensation is predicted and its impact on the CMT drain flow is also predicted well. The condensation effects are enhanced by the mixing that occurs at the top of the CMT. The CMT top node temperatures are also well predicted, particularly at the top of the CMT where the condensation is occurring.

The thermal stratification effects are ranked at a medium importance. NOTRUMP does predict thermal stratification effects; however, the thermal fronts are diffused due to numerical diffusion and are not as sharp as indicated from the data. There does not appear to be an adverse effect of the use of coarse noding and the numerical diffusion of the thermal effects since the predicted CMT drain flow agrees well with the test data. Therefore, the CMT draining phenomena are well represented by the NOTRUMP code and the calculations are in good agreement with the test data.

The highly ranked CMT PIRT phenomena that the CMT separate effects tests address for the CMT recirculation phase include: the natural circulation between the CMT and the simulated reactor system and the cold balance line pressure drop. The natural circulation is well simulated by NOTRUMP as seen by comparing the circulating flows between the CMT and the steam/water reservoir in the test facility. The CMT balance line resistance is set equal to the measured line resistance from the cold shakedown tests so that good agreement is expected. The CMT wall heat transfer model in NOTRUMP was previously compared to the test data in Reference 6-6 and agreed well with the heat transfer calculated from the test data.

Therefore, the CMT separate effects tests provide data to validate the NOTRUMP code against several of the highly ranked PIRT thermal-hydraulic phenomena identified for the CMT component. The NOTRUMP comparisons to the CMT data show that NOTRUMP accurately represents these phenomena.

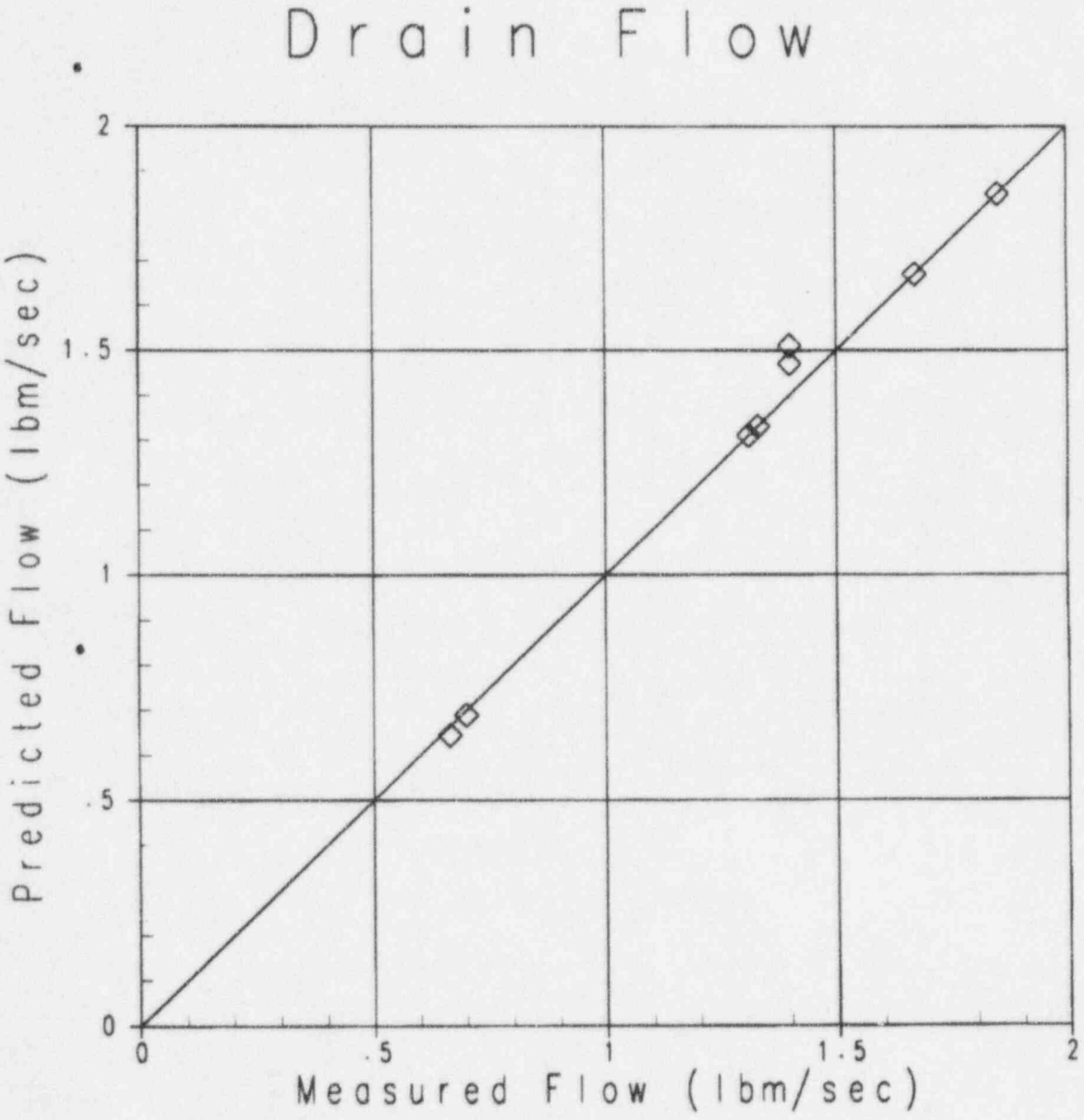

Figure 6.6-1 Summary Comparisions of Average Core Makeup Tank Drain Flow from the 500-Series Test

6.7 Conclusions

NOTRUMP computer code predictions have been compared to the 300-series and 500-series CMT tests, which simulate CMT draindown and the circulation behavior. The computed flow rates from the NOTRUMP calculations agree well for most of the tests and are within the data uncertainty. The calculated time-averaged flow rates over the duration of the test also agree well with the measured data. The average fluid temperatures predicted for the CMT are usually lower for the NOTRUMP calculation, even with the numerical smearing effects caused by the code numerics and coarse noding. However, this appears to have a secondary effect on the resulting circulating and draining flow calculation by the NOTRUMP code. The overall response of the code and the tests are similar, so that the NOTRUMP code captures the thermal-hydraulic effects observed in the tests. The excellent agreement with the majority of the test data for these different series of tests indicates that NOTRUMP captures the key thermal-hydraulic behavior observed in these tests, and the hydraulic phenomenon identified in the AP600 PIRT.

6.8 References

6-1 Westinghouse Electric Corporation, *Core Makeup Tank Final Data Report*, WCAP-14217, November 1994.

6-2 Cunningham, J. C., R. C. Haberstroh, L. E. Hochreiter, and J. Jaroszewicz, *AP600 NOTRUMP Core Makeup Tank Preliminary Validation Report*, Rev. 0, MT01-GSR-001, October 1994.

6-3 Westinghouse Electric Corporation, *AP600 Standard Safety Analysis Report (SSAR)*, June 1992.

6-4 Hochreiter, L. E., K. G. Seraf ni, and D. Aumiller, *Scaling Logic for the Core Makeup Tank Test*, WCAP-13963, Re . 1, January 1995.

6-5 Meyer, P. E., *NOTRUMP, A Nodal Transient Small Break and General Network Code*, WCAP-10079-P-A, August 1985.

6-6 Haberstroh, R. C., J. P. Cunningham, and L. E. Hochreiter, *Core Makeup Tank Test Analysis Repo t*, WCAP-14215, November 1994.